COMPUTER SIMULATION STUDIES OF TITANIUM SURFACE ETCHING WITH HF, HCl and HBr ACIDS

by

DAVID MAGOLEGO TSHWANE

THESIS

Submitted in fulfilment of the requirements for the degree of

DOCTOR OF PHILOSOPHY

in

PHYSICS

in the

FACULTY OF SCIENCE AND AGRICULTURE

(School of Physical and Mineral Science**)**

at the

University of Limpopo, South Africa

SUPERVISOR: PROF H.R CHAUKE

CO-SUPERVISOR: DR R. MODIBA

: PROF P.E NGOEPE

2021

DECLARATION

I declare that the work contained in this thesis has not been previously submitted to meet the requirement for an award or any other higher educational institution. To the best of my knowledge that it is my work in design and execution, and that all material contained herein has been duly acknowledged and referenced.

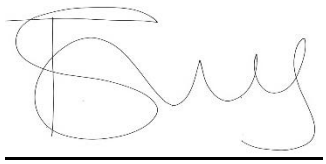

25/10/2021

DM TSHWANE (Mr)

DEDICATION

This work is dedicated to:

My late Mother

Magane Julia Tshwane

My wonderful Father

Mamaile Petrus Tshwane

And,

Tshwane Family

ACKNOWLEDGEMENTS

Firstly, I would like to recognise and greatly appreciate Dr R Modiba for her expertise, guidance and continuous support throughout the research. She supported me in every possible way to achieve my scientific goal. I thank Prof H.R Chauke for his mentorship and planning during the execution of this research. I would also like to acknowledge the important contribution to this work made by Dr G Govender and Prof P.E Ngoepe. I appreciate your help in creating a working environment and learning.

I would like to acknowledge the financial support provided by the Council for Scientific and Industrial Research (CSIR) and the Department of Science and Innovation (DSI) for this PhD project. I would like to say thank you to Centre for High Performance Computing (CHPC) and Material Modelling Centre (MMC) at the University of Limpopo for computational resources.

My thanks also goes to the heart-warmed Advanced Materials Engineering (AME) and MMC staff members for their support and encouragement. My deepest gratitude goes to my Family and Friends for the support and enthusiasm they provided me with to reach my goal. Lastly, I would like to express gratitude to my wife Mahlako for her endless support in the completion of this research. Most of all, I thank God for giving me strength throughout my study.

Abstract

Titanium metal and its alloy components find extensive applications in various industries such as aerospace, medicine and automotive due to its light weight-strength ratio. More importantly, titanium-based components with better surface finishing are required in the titanium manufacturing industries. However, these components suffer from surface roughness and brittleness due to the formation of alpha-case layer. Recently, the etching process has been widely used for metal surface modification, but the etching mechanism and the choice of etchant are not well prescribed. On the other hand, the adsorption of halogen molecules on the metal surface has received much attention due to their technological applications and relevance for material surface processing, corrosion and etching. This is considered as a promising approach towards selecting an effective etchant for the metal surface etching process. In this study, the first-principle approach has been used to study the adsorption behaviour of halogen molecules and ions on Ti (100) and (110) surfaces. Their adsorption mechanism was deduced from the calculated adsorption energy, heats of formation, desorption energy, work function, charge density difference and density of states. In particular, to understand how different etchant can influence the properties of titanium metal surface during etching process.

Firstly, the free halogen molecules (HF, HCl, HBr and HI), as well as the clean Ti (100) and (110) surfaces were investigated to deduce the reactivity and surface stability, respectively. It was established that the HF dissociate easily due to its lowest dissociation energy and higher electronegativity, which suggest stronger interaction with the Ti surfaces. The halogen molecules stability trend was found to follow the order of HF>HCl>HBr>HI consistent with the electronegativity strength. Furthermore, it was also found that Ti (110) is the most stable surface displaying the lowest surface energy as compared to Ti (100) surface.

Secondly, the adsorption of halogen molecules on Ti (100) and Ti (110) surfaces was studied to investigate the chemical interaction and their reactivity. The halogens were adsorbed on three possible adsorption sites (Top, Bridge and Hollow) and their reaction is spontaneous. Moreover, the bridge and top sites were found to be the most favourable sites on Ti (100) and Ti (110) surfaces, respectively. Our results showed that all halogen molecules dissociate spontaneously on both Ti surfaces. The findings revealed that the adsorption of halogen molecules on Ti surfaces is energetically favourable suggesting adsorption energy strength order of $E_{ads}^{HF} > E_{ads}^{HCl} > E_{ads}^{HBr} > E_{ads}^{HI}$. This indicates that the adsorption of HF molecule on these surfaces is thermodynamically more stable than HCl, HBr and HI molecules. Also, our results revealed that the adsorption of halogen ions (F^-, Cl^-, Br^- and I^-) is more favourable than the adsorption of halogen molecules (HF, HCl, HBr and I) on the bridge site in both Ti surfaces considered. The F ion was found to be the most preferable than Cl, Br, and I ions.

In addition, the interaction of halogen ions with Ti surfaces was deduced with regards to electron charge. We found that the amount of electron charge transferred depends on the adsorption energy strength. In particular, it was found that the F atom accepts more electrons than other halogen ions. Moreover, the spherical shape was observed, this suggests that the charge density distribution between Ti atom and halogen exhibit ionic bonding behaviour. We also found that the adsorption of halogen has a stronger effect on the work function of Ti surfaces depending on the halogen ion. The magnitude of the induced work function varies from the halogen ionic order of F>Cl>Br>I.

Lastly, in order to describe the dependence of the surface coverage of an adsorbed molecule, F_2 and Cl_2 molecules were adsorbed on Ti (100) surface at different coverages. We observed the formation of etching products Ti_xF_y and Ti_xCl_y species on the surface. The heats of formation (E_{HF}) and desorption energy of volatile etch products were calculated. Our findings show that the formed volatile molecules (Ti_xF_y and Ti_xCl_y) are energetically favourable ($E_{HF} < 0$), suggesting an

exothermic process. We also found that the Ti_xF_y clusters is more stable with lower heats of formation than the Ti_xCl_y species. Moreover, the desorption energy of the formed volatile (TiF_4) species was found to be lower than $TiCl_4$ indicating that that TiF_4 species desorb easily. This demonstrates that F_2 is more suitable for surface etching as compared to Cl_2.

TABLE OF CONTENTS

LIST OF TABLES

LIST OF FIGURES

Chapter 1

Introduction

This chapter gives a brief background on titanium metal and its applications, the formation of alpha-case layer and the structural aspects for titanium phases. Secondly, the chapter also discuss surface etching and adsorption of halogen molecules. Lastly, the motivation, intention of the study, research hypothesis, research questions, motivation, objectives and outline of the study are presented.

1.1. Background

Titanium and its alloys have a long tradition in the manufacturing of automobile, aerospace and biomedicine components [1]. There are several manufacturing techniques for titanium parts such as machining [2], forging [3] and investment casting [4], but investment casting has become one of the most attractive methods. Investment casting process is the only metal casting process that can produce near-net-shape to a very high-quality standard [5]. However, during investment casting, titanium reacts with oxygen, nitrogen and intermetallic compounds that result in the formation of the alpha-case layer [6]. Formation of this layer causes fatigue and results in material micro-failures due to surface cracks and must be removed before the components go to the application [7].

Etching is one of the most advanced surface modifications in titanium production and plays an important role in the investment casting process [8]. The etching technique is used to remove the top layer from the material through electrochemical reaction [9], corrosion [10] or by breaking the atomic bond that attached at the top surface [11]. Industries rely on etching mechanism essentially for making superior and quality metal components [12]. Basic principle related to etchant is to produce a uniform surface with small surface leakage. There are various studies on the surface

etching phenomenon, but the etching mechanism is not well understood and remain limited, especially at the atomic scale [13].

Previously, various method has been used to modify or etch the alpha-layer from titanium components, such as chemical treatment, electrochemical treatment, chemical vapour and thermal oxidation [14, 15, 16]. Currently, the most commercialist method used to etch the alpha-case layer is through wet chemical milling solutions [17]. A mixture of hydrofluoric acid (HF) and nitric acid (HNO_3) is a common solution used in the wet etching of titanium or metal pieces. However, these solutions are highly exothermic and dangerous, and therefore, compromises workplace safety due to the toxicity of their acidic, particularly HF [18]. The second major problem associated with HF etching is hydrogen embrittlement and the etching mechanism is not well-studied [19].

Other halogen acid solutions can etch titanium substrate, however, the etching types may differ due to their distinction in nature [20] and induce pitting etching [21]. Halide's ions, especially Cl^-, dissolve in water can penetrate through the nature of the alpha-case layer and etch the substrate [22]. Hydrogen bromide (HBr) and potassium hydroxide (KOH) have been suggested as an alternative solution to remove the alpha-case layer on titanium components [23]. Niraula *et al* [24] used a hydrogen bromide-based etching solution to chemically etch the CdTe surface. This etchant offered a highly stable etching where the etching rate was varied by changing the solution composition. Hydrogen iodide is a suitable alternative to conventional chlorine or bromine in the etching process [25]. In order to obtain a better understanding of the etching mechanism and corrosion phenomenon, a computational approach has become an attractive theoretical method [26].

Density functional theory (DFT) was used to investigate the etching mechanism on Al_2O_3 surface by NbF_3 and CCl_4 [27]. Simulations were performed using Schrodinger Material Science Suit with Perdew, Burke and Ernzerhof (PBE) functional. It was demonstrated that the etching mechanism follow two steps, where the etchant (HbF_3) convert part of the Al_2O_3 surface layer into AlF_x which

is the most favourable volatile etch products [27]. Furthermore, Natarajan *et al* [28] utilised DFT-GGA with PBE functional to study the atomic etching of monoclinic alumina surface by HF molecule. It was reported that HF dissociates, resulting in the production of AlF_x species, and that the desorption energies of AlF_3 and Al_2F_6 are high, ranging from +5.08 and +5.25 eV, respectively.

1.2. Motivation

There is a high demand for titanium material components in the production of new commercial automobile and titanium manufacturing industries [29]. This is due to their outstanding properties such as high strength, low density and corrosion resistance makes Ti a more attractive material for their industrial applications [30]. An etching technique is currently the most commercialised approach for modifying and removing the alpha-case layer from the titanium surfaces. Despite the fact that this method is critical in metal production, the etching process is still limited and poorly understood, particularly at the atomic level [31].

Among the manufacturing technology sectors, knowledge and understanding of the etching process, as well as etchant solution is essential for making superior quality metal components. Thus, there is a need to check for other etchant solution, which can provide a desirable outcome. Halogen molecules such as HCl, HBr and HI have the potential to etch the surface metal [20]. The comparison of these halogen molecules and ions with regards to their ability to interact with the Ti surface is significant towards discovering the best etchant.

Halogen molecules and ions play an important role in technological application such as metal surface modification, corrosion and etching [32, 33]. It was noticed that the presence of halogen influences the electrochemical behaviour on the metal surface, which is major to etching, corrosion-protection and electro-catalysis reaction [34, 10]. Halogen adsorption on the metal surface particular on titanium surface is of much interest in the field of electrochemistry and surface modification [35].

Thus, understanding their interaction and the adsorption strength, can be able to provide adsorption stability, electron-charge transfer and charge density differences, which is critical for the etching process.

Adsorption of halogen molecules and ions have received more attention recently due to their higher electronegativity, reactivity, and the ability to form a chemical compound with metal surfaces [36, 37]. However, the halogen ion showed to be the most effective etchant solution than halogen molecules [38]. Investigating the effect of halogen ions on the metal surface is important, and critical for understanding the corrosion and etching process of the metal surface. Thus, from the technological point of view, halogen adsorption on a metal surface is essential in order to understand the fundamental mechanism involved in the etching process. It has also been indicated previously that the key role manner of etching is through ion-metal interaction on the metal surface [39]. Computational technique provides an understanding of chemical bonding and hybridisation of surface interaction with adsorbate molecules and atoms [26].

1.3. Intention of the study

In this study, DFT is used to investigate the adsorption behaviour of halogen molecules (hydrogen fluoride, hydrogen bromide, hydrogen chloride and hydrogen iodide) on titanium surfaces. The goal of this research is to evaluate the adsorption mechanisms and adsorption-desorption energies of various halogen compounds on Ti (100) and Ti (110) surfaces in order to determine their capacity to etch titanium surfaces. The impact of halogen molecules and ions adsorption will be compared and assessed using their adsorption energy values. This will give the chemical interaction between halogen ions and titanium surfaces.

In addition, adsorption coverage on Ti surfaces will be investigated for the most stable halogen ions. Desorption energy and heats of formation will be calculated to examine the energy barrier for an etch product to desorb and form or removed from the surface. Furthermore, charge density difference, Mulliken charge analysis, density of states will be analysed, as a step towards understanding the corrosive nature of ion-metal interaction [10]. The results will give a better understanding of the etching agent and the formation of etchant products, to be able to proceed toward the preferred etching mechanism.

1.4. Research hypothesis

The interaction of titanium metal surface with halogens and ions can enhance the etching. There is significant correspondence between dissociation adsorption mechanisms and the surface etching process. The following questions will be addressed to verify and compare the adsorption of halogen molecules and ions on Ti surfaces.

i. How can the halogen molecules and ions interaction enhance the Ti surfaces?
ii. What is the effect of halogen molecule and ion adsorption on Ti surfaces?
iii. How does the adsorption strength of halogen molecules and ions is affected for different Ti surfaces?
iv. What is the interaction behaviour of different halogen ion at various Ti surface positions?
v. How does halogen adsorption impact/affect the electronic behaviour in terms of charge-electron transfer during adsorbate-adsorbent interactions?
vi. What is the effect of adsorption coverage and etching products?

1.5. Objectives

The main goal of this project is to investigate the interaction of HF, HBr, HCl and HI molecules on titanium surfaces. The objectives of this study are to:

i. investigate the stability of Ti surfaces by calculating the surface energy
ii. investigate the dissolution mechanism of halogen molecules on titanium surfaces by optimisation of both the molecules and titanium surfaces.
iii. investigate the interaction between titanium metal surface with HF, HCl, HBr and HI molecules, to check the most reactive halogen by calculating adsorption energy.
iv. investigate the electronic density of states and charge density distribution of HF, HCl, HBr and HI on titanium surfaces, to check electronic properties and orbital interaction.
v. investigate the effect of halogen ion on titanium surface by calculating the surface work function after adsorption
vi. determines the stability of etch products by calculating the heats of formation
vii. investigate the desorption energy on Ti surface at different coverages, to assess the most preferential desorb etch product.
viii. investigate the Mulliken charge analysis on adsorbed titanium surfaces

1.6. Outline

The outline of this thesis is as follows:

Chapter 1 address a brief background on titanium and its alloyed metal applications, the formation of alpha-case layer and surface etching techniques. The Chapter also gives the main applications of halogen adsorption on the surface, motivation, research hypothesis, research questions, objectives and intentions of the study.

In chapter 2, both experimental and theoretical review on metal surface etching are discussed. This chapter also reflected on the previous work related to etching and metal-molecule adsorption. The main part consists of chemical, halogen adsorption and atomistic metal surface etching.

Chapter 3 present the computational methods and the theoretical techniques that will be used in performing the simulation calculations. In this Chapter, the DFT and plane-wave pseudopotential method, the computer codes and material model properties are described.

Chapter 4 discuss the Ti (100) and Ti (110) surfaces, and halogen molecules. The Chapter discusses the DFT calculation results of Ti (100) and Ti (110) surface properties, and electronic properties of halogen molecules generated in this study.

Chapter 5 present the adsorption mechanism of halogen molecules and ions on Ti (100) and Ti (110) surfaces. The Chapter investigates the interaction of halogen ions with Ti surfaces at different adsorption sites. Adsorption energy strength, bond lengths, work function, charge density redistribution and density of states properties are discussed.

In chapter 6, we discuss the effect of halogen ion adsorption on Ti (100) surface at different atomic coverage. In addition, the formation of titanium halides (etch products) molecules are analysed. We calculated the heats of formation and desorption energy of each etch product molecules formed.

Finally, Chapter 7 present the summary and conclusion on the results obtained in this study, recommendations and future work are also described.

Chapter 2

Literature Review

This Chapter intended to give a scientific background and the work performed previously. It will introduce the theoretical and experimental work on alpha-case layer formation, surface etching, halogen molecule and ions adsorption, and chemical interaction with the metal surfaces. Research on titanium and its alloys continues to be the subject of interest due to the ever-increasing demand for titanium for both architectural and structural purposes. The most research interest in investment casting of titanium is in the surface etching of material components.

Titanium components depend significantly on interstitial impurities, surface modification and the control of removing alpha-case layer [40]. A precise chemical etching technique for a metal surface is essential for manufacturing technology for the fabrication of various metal components. It is well known that etching techniques are frequently used for the fabrication of metal components. Substantial research for chemical etching effort has been devoted previously, however, results remain limited and unclear. Above, all titanium is ubiquitous industrial metal due to high demand in various application.

2.1. Background

Titanium and its alloys materials are of much importance in various specialised application and the great application of Ti-based components are based on their surface properties. Ti-based material can potentially replace other metallic material if they can be produced more competitively [41]. Titanium alloy components are generally fabricated either by investment casting, forging or powder metallurgy [42].

During investment casting, the alpha-case layer is formed on the surfaces of titanium components, this is due to high reactive with oxygen when they are subjected to oxidising environments [43]. The alpha-case layer makes the surface harder and brittle, which results in cracks manifestation and decrease fatigue life [44]. Various causes have been attributed to the formation of the alpha-case layer, this layer is formed due to the reactions between molten metal and investment material [45]. Parthasarathy *et al* [46] found that the alpha-case layer is formed during solidification through oxygen enrichment. The crack initiation and the saturated of periodic was observed on titanium alloy after exposed to ambient air. Work done by Sung *et al* [47] shows that the alpha-case layer is not formed only by interstitial element, but also substitutional metallic element dissolved from mould material. Therefore, the post-fabrication process is required such as surface modification. This post-fabrication remains the main post-process surface and must be taken to avoid unwanted chemical reaction [48].

Surface etching process is the most used technique for metal surface modification and the removal of material from the substrate. Etching of Ti-based material has been problematic because most of the alloyed are designed to withstand oxidation and corrosion [49]. Etching usually removes the surface area, which is not desired on the finished surface. Different etching processes are deployed depending upon the particular materials. The etching process is described in three main steps or terms; adsorption-interaction, production formation (etch products) and product desorption.

Common etching techniques include wet chemical etching [50], reactive ion etching [51] and plasma etching [52]. Chemical etching is employed as a manufacturing surface technique to produce micro-size components and it has long been accepted as one of the non-traditional machining processes. These processes use a strong chemical etchant solution to remove the top surface part in the work piece material [53]. Plasma etching is an extension of the technique of physical sputtering, this technique was introduced to reduce liquid waste disposal in manufacturing and achieve

selectivity's that difficult to obtain with wet chemistry [54]. Reactive ion etching (RIE) combines the plasma and ion beam etching process to achieve both selectivity and directionality. This etching technique has several variable factors that correspond to an output parameter, etch rate, selectivity and surface roughness [55]. The difference in etching mechanism and technique arises from the stability of materials and etchants towards various chemical species. The etching rate and etching selectivity of micro/macro molecules are well connected with the strength of the available bonds in the material [56]. Table 2-1 shows the major difference between wet etching, atomic etching, as well as plasma/dry etching techniques. These etching approaches were found to be the most method for many applications to achieve desired surface structure, morphology or chemistry [57].

Table 2-1. Comparison of wet etching with dry, plasma and reactive ion etching.

	Wet etching	**Plasma/dry etching, RIE**
Etchant	chemicals (acids, alkaline)	reactive gas (ions, radicals)
etchant rate/selectivity	high	good and controllable
Advantage	low equipment, fast process, easy to implement	small etching, no contamination, no hazardous chemical, ecological begin technology.
Disadvantage	high contamination, hazardous chemical, unfriendly technology, high waste process	high equipment cost, potential radiation damage, implementation depend on the application.
Directionality	any isotropic	can be isotropic or anisotropic

Du *et al* [58] investigated aluminium-silicon (Al-Si) alloy etching using both chemical and laser etching. It was demonstrated that the chemical etching and laser finishing removes the surface aluminium layer and exposed the silicon on the surface. Also, the coefficient and weight loss rise as the etching time increases. Furthermore, it was found that when laser power increases, frictional etching and weight loss reduce at first, then rise as chemical etching time increases. In addition, the optimal etching duration was reported to be 2 min for chemical and 1000 W for plasma etching. Wet chemical etching unlike plasma or RIE is usually isotropic and can be highly selective to other materials. The etching technique roughen polycrystalline metals and multiple mixtures or alloy, in which preferentially etching grain boundaries, crystallographic defects and dislocation [59].

Recently, acidic etching treatment is the only adopted approach that can modify both the overall pore structure and its surface of the high reactivity of metal with acidic solution. Zahran *et al* [60] reported that when extending the etching times, both roughness and wetting increased, with the exception of 10 minutes, when roughness rose but moisture dropped. Moreover, the effect of hydrofluoric acid etching rate on titanium topography, chemistry, wettability and cell adhesion was investigated [60]. In addition, it was also reported that HF acid treatment on Ti surface modifies their chemical composition, which becomes stable after 3 min of etching. The wetting and roughness increase with a longer etching time up to 7 min [60]. The etching rate of pure HF is too slow to modify the overall pore structure inside the Ti scaffold. Fluoride formed from the reaction with HF solution further improved capability by attaching fluorine ions to the Ti surface, which confirmed to be a major effect of etching [61]. This proved that due to rapid etching rate of the Ti surface, the porosity, pore size, and pore neck size increased as the treatment time rose. However, explosive hydrogen gases are generated during the reaction. In which it induces the formation of titanium hydride (TiH_x) at the metal surface with consequent embrittlement [61].

Deshmukh *et al* [62] used chemical milling containing a mixture of HF and HNO_3 to remove an alpha-case layer from the titanium surface and after the removal of the alpha-case layer, the titanium surfaces were examined using SEM as well as X-ray diffraction. The results show that the etching time is more effective in completely removing the alpha-case layer by chemical etching. Donachie *et al* [19] confirmed that the material removal rate for chemical etching of titanium in HF is between 0.015 and 0.03 mm/min. As mentioned early that titanium has a high natural attraction to hydrogen, this becomes another concern when using HF acid bath, the hydrogen content can be adsorbed into the surface and create outer layer hydrogen embrittlement. Hence, time-limited that part can spend in the bath.

Previously, Rossouw *et al* [63] used the mixture of 5% HF and 20% of HNO_3 to remove the alpha-case layer however, the results shown are acceptable to no hydrogen retention. The effect of a chemical etching by HCl solution on the surface was investigated, this chemical treatment mostly applicable on a large scale [64]. Oh *et al* [65] investigated the etching characteristic of high-purify Al in HCl solution. The electrochemical etching was carried out in a cell with a carbon cathode at $85\pm 2\ ^0C$. It was demonstrated that HCl solution generated more consistent etching tunnels in this investigation, however due to its strong corrosiveness, the size and distribution of etch pits was not uniform with the low density. Furthermore, Causier *et al* [66] investigated the etching behaviour of the InP surface in HBr/Br_2 aqueous solution. This experiment was performed under controlled temperature and hydrodynamic conditions at constant Br_2 concentration. It was demonstrated that the etching process was found always linear with time, however, its rate depends on the HBr/Br_2 concentration. In addition, dissolution mechanism of InP in HBr/Br_2 solution appears to be ruled by the surface chemical states.

Recently, the stability of titanium surfaces and their alloy in bromide and chloride-containing solution has received considerable attention due to the development of self-organised Ti nanostructures under optimised electrochemical condition [67]. The most common etchant solutions used are summarised in Table 2-2, most widely used contain HF/HNO_2, HCl/H_2O_2, Cl/Ar or HBr/Cl_2. These etchant solutions are in relation to etching condition such as chemical etching, plasma etching and reactive ion etching. In such case of etching, one expects a dependency of the etching yield on the chemical composition of the ions [68].

Table 2-2. Summary of different etchant solutions for different etching processes.

Etchant solution	**material**	**application**	**method**	**Ref:**
HF/NaCl	AISI 302	chemical etching	experimental	[69]
HF/H_2O_2	Ti_3SiC_2	wet etching	experimental	[70]
HCl/Stearic acid	ZnO	chemical etching	experimental	[71]
F^-/H_2O_2	Cu	wet etching	experimental	[72]
Cl_2/Ar	Ti nanostructure	RIE	experimental	[73]
HF/HNO_2	Ti-6Al-4V	chemical etching	experimental	[62]
HBr/Cl_2	Si/SiO	plasma/dry etching	experimental	[74]
HF	AlO_2/Al	thermal etching	theoretical	[75]
CHF_2	Si/SiO	DFT/Plasma	theoretical	[76]
HCl/H_2	SiC	DFT/ chemical	theoretical	[77]
HF	TiO_2/Al_2O_3	DFT	theoretical	[13, 78]
F_2	Si (100)/(111)	DFT	theoretical	[79]

Atomic layer etching (ALE) opened a new degree of control in material processing and lowering the cost by removing the need for etching steps [80]. It becomes increasingly important method for advancing the understanding of metal surface etching. Continues improvement of the ALE method and equipment will undoubtedly progress the field of etching. Atomic layer etching has been introduced as the most suitable method for extreme nano-scale devices because it can etch a material at an atomic scale without physically and chemically damaging the substrate [81]. ALE process is sequential based on halogenation and bombardment of energetic ions that lead to anisotropic etching. Positively charged ions gain directionality by being accelerated normal to the surface via a negative voltage bias on the substrate. To remove layer from the wafer surface, energetic ions act in tandem with neutral chemical species from the plasma [82].

Generally, an atomic layer etching process is thermal chemistry and the reaction taking place involves surface modification by adsorption of reactive ion species that activate the metal surface. Secondly, the atomic layer etching is a reactive ion that produces stable volatile etch products. It was found that the HF reactant converts Al_2O_3 to AlF_3 as a reaction intermediate, allowing SnF(acac) and H_2O to exit as reaction products [83]. Many ALE method techniques are based on fluorination and exchange ligands reaction on the metal surface. However, the chemical details of ligand-exchange lead to selective ALE between various materials [84]. Lee *et al* [85] investigated atomic layer etching of Al_2O_3, HfO_2 and ZrO_2 surfaces using HF and dimethylaluminum chloride (DMAC). The results analysis shows that the exposure of the surface in HF/DMAC led to efficient etching attributed to the formation of stable and volatile chloride or fluoride species. All surfaces were etched linearly with respect to the HF/DMCA coverage. The magnitude of fluoride had the same ordering as etch rates for all surfaces.

Walch *et al* [86] investigated the etching of Si (100) surface by F and Cl using DFT with B3LYP functional. The computations were done with the GAUSSION-94 code, with 6-31G basis set for F and 4-31G basis set for Cl and Si. It was reported that Cl differs from F in that it has lower binding energies and considerably larger non-bonded repulsions. Furthermore, the study discovered a lower pathway to SiF_4 with no barrier to adding F atoms. It was also reported that fluorine etching was accomplished by the production of SiF_x species as etch products in the gas phase, although the mechanism of F etching was unknown [86]. Migani *et al* [87] reported that the formation of this volatile species such as SiF_x and $SiCl_x$ upon halogenation or halogen adsorption on the metal surface plays a crucial role in the purification or etching metal surface [87].

First-principles calculations utilising a plane-wave pseudopotential method within the VASP code was used to investigate the production and desorption process of etchant products [88]. The simulations were run using the Cerperley-Alder exchange-correlation functional and the local density approximation. I was found that the desorption of etchant products occurs when there is more than 1ML coverage adsorption on the metal surface. In addition, $SiCl_3$ formation and desorption were observed to be less favourable than $SiCl_4$. However, this poses some difficulty in building up a surface model for $SiCl_4$ formation and desorption. Furthermore, the findings revealed that desorption of $SiCl_2$ can occur at high temperatures, reducing the likelihood of $SiCl_4$ formation [88]. Winters and Coburn [89], explored metal surface etching using halogens such as fluorine atoms or molecules, the study used ion bombardment for metal surface etching. It was reported that the inherent characteristics of halogen atoms, as well as their propensity are the major causes creating a stable volatile compound [89]. It was found that ion adsorption etched a material surface wherever the surface's interaction state leads to the production of stable volatile compounds. In another study, reactive ion etching was conducted using ions bombardment to promote the production and desorption of etching reactive products [68].

2.2. Structural aspect

Titanium is the 22nd element in the periodic table and the first in a group of metal known as transition metals. The density of titanium is 4.5 g/cm^3 in which is almost half that of copper and less than 60% the density of stainless steels [19]. The tensile and yield strength of titanium are comparable to those of most stainless steels, this results in a high strength-to-weight ratio account for the widespread use of titanium components, in various industry applications [90]. Nearly more than 80% of titanium is used in the aerospace industry and found widespread application in the medical industry as well as chemical processing [91].

Titanium ore exists in one or a mixture of the two different crystalline structure: α-phase which is a hexagonal closed packed (HCP) structure with a space group of P63/mmc and β-phase which is a body-centred cubic (BCC) structure with a space group of Im_3m [92]. The transition temperature between alpha-beta phases is about 882 ^{0}K for pure titanium, which is the most fundamental phase transformation in titanium casting. Figure 2-1 shows the atomic arrangement of two titanium crystal structures: (a) titanium crystal structure arranged in a body cantered cubic (BCC) (b) titanium crystal structured arranged in hexagonal closed packed (HCP) structure and (c) atomic arrangement in face centred cubic.

Generally, different titanium crystal structure plays an important role in determining respective structural properties. For example, in α-phase causes an improvement in creep strength, high-temperature strength, while increasing the β-phase fraction increases room temperature strength [93]. Among all Ti-based material, commercially pure titanium is the most commonly used within the α-phase. However, interstitial site (elements) in HCP crystal structure produces non-symmetric strain field and therefore effectively interact with dislocation [94]. As a result, in strengthening effect because exploited in commercialist pure titanium.

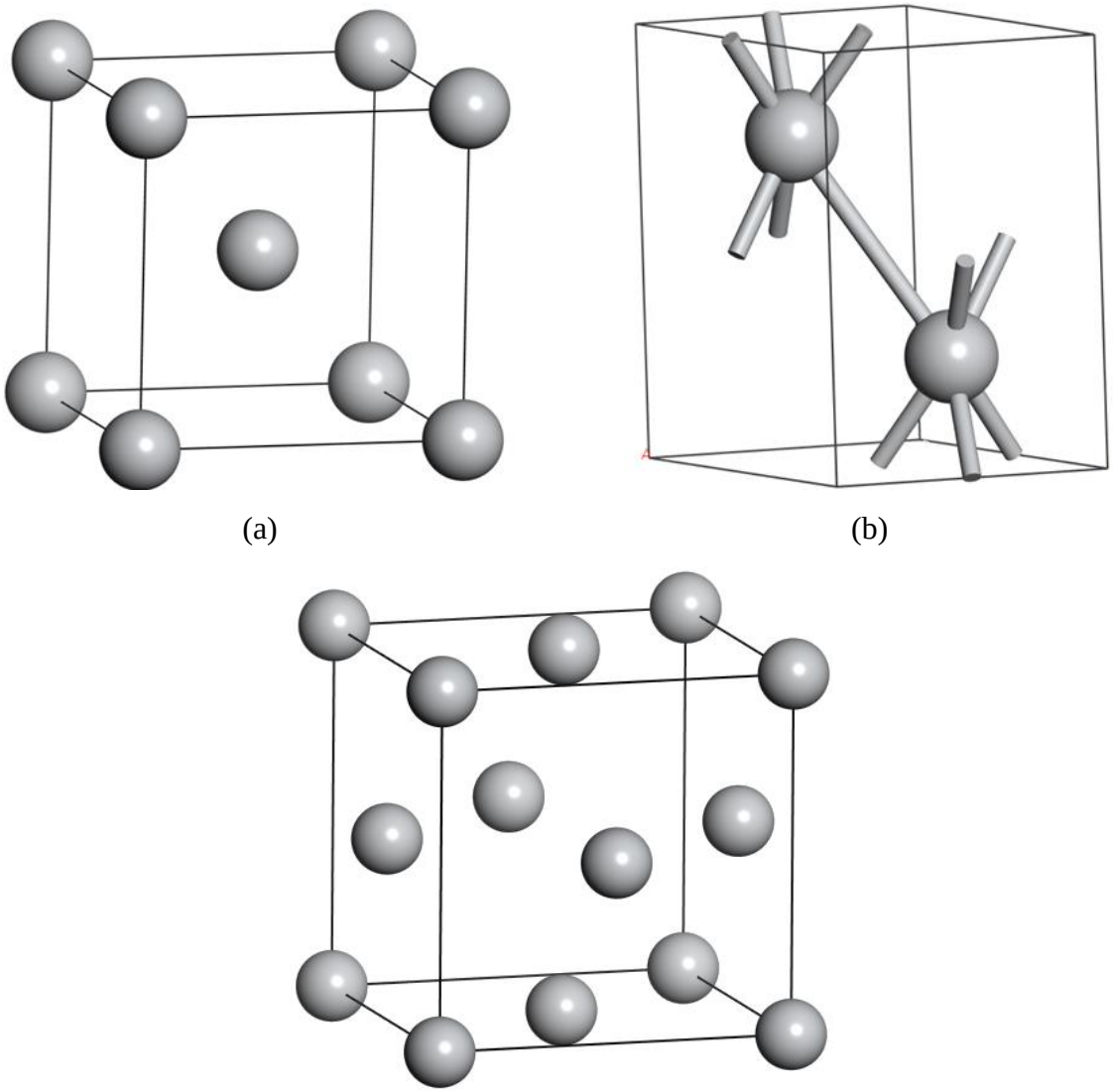

Figure 2-1: Atomic arrangement of titanium crystal structures (a) Body centred cubic (BCC), (b) Hexagonal closed packed (HCP) and (c) Face-centred cubic (FCC).

2.3. Fundamental principle of etching

As explained in the previous section, conventional treatment for removal of alpha-case layer using chemical etching. Generally, metal etching treatment results in dissolution, i.e. etching away material from the surface via corrosion mechanism [95]. To enable a better content of etching processes it is fundamental to understand, at atomic scale, the basic mechanism involved. Most structural surfaces are in fact metallic or metal alloys, it is important to consider how metal surfaces are etched.

2.3.1. Metal etching

Etching of metal in solution/ion is defined as a simultaneous transfer of mass and charge across the metal-solution interface. Etching relies on the action of a corrosive etchant to dissolve away the unwanted surface area, the selective removal of material from the surface through chemical action of an etchant species [96]. The direct charge transfers between the surface and the solvent are via electronic contact [97]. This is a physiochemical process that involves the making, breaking or rearrangement of bonds between atoms. The main reactants that contribute to aqueous corrosion are electrochemical. Following the mass loss from structural components, may be embodied by the general dissolution reaction:

$$M \rightarrow M^{Z+} + ze^{-} \tag{2-7}$$

This reaction is accelerated by the complexation of the surface metal atoms by species in the environment. The atomistic investigations of this process show that the surface structure provides a high degree of control leading to surface faceting. In the case when the metal surface is covered by thin oxide, deleterious etching/corrosion effects arise from the dissolution of metal atoms directly exposed by virtue of cracks or pores [98]. In many applications, the surface materials are treated concurrently during manufacturing processing, each metal surface must be chemically treated with unique functional groups that allow the growth of a distinct material surface [99].

The removal of atoms from the surface by etching is a complex process that involves chemical and electrochemical reaction [9]. These are distinguished by the fact that it involves the participation of free charge carrier. The first neighbourhood of an atom at the surface directly affects the probability with which the etchant can break its back-bond to the rest of the structure and the atom is removed or remain attached. Removal of material from the surface occurs, as results of the chemical reaction between surface atoms and the etchant molecules. Figure 2-2 shows a schematic illustration of metal

surface etching [100]. The reality is that the form of the material changes when it is exposed to etchant, and various materials respond to etchant in different ways. The atomistic model of chemical etching is a non-equilibrium process in which both atomistic (microscopic) morphology and macroscopic orientation-dependent etch rate are determined by the relative values of atomistic reaction rates. Surface termination plays an important role in catalysing the removal of the surface atoms by following a back-bond attack. The active etching species, which produce the back-bond attack during the etching sub-process, is a polar molecule. The weakening of the back-bond depends only on the total number of terminated atoms sharing the bond and is independent of the particular distribution.

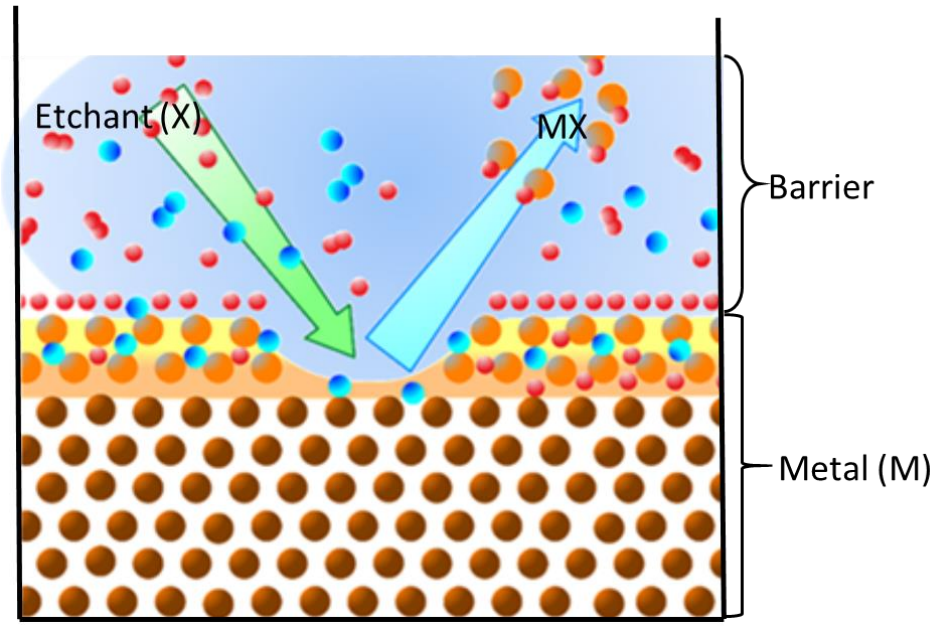

Figure 2-2: Schematic illustration of etching process on the metal surface *[100]*.

2.3.2. Metal dissolution

Metal dissolution involves some mystery, due to the transition of a neutral metal atom bound to its neighbours through metallic bonding across the electrochemical layer, this phenomenon has been in the recent year highlighted [101]. Metallic dissolution is usually controlled by multiple surface reaction mechanism that involves chemical effects. The metal dissolution in an acidic medium has

been studied and its dissolution depends mainly on the concentration of acid and temperature [102]. This reflects the complex structure of an alloy surface at wet solution, atomic and mesoscale level [103].

Previous studies reported that Ti metal dissolution in acidic media indicates the existence of three regimes of dissolution via active, passive and trans-passive [104]. In which one major limitation of the previous studies are that the species attacking the metal surface is not clearly identified. Only the overall reaction kinetics with respect to nominal concentration is reported, with limited information on the detailed mechanism [104]. Taylor *et al* [105] used DFT to investigate and model electrochemical interface to the simulation metal atom deposition and dissolution mechanism. The simulations were carried out with the VASP software, which included the PW91 exchange-correlation functional and an ultrasoft pseudopotential. A model is shown to provide a flexible basis for understanding the effect system perturbation to the surface structure of dissolution potential energy. The change in potential energy of dissolving ion as a function of its progress across the electrochemical layer shown to be highly dependent.

2.4. Surface etching

Surface etching is one of the various surface treatment method that is recently applied and under investigation. Surface treatment introduces the possibility that the change in geometry produced by the treatment may affect the mechanical properties of the material [99]. Even though, the effect changes in surface morphology on mechanical properties of metallic due to surface etching, the treatment has not yet discussed fully [106]. The etching of Si (111) surface in HF solution has been studied, the etching process characterised based on different etching rates for each individual surface species. It was reported that the etching procedure causes full H-termination on the surface, and the stepped Si (111) surface was used to determine the surface morphology as the etching solution pH ranged from 2 to 8. [107]. Ramakrishnaiah *et al* [108] investigated the effect of

hydrofluoric acid etching duration on silica-based ceramic surfaces. It was reported that the surface was etched with 5 percent HF for four different time intervals before being inspected under a scanning electron microscope to analyse the patterns. It was also seen that the microstructure of silica-based ceramics was dramatically altered by increasing the etching time with hydrofluoric acid, as well as the surface roughness and wettability. The results reveal a significant change in the crystal structure and surface roughness. However, it was discovered that etching over a longer period of time led in an increase in the number and breadth of pores, with the number of pores increasing at a quicker pace than the depth of the pores.

Moreover, Juodzbalys *et al* [109] used different acids such as HCl, HCl-H_2SO_4, H_2SO_4/HCl-H_3PO_4 and H_2SO_4-HCl to study Ti surface etching. It was found that the precise etchant selection and processing sequence are critical in preparing the rough Ti surface. In addition, it was also reported that treatment with just hydrochloric acid or sulphuric/hydrochloric acids and phosphoric acids produced fairly comparable outcomes. The best results were obtained using sulphuric and hydrochloric acids in sequence and at different times. However, HCl/H_2SO_4 etching generated sporadic holes. Work by Le Guehennec *et al* [110] proved that numerous holes could be etched by using a mixture of HCl and H_2SO_4 at a temperature higher than 100^oC. Metal surface treatment technology, combined with Ti and its alloy can retain the original corrosion resistance. The previous research on the detailed parameter of the metal etching recipe, concentration, temperature and time limitation has been proposed are different [111].

Gosalvez *et al* [112] investigated the atomistic simulation of wet chemical etching of crystalline silicon surface at different coverage using Cellular Automaton (CA) approach. The gradient corrected BLYP functional was used to conduct ab initio calculations using the Amsterdam density functional code (ADF). It was reported the dependence of the etching process on coverage, including the dependence of the fastest etched plan orientation. Only the fastest etched plane on

coverage is controlled by only a few surface configurations involving indirect second neighbours and the relative value of the corresponding removal probabilities. David and his co-workers [12] used first principle calculations employing plane-wave pseudopotential method within the DACAPO code, to investigate the reactivity of ion etching on the metal oxide surface such as Fe_3O_4 and NiO. It was reported that the RIE technique is influenced by bond making and bond breaking at the etching surface is due to orbital interaction.

Silicon etching yields in F_2, Cl_2 Br_2 and HBr have been investigated as function of ion bombardment energy and angle in high density plasmas [113]. It was observed that etching-speed in HBr plasmas is lower than in Cl plasmas, and that etching yield decreases fast at ion angles greater than 60^o. The probability of a spontaneous chemical reaction in a fluorine-based system was reported to be much higher as compared to the Cl/Br based system [113]. This effect was related to the atomic size (halogen atom size). Thus, the fluorine with a smaller size ensures the entry of this particle into the metal surface layers of the treated material and the formation of volatile molecules [113, 114]. Moreover, the chemical reaction of Cl/Br atoms with Si metal surface is only by a finite number of the bonds and the absolute values of etching rates are slower as compared to the fluorine under similar range conditions [113, 115].

In addition, Lim *et al* [116] studied the etching kinetics and surface conditions for KNb_xO_y thin films in both fluorine and chlorine-based plasma chemistry. Variable processing parameters included feed gas Ar content (0-75% Ar), gas pressure (4-10 mTorr) and input power (400-700 W) at a constant biase power of 100 W. It was observed that the fluorine-based etching chemistry shows higher etching rates than chlorine-based. In correlations between F and Cl based, the etching regime with lower effective reaction probability between KNb_xO_y to Cl atom. This effect was associated with to lower volatility of $NbCl_x$ than the NbF_x molecule.

Previous researchers [117] studied atomic layer etching on Si (100) and Si (111) surfaces by Cl_2 adsorption and desorption. The results observation showed that the etching rate of silicon surfaces depend on the Cl_2 pressure. In addition, the adsorption of these ions at various coverage resulted in the desorption of the formed atomic halide species [118]. Pavlova *et al* [119] used the first principle to demonstrate the adsorption and desorption of Cl on Cu (111) surface. The calculations were carried out using DFT and PBE functional within the VASP program. It was found that Cu (111) surface was etched, and the etched products desorbed in the form of $CuCl_x$ molecules from the step edge.

Previously, molecular dynamics calculations were used to study the etching simulations on titanium metal and oxide by Cl_2 and HCl molecules. The etching ratio between HCl and Cl were found in good comparison with experimental results [38]. Bright *et al* [120] investigated the dissolution kinetics of TiO_2 powder in HF-HCl solutions as a function of time, temperature, and acid content. It was found that the rate of dissolution is linear with time and proportional to HF but independent of HCl. Work by Fracassi and his co-workers [121], found that fluorine atoms act by making titanium atoms more reactive towards chlorine gases in fluorinated and chlorinated gases mixture. Previous reports have exclusively concluded that surface fluorination under acidic condition is responsible for lowering the surface energy [122]. In general, it is useful to investigate if and how the action of ions changes the metal surface.

Ma *et al* [123] investigated how fluorine adsorption affected the relative stability of (100) and (110) surfaces of TiO_2 using DFT approach employing GGA-PBE functional as implemented on VASP code. It was revealed that F adsorption significantly weakens the Ti-O bond in (110) but strengthen the Ti-O bond in TiO_2 (100) surface. DFT has been demonstrated to be a high-quality approach to investigate surface adsorption of molecules or ions on metals and as well as at the metal/solution interface [33, 124]. Most previous theoretical studies explored the interaction of halide atoms with

metal oxide, very few studies have focused on bare metal (Ag, Ni) [125, 126]. Grassman *et al* [127] used experimental and DFT to investigate the Cl_2 etching reaction on Al (111) surface. The experiments were carried out under ultra-high vacuum (UHV) with a base chamber pressure of 2 x 10^{10} Torr, while DFT calculations were performed using VASP code utilising GGA-PW91 functional model. It was found that at 100 K, the etch product was determined to have a most-probable velocity of 517±22 m/s. In addition, it was also reported that the adsorption of Cl_2 formed aluminium chloride and the present of activator $AlCl_3$ chemisorption having potential energy above vacuum level. The calculations yield results that are consistent with experimental findings and mechanistic description.

Kim *et al* [128] used a quantum mechanics training set implemented on the Amsterdam density functional program to simulate etching of SiO_2 surfaces with an HF etchant. The molecular dynamics simulations were performed using optimised ReaxFF. It was found that when HF molecules adsorbed and collided with SiO_2 surface, the H-F molecule dissolved, and a new Si-F bond was formed. It was discovered that a single layer of SiO_2 substrate was removed and SiF_x (x=4, 5 and 6) and H_2O molecules were produced with different incident energies with respect to time. Furthermore, among the SiF_x that contributed to the etching process, SiF_4 species was revealed to be the major volatile molecules. SiF_5^- and SiF_6^- were also produced from unreacted active HF reacting with SiF_4 [128].

Fluorine-based etchants are commonly employed in processing etching because F ions and molecules are the most reactive of all the halogens, producing volatile compounds like SiF_4 when they react with metal surfaces [129]. Hamaguchi *et al* [130] performed classical molecular dynamics simulations for Si and SiO_2 etching using F and Cl. Authors employed the SW potentials to represent the Si and halogen interaction while for SiO_2 and halogen interaction potentials were constructed from SW potentials. It was reported that for the same impact energy, the fluorinated layer was found

to be considerably bigger than the chlorinated layer. Furthermore, during F etching, the etch products include more halogen atoms per Si than for Cl etching.

Some metal surfaces, such as V, Nb, Ta, Mo, Ti, and other metal alloyed surfaces, were spontaneously etched using fluorination reactants stronger than HF, such as XeF_2 and F_2 [131]. However, after etching the top layer, it was found that the underlying metal layer was also damaged. After fluorination all these metal yields volatile metal fluorides VF_5 (-68 kJ/mol), TaF_5 (-79 kJ/mol), NbF_5 (-74 kJ/mol), MoF_6 (-53 kJ/mol), TiF_4 (-62 kJ/mol) [131]. The reaction formation for these metal fluorides was reported to be favourable at 250 ^{0}C and all are volatile. On the other hand, other metal surfaces are difficult to etch utilising the fluorination and oxidation reactions due to their unfavourable and unstable surfaces. Because PtO_3 is not a stable oxide, it may be difficult to etch platinum metal or oxide surfaces using fluorination. Although the production of PtO_2 on the Pt surface is conceivable, PtF_4 is not a volatile substance [132].

2.5. Titanium surface etching

The etching phenomena of Ti surfaces in halides media is important not only in corrosion but also in several technologies and industrial applications such as pickling of Ti, manufacture of Ti-based automobile parts [133], and formation of self-organised TiO_2 nanotubes [134]. The composition nature, thickness and hence the resistance of the protective titanium to etching depends on the environmental conditions. In the presence of halides, the titanium oxide is not immune anymore and localised corrosion commences relatively easily resulting in passivity breakdown and high dissolution [135]. Etching behaviour of titanium oxide surfaces and its alloys in etchant containing different corrosive species or ions such as HF–HNO_3 have been reported [136]. The etching mechanism showed two stages are involved: F- destruction of the titanium oxide layer and pure titanium substrate dissolving. It was reported that the titanium substrate dissolved quickly in HF

solutions containing less than 0.1 Mol. L-1. Furthermore, fluoride enhances both etching and HER rates, according to the findings. It was also reported that increasing HF concentrations, the quantity of dissolved titanium from S-Ti increased. Shankar *et al* [137] studied the etching resistance of thermally oxidised Ti in boiling HNO_3 solution. The polarisation curve of Ti etching was reported with respect to pH related solution [137].

Wang *et al* [138] investigated Ti metal surface corrosion in fluoride solution based with critical concentration values between 0.0005 M-0.002 M. It was observed that the fluorine ion accelerates the corrosion of titanium and destroying the protectiveness of the film. It was demonstrated that, at greater concentrations, the fluoride ion may interact not only with the outer layer but also with the interior layer. Work by Ban *et al* [139] investigated the surface etching of commercially pure titanium (cp Ti) surface in concentrated H_2SO_4. This study shows that etching cp Ti with concentrated H_2SO_4 is an efficient way to modify the cp Ti surface for biological application. The activation energy for cp Ti to dissolve in H_2SO_4 was observed to be 67.8 kJ/mol.

The effect of HF on Ti metal surface was investigated using potentiodynamic polarisation. Results analyses reveal that HF and HF_2 remain the species that influence chemical and electrochemical dissolution steps. The electrochemical dissolution increases as the HF concentration rises at a fixed voltage [140]. Other important mechanistic details include the transfer of metal ions, the interfacial chemistry occurring between the Ti surface and the solution. Liu and his co-workers [141] studied the chemical etching behaviour of titanium in a bromine-methanol electrolyte. The etching procedure was carried out for 10, 30, 120, and 300 seconds in a 1 to 9 by volume combination of liquid bromine and methanol electrolyte. The study provided evidence that pitting corrosion is induced on the bare titanium due to the attack of bromine. Furthermore, as the etching duration rises, the roughness of the titanium substrate increases due to the increased pitting corrosion.

Titanium implants surface were chemically etched using HF and HCl/H_2SO_4 solutions. The initial exposure was to hydrofluoric acid, followed by a mix of hydrochloric acid and sulfuric acid. As a results, implant surfaces that have been chemically acid etched have better osseointegration strengths than those that have been machined. The difference in HF volume percent and removal torque have a weaker relationship [142]. Towards an attempt to explore the use of a new electrolyte that can etch titanium other than fluorides. Jiang *et al* [143] recently explored the metastable pitting of Ti surface using potentiodynamic and potentiostatic polarisation in Cl^- containing solutions. This modified mechanism is well compared with the one described for pit initiation on the passive films of other metals.

Despite the frequent use of HF, many questions remain unresolved, including the optimal etching time and its effect on the surface remain unclear [60]. Kim *et al* [144] used acid-etched with 10% HCl acidic and laser etched to treat titanium ASTM grade-2 surface. Therefore, laser etching of titanium surface was effective in improving bond strength as compared to the acid etching method. Previous work proved that a uniform surface could be fabricated after etching in H_2SO_4 for 72 h and through HCl etching for 30 h [109]. Work by Zhang *et al* [145] modified the surface morphology of TiO_2 nanorods using aqueous H_2O_2-NH_3 and H_2SO_4 solutions. The etching rate with H_2O_2-NH_3 was fast and the morphology was modified from the top faces.

Recently, the insight into etching of metal surface by halogen ions/atoms have become from studies that probe surface structure with atomistic scale precision [146]. Researchers have applied molecular modelling to understand the mechanism, pathways and their associated parameters, however, a complete analysis remains a significant challenge. Work done by Wang *et al* [13] found that a selective etching phenomenon occurred on the anatase TiO_2 (100) surface by HF using DFT approach with Quantum Expresso software. The results revealed that HF stabilises the grown facets at low concentration but selectively destroy the grown (100) facets at high temperature.

It has been reported that aqueous solution containing bromine act as effective etchants for etching crystal faces. The $TiBr_4$ compounds were observed during the chemical etching of titanium with bromine-methanol electrolyte [141]. In addition, it was found that etching in the bromine-methanol electrolyte causes pitting corrosion to occur on exposed titanium. Due to the breakdown of the metal substrate, the depth of pits rises as the etching duration increases [141]. Work done by Sazuo *et al* [147] shows that titanium exhibits a much higher susceptibility to localised corrosion in bromide compared with chloride. It was also suggested that pit initiation of unalloyed titanium in bromide solution is related to the adsorption of Br- on bare titanium or the formation of bromide nuclei.

Surface etching technique can be typically accomplished based on halogen ion adsorption on the metal surface [10], because the key role manner of etching is through ion-metal interaction. This was complemented by studies that have explored halogen adsorption, surface chemistry and the nature of the species from the metal surface [39]. The removal of material from titanium metal surface by etching is key in various industries. Even though chemical etching has been practiced for centuries, atomistic detailed mechanisms are not yet being disclosed. Various etching processing has been explored; it was found that aqueous halides solution and dry gas could be used to etch the metal surface. Therefore, if the halogen adsorption mechanism is well understood it could help in the development of new electrolyte metal surface etching [148].

Lemaire *et al* [149] investigated thermal and chemical selective TiO_2 vapor etching with WF_6, as well as self-limited atomic layer etching with WF_6 and BCl_3 using HSC Chemistry 7.1 software. It was reported that the WF_6 easily etched TiO_2 which was attributed to TiO_2's capacity to more easily extract volatile compounds at low process temperatures. Furthermore, WF_6 interacts with TiO_2 at ambient temperature to create solid WO_3 and TiF_4, solid TiF_4 was entirely volatilised at 125 ^{0}C, and WF_6 began to etch solid WO_3 to form volatile WF_2O_2 at 150 ^{0}C [149].

Kim and Duin [38] used the ReaxFF reactive force field to simulate the etching of titanium metal and titanium dioxide by chlorine and hydrogen chloride [38]. Quantum data was obtained using DFT calculations within Jaguar 7.0 program with the B3LYP hydride functional and a LACV3P basis set for the Ti and Cl atoms. It was founded that Cl_2 is more effective than HCl in terms of etching point of view and the etching mechanism is significantly different between Ti metal and TiO_2. Furthermore, because $TiCl_4$ must be produced, a large number of Cl_2 molecules are necessary to etch the Ti metal. $TiCl_4$ species have been identified as the most volatile Ti_xCl_y species, contributing the most to etching [38].

2.6. Halogen adsorption

Halogen adsorption has emerged as a prominent interaction in many applications including catalysis, corrosion, supra molecular and etching [121]. There is a growing interest in studying the interaction of halogens with metal not only because they are among the best-known oxidising agent but they play an important role in atmospheric chemistry.

2.6.1. Molecules and ions adsorption

The adsorption phenomenon of halogen molecules or ions has captured the attention of researchers for several reasons including relatively small volume, surface modification and strong adsorption ability [150, 151]. Despite the importance of halogen molecule, atomistic-level quantification remains unclear. Adsorption of halogen molecules and ions on metallic surface presents an important question in a different field, which has particular importance in electrochemistry [33, 32]. Many properties of molecules/ions and metal surface are dictated by the chemical interaction of the material and interfaces with its ambient condition. Therefore, the understanding of halogen bonding with Ti surface is of uttermost importance. Hence, in this present study, the main focus is on the interaction of halogen ions with Ti atoms.

Halogen ions (F^-, Cl^-, Br^- and I^-) are known as strong corrosive species and chemically very reactive to metals [152]. The media containing this kind of ions are commonly used in various industry for material surface processing. It has been reported that these media would etch/corrode component made of metals [153]. Currently, literature information available for the interaction of halogen molecules with metal surfaces is limited [154]. The halogen atoms on a metal surface are considered a model for understanding more complicated systems under acid condition. It has been observed that adsorption ions affect the number of electrochemical reactions, including adsorption ordering from the electrolyte, the kinetics of the electrochemical reaction, metal deposition, etching and corrosion [32].

Halogens form a particular group in the periodic table, therefore, due to their extremely high electronegativity can form chemical compounds with all metals and most non-metals [36]. In this interconnection, one can expect significant changes in the atomic arrangement and electronic structure of the surface when covered with halogen molecules. The first strive to understand halogen interaction with metals and its alloys were related to the importance of the etching process in the industry [155]. Surface chemistry of halogens on metals is relevant to corrosion, analysis and electrochemistry. In particular, the adsorption mechanism for halogen molecules with sufficiently high electron affinities is the possibility of electron transfer of the incident molecules at a long range. Halogen molecules and its ions are widely used to modify the properties of transition metal catalyst, which the most striking example is the hydrofluoric molecule one of the most important industrial chemical reactions [155].

Adsorption of halogen on a metal surface is much important from the scientific point of view and because of potential technological application [156]. Halogen molecule/ions on the metal surface are typical electrochemical systems since they constitute one of the models for specific adsorption [36]. Knowledge about halogen adsorption on crystal surfaces accumulated, it became clear that

this system is of interest from a fundamental point of view. In addition, the halogen adsorption on the metal surface is also very attractive for studying phase transition in two-dimensional systems. In which phase transitions in halogen could be governed by the electronic properties of the surface [157]. However, since halide ions have different chemical compound, the chemical state of the halogen molecules within the halide is strongly different [158]. Understanding the role of these extensive elements in affecting the corrosion of structural and functional materials across every industry. The first attempts to understand halogen interaction with metal surface and semiconductors were related to the importance of this process industry, firstly in heterogeneous catalysis and microelectronics [155].

Secondly on an industrial chemical reaction in which ionic species play a central role [159]. In particular, interesting molecules with sufficiently high electron affinities is the possibility of electron transfer from the surface. Halide ions adsorption on metal oxide surface has been investigated in detail but scares research for the bare metal surface. The presence of specifically adsorbed anions influences the electrochemical behaviours of a metal or alloy surface that is of major relevance for electro-catalysis reaction [124], etching [10, 95] and corrosion protection [160, 34]. Their adsorption on transition metal surfaces has been investigated but very scarce research for titanium and alloy surfaces [161]. It was observed that the adsorption energy value depends on the halogen and the metal surface plane. Moreover, the metal-halogen adsorbate energies (Cl, Br and I) shows the same periodic trend were decreasing down the group 11 and 10 metals [161].

Gases containing halogens such as chlorine-based Cl_2, CCl_4 [162] and fluorine-based CHF_3, and CF_2 [163] are proposed the most dominant etchants in etching substrate. These gaseous etchants produce active radicals that can react with the compound or substrate to form volatile by-products. Moreover, the fluorine-based etchant is favourable than chlorine-based due to their good etching selectivity and environmentally friendly features [162, 163]. Cheng *et al* [164] investigated

dissociation chemisorption of CH_3F for atomic layer etching of silicon nitride (0001) surface using DFT calculations through VASP code with GGA-PBE functional. It was revealed that the CH_3F molecule dissociates via an exothermic process with an adsorption energy of -0.74 eV. Furthermore, it was reported that the most plausible process began with molecular adsorption with -0.20 eV exothermicity.

A computational study used DFT with PAW method based on VASP code was carried out to look at the mechanism of halogen-based (Br and I) covalent on metal (Au, Cu, and Ag) (111) surfaces [165]. It was found that the metal surface reduces the barrier to halogen split, with the largest barrier for Au and the least for Cu (111). Furthermore, it was reported that the dissociated iodine barrier is lower than that of bromine. Dehalogenation also causes a substantial downshift of the halogen's core-level in the range of 1-2 eV, depending on the halogen and underlying surface [165].

Adsorption of F on Cu, Au, Pd, and Pt (111) surfaces was studied using DFT with PBE functional as impended on Quantum ESPRESSO [166]. It was found that the greatest adsorption energy amounting to -4.49 eV was calculated in the case of the Cu (111), Pd (111) (-3.84 eV), Pt (111) (-3.62 eV) and Au (111) (-3.29 eV). Furthermore, the authors observed that the Cu (111) and Au (111) surfaces interact with the F atom solely via the sp-band, whereas the Pt and Pd base surfaces interact via the d-band. This also verified that the nature of the highly electronegative F atom's surface interaction with a metallic surface is greatly dependent on the nature of the metal surface [166]. DFT calculation with GGA-PW91 functional was performed using VASP code, for chemisorption of atomic chlorine on (001) metal surfaces of Cu, Ag, Rh, Pd, and Pt [87]. It was discovered that depending on the surface metal, the surface work function generated by the presence of the adsorbed halide is either positive or negative [87].

2.6.2. Adsorption comparison

The adsorption of anions on the metal is of interest in electrochemistry, adsorption of halides anions specifically forms a chemical bond with the metal surface [32]. The adsorption not only affects the chemical properties [167] but also directly participate in reaction at the surface by simply blocking adsorption and reaction site [33]. Most recent surface science studies of an etching by halogens have focused on issues relating to semiconductor dry processing technologies rather than the etching of metals. Their adsorption on metal single-crystal surfaces has been investigating but very scarce researcher on metallic surfaces.

Adsorption of chlorine and fluorine on the Mg (0001) surface was studied using DFT as impended in CASTEP code with ultra-soft pseudopotential and PBE functional [168]. It was found that F atom attach to Mg stronger than Cl. The author has established periodic trends in metal-halogen vibrational frequencies with metal electrode-halogen bonding. Zhu *et al* [169] reported the study of halogens adsorption on intermetallic (Al_2Au and Al_2Pt) surfaces using VASP package with a PBE functional. Based on the analysis of the results, the adsorption energy of fluorine was found to be stronger than all the halogen atoms (Cl, Br and I) on both surfaces. The adsorption energies (E_{ads}) and Bader net charges (Q_{Bader}) strength were found to follow the order of periodic rule: $E_{ads}^{F} > E_{ads}^{Cl} > E_{ads}^{Br} > E_{ads}^{I}$ and $Q_{ads}^{F} > Q_{ads}^{Cl} > Q_{ads}^{Br} > Q_{ads}^{I}$.

Previously, Tada *et al* [170] used DFT with PBE and PBE + U exchange functional to investigate the effect of halogens interaction with TiO_2 (110) surface. Halogen atoms were reported to occupy the oxygen sites and decrease the stability of a metal atom on the surface due to electron transfer. Moreover, the adsorption energy strength was observed to vary in the order F>Cl>Br>I which is a similar order of electronegativity strength. Pasti *et al* [171] used Quantum ESPRESSO package to investigate the adsorption of halogens (Cl, Br and I) on crystallographic (111) planes of palladium,

platinum, copper and gold using DFT-PBE functional. The adsorption energies were reported to be decreasing with increasing in halogen atom size. In addition, the 3-fold sites were found to be the strongest adsorption site for halogen atoms for surfaces.

Using the DFT method, the influence of various halogen (Cl, Br, and I) and O atoms on the Ag (111) surface was studied [172]. The calculations were performed using Amsterdam density functional package and GGA with local parameterization augmented. The adsorption strength on Ag (111) surface was found to be in the order O>Cl>Br>I. Despite the fact that iodine's interaction with Ag is weaker, it had the biggest influence on the structure, which was attributed to its enormous size in comparison to other adsorbates atoms. Using Ab initio pseudopotential DFT and a molecular dynamics software package with the GGA correlational function, the interaction of halogen atoms on Ag (110) surface was studied [173]. It was showed that the adsorption energy increase in the order I<Br<Cl<F. The highest adsorption energy of F was linked to the atom's greater electronegativity. Furthermore, halogen adsorption was shown to affect structural and electronic characteristics, as seen by the electronic transferred to halogen atoms.

DFT was used to examine the specific adsorption of aqueous F^-, Cl^-, Br^- and I^- on Cu (100), Cu (111) and Cu (211) using VASP code with GGA-PBE functional [174]. It was reported that the adsorption potential increasingly favourable in the order of F<Cl<Br<I. This follow a periodic trend and more favourable for I than F atom which is inconsistence with the report by Wang *et al* on [173] Ag adsorption. Moreover, halides adsorption is most stable on Cu (100) and least stable on Cu (111) surfaces. Theoretical investigation of halogen atoms adsorption and co-adsorption on metal surfaces such as Al and Si have shown a variety of phenomena that halogen atoms form ionic bonds with the metal atoms surface [175]. The halogen atoms are absorbed/adsorbed on the surface with no energy barrier [176]. The atomistic first principle calculation for the halogen/titanium system has

not yet performed so far. Recently, reactive (halogen) ions are used as etchants with the advantage of good selectivity, controllability, repeatability and fine etched structure [177].

Jenichen *et al* [178] investigated GaAs (100) surface etching by halogen molecules adsorption using DFT-Hartree-Fock (HF). It was reported that the halogen molecules cause the desorption of GaX_n (X= F, Cl, Br, I and n = 1-3) and As_2 species. The reaction energies were calculated from the desorption of volatile species where the volatility increase for GaX_n from F to I. It was also found that under low F_2 exposure, AsF and GaF species were formed and desorbing from the GaAs (100) surface.

The adsorption of halogen atoms F, Cl, Br, and molecules F_2, Cl_2, and Br_2 on the CoP surface was investigated using DFT and time-dependent DFT (TD-DFT) simulations [179]. The computations were performed using the B3LYP level of the Gaussian-09 suit software. Adsorption of F, Cl, Br atoms, and F_2 molecule is chemisorption, whereas Cl_2 and Br_2 molecules are physisorption, according to the adsorption energy value. The negative charges that develop on halogen follow the F>Cl>Br trend, which was also the same order as the adsorption energy.

2.6.3. Coverage adsorption

Coverage halogen adsorption or adatoms induce reconstruction of the substrate surface. Through this approach the increase in coverage adsorption decreases the outmost surface layer [180]. Saraireh *et al* [181] studied the coverage (0.5-l ML) adsorption of Cl on Fe (100) surface at different sites (top, bottom and bridge site) using nanosystem's DFT through VASP package and employed PAW-GGA method with PW91 functional. It was reported that for all coverages Cl adsorption at the bridge and hollow sites is more preferred than on top sites with adsorption energies ranging to -4.44 eV, -4.39 eV and -4.06 eV, respectively. At 0.5 ML coverage, the top site was observed to be less preferential than both bridge and hollow sites [181].

Liu *et al* [182] also used DFT with PW91-GGA functional to investigate Al pitting corrosion in an electrolyte containing chloride ions at different coverages (0.25-1 ML). Calculations were carried out using the $Dmol^3$ computer code, which included double numerical basis sets and polarised functions (DNP). It was found that the adsorption of Cl on the top site was shown to be preferable with the adsorption energy of -3.32 eV than hollow (-3.02 eV) and bridge (-3.08 eV) sites. Furthermore, when the ML coverage increased by 2/3, it was seen that the Al surface gradually dissolved, forming substructures such as $AlCl_3$ and Al_2Cl_3. The Cl- ion assisted pitting start by aiding in the dissolution of the reaction at the Al surface.

Theoretical studies are greatly demanded to explore the formation, stabilities and structure of volatile compounds or gas phases and the main factor influencing the etching processing. Major frontiers still exist in the formation mechanism of metal complexes over the metal surface during the etching process [183]. Acker *et al* [184] studied the impact of the chemical form of different sources formation of etch products and found that the volatile etch products are formed by the reaction between the metal surface and halogen molecules [184]. No DFT studies have so far been concerned with the adsorption competition between halogen and bare titanium surfaces. The first step in etching chemical, a precursor is introduced into the reactor and adsorbed at the surface, in this case, is the halides molecule or ions.

Chapter 3

Theoretical Methodology

This chapter focuses on the computational methods used in this study. Theoretical concepts and computational approaches for atomistic simulation have been a major part of solid-state physics, quantum chemistry and material science. Atomistic modelling simulation has witnessed tremendous progress in the development of an approach for performing ab initio calculations. Ab initio method provides a high-quality quantitative prediction for a broad range of systems, including metals. This approach to simulation is extremely ambitious, given that the aim is to use no empirical data but to rely purely on quantum mechanics. The other way to study the atomistic modelling is through classical mechanics, however, this study mainly focused on quantum mechanics. The foundation of this is laid by density functional theory (DFT), which casts the intractable complexity of electron-electron interactions in many electron systems into an effective one electron potential. In the next section, a description of DFT is outlined.

Material Studio software package [185] was used to build the molecules and construct the metal surfaces at lower Miller index. The current study investigated the interaction of halogen compounds with titanium surfaces using a plane wave pseudopotential method and the CASTEP algorithm [186]. The CASTEP code allows you to model surface contact and solid-state characteristics. DMol^3 code [187] was used to model the electronic properties of halogen molecules, due to its ability and uniqueness to represent molecules [187].

3.1. Density functional theory

Density functional theory (DFT) approach is a quantum mechanical theory that is used to predict the material properties of different classes of materials [188]. The field of DFT is based on two mathematical theorems proved by Hohenberg and Kohn [188], as well as the derivation of a set of equations by Kohn and Sham [189]. Based on the famous theorems provide a solid foundation to develop computational strategies to obtain information about the energetic, structure and properties of atoms or molecule at lower computational costs. In order to understand the principle of DFT the theory are discussed in the next sections.

3.1.1. Hohenberg-Kohn theory

DFT was first formulated by Hohenberg and Kohn theorem [188] in 1964, which states that the ground-state energy E can be expressed as $E[\rho]$ where is the electron density. Therefore, the expression of the total energy of the system is a function of its electron density.

$$E = E[\rho]. \tag{3-1}$$

This proves that the total energy of the system in solids, surfaces, molecules and interfaces depends on the electron density. This idea of using the electron density as a fundamental entity of a quantum mechanical theory of matter arises in the early 1920's especially in the work of Thomas [190] and Fermi [191]. Then, in the subsequent decades, it was rather the Hartree-Fock approach [192, 193], which was developed and applied to small molecular systems. However, calculation on realistic solid-state systems was then inaccessible. Therefore, in 1951 Slater [194] used ideas from the electronic gas with the intention of modifying Hartree-Fock theory to a point where electronic structure calculation on solid became achievable. Slater's work has contributed tremendously to the development of electronic structure calculations, which led to so called X_α method [195]. The

electron density in solid-state systems, molecules and atoms, is a scalar function, which is defined at each point r in real space,

$$\rho = \rho(r). \tag{3-2}$$

The electron density and the total energy depend on the type and arrangements of the atomic nuclei. Therefore, one can express as:

$$E = E[\rho(r), \{R_\alpha\}], \tag{3-3}$$

The set $\{R_\alpha\}$ represent the atomic position for all atoms, α is the system under consideration. Equation (3-3) is the key to the atomic-scale understanding of the structural, electronic and dynamic properties of a material. In order words, is possible to evaluate the expression (3-3), for example, predict the equilibrium structure of solid, one can predict the reconstruction of surfaces and the equilibrium geometry of molecules adsorbed on the surfaces.

The derivative of the total energy Eq. (3-3) with respect to the nuclear position of an atom gives the force acting on that atom. This enables the efficient search for stable structures and more importantly, the study of dynamic processes such as diffusion or the reaction of molecules on the surfaces. Most of the considerations are based on the Born-Oppenheimer approximation in which it is assumed that the motions of the electrons are infinitely faster than those of the nuclei. From a practical point of view, this means that the electronic structures are calculated for a fixed atomic arrangement and the atoms are then moved according to classical mechanics. This is a good approximation for heavy atoms like tungsten (W), however, it may cause errors for light atoms such as hydrogen (H) or lithium (Li).

In DFT, the total energy in Eq. (3-1) is decomposed into three terms, Kinetic energy, and Coulomb energy due to electrostatic interaction among all charged particle in the system and the last term is exchange-correlation energy E_{xc} that represents all many-body interactions. Thus,

$$E = T_0 + U + E_{xc}, \tag{3-4}$$

where U is the Coulomb energy, it is purely classical and contains the electrostatic energy originated from the Coulomb attraction between electrons and nuclei U_{en}, the repulsion between all electronic charges U_{ee} and repulsion between nuclei U_{nn}, written as:

$$U = U_{en} + U_{ee} + U_{nn}, \tag{3-5}$$

with

$$U_{en} = -e^2 \sum_\alpha Z_\alpha \int \frac{\rho(r)}{|r-R_\alpha|} dr, \tag{3-6}$$

$$U_{ee} = e^2 \iint \frac{\rho(r)\rho(r')}{|r-r'|} dr dr', \tag{3-7}$$

$$U_{nn} = e^2 \sum_{\alpha\alpha'} \frac{Z_\alpha Z_{\alpha'}}{|R_\alpha - R_{\alpha'}|}, \tag{3-8}$$

where e is the elementary charge of a proton and Z_α represent the atomic number of atoms α. The summations extend over all atoms and the integration of overall space. Once the atomic number and electron density and the positions of all atoms are known, expression (3-6) to (3-8) can be evaluated using the classical electrostatics techniques [196]. The kinetic energy term T_0 is more subtle.

In DFT, “effective” electrons with the same charge, mass and density distribution replace the “real” electrons of a system. However, effective electrons move as an independent particle in an effective potential, whereas the motion of a “real” electron is correlated with those of all other electrons. The T_0 term is the sum of the kinetic energies of all effective electrons moving as independent particles. Often, one does not explicitly make this distinction between real and effective electrons.

If each effective electron is described by a single particle wave function, Ψ_i, then the kinetic energy of all effective electrons in the system is given by this expression Eq. (3-9):

$$T_0 = \sum_i n_i \int \Psi_i^* (r) [\frac{-\hbar^2}{2m}\nabla^2]\Psi_i(r)dr. \quad (3\text{-}9)$$

This expression (3-9) is the sum of the expectation values of one-particle kinetic energy; n_i represent the number of electrons in state i. By construction, the dynamic correlation between the electrons is excluded from T_0. The third term of Eq. (3-4), called exchange-correlation energy,E_{xc}, includes all remaining complicated electronic contributions to the total energy. The most important of these contributions is the exchange term.

3.1.2. Kohn-Sham theory

In 1965 Kohn and Sham theory [189] provided a foundation for accurate prediction of material properties, which states that the total energy is at its minimum value for the ground state density and that the total energy is stationary with respect to first-order variations in the density, i.e.

$$\frac{\partial E[\rho]}{\partial \rho}|_{\rho-\rho_0} = 0. \quad (3\text{-}10)$$

In conjunction with the kinetic energy, we have introduced a one-particle wave function Ψ_i, which generate the electron density, as seen in expression (3-11).

$$\rho(r) = \sum n_i |\Psi_i(r)|^2, \tag{3-11}$$

where n_i denotes the occupation number of the eigenstate i, which is represented by the one-particle wave function Ψ_i. By construction, ρ in Eq. (3-11) is the exact many-electron density. Therefore, one can derive the equations that can be used for practical density functional calculations. The variation condition (3-10) can be used to derive the conditions for one-particle wave functions that lead to the ground state density. To this end, if Eq. (3-11) is substituted in expression (3-10) and varies the total energy with respect to each wave function. The expression leads to the following equation:

$$\left[-\frac{\hbar^2}{2m}\nabla^2 + V_{eff}(r)\right]\Psi_i(r) = \varepsilon_i \Psi_i(r), \tag{3-12}$$

with

$$V_{eff}(r) = V_c(r) + \mu_{xc}[\rho(r)]. \tag{3-13}$$

Equations (3-12) and (3-13) are called the Kohn-Sham equations. The electron density, which corresponds to this wave function, is the ground state (3-12) density, which minimizes the total energy. The solution of the Kohn-Sham equation forms an orthonormal set,

$$\int \Psi_i^*(r)\,\Psi_j(r)dr = \delta_{ij}. \tag{3-14}$$

This additional constraint is achieved by introducing Lagrange multipliers, ε_i in Eq. (3-12). These Lagrange multipliers are effective one-electron eigenvalues. The eigenvalues are used to determine the occupation number n_i and are ordered according to increasing eigenvalues. For non-spin polarized systems each state is occupied by two electrons until all electrons are accommodated, while in spin-polarised systems, each state is occupied by at most one electron. Because of the partitioning of the total energy (3.14), the Hamilton operator in the Kohn-Sham equation (3-12)

contains three terms, one for kinetic energy, the second for the Coulomb potential and the third term for the exchange-correlation potential.

The kinetic energy term is the standard second-order differential operator of a one-particle Schrodinger equation, and its construction does not require specific knowledge of a system. In contrast, the Coulomb potential operator V_c and the exchange-correlation potential operator μ_{xc}, depend on the specific electron distribution in the system under consideration. The Coulomb potential V_c at point r is generated from the electric charges of all nuclei and electrons in the systems. It can be evaluated directly in real space,

$$V_c(r) = -e^2 \sum \frac{Z_\alpha}{|r-R_\alpha|} + e^2 \int \frac{\rho(r')}{|r-r'|} dr'. \quad (3\text{-}15)$$

In condensed systems, it is more convenient to use Poisson's equation (Eq. 3-16) to calculate the electrostatic potential.

$$\nabla^2 V_c(r) = -4\pi e^2 q(r), \quad (3\text{-}16)$$

The $q(r)$ denotes both the electronic charge distribution $\rho(r)$ and the positive point charges of the nuclei at position R_α.The exchange-correlation potential is related to the exchange-correlation energy by:

$$\mu_{xc} = \frac{\partial E_{xc}[\rho]}{\partial \rho}. \quad (3\text{-}17)$$

Equation (3-17) is formally exact in the sense that it does not contain any approximations to the complete many-body interactions. Therefore, from the above argument, the Kohn-Sham total energy functional can be expressed as:

$$E = \frac{1}{2}\sum_{occ} \varepsilon_i + U_{nn} - \frac{e^2}{2} \iint \frac{\rho(r)\rho(r')}{|r-r'|} dr dr' + E_{xc}[\rho(r)] - \int \rho(r)\, \mu_{xc} dr. \quad (3\text{-}18)$$

However, the exchange-correlation energy is not known, and one has to make approximations, which will be discussed in full details in the next section.

3.1.3. Exchange correlation functional

This section provides a historical picture of the evolution of the exchange correlation functionals and their application. Moreover, importantly it will outline some of the key advantages that have led to modern DFT. Various schemes have been developed to obtain approximation forms of the functional, for the exchange-correlation energy.

3.1.3.1. Local density approximation

Local density approximation (LDA) is the description of the exchange-correlation energy of the electronic system that was motivated by Hohenberg-Kohn theorem [188]. Hohenberg-Kohn theorem gives some incentive to describe exchange-correlation energy as a function of electron density. According to LDA exchange-correlation energy, an electronic system is constructed assuming that exchange-correlation energy per electron at a point r in the electron gas and the expression is given by:

$$E_{xc}[\rho] \approx \int \rho(r)\, \varepsilon_{xc}^{0}[\rho(r)]dr, \tag{3-19}$$

Where the exchange-correlation energy is from the known results of many-electron interaction per particle for a uniform electron gas system. The LDA assumes that the exchange-correction energy function is purely local. However, LDA ignores correction to the exchange-correlation energy at a point r due to its inhomogeneity's in the electron density. LDA is the first principle approximation in the sense that quantum mechanical problem can be resolved without adjusting and arbitrary dependent on parameters [197].

3.1.3.2. Generalised gradient approximation

Generalised gradient approximation (GGA) functional [198] evolve in two main orientations first one is parameter-free, where the new parameters are determined from known expansion coefficients and other exact theoretical conditions and the second is empirical with parameters determined from fits to experimental data or accurately calculated atomic and molecular properties. The most commonly used GGA functional in physics is the Perdew, Burke and Ernzerhof (PBE) [198] and Perdew–Wang [199] from 1991 (PW91), and regarded as parameter free [200]. PBE functional is designed to have a smoother effective potential than PW91, which is prone to numerical instabilities. Most GGA functional used in chemistry applications is Becke, Lee, Parr and Yang (BLYP), Becke three-parameter hybrid functional combined with LYP functional (B3LYP) and there are empirical [201]. The BLYP correlation employs the density's Laplacian (second derivative) and thus formally belongs to the third rung of Jacob's ladder, but it is commonly classified as a GGA.

The basic idea in these schemes is the inclusion of a term in the exchange-correlation expressions. This depends on the gradient of the electron density and not only on the density at a particular coordinate r but also take into account the gradient of density at the same co-ordinate [202], there exists an explicit dependence of the integral f on the densities and their gradients [203].

GGA is the function of this form:

$$E_{xc}^{GGA}[\rho_{\uparrow}, \rho_{\downarrow}] = \int f(\rho_{\uparrow}, \rho_{\downarrow}, \nabla\rho_{\uparrow}, \nabla\rho_{\downarrow})\, dr. \tag{3-20}$$

The GGA adds the gradient of the density as an independent variable. The gradient introduces non-locality into the description of exchange and correlation.

The GGA still entails some locality, however, it also takes into the gradient of the density, and the density at the same coordinates is given by:

$$E_{xc}[\rho_{\uparrow}, \rho_{\downarrow}] = \int \varepsilon_{xc}(\rho_{\uparrow}, \rho_{\downarrow}, \nabla\rho_{\uparrow}, \nabla\rho_{\downarrow})\rho(r)d^3r, \quad (3\text{-}21)$$

where ε_{xc} is the exchange-correlation energy, ∇n is the gradient term and $\rho_{\uparrow}$ and $\rho_{\downarrow}$ spin up and spin down densities, respectively. GGA corrects the over binding tendency inherent in the LDA. Other equilibrium properties that are sensitive to the lattice constants are corrected by GGA. GGA produce the correct ground for magnetic transition metals. Although LDA and GGA provided relatively accurate calculation and widely used other approaches are also utilized. Other functionals have been introduced based on the combination of the local approximations from LDA to GGA. The move from LDA to GGA brought about a massive improvement in functional.

The other alternative functional within GGA is meta-GGA and hyper-GGA [204]. Meta-GGA is the third Laplacian derivative of the density and kinetic energy and the degree of freedom added. Moreover, there are also empirical meta-GGAs with parameters determined by fitting. Furthermore, hyper-GGA normally known to belong to the fourth rung of Jacobs ladder. This functional include the contribution of exact exchange with the GGA functional. The hyper-GGA functional is mostly used in the B3LYP functional. However, it worth noting that B3LYP does not meet the uniform density limit and the tree parameters are chosen to empirically optimise the performance of the functional for large molecule properties such as bond length, formation energy etc.

3.1.4. Plane wave and pseudo potential method

The plane wave pseudo potential method has been used in the implementation of DFT, it combines a plane wave basis set with the pseudo potential method, in which the nuclear potential and the inert core electrons are replaced by pseudo potential so that only valence electrons are included explicitly in the calculation [205]. Plane wave pseudo potential method has become a powerful and reliable tool to study the properties of a broad class of material. The main idea of the method is to simplify the DFT problem by considering only valance electrons. These methods provide a very accurate

description approximation, but the computational cost is rather high especially for calculation, which involves transitional metals [206].

3.1.4.1. Plane wave basis

The use of a plane wave basis has several immediate advantages than infinite plane wave basis set, which is used to expand the electronic wave function of the system. Modern electronic structure approach falls into two classes, which depend on the choice of the basis set for the expansion of the valence orbital, charge densities and potentials [207].

The method is described well using Bloch's theorem, which states that the electronic wave function at each k-point can be expanded in terms of a discrete plane wave basis set:

$$\Psi_{ki}(r) = \exp[ik.r]f_i(r). \quad (3\text{-}22)$$

The expression has a wave-like and cell-periodic part. Function $f_i(r)$ defines the periodicity of the solid and can be expanded using a basis set with a discrete set of plane waves, which is written as:

$$\mathrm{f_i(r)} = \sum \mathrm{C_i G^{[iG.r]}}. \quad (3\text{-}23)$$

In which the value of G is the reciprocal lattice vectors in the periodic cell, each electronic wave function can be written as the sum of plane waves.

$$\Psi_{\mathrm{ki}}(\mathrm{r}) = \sum \mathrm{C_{i,k}} + \mathrm{G^{[i(K+G).r]}}, \quad (3\text{-}24)$$

where $C_{i,K+G)}$ are the coefficients for the plane waves that need to depend entirely on the specific kinetic energy,

$$\frac{\hbar^2}{2\mathrm{m}}|K+G|^2. \quad (3\text{-}25)$$

The convergence of this expansion is controlled by the choice of the kinetic energy cut-off. The introduction of an energy cut-off to the discrete plane wave basis set produces a finite basis set. The

truncation of the plane wave at finite cut-off energy will lead to an error in the computed total energy. However, it is possible to reduce the magnitude of the error by increasing the value of the cut-off energy. In practices, cut-off energy should be increased until the calculated energy has converged.

3.1.4.2. Pseudopotential method

In order to avoid having to explicitly handle the tightly bonded and chemically inert core electrons, a pseudopotential method has been developed [208]. They are exploited in both plane-waves and localised basis sets to reduce the computational effort, as the electronic density from core electrons exhibit very strong oscillation that require very high cutoffs or very refined and complete basis sets. Valence electrons are those that are primarily involved in the physics-chemical properties. A weaker pseudopotential replaces the core electrons and the strong attractive Coulomb potential inside the ionic core, describing all of the prominent characteristics of a valence electron traveling through the crystal, including relativistic effects.

The pseudopotential method is constructed ideally so that its scattering properties or phase shifts for the pseudo wave functions are identical to the scattering properties of the ion and the core electrons for the valence wave functions, but in such a way that the pseudo wave functions have no radial nodes in the core region. In the core region, the total phase shift produced by ion and the core electrons will be greater by $\prod$, for each node that the valence functions had in the core region. Figure 3-1 illustrate all-electron potential (Z/r), the valance wave function (v) the corresponding pseudo potential (Vpseudo) and pseudo wave function (Ψpseudo) [209].

If one replaces strong ionic potential with weaker pseudo potential that gives identical valence electron wave functions outside the core region, $r > \mathrm{r_c}$ this gives identical scattering properties. However, pseudo-wavefunction has no nodes for $r > \mathrm{r_c}$ unlike true wave function. Ab initio

pseudo potential is calculated from all-electron DFT calculations on a single atom and can be calculated using relativistic.

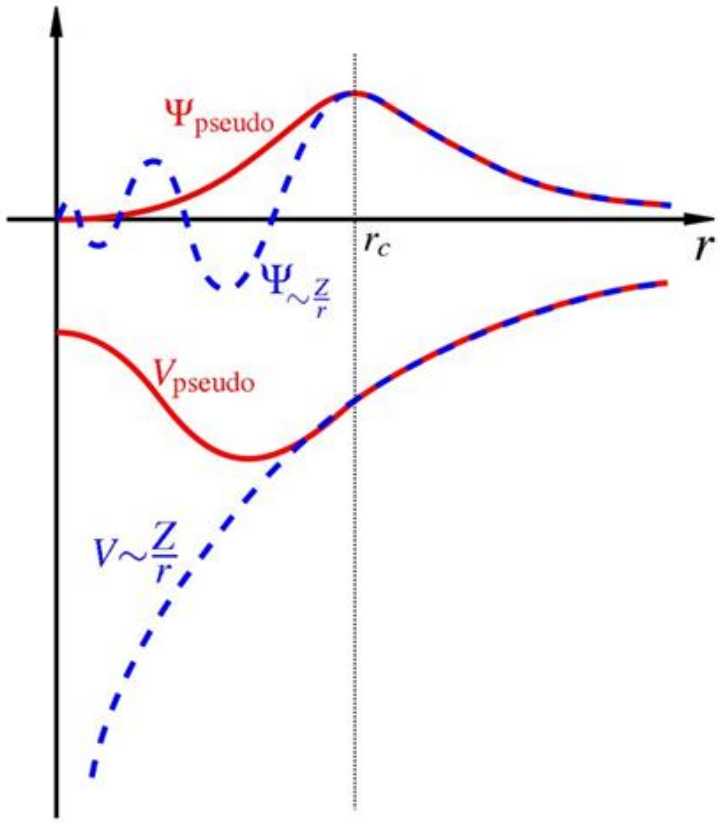

Figure 3-1: Schematic illustration of all-electron potential (solid line) and pseudo electron potential (dashed line) with the corresponding valence wave function (V) and pseudo wave function (pseudo).

Theory of pseudopotential is mature; therefore, the practice of constructing accurate, transferable and efficient pseudopotentials is far from straightforward. The method to generate pseudo potential includes the norm-conserving pseudopotential [210] and ultra-soft pseudopotential [211]. The criteria for the quality of a pseudopotential is well reproducing the results of accurate for all electrons calculations. Drawback of pseudopotential calculations is that because of the non-linearity of the exchange interaction between valance and core electrons, elaborate non-linear core correction [212], are required for all systems where the overlap between valance and core electrons densities is not completely negligible. This deficiency may be removed by using the projector-augmented wave function.

3.1.4.3. Projector augmented wave

Projector augmented wave (PAW) method was firstly introduced by Blochl [213]. This approach accounts for nodal features of the valence orbitals and ensures orthogonality between valence and core wave functions. PAW method represents mainly to achieve simultaneously the computation efficiency of the pseudopotential method as well as the accuracy of the full potential linearized augmented plane wave method [214], which is known as the benchmark of DFT calculation on solids. In the PAW approach method, all electron valence (AE) wave functions φ_n^{Ps} (n is the band index) are reconstructed from pseudo potential (PS) wave function via linear transformation:

$$|\varphi_n^{AE}\rangle = |\varphi_n^{Ps}\rangle + \sum_i |\varphi_n^{Ps}\rangle - \left|\emptyset_i^{AE}\right\rangle\left\langle P_i^{Ps}\middle|\varphi_n^{Ps}\right\rangle, \quad (3\text{-}26)$$

φ_n^{Ps} (AE) (n is the band index) is the variation quantities and are expanded in plane wave and AE-partial wave $\emptyset_i^{AE}$ are solution of the spherical relativistic equation for non-spin polarized atom.

In the regions between the PAW spheres surrounding the atoms, the φ_n^{Ps} are identical to the AE wave functions φ_n^{AE}, but inside the spheres the φ_n^{Ps} are only a bad approximation to the exact wave functions, they are used only as a computational tool. The AE partial wave $\emptyset_i^{AE}$ resolutions of the spherical scalar-relativistic Schrodinger equation for a non-spin-polarized atom at reference energy ε_i in the valence regime and for angular momentum l_i. The projector functions P_i^{Ps} are constrained to be dual to the partial waves and constructed by a two-step procedure: First, immediate functions χ_i are computed via,

$$|\chi_i\rangle = (\chi_i + \tfrac{1}{2}\nabla - v_{eff}^{PS})\left|\phi_i^{PS}\right\rangle, \quad (3\text{-}27)$$

Where v_{eff}^{PS} is the spherical component of the effective pseudopotential, which can be chosen arbitrarily inside the radius r_c but must match v_{eff}^{PS} for $r \geq r_c$. The projector functions are linear combinations of the χ_i [215].

$$|p_i^{PS}\rangle = \sum_j B_{ji}^{-1}|\chi_i\rangle, \tag{3-28}$$

$$B_{ij} = \langle \phi_i^{PS}|\chi_i\rangle, \tag{3-29}$$

such that the ϕ_i^{PS} and P_i^{PS} are dual $\langle p_i^{PS}|\phi_j^{PS}\rangle = \delta_{ij}$, and $\langle r|p_i^{PS}\rangle = 0$ for $r > r_c$.

The PAW method has been described for all-electron (AE) methods, this is corrected in the sense that it correctly describes the model features of the valence orbital which are also correctly orthogonalised to the core wave functions. The exact all-electron wave function and charge density displaying the full nodal character are reconstructed by subtraction of the pseudo-on-site term and the addition of the exact on-site term. However, both are expanded on a radial support grid. An analogous decomposition with no cross-terms between on-site and plane wave terms holds for all expectation values of quantum mechanical operators and particular for the total energy of the electrons i.e.,

$$E = E^{PS} + E^{PS,1} + E^{AE,1}, \tag{3-30}$$

where each of the three terms consists of a kinetic, Hartree and exchange-correlation contribution.

3.2. Energy minimisation

Energy minimisation is a numerical procedure for finding a minimum on the potential energy surface starting from a higher energy initial structure. The energy minimisation generates individual minimum energy configurations of the systems. Information provided by the energy minimisation can be sufficient to predict accurately the properties of the systems. If all minimum configurations

on the surface can be identified, then statistical mechanical formulae can be used to derive a partition function from which thermodynamic properties can be calculated.

However, this is possible only for relatively small molecules or small molecular assemblies in the gas phase. When structures are built in a computational chemistry software package, the initial geometry does not necessarily correspond to one of the stable conformers. Therefore, energy minimisation simulation is usually carried out to determine stable geometry, this process is well known as geometry optimisation. In this study, geometry optimisation was performed with Broyden-Fletcher-Goldfarb-Shanno (BFGS) [216] algorithm as implemented in CASTEP [217] and DMol^3 [187]. Equilibrium atomic position with electronic and ionic optimisation criteria was set up to 10^{-5} eV and 10^{-2} eV, respectively, and the conjugate gradient techniques were adopted. The forces on each atom were converged to 0.003 eV/Å, stress on each atom was converged to 0.05 GPa and the displaced was converged to 0.001 Å.

3.3. Computational code

Computational simulation of material with atomistic details has become a very prominent tool in physics chemistry and material sciences. Simulation findings can be used to understand experimental observations that are used to forecast material characteristics and create new materials in this sector.

3.3.1. Materials studio

Materials Studio Biovia [185] is a complete modelling and simulation environment designed to allow computational researchers in material sciences, physics and chemistry to predict and understand the relationship of the atomic and molecular structure with its properties and behaviour. Materials Studio software package covers many applications including catalysts, composites, metals and alloys. Materials Studio analytical and crystallisation software investigate, predict and

modify crystal structure and crystal growth. It can be used to simulate particle morphology, predict the structure and understand polymorphism, study surface interactions and design growth mediating additives. Materials studio can also be used to calculate various properties such as electronic, structural, thermodynamics and mechanical properties. All DFT calculations in this work were done with the CASTEP version integrated in Materials Studio.

3.4.2. CASTEP code

CASTEP code [217] is a fully featured first-principle quantum mechanical code for performing electronic structure calculations and its capabilities are numerous. Payne and his co-workers originally developed it in the late 1980's and early 1990's [197]. It quickly became a widely used computational code for electronic structure calculations. Within DFT, it can be used to simulate a wide range of material including crystalline solids, surface, molecule, liquids and amorphous materials. Whereby the basic quantity is the total energy, from which many other quantities are derived. Any material properties that can be thought of as an assembly of nuclei and electrons can be simulated with only the limit of finite speed and memory of the computer. This simulation approach is extremely ambitious given that the aim is to use no empirical (experimental) data but to rely purely on quantum mechanics. The derivative of total energy with respect to atomic positions results in force and the derivatives with respect to cell parameters gives stresses. This is then used to perform fully geometry optimisation and possibly finite temperature molecular dynamics on material models.

3.4.3. DMol^3-code

DMol^3 software package [187] is a modelling program that uses DFT to simulate properties of the material, within a numerical radial functional basis set to calculate the electronic properties of molecules, cluster, crystalline materials and surfaces. DMol^3 is part of the Material Studio software

environment. Delley initiated the DMol^3 method [218] in which the computation effort for this method grow to lead order with the cube of the molecule size. It is broadly applicable to research problems in chemistry, material science, chemical engineering as well as solid-state physics.

The localised numerical orbitals are used as bases set to designed and give a maximum accuracy for a given basis set size. DMol^3 method describes the local orbital density functional, which involves from gas phase molecular to an insulating and metallic solid. In principle, this method uses any type of functional, which satisfies the regularity and renormalisability condition for molecule orbitals. DMol^3 require no further analytical properties for its orbital expansion function than the ones guaranteed by the single electron theory of bound states [187].

3.4. Materials model

In the following section, a brief description is given by general concept and physical properties used in theoretical studies of molecule and surface adsorption. The use of both density functional theory and the current computing resources make it is possible to solve a large range of surface science problems. Studying molecules and ions on the surface or chemical reactions in general, both the geometrical configurations and interaction are of much interest.

3.4.1. Surface properties

To describe the nature of a chemical reaction at the surface. Firstly, a reliable model surface needed to be employed and the slab layers thus need to be relaxed. A common model for a surface is a periodic slab or non-periodic cluster modes. Uniform surfaces with will defined sites play a central role in surface science and catalysis. The use of periodic slab allows for the employment of a computational elaborate method. For slab models, it is important to take atom in order to avoid

unwanted interaction between the periodic mirror image. This often results in the need to use large supercell normally when considering adsorption interactions.

This means one should always check that a studied property has converged with the respect to i) surface supercell size ii) number of atomic layers in the slab iii) vacuum distance between slabs. The model slabs of the surface and slab layers thus need to be relaxed. Surface slab properties are closely articulated to the surfaces geometric, surface energy and electronic structure, in which the surface energy of a material varies largely with the surface structure and the composition, dictating e.g. its wettability, adsorbate affinities and conductivity. This is liked with the electronic configuration of the surface that can be described by its band structure and density of state (DOS) its wave function.

It's crucial to think about the particular properties of crystalline solids on the metal surface. In most cases, crystalline formations are tightly packed and made up of repeating units. Cutting the crystal into two halves allows for the creation of surfaces. The surface energy is a measure of the cost of producing a certain surface and is related to its reactivity. DFT methods allow you to accurately adjust the composition's surface characteristics. Surface energy is the amount of energy that surface atoms have owing to a variety of circumstances, such as a broken link length that results in undercoordinated atoms. Surface slab (vacuum slab) approach performing surface energy calculation is required to avoid the interaction. Surface energy expression is defined as:

$$\gamma = \frac{1}{2A}\left(E_{tot.}^{surf} - nE_{tot.}^{bulk}\right), \tag{3-53}$$

where $E_{tot.}^{surf}$ present the total energy of the crystal surface region which normally consists of several atomic layers, $E_{tot.}^{bulk}$ represent the total energy of a bulk, n and A represent the number of atoms and area of the surface, respectively. Surface energy is defined as the surface excess free energy per

unit area of a particulate crystal surface, is one of the basic qualities in surface physics and determines the equilibrium shape of crystals. In order to lower the surface energy or to adapt to adsorption interactions, the surface can be reconstructed forming new structural patterns.

The relevance of atomic coordination on the surface's interaction characteristics cannot be overstated. Surface coverage, surface work function, and adsorbate affinity are some additional significant features and qualities. The energy differential between the adsorbate-surface and the free molecule and surface determines the adsorbate affinity or adsorption (interaction) energy. In Chapter 4, the characteristics and analyses of Ti surfaces and halogen molecules are explored.

3.4.2. Adsorption

Adsorption is the bonding of a soluble particle from a solution to a specific substrate at the surface. The adsorbed-adsorption substrate's strength is a critical feature for determining the adsorbate's involvement on the substrate. The majority of experimental data, however, do not provide direct information on the nature of chemical bonding. Many fields of chemical and material sciences rely on surface adsorption and interfaces [219]. Adsorption is a well established and powerful technique for treating domestic and industrial effluents. Surface interaction process entails many kinds of materials, such as composites, corrosion, etching, metals and alloy and other various semiconductors. This study focuses on the surface interaction characteristics of non-alloyed transition metal surfaces with halogen molecules.

The large focus is directed towards the computing of surface properties and adsorption characteristics. Molecule-surface interaction can be interpreted by analysis of the wave function of the adsorbate and the metal substrate prior to and after adsorption. This interaction normally leads to a large perturbation in the chemisorption process, whereas the physisorption process relates to a smaller rearrangement of the wave functions. The favourable adsorption position and the bond

strength can largely be rationalised by the local orbital-bond overlap as well as by occupation and distribution of electron energy levels of the interaction.

Adsorption process is modelled asymmetrical the atom or molecule is adsorbed only on the top side of the slab. To improve the accuracy of the slab model by keeping layers on one side of the slab fixed. By fully optimising the adsorbed molecule/ion together with the top slab layer, describes both the molecular geometry and the influence of the molecule on the surface structure. Adsorption and interaction energies are defined with opposite signs. The adsorption strength (interaction) or adsorption energy (E_{ads}) is given by the energy difference between adsorbate-adsorbent and the sum of the free molecule (adsorbate) and surface (adsorbent).

$$E_{ads} = E_{surf-mol} - (E_{surf} + E_{mol}), \tag{3-54}$$

where $E_{surf-mol}$ is the total energy of the adsorbed surface, while E_{surf} and E_{mol} represent the total energy of isolated surface and free molecule, respectively. The adsorption strength and adsorption energies are defined with the opposite signs. Moreover, the negative energy means that the reaction/interaction is exergonic (favourable) while a positive means that the reaction/interaction is endergonic (unfavourable). Large negative value of adsorption energy implies more stable and stronger interaction between adsorbate (molecule) and adsorbent (metal surface) [220]. Adsorption energies are then usually compared to experimental data obtained by thermal desorption spectroscopy (TDS). The adsorption interaction of halogen molecules with a titanium surface will further discussed in Chapter 5.

3.4.3. Charge density analysis

In the previous subsection (3.8.1-3.8.2), describe the important physical geometrical properties of the surface and adsorption energy (interaction). However, they do not give any insightful context

of any quantum-mechanical interaction of the adsorbates and substrate's electrons. Importantly, the quality to analyse the chemical interaction is the changing density. Bond formation and anti-bonding levels reflect directly in the electron density n(r), as an accumulation or depletion of electrons. It worthwhile looking at the electron density difference of coupled and uncoupled systems. The redistribution of charge density for complex systems cannot easily be identifiable.

One can easily compute the charge densities of the molecules (adsorbates) and the substrates separately, but at the position of interacting adsorbates-adsorbents systems, the electron-density difference can be computed as:

$$\Delta n = n(\text{interacting system}) - \sum_i n\ (\text{non} - \text{interaction subsystem i}). \quad (3\text{-}55)$$

It is thus possible to localise any interaction in real space and get an idea about induced charge redistribution and hybridisation of the interacting systems. The analysis of the charge density can further be perused along with the ideas of atoms in a molecule. In this thesis, only stick to the basic of charge density analysis.

3.4.4. Density of states

Chemical bonding can be considered as the composition of an atomic Frontier orbital whereby the state in the bands and their dependence on energy described by the density of state (DOS). To analyse the electronic configuration and nature of orbital the density of states is analysed. Density of state presents the interaction of any substrate to adsorbate, for computation this quality is directly accessible in the density of state is defined as:

$$N(E) = \sum_{i=1}^{\infty} \delta(E - \varepsilon_i), \quad (3\text{-}56)$$

where the sum extends over all eigenstates. The total density of states compresses all electrons of the systems. The applicability of the DFT DOS curve has proven to be good enough for qualitative analysis of bond formation and breaking. However, the interest is what happens to the electronic orbitals of the directly involved orbitals of the adsorbates and substrate. This information cannot be directly identified in the total density of states. However, this can be achieved by computing the partial density of states (PDOS) as shown:

$$n_{\propto}(E) = \sum_{i=1}^{\infty} |\langle \emptyset_{\alpha} | \varphi_i \rangle|^2 \, \delta(E - \varepsilon_i), \tag{3-57}$$

where $\emptyset_{\alpha}$ is a properly chosen localised function. The formation of bonding and anti-bonding hybridisation orbitals can be traced down to atomic origin. The density of states turned out to be another successful analysis tool in this study.

3.4.5. Work function

Another crucial variable surface parameter to analyse is the electrostatic potential (Φ) known as work function. The work function is the minimum amount of energy required to remove or extract an electron from a crystal surface in a vacuum. This is the most fundamental parameter of crystal solid surface to understand the wide range of structural, physical phenomena and chemical surface condition [221]. Computed work function is thus another parameter that might be compared to experimental data. Generally, the computed work function of a specific solid surface is defined as the difference between vacuum potential from the surface and Fermi energy level [222]. The electrostatic potential is described as using the expression:

$$\Phi = E_{vac} - E_{F,} \tag{3-58}$$

where E_{vac} and E_F represent the electrostatic potential energy of the vacuum and Fermi energy level, respectively. The electrostatic energy value is mainly determined by the charge rearrangement

of electrons and ions near the surface. In addition, the work function of the metal surface generally depends on the crystalline orientation of the surface, indicating that the work function of different surfaces can differ slightly. Work function changes as small as a few MeV can be measured and identified, for crystal with N number of electrons E_N is the initial energy of the crystal surface.

Figure 3-4 present the schematic plot of the electrostatic potential along with the slab model. The energy barrier of electrostatic potential along the metal surface can be visualised. Then E_{N-1} represent the crystal with one electron removed to a region of electrostatic potential vacuum. Numerical uncertainty on the value of the work function is estimated to be ~0.03 eV. In computational simulation calculation, the work function is done through the supercell approach. The chosen vacuum region has to be large enough so that the electrostatic potential is allowed to relax to its real vacuum level. Work function of an electron in a vacuum is thus determined by both electrostatic potential and long-range image contribution.

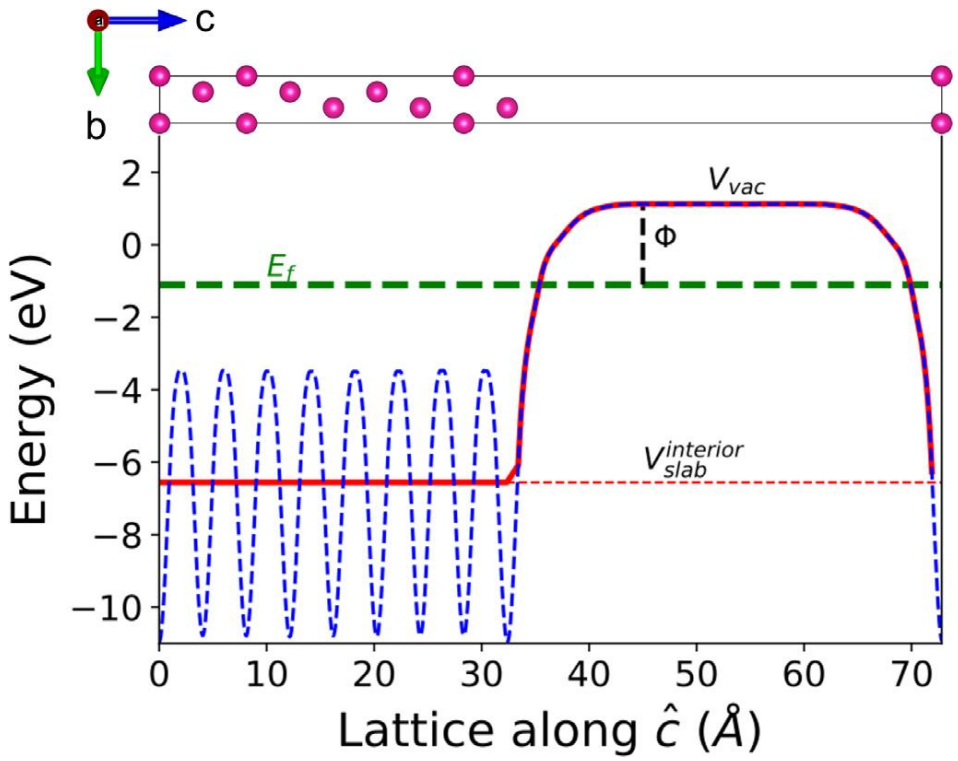

Figure 3-2: Schematic plot of the electrostatic potential along with the slab model. The Fermi energy (E_F), electrostatic potential of the vacuum region (V_{vac}), average electrostatic potential of the slab region ($V_{slab\ interior}$) and work function (Φ) [223].

3.4.6. Heats of formation and desorption energy

The development of a quantitative approach to molecular desorption on the surface is important for a chemical understanding of the fundamental etching process as molecule self-assemble at the top surface. Desorption energies are calculated for all molecules formed in order to understand the etching mechanism for different desorption molecules on the surface. Etching means that atoms/molecules are formed and removed from a surface by breaking the bond that attaches to them, which means overcoming an energetic barrier known as desorption energy and heats of formation. In brief, the negative heats of formation imply the formation of new compounds involving a heat release process, while a positive value indicates the compound cannot exist stably at the equilibrium state because the formation of the compounds needs more energy from the surroundings. Understanding the desorption energy and formation energy opens up to understand surface etching. Therefore, in order to investigate the etching mechanism on the metal surface, the desorption energy

and heats of formation provide the crucial analysis. Heats of formation (E_{HF}) of the molecule reflect the stability of the molecule and is calculated as follows:

$$E_{HF} = E_{surf-mol} - (E_{surf} + nE_{mol}) \quad (3\text{-}59)$$

Here, $E_{surf-mol}$, E_{mol}, and E_{surf}, refers to the energies of the surface with a molecule, free crystal molecule and pure surface structure, respectively and n is the number of atoms. The accurate determination of desorption energy of an isolated molecule from the surface remains a challenging problem both experimentally and computationally. To investigate desorption from the surface for probable desorption products. The desorption energy (E_{des}) of molecules from the metal surface is calculated using expression (3-43):

$$E_{des} = -[E_{a/s} - (E_a + E_s)] \quad (3\text{-}60)$$

where $E_{a/s}$ is the potential energy of the adsorbate-surface, E_a and E_s represent the potential energies of each adsorbate and surface separately.

3.5. Computational details

All the DFT calculations in this study were performed using Materials Studio (MS-2018) Environment [185]. Geometry optimisation for both clean Ti (100) and Ti (110) surfaces, and halogen molecule adsorption was performed using the CASTEP code [217]. Generalised gradient approximation (GGA) of Perdew-Burke-Ernzerhof (PBE) approach functional [198] was applied for exchange-correlation energy calculations. A k-point sampling method was used as proposed by the Monkhorst-Pack approach [224] for energy integration, k-points grids of 4x4x1 and the energy cut-off of 400 eV were used, which was found to be sufficient to converge the structures. The interaction between valence electrons and the core ionic was described by norm-conservation pseudopotential [225].

Halogen molecules properties were calculated using the $DMol^3$ program as embedded on Materials Studio with a double numerical basis set and polarisation function (DNP). The k-point mesh interaction was selected as 4x4x3 and the kinetic energy cut-off of 500 eV was used, which were sufficient to converge. All the halogen molecules were fully optimised and electronic properties such as HOMO-LUMO energy; electronegativity and energy gap were studied to investigate halogen molecule reactivity. The binding and dissociation energies were calculated to determine the stability and dissociative halogen molecule. The HOMO-LUMO energy was analysed to investigate the electronic affinity and electron withdrawal while the electronegative was calculated to determine the most reactive halogen molecule.

All the structures were relaxed to their equilibrium atomic position with electronic and ionic optimisation criteria set up to 10^{-5} eV and 10^{-2} eV, respectively, and the conjugate gradient techniques were adopted. For geometry optimisation the forces on each atom were converged to 0.003 eV/Å, stress on each atom was converged to 0.05 GPa and the displaced was converged to

0.001 Å. Pure surface calculations were performed to investigate the stability of the surfaces, the most stable surface was determined by calculating the surface energy, work function and density of states. Surface energy measures the excess energy of surface atoms due to various factors such as the broken bond length yielding undercoordinated atoms. Adsorption calculations were performed to understand the halogen adsorption stability and interaction by comparing the adsorption energy, electron-charge transfer, work function charge density distribution and density of states. The adsorption strength of adsorbed-substrate is a crucial characteristic that allows estimating the role of adsorbate on the substrate. Desorption energy was calculated to measure the barrier of the etch product to desorb or removed from the surface.

Furthermore, electron-charge transfer was calculated to determine which halogen adsorbate withdraw electrons during the interaction. Work function was investigated to analyse the surface properties after adsorption. In addition, charge density difference was determined to visualise the nature of halogen bonding on the metal surface. Importantly, the quality to analyse the chemical interaction is the changing density for ion-metal interaction. The density of states (DOS) curves was plotted to describe and investigate the electronic and hybridisation of halogen and surface orbitals. The formation of bonding and anti-bonding hybridisation orbitals can be traced down to atomic origin, therefore, the density of states turned out to be another successful analysing tool.

Figure 3-4 present the flowchart on the computational model indicating computer software, codes and calculated properties considered in this study. The flowchart can be summarised as follows:

- The study is based on density functional theory using Material studio software package
- Two codes DMol^3 [187] and the CASTEP programs [217] were employed
- DMol^3 code was used to study the properties of free halogen molecules
- CASTEP code was used to study the properties of clean and adsorbed surfaces

- Dissociation, binding and bond energies were calculated to investigate the most stable halogen molecule
- Electronegativity, HOMO-LUMO and Fukui indices were determined to investigate the most reactive halogen molecules
- Surface energy, work function and density of states were analysed to determine the most stable surface
- Adsorption energy was calculated to investigate the halogen-surface interaction strength
- Electron transfer was studied to investigate which halogen withdraw more electrons from the surface
- The density of states was analysed to investigate the orbital hybridisations
- Work function was calculated to analyse how the interaction of halogen affect the surface property
- Charge density differences were analysed to determine the nature of bonding between halogens and the surface
- Heats of formation and desorption energy were calculated to investigate the formation and desorption of the etch products

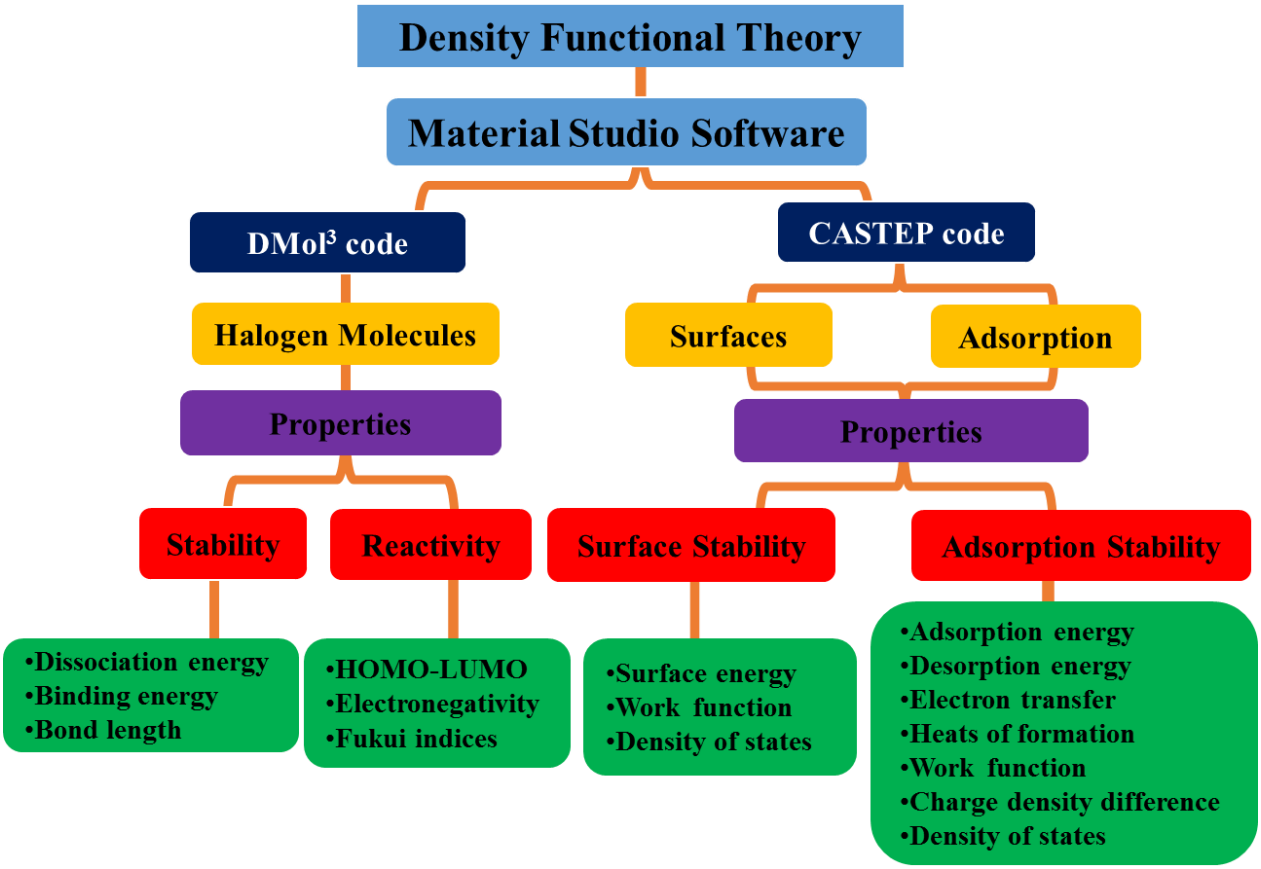

Figure 3-3: Flowchart on computational model indicating computer software, codes and calculated properties considered in this study.

Chapter 4

Halogen molecules and titanium surfaces

This Chapter focuses on the description of titanium surfaces and halogen molecules consider in the study. The general concepts, electronic and chemical properties of titanium surfaces and halogen molecules especially those used in the theoretical studies of electrochemical field and etchant are briefly described.

4.1. Halogen molecules

In this section, the structural and electronic properties of all halogen molecules are investigated. Their dissociation and binding energy, Frontier orbital theory and electronegativity are also discussed. The electronic properties of the molecule were investigated to provide insightful information about the tendency of a molecule to interact with the metal surface. Both the highest occupied molecular orbital (HOMO) and lowest unoccupied molecular orbital (LUMO) energy level are analysed.

4.1.1. Geometry optimisation of halogen molecules

All halogen molecules were initially subjected to full geometry optimisation by allowing both the cell and volume to change, and their dissociation energy and equilibrium separation properties are listed in Table 4-1. The dissociation energy was calculated, it is found that the HF molecule is lower (-5.12 eV) than that of HCl, HBr and HI molecules which suggest that the HF molecule will become more reactive. It was found that the dissociation energy strength follows the decreasing order as HF>HCl>HBr>HI. This is consistent with the previous observation however the different in the values is because the dissociation energy were carried out using Gaussian[9447] and Gaussian[9848]

program suites using restricted and unrestricted Hartree-Fock (RHF-SCF) wave functions [226]. While DFT tends to underestimate Electron-Affinities and Ionization Potentials as well as binding energies and dissociation energies, Hertree-Fock overestimate them.

The halogen equilibrium separation order increases HF<HCl<HBr<HI as shown in Table 4-1. The strong bond is determined by short equilibrium separation length; of all the hydrogen halides HF has the shortest bond length indicating strong atomic bonding than H-Cl, H-Br and H-I [227]. Moreover, the bond energy of HF is lower (-2.90 eV) among all the halogen molecules. Equilibrium separation for halogen molecules was calculated to describe the halogen atoms interaction. Separation length between halogen atoms was presented in Table 4-1 whereby the bonding of H-F has the shortest (0.94 Å) interaction length than H-Cl, H-Br and H-I molecules, which agrees well with previous work [228].

Table 4-1: Dissociation energies and equilibrium separation for the halogen (HF, HCl, HBr and HI) molecules.

Molecules	**Dissociation Energy (eV/atom)**		**Bond energy (eV)**	**Equilibrium separation (Å)**	
	TW DFT	**Hartree-Fock** [226]		**present**	**previous** [228]
HF	-5.12	5.891	-2.90	0.94	0.92
HCl	-3.61	4.489	-0.915	1.28	1.27
HBr	-3.19	3.827	-0.705	1.43	1.41
HI	-2.87	3.136	-0.225	1.63	1.61

In addition, the strength of the halogen molecule depends not only on the withdrawing power of the attached but also on the stability of the halogen ion. The concept is analogous to conventional hydrogen bonding in that a –covalent bond forms between an electron donor and acceptor [229].

The notion of halogens bonding to both types of molecules was initially puzzling since it implied that halogens could be treated as being either entirely positive or negative.

4.1.2. Electronic properties

In Table 4-2, the electronic properties; highest occupied molecular orbital (HOMO), lowest unoccupied molecular orbital (LUMO) and energy gap for the halogen molecules are presented. According to Frontier Orbital Theory, the reaction of reactants mainly occurs on the HOMO and LUMO. The energy densities of HOMO and LUMO are the key electronic parameter for characterising the chemical reactivity of the halogen molecules [230]. The difference between the energy levels of the orbitals is important in evaluating their chemical efficiency. Therefore, the electron-accepting capacity of a molecule can be estimated from its LUMO energy.

Based on the HOMO energy, it indicates that HF is more reactive with the lowest energy of -8.353 eV as compared to -7.631 eV of HCl, HBr (-6.761 eV) and HI (-6.488 eV), The LUMO and HOMO of all halogen are considered in order to analyse the chelation processes of chemical adsorption. Chelation process predicts the capacity of a molecule to accept an electron from the metal surface and is referred to as the LUMO energy (E_{LUMO}). The E_{LUMO} for HF/HCl molecules is lower than that of HBr/HI molecules indicating that HF will easily accept E_{LUMO} (-0.333 eV) electron as compared to Hl E_{LUMO} (-1.707 eV). The results compare well with previous findings by Al-Amiedy using DFT with B3LYP functional [231]. Descrepancies between our calculated values and Ref [231] are due to the different level of theory and the inclusion of a Fock fraction in [231]. The delocalised HOMO has a greater tendency to donate electrons to an unoccupied d- orbital of the metal, while the molecular region covered by delocalised LUMO is likely to accept electrons from metal atoms this is indicated that by the value of E_{HOMO}. HOMO energy is also related to ionisation energy while the energy of LUMO is directly related to electron affinity [232]. A high value of

E_{HOMO} indicates the proclivity of the molecule to donate electrons to appropriate acceptors with lower or empty d- orbital form a coordinate bond.

Table 4-2: Electronic properties for HF, HCl, HBr and HI molecule.

Molecule		**E_{HOMO} (eV)**	**E_{LUMO} (eV)**	**E_{gap}**
TW PBE	HF	-8.353	-0.333	8.02
	HCl	-7.631	-1.034	6.59
	HBr	-6.761	-1.825	4.93
	HI	-6.488	-1.707	4.78
B3LYP [231]	HF	-10.745	0.710	10.03
	HCl	-9.251	-0.241	9.01
	HBr	-8.443	-0.621	7.822

The lower the value of E_{LUMO} the stronger the electron-accepting ability of the molecule. Therefore, the binding strength of the molecule to the surface increase with increasing E_{HOMO} and decreasing of the E_{LUMO} values, a similar analysis has been reported by Obi-Egbedi *et al* [26]. In Table 4-3 the binding energy, electronegativity and Fukui indices for halogen molecules are presented. Halogen molecules possess lower binding energy of -6.95 eV for HF, -4.43 eV (HCl), -3.08 eV HBr and HI -3.36 eV, which compare well with the dissociation energy strength above (in section 4.1.1). Electronegativity is the ability of a molecule or an atom to attract electrons from other atom compounds. The electronegativity parameter is related to the chemical potential wherein a higher value indicates better chemical potential. It was found that HF molecule has the highest electronegativity (4.62 eV) than other molecules which suggests that HF will attract more electrons when interacting with the metal surface as compared to other halogen molecules. This is comparable with the work by Al-Amiedy [231]. The more electronegative a molecule the better able it is to bear a negative charge.

Table 4-3: Binding energies (eV) and electronegativity of HF, HCl, HBr and HI molecule.

Molecule	**Binding Energy**	**Electronegivity**		**Nucleophilic**		**Electrophilic**
		TW DFT	**B3LYP** [231]	**TW DFT**	**Ref.** [233]	
HF	-6.95	4.62	5.01	0.85	0.58	-0.093
HCl	-4.43	4.33	4.75	0.87	0.77	0.203
HBr	-3.08	4.29	4.53	0.88	0.80	0.255
HI	-3.36	4.20	-	0.86	0.71	0.559

It is clearly seen that all the molecules have a higher electronegativity value than the Ti atom (1.5 eV) [234], therefore, the transfer of electrons from the surface to a molecule may occur. The local reactivity for each molecule can be analysed through Fukui indices (nucleophilic and electrophilic [235]. These measurements provide the chemical reactivity and indication of the reactive region. The electron-donating/accepting capacity of molecules is measured by high/lower values of nucleophilic/electrophilic. The nucleophilic and electrophilic values decrease from HF to HI indicating that HF attacks positive charges easily than other molecules. The Fukui function for HF molecule was found to be the smellest while HBr was shown to be the largest, this is consistent with previous work [233]. Furthermore, the HF possess lowest electrophilic which suggest that the molecule can accept electron pair from the metal surface [236].

4.2. Ti (100) and Ti (110) surfaces

This section focuses mainly on the clean Ti (100) and (110) surfaces considered in this study, which is one of the most widely used metallic substrates. Only the lower miller index facets Ti (100) and Ti (110) surfaces are considered and seemly they are regarded as the most stable Ti surfaces [237]. The Ti surfaces are represented with atomic slab models in a supercell that is bounded with periodic

lateral boundaries and separated by vacuum space perpendicular to the surface. All the Ti surface models were generated from the cleavage of optimised bulk Ti single crystal with a space group of P63/mmc and lattice parameter a=b=4.57 Å and c=2.82 Å.

The entire Ti surface slabs were constrained to have a symmetric top and bottom layer. A fundamental element in understanding the substrate is a quantitative description of its geometry structure to investigate its surface properties. The stability of Ti surfaces is described by structural relaxation, surface energy and work function. Structural determination has been performed as a function of the number of adaptable layers. In order to archive surface properties, the surface was allowed to relax during geometry optimisation.

4.2.1. Geometry structures of Ti (100) and Ti (110) surface

To describe the atomic chemical reaction at the surface plane, a reliable model of Ti surface was employed that includes slab thickness and vacuum region. Atomic structures and the composition of surfaces largely dictate their properties, even small structural difference can have a significant influence. Figure 4-1 (a-b) presents the optimised slab of Ti (100) and (110) surface layers separated by a vacuum region of 25 Å, with 64 atoms and 46 atoms, respectively. Ti (100) surface consists of 4-atomic layers terminated by four-fold titanium atoms whilst Ti (110) surface consist of 5-atomic layers terminated by three-fold titanium atoms. The difference in the orientation of the atom surface can detect changes in the adsorption of a molecule.

We noted that Ti (110) surface is a rather open surface with large interlayer distancing and a higher density of steps while Ti (100) surface is closely packed layer atoms. After geometry optimisation, the equilibrium bond length (Ti-Ti) was found to be 2.876 Å and 3.086 Å for both Ti (100) and (110) surfaces, respectively. Figure 4-1 also show the possible adsorption sites for each surface, that is the top (T), bridge (B) and hollow (H) sites. This will be discussed in details in Chapter 5.

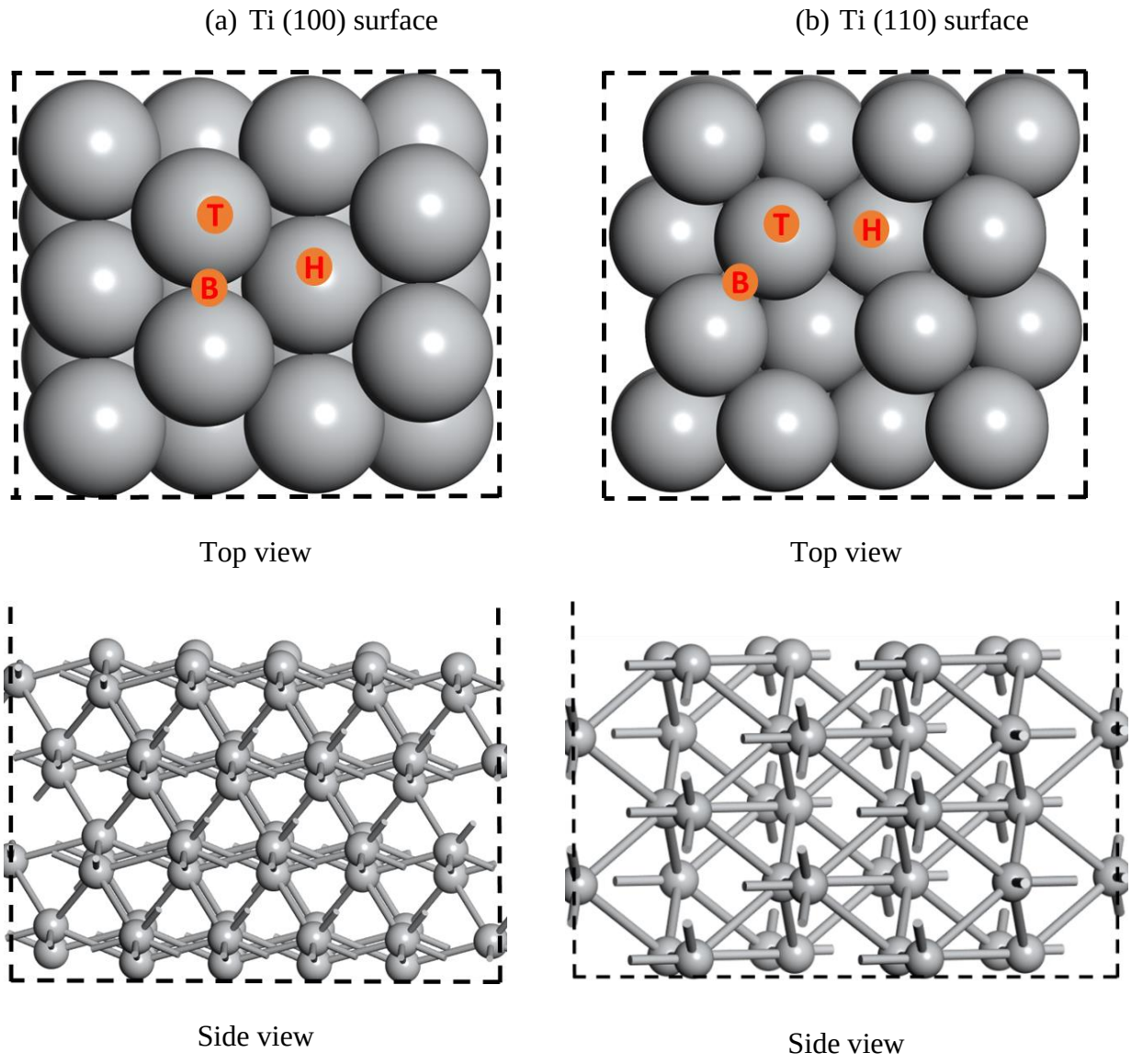

Figure 4-1: Optimised atomic structure of titanium surface model: (a) Ti (100) surface and (b) Ti (110) surfaces. Top view showing possible adsorption sites, Top (T), bridge (B) and hollow (H) site.

4.2.2. Ti (100) and (110) surface energies

In order to determine the surface properties, surface energy is a fundamental property of the different facets of a material's surface and can be used to describe its stability. Surface energies of Ti (100) and Ti (110) surfaces were calculated using Eq. (3-36) and their results are listed in Table 4-4. Note that the higher energy of a structure, the less closed-packed the surface. The higher the surface energy of the model indicates less stability [238]. Comparing their surface energy values,

Ti (110) surface was found to be the most stable with a lower value of 0.126 eV/A^2 than that of Ti (100) surface (0.141 eV/A^2). The difference between Ti (100) and (110) surface energies is relatively small with the order of 0.026 eV. Clearly, the model Ti (110) surface is more stable than the (100) surface. This prediction is in good agreement with the results reported by Hennig *et al* [237] using DFT with PW91 functional.

Table 4-4: Calculated surface energies for Ti (100) and (110) surface.

Index	**Bond Length (Å)**	**Surface Energy (eV/A^2)**	
		Present	**Previous** [237]
(100)	2.876	0.141	0.153
(110)	3.086	0.126	0.121

4.2.3. Density of states for Ti (100) and (110) surfaces

To understand the electronic properties of Ti (100) and (110) surfaces and their stability, the partial density of state (PDOS) and total density of states (TDOS) were investigated. Figures 4-2 and 4-3 presents PDOS for Ti (100) and (110) surfaces, respectively. The typical interest is on the electronic orbitals that are directly involved in the Ti metal surface. Accordingly, their electronic peaks consist mainly of $4s^2$ $3p^6$ and $3d^2$. PDOS curves for Ti (100) and Ti (110) surface display similar features. The partial contributions of s, p and d orbital of Ti atoms are displayed in Figure 4-2 and 4-3, in all the PDOS plots, the Fermi level is located in the deep pseudogap of the p- orbital peak.

It is clearly seen that the large contribution to the density of state is from d- orbital electrons compared with s- and p- orbital electrons contribution. The surface of the transitional metal is balanced by the attraction force of d- bonds against the repulsion force of the s-p electrons [239]. The PDOS plots show that the d- state contributes much on the E_F level suggesting that both Ti

(100) and (110) surface are metallic. Figures 4-2 and 4-3 clearly show the states are well pronounced and overlap from the valence to the conduction. The PDOS curves for Ti (100) surface slightly shifted away from E_f towards the valence band region whilst Ti (110) almost tallying at E_f. Moreover, there is a significant difference in PDOS peaks height wherein Ti (100) PDOS peaks are higher compare to Ti (110) surface indicating that there is a large number of electrons in Ti (100) surface.

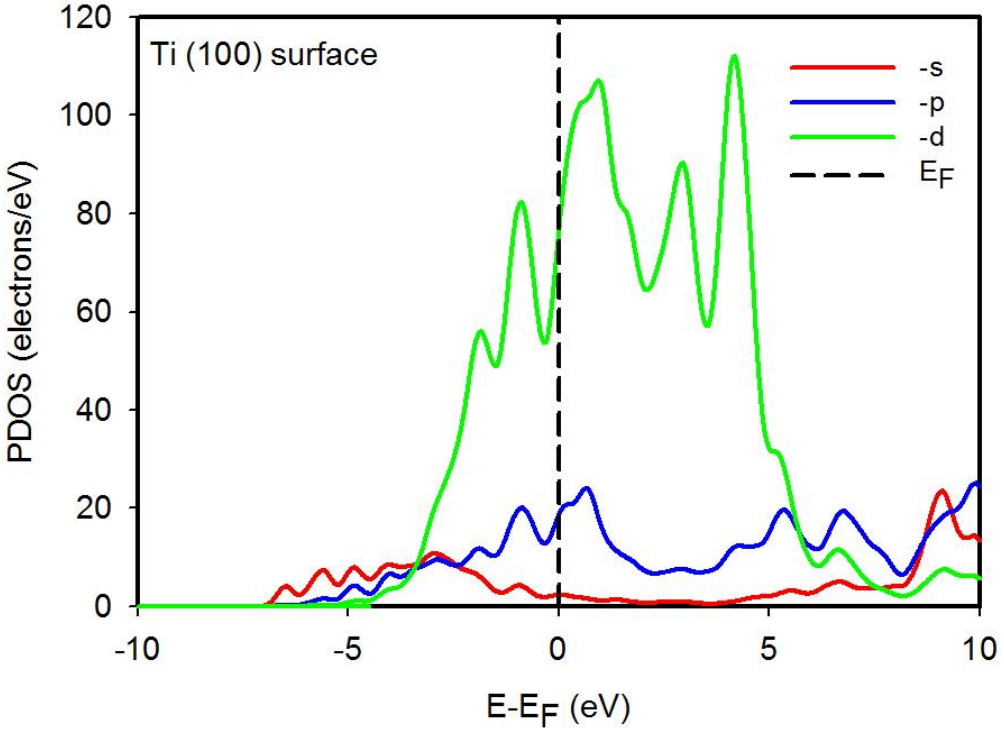

Figure 4-2: Partial density of states of the typical configuration for pure Ti (100) surface. The Fermi energy is taken as the energy zero.

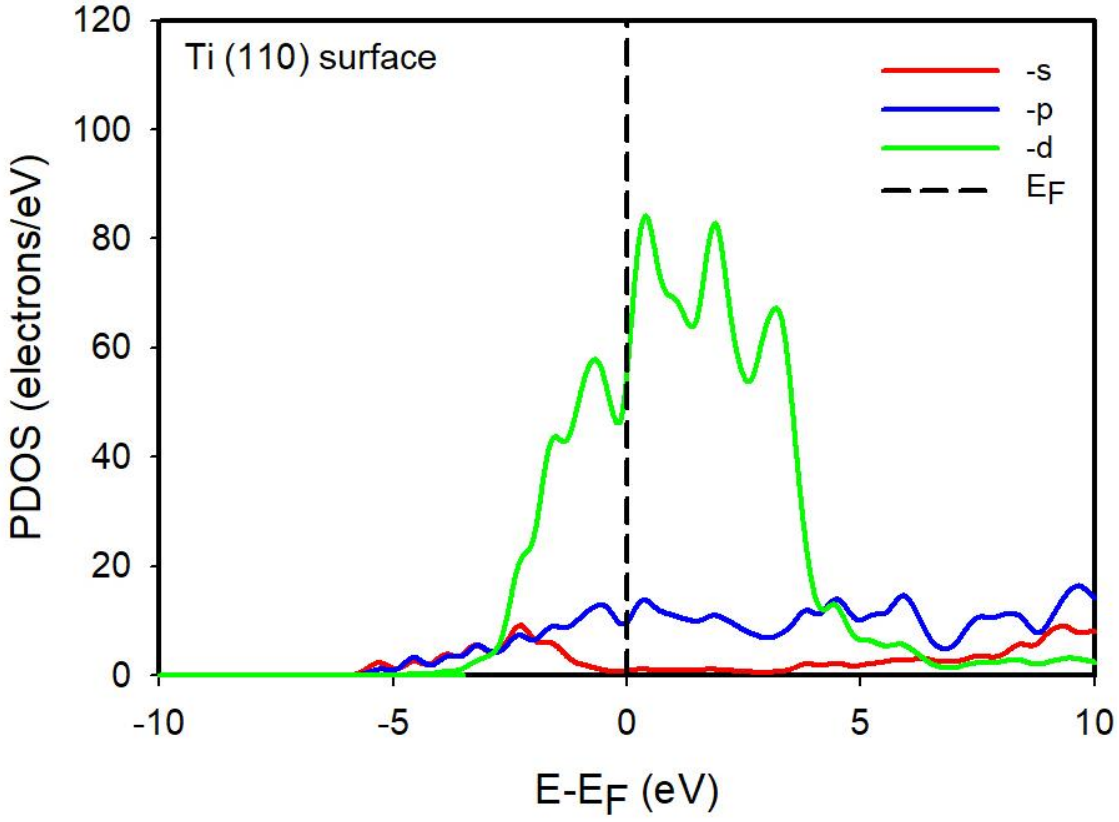

Figure 4-3: Partial density of states of the typical configuration for pure Ti (110) surface. The Fermi energy is taken as the energy zero.

Figure 4-4 presents the embedded total density of states (TDOS) plots for the Ti (100) and (110) surfaces. This is to allow direct comparison of Ti surface stabilities and description. It is the surface states at the high-level area and the reduced electronic density of state at low energy level area that makes surface structure high state relative to the energy of the crystal structure [239]. It is seen that the most contribution to the TDOS is the 3d- orbital electrons. Moreover, the lower TDOS at the E_f level represents the number of electrons at the high energy level. Therefore, the TDOS of Ti (110) surface is lower than the TDOS of Ti (100) indicating that Ti (110) is more stable than Ti (100) surface.

The electron energy of Ti (110) surface is lower and surface energy also small as a result. Suggesting that Ti (110) is the most stable surface than Ti (100). This is in agreement with the calculated surface energy observed in section 4.2.2. It worth noting that the TDOS curves for the Ti (100) surface are slightly broader than that of the Ti (110) surface. This behaviour is a result of the difference in partial localisation of the d- state electrons. In addition, the E_F cuts the middle neck of the d- state towards the minima of the TPDOS curve. However, the Fermi level falls closer to the pseudogap for Ti (110) surface and is situated to the left for Ti (100) surface.

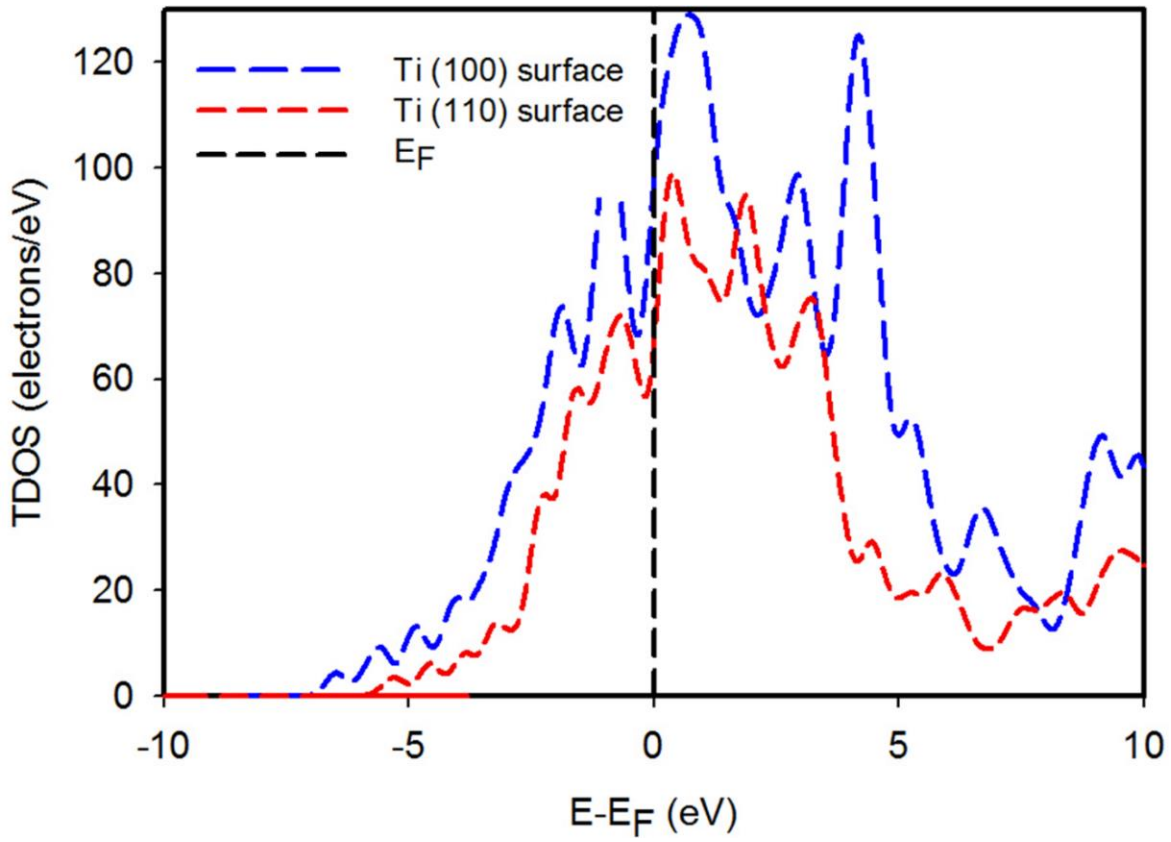

Figure 4-4: Total density of states of the typical configuration for pure Ti (100) and Ti (110) surfaces. The Fermi energy is taken as the energy zero.

4.2.4. Work function

Electrostatic potential is the minimum amount of energy required to remove or extract an electron from a crystal surface in a vacuum, normally known as work function (Φ). Computed electrostatic potential of Ti (100) and Ti (110) surfaces were calculated using Eq. (3-41) to understand the physical properties. In Figure 4-5 and 4-6, the work function plots for Ti (100) and Ti (110) surfaces are presented. It was found that Ti (100) surface has a larger numerical value of the work function (3.665 eV) than that of the Ti (110) surface (3.011 eV). The difference between both Ti surfaces has a magnitude of 0.65 eV, which is influenced by surface atomic relaxation and surface termination. Our calculated work functions of Ti surfaces are slightly lower than (4.33 eV) that observed by Nicholas *et al* [240], which may be due to different surface slab and calculation parameters.

In addition, the work function of the Ti surface decrease from the (100) to (110) surface orientation, this is due to the spreading of negative charge. The surface with a lower work function easily transfers electronic charge to any adsorbate with higher electronegativity that results in ionic bonding [241]. Comparing the work function of Ti (100) and Ti (110) surfaces, the Fermi energy of the Ti (110) surface is lower than that of the Ti (100) surface. This follows the same trend of PDOS analysis in section 4.2.3. The induced changes in the work function are due to atomic charge rearrangement on the surface whereby the spreading of negative charge increases the work function. Lower work function value suggests that there is a much easier electron extraction on Ti (110) than on Ti (100) surface. Wei *et al* [242] have reported similar analysis previously on TiN (100), (110) and (111) surfaces, which is consistent with the current study.

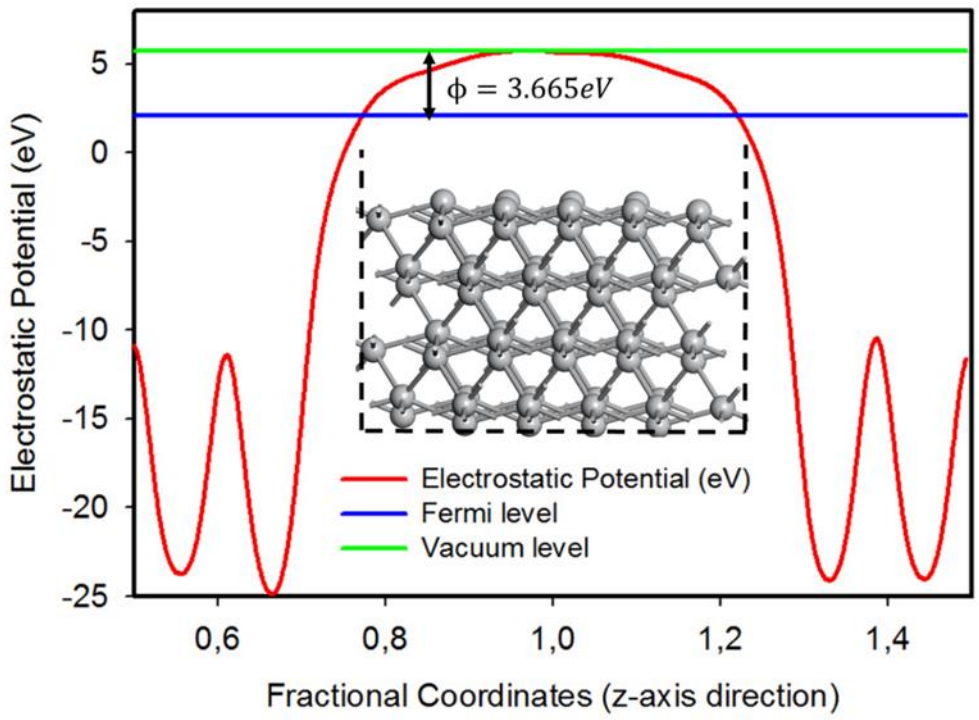

Figure 4-5: Electrostatic potential energy (Φ) of Ti (100) surface.

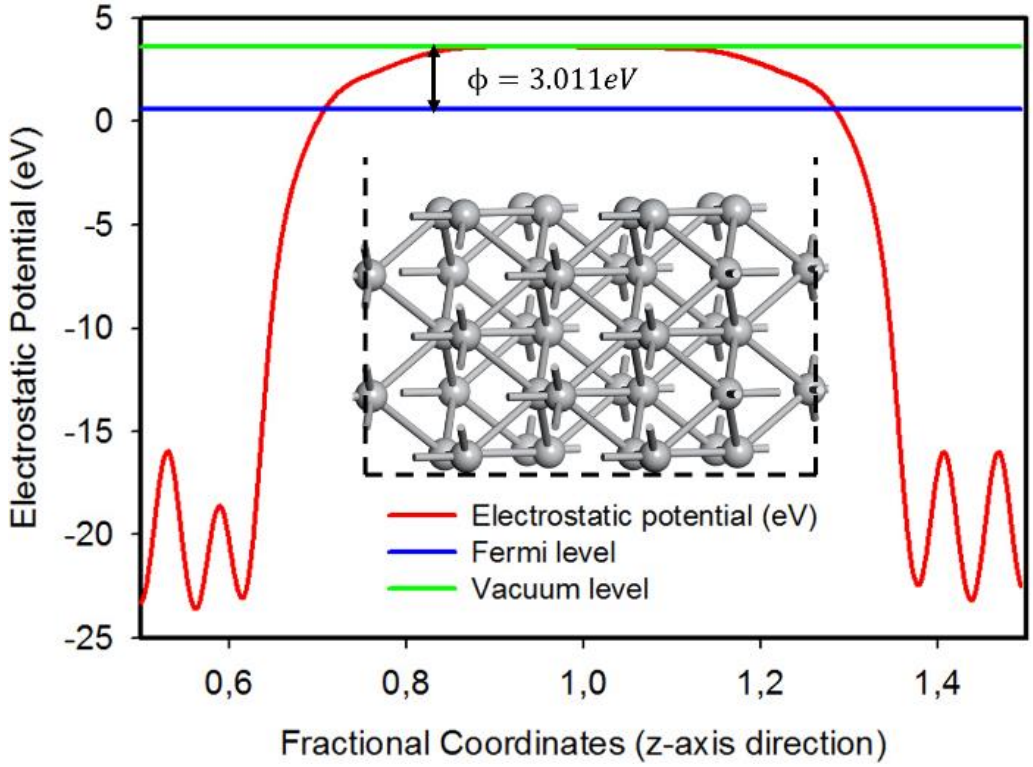

Figure 4-6: Electrostatic potential energy (Φ) of Ti (110) surface.

4.3. Summary

In this chapter, DFT calculations were performed to study free halogen molecules as well as the clean Ti (100) and (110) surfaces. In each halogen, molecule electronic properties such as dissociation energy, electronegative and Frontier Orbital Theory were investigated to determine the possible reactivity towards the Ti metal surface. The HF molecules was found to be the most reactive halogen molecules with lower dissociation energy of -5.12 eV than other halogen molecules. Furthermore, the halogen molecules were found to possess the higher electronegativity whereby the trend follows an atomic period of HF>HCl>HBr>HI, which is the same trend of the Frontier Orbital Theory energy (E_{HOMO} (eV)).

In the case of Ti (100) and (110) surfaces, the surface energies, PDOS and work function (Φ) properties were examined to investigate the surface stability. It was found that the Ti (110) is the most stable with a lower surface energy of 0.126 eV/A^2 than the Ti (100) surface (0.141 eV/A^2). This surface stability trend was also confirmed by the TDOS and PDOS curves. Moreover, the PDOS curves showed the localised d- orbitals positioned at the Fermi energy level denoting metallic character. Moreover, the work function (Φ) value of Ti (100) and (110) surfaces were analysed. The results show a decrease in Φ from Ti (100) to Ti (110) surfaces revealed that the most stable Ti (110) surface possess a lower work function. This shows charge rearrangements on the surface metal atoms that induce changes in the work function.

Chapter 5

Adsorption of halogens on Ti (100) and (110) surfaces

This Chapter investigates the fundamental characteristics and mechanism of halogen molecules (HF, HCl, HBr and HI) and ions adsorption on bare Ti (100) and (110) surfaces. The essential concepts of adsorption, adsorbent, adsorbate and factors that influence adsorption are described. Halogen molecules are placed on top of Ti surfaces, and a sequent structural relaxation was performed using the CASTEP code with similar computational details as described in Chapter 3 (section 3.7.5). The study will provide an insight on ion-metal atom interaction. Both Ti surfaces and adsorbates are allowed to relax during geometry optimisation to determine the adsorption strength. Atomistic level modelling of the electrochemical adsorption of halogen will be investigated taking into account both the solvation and partial charge effect. The first part of this Chapter forms the Ti (100) and the second part on the Ti (110) surface.

5.1. Adsorption of halogen molecules on Ti (100) surface

In this section, the adsorption mechanism of halogen molecules and ions on the bare Ti (100) surface is investigated. All halogen molecules were initially placed 2 Å distance on top of the Ti (100) surface. The key characteristics of molecules and ions interacting with the Ti (100) surface atoms such as dissociation mechanism, adsorption energy, charge density redistribution and density of states are analysed. The interaction energy strength of adsorbate with the Ti atom was determined by comparing the adsorption energy, charge density distribution and density of state.

5.1.1 Dissociative adsorption of halogen molecules on Ti (100) surface

Adsorption behaviour of halogen molecules on Ti (100) surface was investigated. The entire Ti (100) surface including halogen adsorbents were allowed to relax during geometry optimisation to investigate the nature of adsorption. Dissociative adsorption is one of the most fundamental chemical reactions at the surface since it involves strong covalent molecular bond and the formation of new chemical bonds of atomic [243]. Figure 5-1 (a-d) describe the initial, intermediate and dissociation adsorption steps of halogen molecules on the Ti (100) surface. The intermediate step mainly emphasised the attractive force from a positive charge of the Ti atom surface. It was observed that the molecules approach the Ti (100) surface leading to halogen molecules bond length elongated and ruptured. The halogen bond distances were found increasing to (HF= 2.928 Å), (HCl= 3.067 Å), (HBr= 3.131 Å) and (HI= 3.219 Å) as presented on the intermediate step.

All the halogen molecules dissociate completely on Ti (100) surface resulting in titanium halides and hydrides bonding (Ti-H). This is due to an applied potential difference that occurs during electrochemical interaction. The formation of Ti-H bonding is consistent with the experimental observations that etching Ti metal surface with HF/halogen molecule or aqueous solution induces hydrogen embrittlement [19]. Interestingly, all the halogen ions (F^-, Cl^-, Br^- and I^-) prefer to be adsorbed on the bridging site. It was found that all the halogen ions preferred a bridging adsorption site on Ti (100) surface and bond to the nearest Ti atoms with an average bond length of 2.045 Å for Ti-F, Ti-Cl (2.452 Å), Ti-Br (2.605 Å) and Ti-I (2.818 Å). The Ti-F bond length value was found to be shorter than all bond lengths suggesting stronger interaction between Ti-F. In addition, the bond length of Ti-H after dissociation is 1.869 Å for H-F, 1.870 Å both (H-Cl and H-Br) and 1.866 Å (H-I). Tshwane *et al* [244] reported a similar dissociative mechanism of HF molecules on the titanium oxide surface.

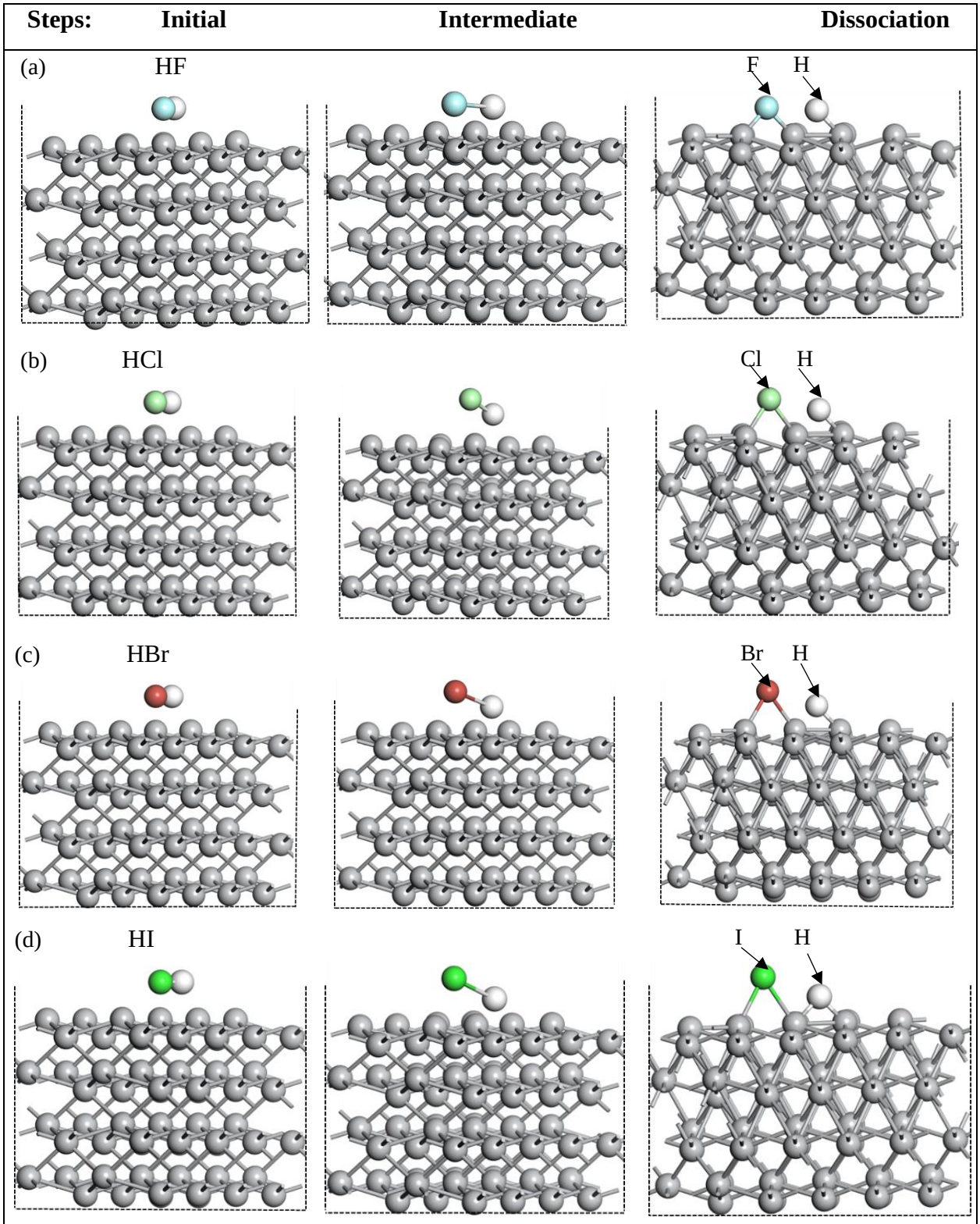

Figure 5-1: Atomistic side-view of halogen molecules (HF, HCl, HBr and HI) adsorption process on Ti (100) surface. Each adsorbate shows the initial configuration step, intermediate and dissociated adsorption. The surface of Ti atoms shown in grey, whereas the atoms for the specific molecules indicated by the arrow.

Moreover, when halogen molecules dissociate on the Ti (100) surface depends again on the adsorption energy between halogen molecules and the Ti surface. To further analyse the effect of adsorption behaviour on the Ti (100) surface, the successive adsorption energy of each molecule were calculated using Eq. (3-37). Adsorption energy is the fundamental characteristics of adsorbate (halogen molecules) interaction with an adsorbent (Ti surface). Figure 5-2 present the adsorption energy relation for adsorbed molecules on Ti (100) surface. We observed that all the halogen molecules possess negative adsorption energy on the Ti (100) surface indicating a spontaneous reaction. The adsorption energies were found to be thermodynamically favourable.

Adsorption energy of HF molecule on the Ti (100) surface was found to be more energetically favourable than other halogen molecules. HF molecule possesses stable adsorption energy (E_{ads}) of -4.23 eV while the HI is the least stable with an adsorption energy of -3.55 eV. The trend of adsorption energy for the halogen molecules follows the periodic rule $E_{ads}^{HF} > E_{ads}^{HCl} > E_{ads}^{HBr} > E_{ads}^{HI}$, this is due to the repulsive lateral between the adsorbates on the Ti surface (Figure 5-2). Similar adsorption energy strength of halogen molecules was also reported by Zhu *et al* [169] on the Al_2Pt surfaces using DFT-PBE functional within VASP code. A similar trend was observed on surface etching strength whereby fluoride etchant was reported to be more reactive than other halogen etchants [245].

Furthermore, the formed Ti-F bond has the shortest bond length (2.045 Å) than all the adsorbed bond length on the Ti (100) surface, which is supported by the stability of its adsorption energy configuration. It was found that the binding between F-Ti atoms is strongest among all other halogen atoms (Cl, Br and I). Present findings suggest that the adsorption stability configuration of halogen molecules are closely related to the bond formation. Comparing with the aqueous solution, the halogen molecule dissociates to produce halogen ions that can strongly interact with the metal atoms and thus modify the structure of the metal surface. The crucial effect of halogen molecules

adsorption is the interaction between halogen ion with Ti atom, thus, the adsorption of halogen ion on Ti (100) surface is discussed in the next section. Halogen ions are presented in the form of F^-, Cl^-, Br^- and I^- where the formal charge generated, become the major components. The adsorption of halogen ions on the Ti (100) surface is presented in the next section 5.1.2.

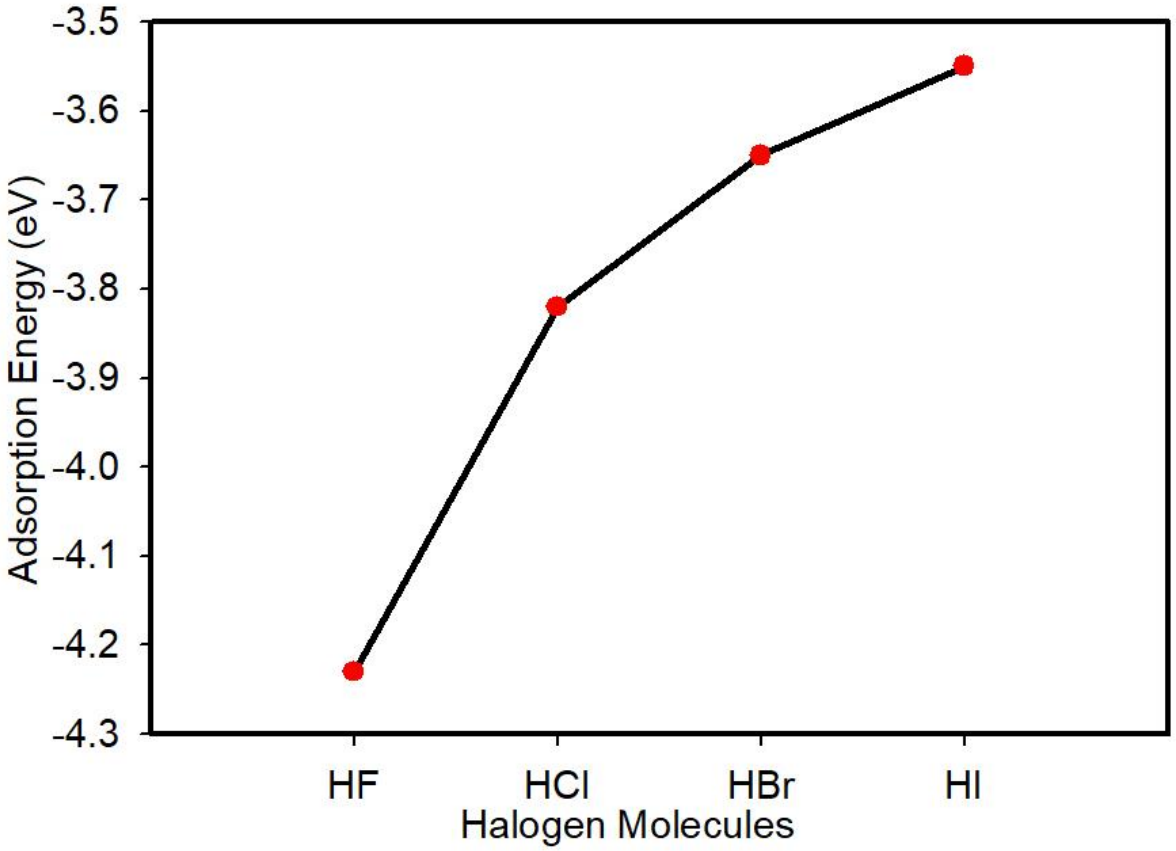

Figure 5-2: Adsorption energies for halogen molecules (HF, HCl, HBr and HI) on Ti (100) surface.

5.1.2. Adsorption energy of halogen ions on Ti (100) surface

In chemical reactions, etching of metal surface is through an aqueous solution in which halogen ions play a central role [246], whereby, the most specific effect is the interaction of ion and surface atoms. In order to understand better the halogen ions interaction mechanism, all halogen ions were adsorbed on Ti (100) surface at different adsorption positions, top, hollow and bridge sites. The stability order of the adsorption positions of the halogen ions is analysed in terms of their local reactivity. The calculated adsorption energy strength for the halogen ions on the Ti (100) surfaces is considered.

In Table 5-1, the comparative adsorption energy of halogen ions on the Ti (100) surface at different adsorption sites are presented. The energetic preferable position for halogen ions adsorption was found to be a hollow position site with lower adsorption energy for each halogen. This support the findings in section 5.1 wherein the bridging site adsorption was found to be more stable while the top and hollow sites were found to be least stable for all adsorption molecules. This indicates that the bridging site is the most preferred adsorption site with the lowest adsorption energy than the top and hollow sites. Adsorption energy for the three sites were found to be negative suggesting that the adsorption reaction would happen spontaneously denoting that all three sites can adsorb halogen ions effectively.

The adsorption energy of F ion at corresponding adsorption sites is lower than that of other halogen atoms denoting that there is a strong stable interaction between Ti atom and F ion at all adsorption position. Fluorine ion was found to be the most stable adsorbate when comparing the adsorption energy of all halogen ions at different adsorption sites. The calculated adsorption energy for F^-, Cl^-, Br^- and I^- at different adsorption sites are shown in Table 5-1 wherein the adsorption energy of fluorine is greater as compared to the top and bridge sites.

It is also noted that the adsorption energy of fluorine on the Ti (100) surface adsorption site is more stable than all halogen ions. It was observed that the adsorption energy strength increases following the order of $E_{ads}^{F} > E_{ads}^{Cl} > E_{ads}^{Br} > E_{ads}^{I}$ for all adsorption sites. Similar trend was observed by Tada *et al* [170] using DFT+U and PBE functional on TiO_2 (110) surface. Complementary findings were also reported by Nguyen *et al* [247] on adsorption of halogen on silicon using spin-polarized DFT-PBE functional implemented in VASP.

Table 5-1: Calculated adsorption energies (eV) for halogen ions at Ti (100), TiO_2 (110), Si and Pt (111) surfaces at different adsorption site.

Adsorption site		**F^-**	**Cl^-**	**Br^-**	**I^-**
Present @ Ti (PBE)	Top	-5.850	-5.071	-4.549	-3.700
	Bridge	-5.951	-5.108	-4.590	-3.700
	Hollow	-5.800	-5.070	-4.550	-3.626
[170] @ TiO_2 (PBE+U)	-	-6.10	-4.09	-3.37	-2.55
[247] @ Si (PBE)	Top	-5.29	-3.24	-2.41	-1.29
[171, 166] @ Pt (PBE)	Top	-3.62	-2.95	-2.73	-2.37
	Bridge	-3.37	-2.96	-2.85	-2.68
	Hollow	-3.32	-2.97	-2.86	-2.74

In Figure 5-3, the dependence of adsorption energy per bound halogen ion on the bridging site is shown. The adsorption energies for all halogen ions are negative this denotes that the interaction between the halogen ions and Ti atoms is spontaneous. It was found that the trend of adsorption energy strength varies in the order of F>Cl>Br>I, which follows the same order with electronegativity strength [39]. Similar adsorption energy trend was observed by Tada *et al* [170]

on the TiO_2 surface. This suggests that the stability of halogen ion adsorption on the Ti (100) surface increases with increasing electronegativity.

We noted that the adsorption energy of the F ion on the Ti (100) surface is more stable than all halogen ions in all adsorption sites. Fluorine ion showed the most stable adsorption energy of (E_{ads}^{F}) -5.951 eV while iodine is less favourable with (E_{ads}^{I}) -3.700 eV on hollow site. The interaction between F-Ti is stronger than that of Cl-Ti, Br-Ti and I-Ti interaction. This reveals that interaction strength decrease with increasing halogen atomic size. Similar observations were reported by Vital *et al* [113] on halogen adsorption on the silicon surface.

The adsorption energy changes slightly with an atomic difference, which shows different attractive interaction between the adsorbate-adsorbent. Generally, the smaller atomic radii suggest a stronger polarisation effect inducing a stronger binding during the interaction [248]. Our results show a clear dependence between the adsorption energy and atomic radius wherein F atom with smallest atomic radii and strongest polarisation result in a strong adsorption strength whilst I atom with largest atomic radius showed the lowest adsorption energy as shown in Figure 5-3. Differences in calculated adsorption strength between halide ion are relatively small all less than 1 eV. Therefore, the lateral adsorption energy of halogen on the Ti (100) surface contribute to the reactivity mechanism. Comparing adsorption energies of halogen molecules and ions in section 5.1 and 5.3 respectively, it reveals that the adsorption energy of ions is more stable than adsorption energy of halogen molecules. The adsorption energy of halogen ions on the Ti (100) surface is lower than that of the halogen molecule. This suggests that halogen ions are more reactive to the Ti atom surface than halogen molecules.

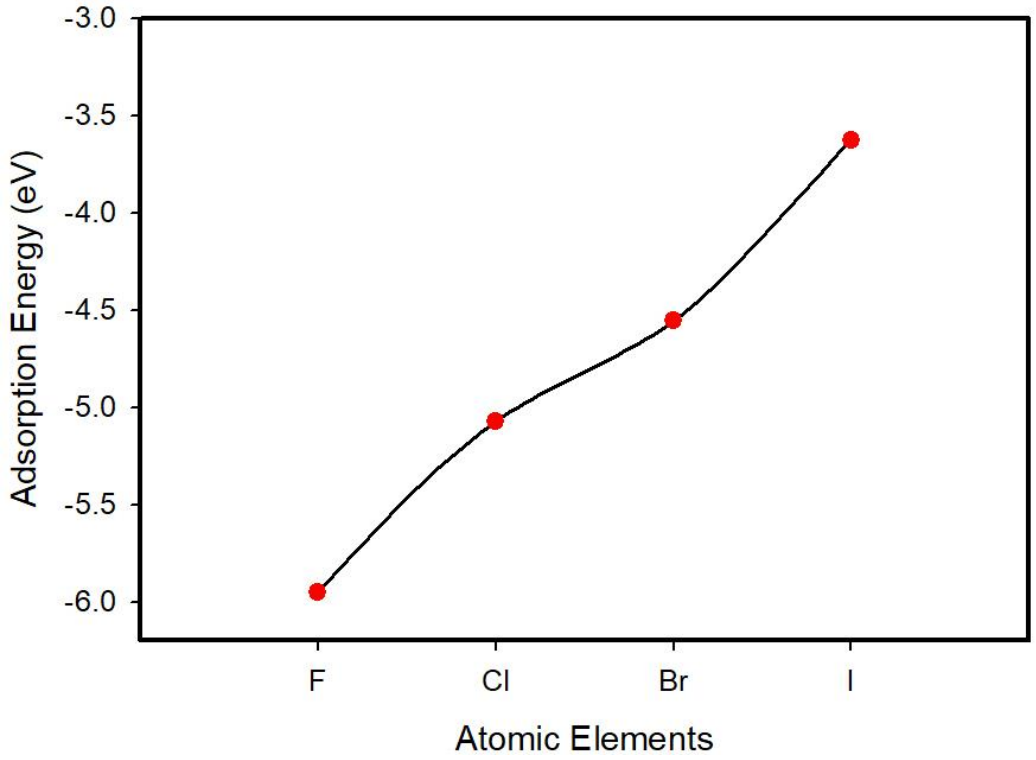

Figure 5-3: The adsorption energy of halogen ions on Ti (100) surface.

5.1.3. Adsorption geometry of halogen ions on Ti (100) surface

In an aqueous solution, halogen molecules are presented in the form of F^-, Cl^-, Br^- and I^-, wherein the formal charge generated become the major component. In addition, the characteristics of halogen ion adsorption will avoid the formation of the Ti-H bond (titanium hydride), which is the major problem of etching metal surface with hydrofluoric acid [19]. Thus, halogen ions were considered as the possible components in the adsorption process. Figure 5-4 (a-d) present the geometry optimisation of halogen ions adsorption on Ti (100) surface. Only the geometry of the hollow site is considered as this configuration was found to be the most preferred site as in section 5.1. All halogen ions were initially placed same distance (2 Å) from the Ti (100) surface. Since the calculation system is related to geometry relaxation, after optimisation halogen ion chemically bonded to Ti atoms with a different bond length of Ti-F (2.012 Å), Ti-Cl (2.427 Å) Ti-Br (2.580 Å) while for Ti-I (2.782 Å) which are in good agreement with the result by Pradhan *et al* [249].

In Figure 5-5 displays the adsorption energy strength of halogen ions on the Ti (100) surface as a function of adsorption bond distance. We observed a linear relationship between bond distance and adsorption energy. The analysis shows that the adsorption distance between titanium and F, Cl, Br and I increase with decreasing adsorption energy strength. It was noted that the displacement between Ti-F was shorter while Ti-I interaction possesses a larger bond distance. Moreover, the bond length displacement of Ti with halogen atom follows the sequence of F-Cl-Br-I. The analysis of this fact shows that the stable adsorbate possess a stronger (shorter bond length) interaction

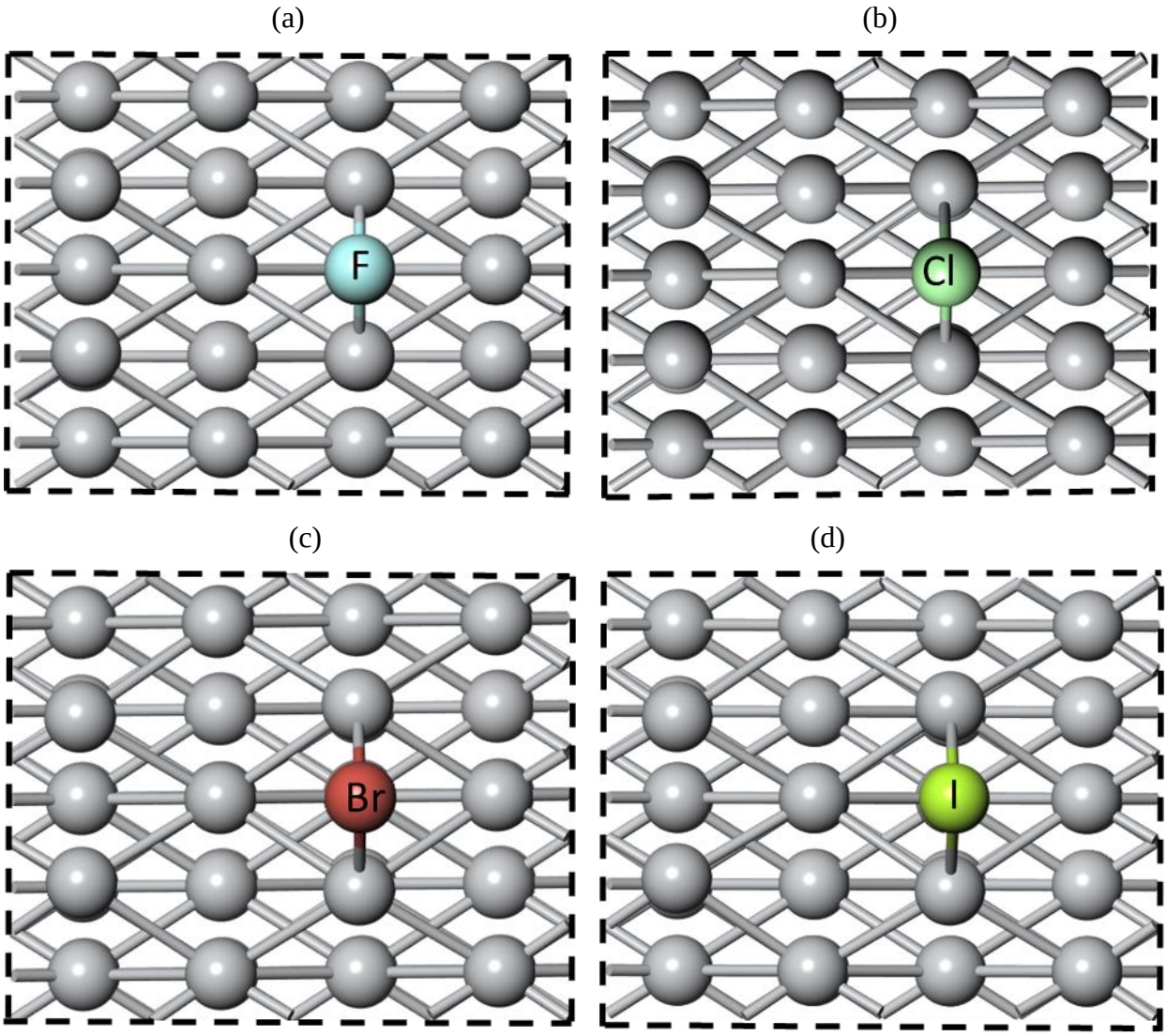

Figure 5-4: Optimised atomistic structures of halogen ions adsorption on Ti (100) surface: (a) F-Ti, (b) Cl-Ti (c) Br-Ti and (d) Ti-I.

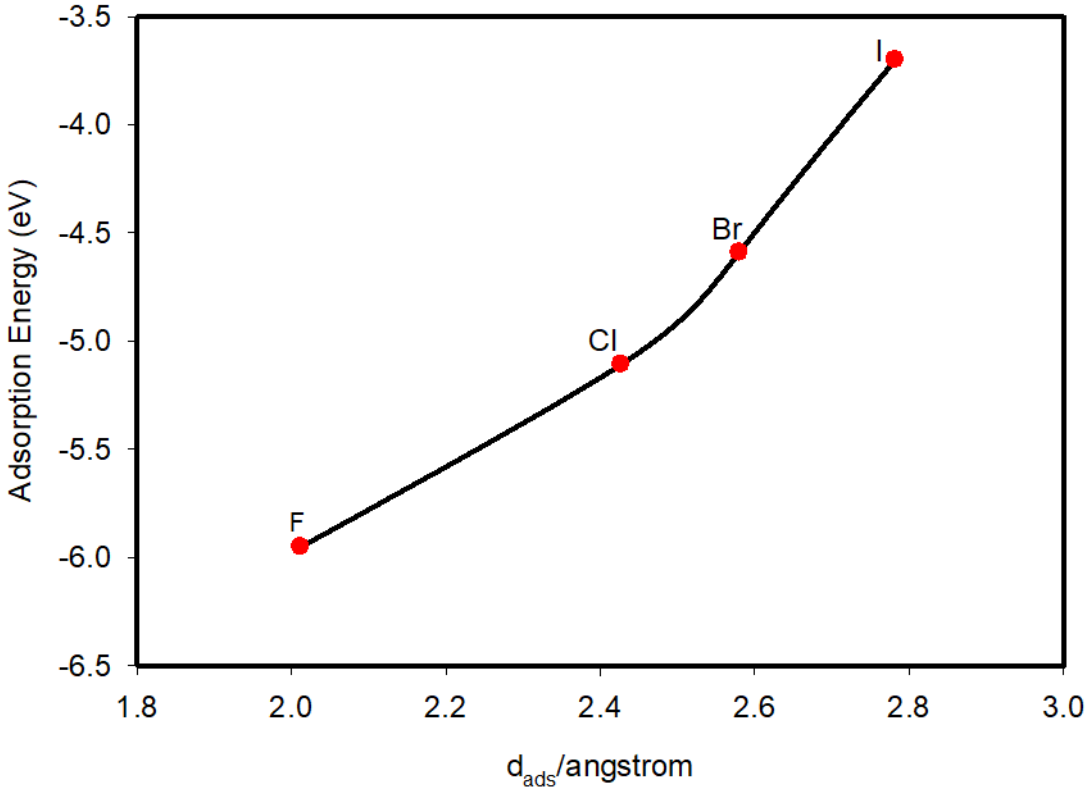

Figure 5-5: The adsorption energy of halogen ions with respect to adsorption distance on Ti (100) surface.

5.1.4. Electronic properties of halogen adsorption on Ti (100) surface

In order to fully understand the electrochemical interaction of halogen ions with Ti (100) surface, electronic properties are investigated. The interaction between halogen ions with Ti atom surface implies significant electronic changes. Therefore, in this section electronic charge transfer, charge density distribution (map) the density of states are analysed.

5.1.4.1. Electronic charge transfer

The electronic charge transferred between the adsorbent and metal play a crucial role in the manifestation of a metal corrosion and etching process [250]. The binding between halogen and titanium atoms is a typical covalent bond that reaches several electron volts, depending on the

atomic electronegative strength and adsorption energy stability [169]. During the adsorption, all halogen atoms withdraw a substantial amount (-0.48 |e|) of charge from Ti atoms.

The influence of the charge transfer effect on the adsorption energy profile has been explored. Furthermore, to gain insight into the interaction of halogen ion with titanium atoms the calculated adsorption energy and charged transferred curve is plotted as shown in Figure 5-6. It was found that all the adsorbents accept electron with a charge ranging from 0.04 to 0.48 |e|. We found that the more stable adsorption energy the more electron transfer during the interaction. A halogen atom interacting strongly with Ti atoms also accept more electron from the Ti (100) surface. It can be seen that electron transfer is induced by adsorption stability. The adsorption energy of halogen ions on Ti (100) surface are -5.951 eV (F^-), -5.108 eV (Cl^-), -4.590 eV (Br^-) and -3.700 eV (I^-) which corresponding to charge transfer of 0.48 |e|, 0.27 |e|, 0.17 |e| and 0.04 |e|, respectively. We found that the trend of charge transfer strength varies in the order of F>Cl>Br>I, this is the same order of adsorption energy stability and electronegativity strength. These findings are consistent with previous observation of Bader charge analysis of halogen adsorption on intermetallic surfaces [169].

The absolute value of the electron on F- atom adsorption onto the Ti atom is larger than other halogen atoms due to its higher electronegativity and adsorption energy strength. The present results reveal the idea that adsorbents adsorb strongly on the Ti (100) surface when the adsorbate accepts more electrons from the surface. According to Figure 5-6, more electron transfer accompanies the stronger interaction. It was found that the higher value of charge/electron of F than other than halogens is due to the higher electron-accepting capacity of the F atom. We observed that the adsorption energy is linearly related to the charge of transferred; this is because the electrostatic interaction is an important part of bonding between adsorbate-adsorbent [248].

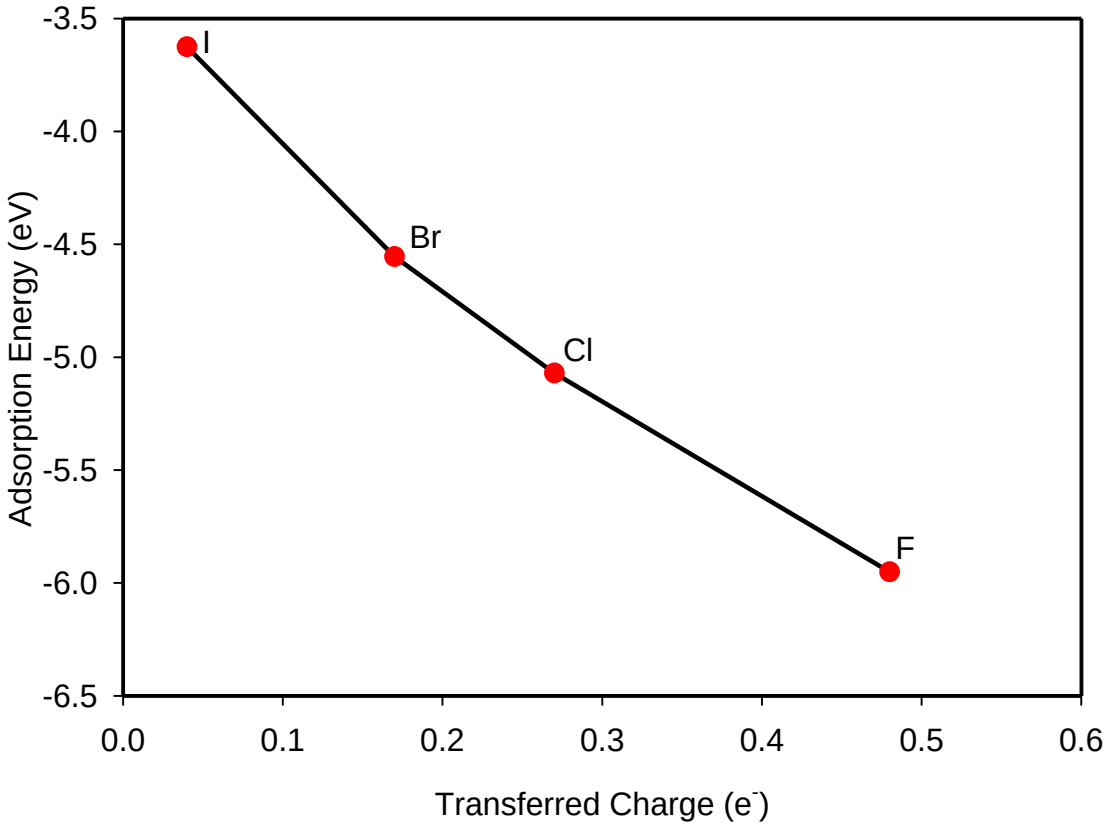

Figure 5-6: Charged transferred during halogen ion adsorption on Ti (100) surface.

5.1.4.2. Charge density difference

Interaction of halogen ions with Ti (100) surface influences charge transfer distribution of active species involved in the reaction, hence it becomes more crucial to analyse the charge density distribution after ion adsorption. The change in the electrochemical potential or electron activity at the metal surface has a profound effect on the rate of corrosion reaction. Charge density distributions were calculated by subtracting the charge density of the clean surface and that of a single halogen ion from the total charge density of the system as described in Eq. (3-38). All the charge density analysis between halogen ion and Ti atom were visualised by plotting a charge density difference. Figure 5-7 presents the charge density difference of the adsorbed halogen on the Ti (100) surface. The measurement of the charge is presented by different coloured regions, where the yellow and blue iso-region represent the charge depletion and accumulation, respectively.

Charge accumulation were established above the top-most Ti atoms, however, significant charge depletion is found to depend on the halogen atom. Different charge redistribution is observed during halogen ion interaction with Ti atoms. Figure 5-7 displays a charge accumulation along the adsorbates whilst the charge density towards Ti atoms decreases (yellow region), suggesting an apparent charge redistribution around the atoms. Previous researchers have demonstrated that the accumulation of electrons between adsorbed atom and a surface determines the interaction [251]. The 3D iso-surfaces of charge redistribution at the interface indicates that the charges are localised mostly on the F-Ti interaction.

The large charge redistribution leads to stronger electron depletion during the interaction [252]. Looking at the charge density analysis in Figure 5-7, it is apparent that the charge transfer is more pronounced on the F-Ti interaction than Cl-Ti, Br-Ti and I-Ti interaction. We noted that the effect charge redistribution is local and only the atoms involved in the adsorption bonding are affected. There is more charge density distribution observed on F-Ti interaction than other halogen atoms (Cl, Br and I). A large amount of charge transfer and their corresponding high adsorption energies indicates the stronger interaction between the halogen ions and Ti atom. It can be seen in Figure 5-7 that the electron charge density surface takes place in more than one Ti atom suggesting that the adsorption site involves an ionic interaction with more than one Ti atom from the surface. The stronger charge accumulation on the F atom indicates that more electron will exit from the Ti surface. These observations are in good agreement with the Mulliken charge analysis of -0.48 for F, -0.27 |e| Cl, -0.17 |e| Br and -0.04 |e| I. In addition, the values of the charge transfers also indicate that the Ti atom donates electrons to F, Cl, Br and I atoms. Amount of charge transferred is relative to the interaction strength between Ti and F, Cl, Br, I atoms.

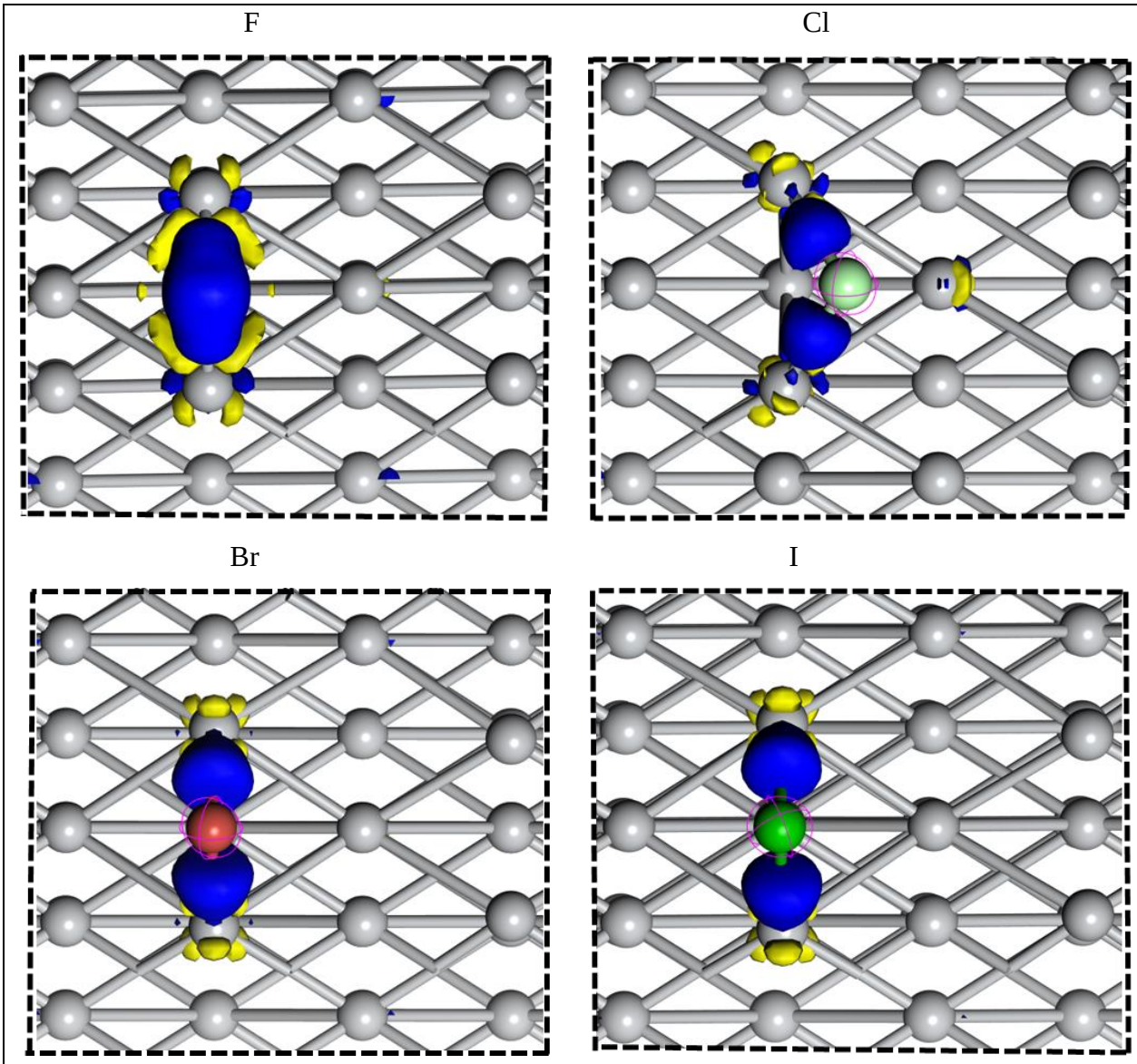

Figure 5-7: Charge density difference for (a) F-Ti, (b) Cl-Ti, (c) Br-Ti and (d) I-Ti. The blue region shows electrons accumulation while the yellow region shows electrons depletion.

5.1.4.3. Electronic density map

Electrochemical reaction either produce or consume electrons, thus the rate of electrons flow to or from a reaction interface is a measure of reaction rate [253]. Electron transfer during the interaction can be seen clearly on the electron density map, this facilitated the reaction between adsorbate and adsorbent. The distribution of charge for halogen ion adsorption was also examined using an electron density map. In Figure 5-8 and 5-9, show the exhibits of electron density population for each adsorbate on Ti (100) surface. In this 2D plot, the blue region indicates electron depletion, while electron enrichment is indicated in the red region. It can be that Ti atoms lost electrons whilst the halogen ions consumed electrons. This corresponds well with the aforementioned analysis of charge density difference analysis. A region of electron accumulation and loss differ with adsorbate, this is due to the electron-accepting ability and the nature of bonding between the halogen ions and Ti atoms.

For fluorine ion adsorption, the electron gain region is spherical and closely packed, while for chlorine, bromine and iodine we observed electron loss around the halogen atom. This is relative to the atomic radii of halogen ion and their electronegativity. There is stronger ionic bonding between the halogen ions and Ti atom and more electrons are gathering on the halogen ion atoms. However, the electronic region differs from ion adsorption. The electronic region for Ti-F is more than the electronic region on Ti-I this is due to different bonding strength between the ion and Ti atoms.

F Cl

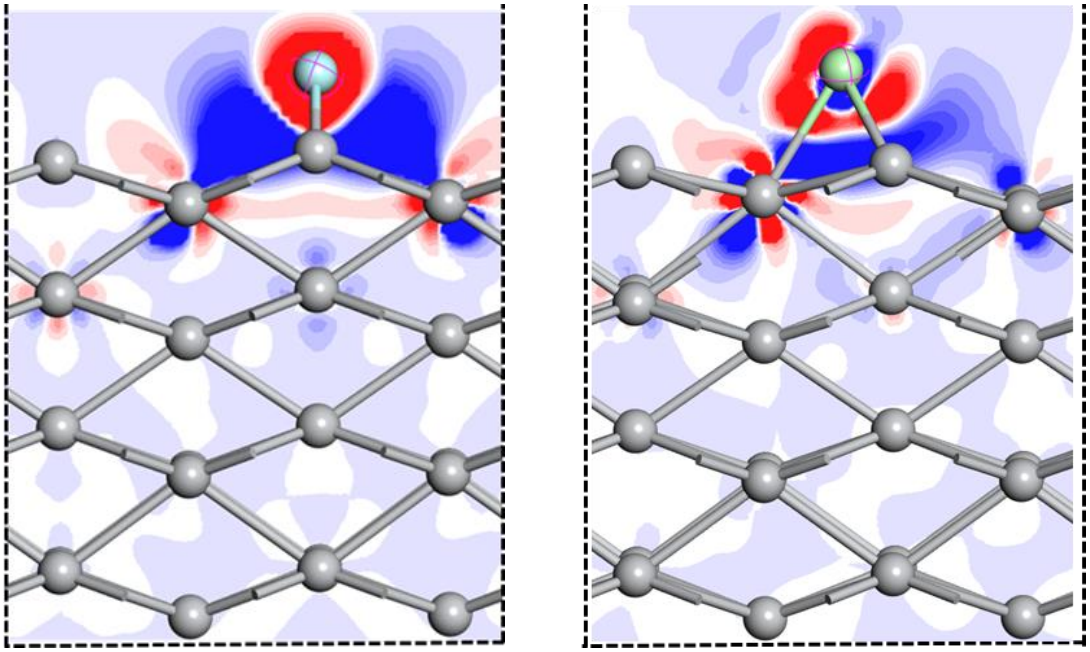

Figure 5-8: Electron density map of F and Cl adsorption on Ti (100) surface, with spectrum from -0.02 to +0.02 and set value of 16 bands. Blue and red region indicate electron loss and gain, respectively.

Br I

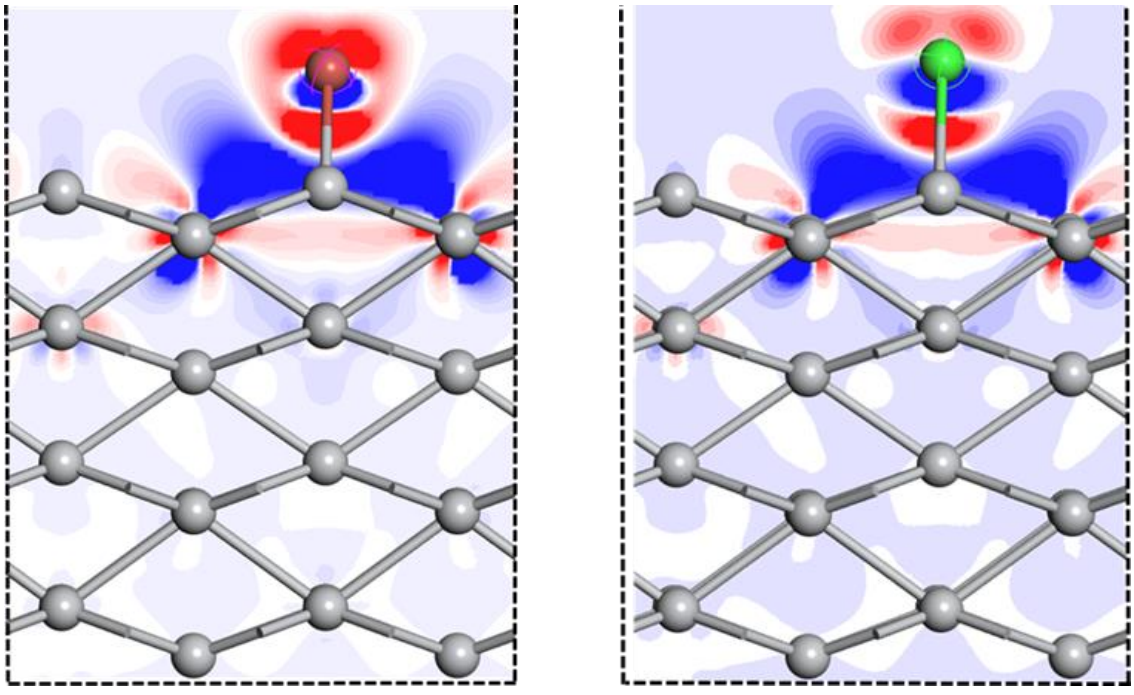

Figure 5-9: Electron density map of Br and I adsorption on Ti (100) surface, with spectrum from -0.02 to +0.02 and set value of 16 bands. Blue and red region indicate electron loss and gain, respectively.

5.1.4.4. Partial density of states

In order to evaluate the electronic interaction of halogen ions and Ti atoms, the corresponding partial density of states (PDOS) was plotted. The PDOS for free halogen molecules, pure Ti (100) surface and adsorbed Ti surfaces were analysed to understand the essential number of orbital states at the particular energy level. Figure 5-10 presents the PDOS profile for HF free molecule, pure and adsorbed Ti (100) surface. The PDOS plots for pure and adsorbed Ti (100) surface (Figure 5-10 bottom panel) show clearly that the states are well prominent and overlap from the valence to conduction band indicating metallic behaviour. The electronic peaks for a pure Ti (100) surface (Figure 5-10 middle panel) consist mainly of $3s^2\ 3p^6\ 3d^2\ 4s^2$, with predominately 3d-orbital states and less contribution from s- and p-orbital at the Fermi level. Furthermore, all the PDOS plot are characterised using pseudogap at the Fermi energy (E_F), which emerge from d- and p-orbitals. In all PDOS curves, the Fermi energy is located in the deep pseudogap of the p-orbital peak. PDOS for HF molecule (Figure 5-10 top panel) constitute of an electronic peak at -23.5 eV and -4.5 eV corresponding to s- and p- states.

After adsorption HF-Ti (100) surface the new peaks appear at the valence region at -29 eV and -7.5 eV, this shows the presence of fluoride-ion on Ti (100) surface as compared to PDOS of pure Ti (100) surface. Both the d- electronic curves for pure and adsorbed surface lies lower at the Fermi level. Comparing the adsorbed PDOS plot there is no significant difference for HCl, HBr and HI PDOS as compared to the clean Ti (100) surface, except the new electronic peaks emerging at different energy level. Figure 5-11 (top panel) depicts the PDOS plot for free HCl molecule shows electronic peaks at valence bond region around -13 eV and -3.5 eV, this electronic peak corresponds to s- and p- orbital for Cl atom. The Cl s- electronic peak lies very lower this suggests that s- orbital has no impact on bonding. In pure Ti (100) surface PDOS (Figure 5-11 middle panel) curves the d-band lies lower at the Fermi energy while after HCl adsorption the d- orbital lies at the top of the

Fermi energy. The electronic peak corresponding to the p- orbital state lies closer to the Fermi with less hybridisation from the s- orbital, this contributes to the formation of Ti-F and Ti-Cl bonding.

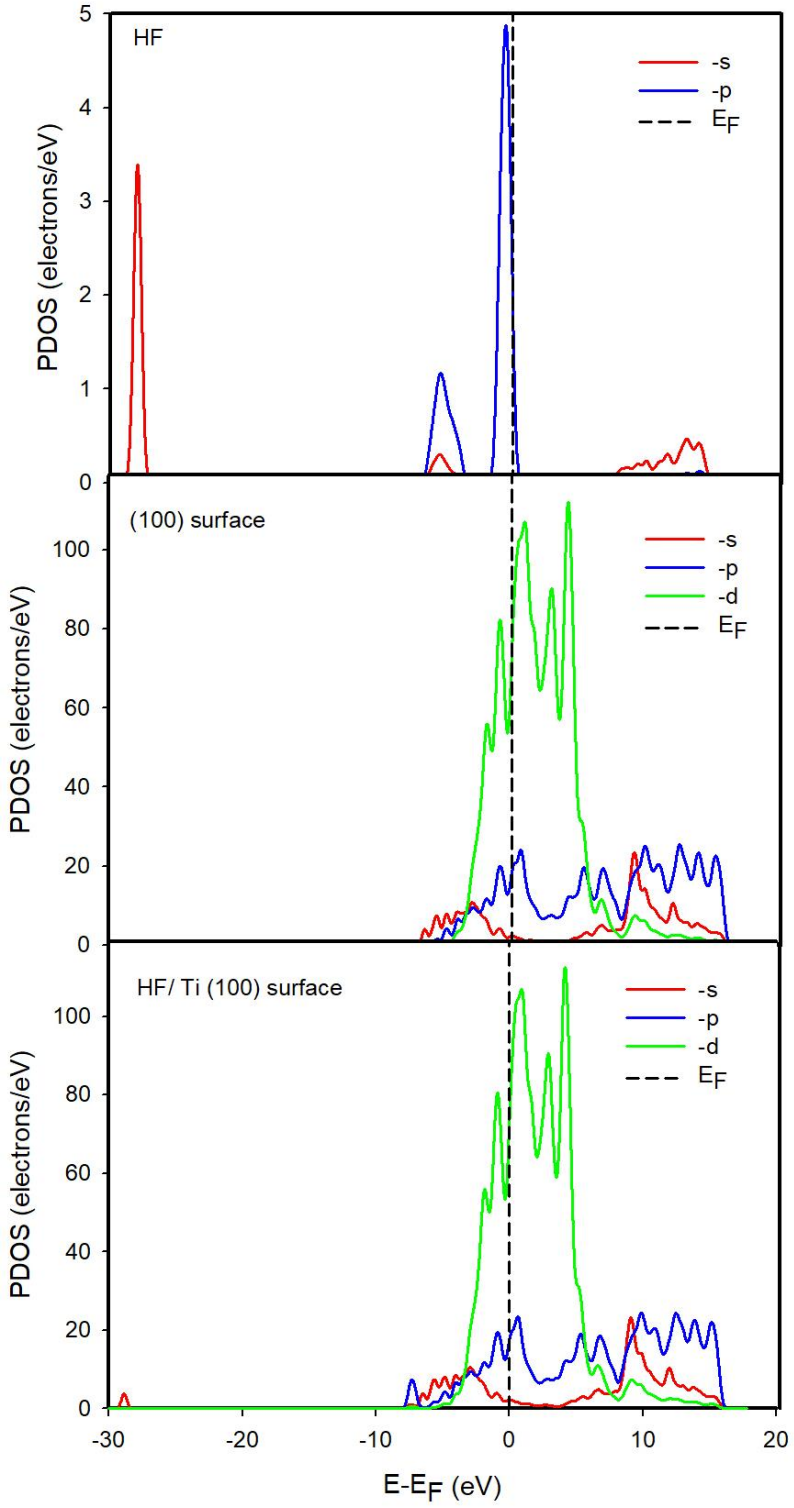

Figure 5-10: Partial density of states (PDOS) for HF free molecule, clean Ti (100) surface and HF/Ti (100) surface. The Fermi energy is taken as the energy zero.

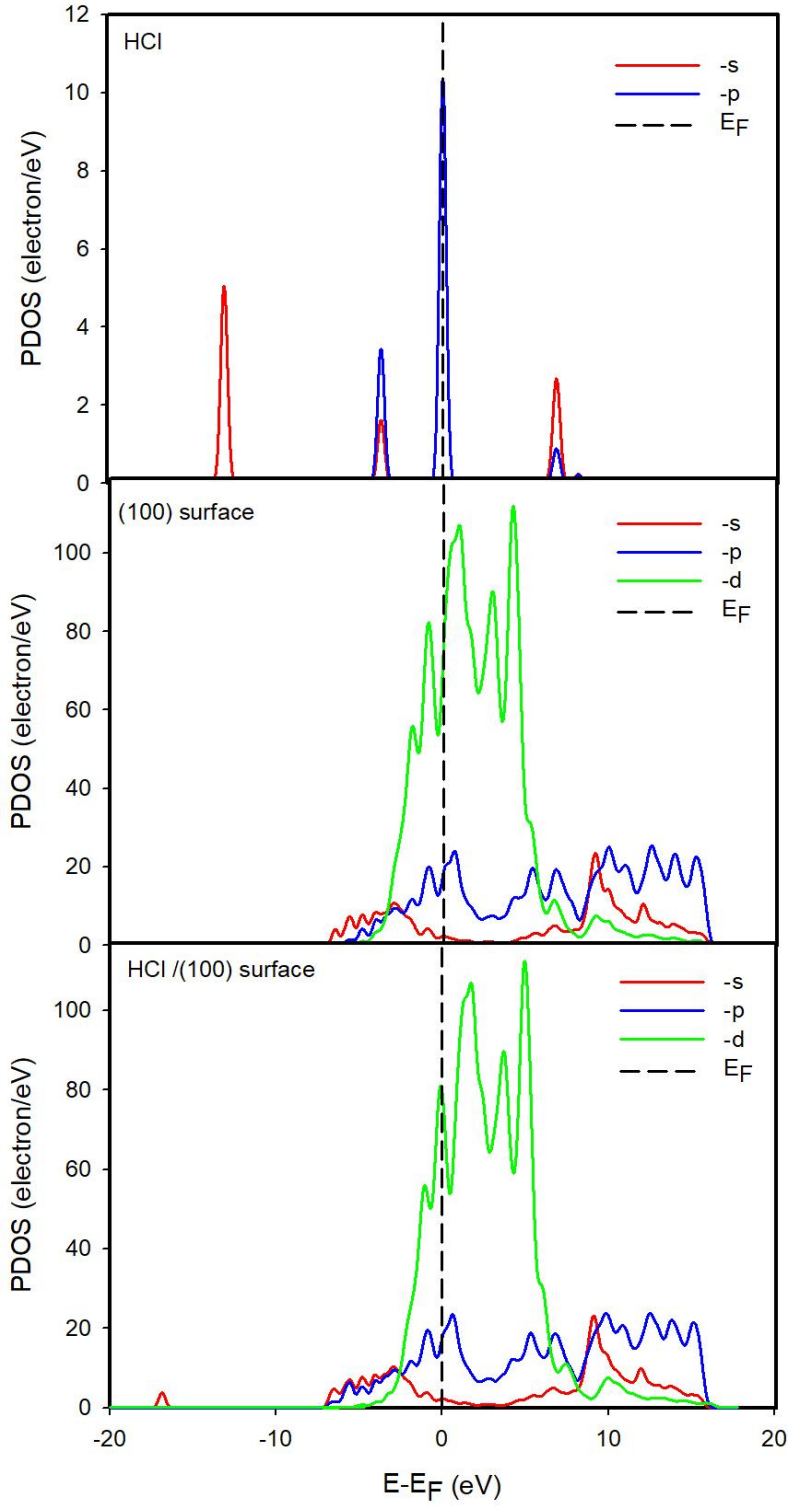

Figure 5-11: Partial density of states (PDOS) for HCl free molecule, clean Ti (100) surface and HCl/Ti (100) surface. The Fermi energy is taken as the energy zero.

Comparing the PDOS of a free molecule, clean surface and after adsorption, the PDOS plots show a significant change in electronic positioning especially for s- and p- orbitals for halogen atom. In Figures 5-12 and 5-13, show the PDOS for HBr and HI adsorption on Ti (100) surfaces, respectively. The molecular orbital for free HBr molecule present electronic peak (Figures 5-12 top panel) with -15 eV, -6.2 eV and -3.4 eV at valence bond region, mostly these electronic peaks corresponding to Br s- and p- orbital. However, Br s- orbital (-16.3 eV) lies very lower, this implies Br s- orbital plays no impact in bonding.

The PDOS for HBr-Ti (100) surface (Figures 5-12 bottom panel) shows a new peak at the VB region around -16.3 eV and -6.2 eV this corresponds to Br s- orbital and Br p- orbital respectively. However, the electronic peak around -6.2 eV (Br p- orbital) combine with some contribution from Ti s- and d- orbital. This suggests some hybridisation between the orbital. Figure 5-13 (bottom panel) present the PDOS profile for HI adsorption, for free molecular orbital the electronic peak for I s- orbital lies around -12.4 eV while I p- orbital appears around -5.5 eV. Comparing both PDOS profiles for a clean and adsorbed surface, the PDOS shows significant changes in the peak shape and positioning as well as a slight decrease in Ti d- orbital states. This implies that the total energy decreases after HBr and HI adsorption.

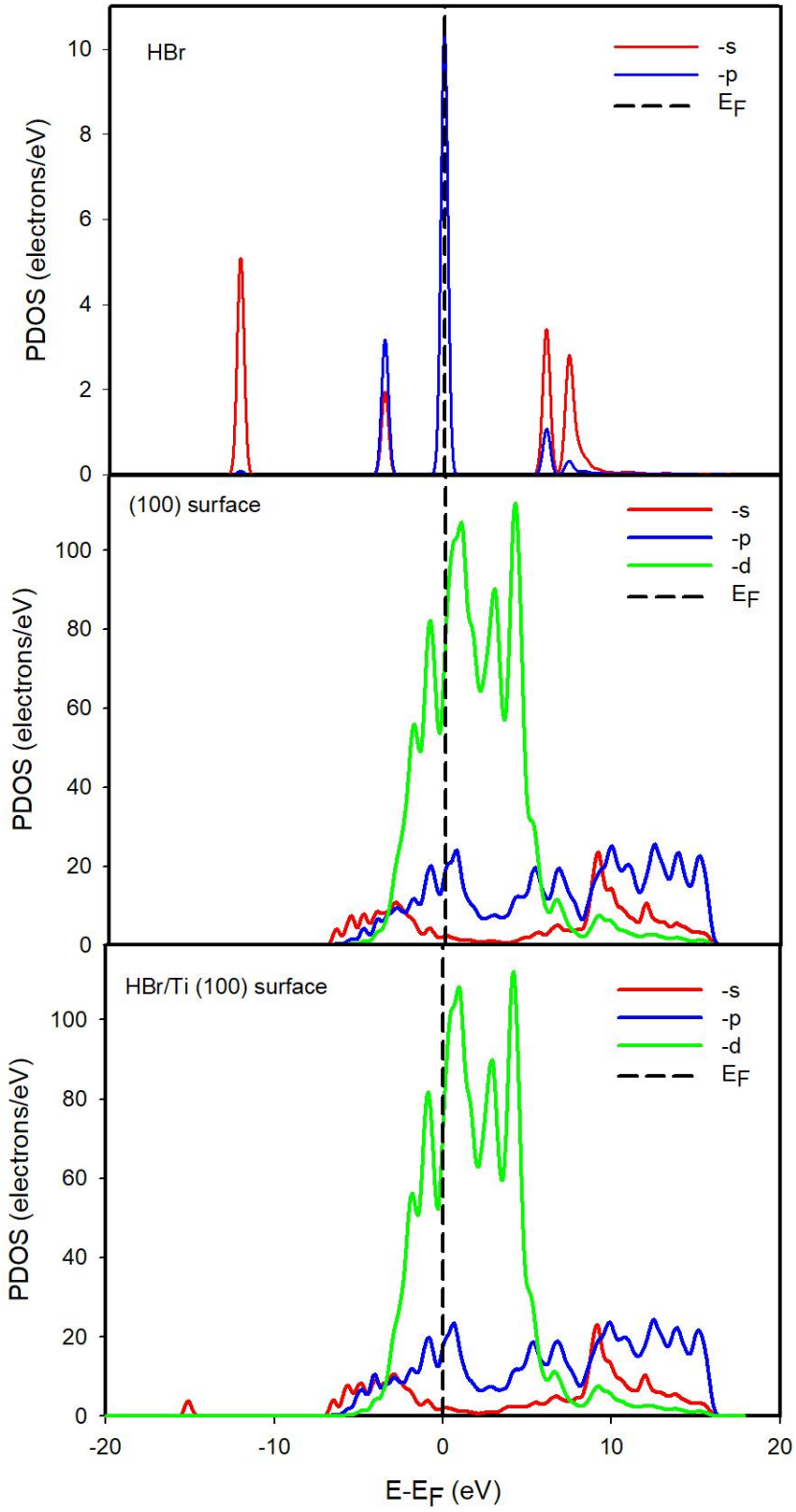

Figure 5-12: Partial density of states (PDOS) for HBr free molecule, clean Ti (100) surface and HBr/Ti (100) surface. The Fermi energy is taken as the energy zero.

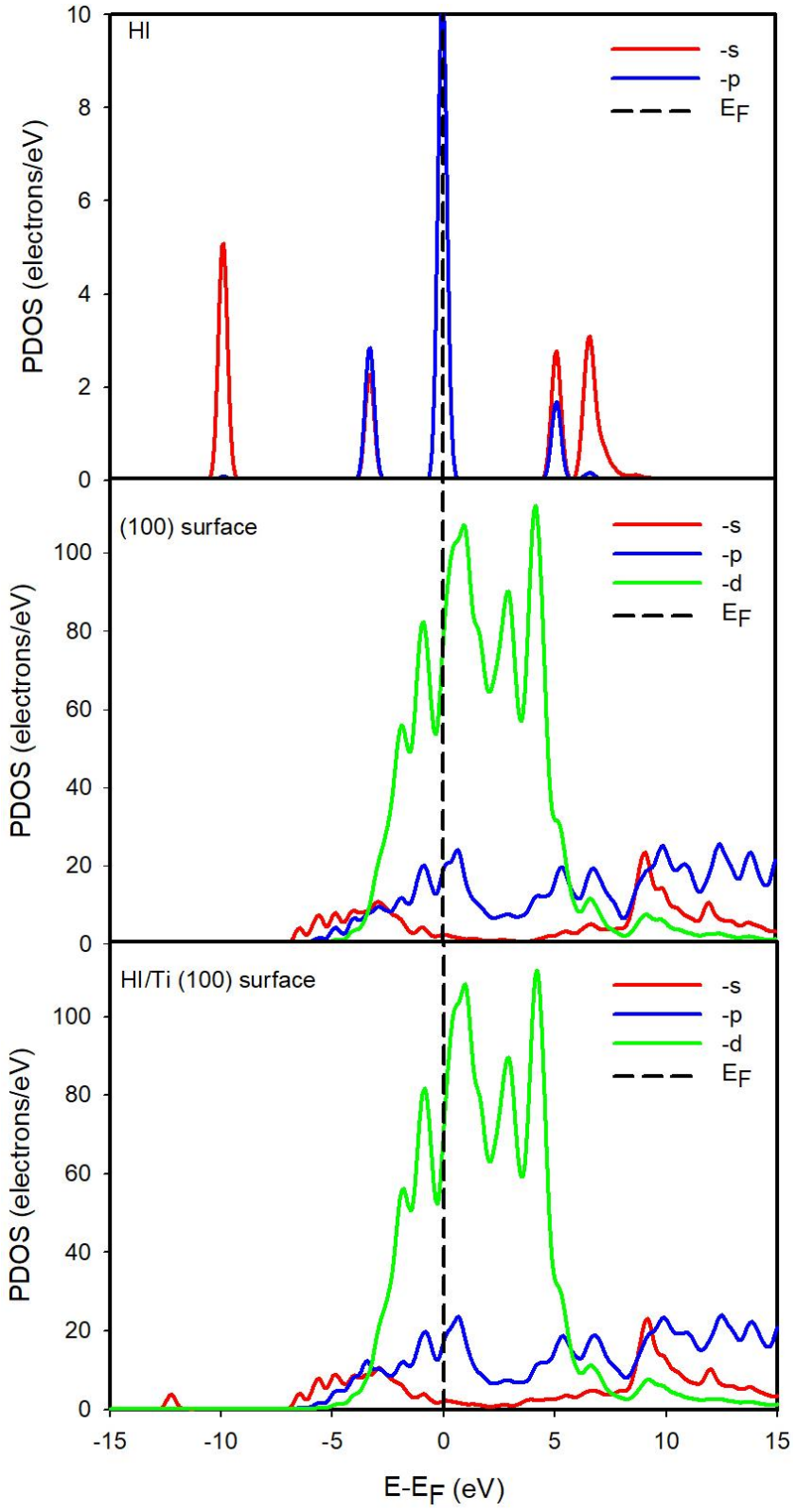

Figure 5-13: Partial density of states (PDOS) for HI free molecule, clean Ti (100) surface and HI/Ti (100) surface. The Fermi energy is taken as the energy zero.

5.1.5. Work function

The computed work function (Φ) of adsorbed Ti (100) surface is presented in Figure 5-14. In the adsorption system, the work function also play important role in understanding the interaction [254]. It was found that all halogen ion adsorbed changes the work function as compared to the clean surface (3.665 eV). The magnitude of the induced work function varies from the halogen-adsorbed atom. We note that the adsorption of F, Cl, and Br increase the value Φ while I decrease the work function. The value of work function after F adsorption was found to be 3.797 eV, for Cl (3.727 eV), Br (3.672 eV) and I (3.626 eV). This suggests that the stronger adsorption halogen ion (F, Cl and Br) lead to the increase of the work function as compared to the free Ti (100) surface.

Depending on the halogen ion adsorption, the work function value decreases with respect to the halogen atom as seen in Figure 5-14. The decrease of Φ value as a function of adsorption is due to the increase of halogen atom size and decrease in electronegativity [241]. Moreover, we noted that the work function of adsorbed Ti (100) surface decrease with decreasing in charge transfer during halogen ions (F, Cl, Br and I) interacting with Ti atoms. Correspondingly, the Φ and charge transfer during Ti-F interaction is 3.797 eV and 0.48 |e| whereas for Ti-I bonding the work function and charge transfer is about 3.626 eV and 0.08 |e|, respectively. Previously, the study demonstrated that the decreasing of work function was related to the charge transfer after halogen adsorption [254].

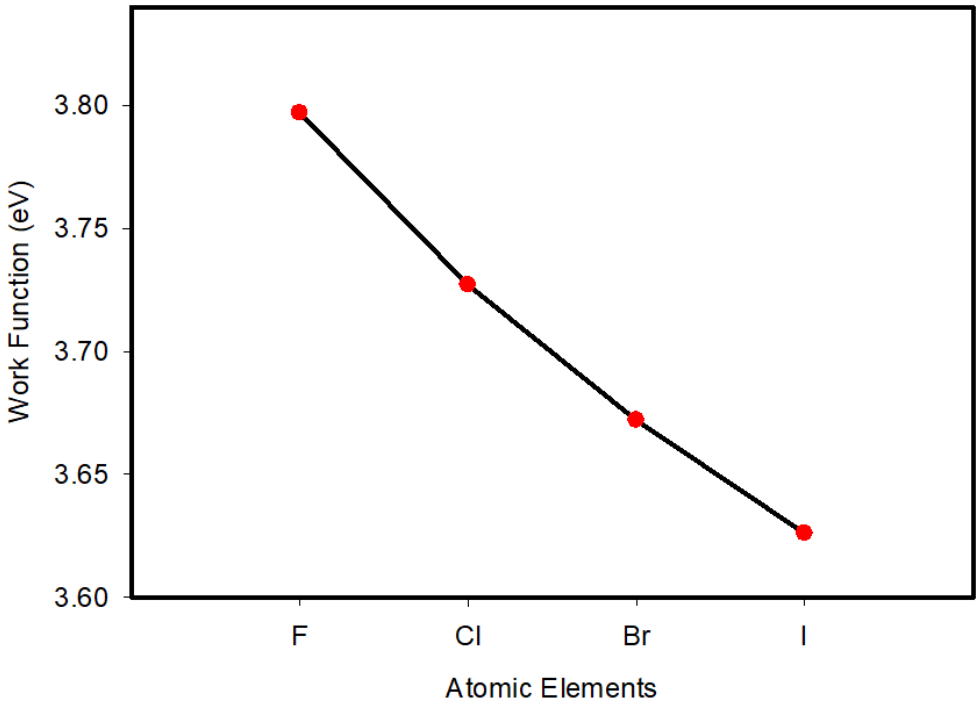

Figure 5-14: Calculated work function (Φ) against halogen ions adsorbed on Ti (100) surface.

5.2. Adsorption of halogen molecules on Ti (110) surface

All halogen molecules and ions were adsorbed on Ti (110) surface slab to explore their adsorption behaviour and interaction. The adsorption energy, charge density difference as well as density of states for the halogen molecules adsorbed on the Ti (110) surface are analysed. Some of the results in this section have been published [255]. The interaction strength of halogen ions and molecules has been determined by comparing their adsorption energies,

5.2.1. Dissociative adsorption of halogen molecules on Ti (110) surface

The dissociative adsorption process of molecular species and atomic at the surface is a key factor governing surface chemistry, in some aspects this is the same process discussed in the previous section (section 5.1.1). Dissociation adsorption of halogen molecules on Ti (110) surface is considered to evaluate their interactions and molecule splitting reaction. This surface reaction is accompanied by structural and chemical changes.

In Figure 5-15 the description of halogen molecules interacting with the Ti (110) surface is shown. The minimal bond length between the halogen molecules was estimated from 0.924 to 1.961 Å (HF-HI) that agrees with the experimental bond length value [256]. All halogen molecules were placed on top Ti (110) surface, the initial position (2 Å) was taken as minimum height positions above the Ti (110) surface. The use of initial positions of the molecule closer to the Ti surface is due to dissociation into a pair of separate during the optimisation. Figure 5-15 (a-d) presents the adsorption steps (initial, intermediate and dissociation adsorption) for all halogen molecules adsorption on the Ti (110) surface. We observe that during optimisation, the molecules approach the Ti (110) surface, which led to bond length elongation and rupture (molecule dissociation). The halogen bond length stretched to (HF= 3.65 Å), (HCl= 3.99 Å), (HBr= 3.39 Å) and (HI= 4.65 Å) as shown on the intermediate step. The bond length of halogen molecules ruptured forming titanium halides, denoting that the entire halogen molecule dissociates completely on Ti (110) surface.

In this process, the dissociated halogen ions remain negatively charged and bonded to the positive charge of Ti atoms whilst the hydrogen (H^+) atom remaining positively charged. More importantly, the halogen ions (F^-, Cl^-, Br^- and I^-) are chemically bonded to the neighbouring Ti atoms with a bond length of 1.930 Å for Ti-F, Ti-Cl (2.28 Å), Ti-Br (2.62 Å) and Ti-I (2.74 Å). Note that no lattice hydrogen atom is bonded to the surface. The distance between hydrogen and the nearest Ti atom after dissociation is 1.97 Å for H-F, 1.97 Å (H-Cl), 1.95 Å (H-Br) and 1.93 Å (H-I). This hydrogen distance value turns to be less for HI molecule than HF, HCl, and HBr. Thus, the interaction of halide ions with Ti atom is crucial for molecule splitting reaction to take place [39, 244]. Tshwane and his co-workers reported similar dissociation mechanism on TiO_2 (100) and Ti (110) surface [257]. A similar phenomenon of dissociative adsorption of halogen molecules was reported experimentally and theoretically [258, 259].

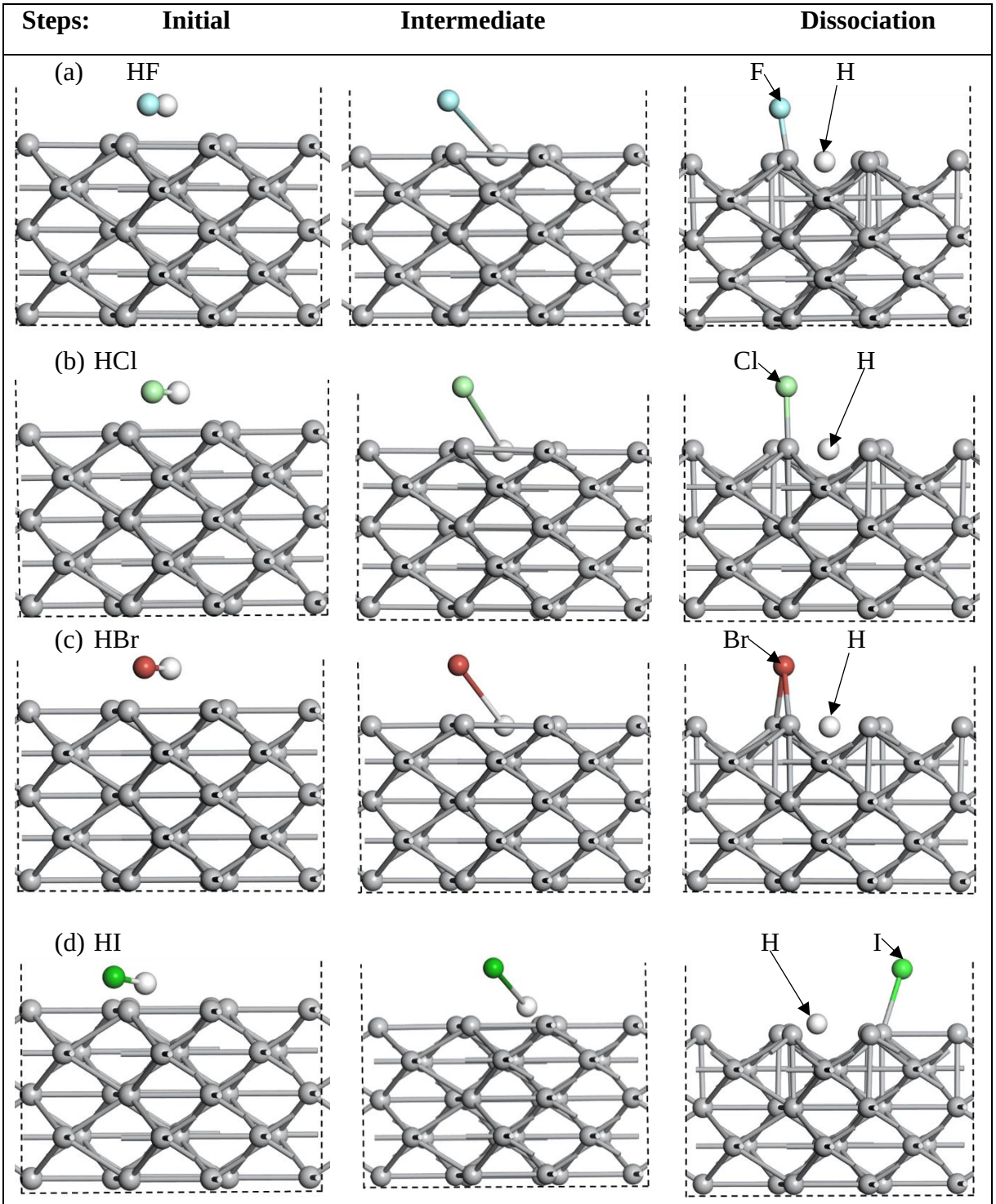

Figure 5-15: Optimised atomic side-view of halogen molecules (HF, HCl, HBr and HI) adsorption process on Ti (110) surface. Each adsorbate shows the initial configuration step, intermediate and dissociated adsorption. The surface of Ti atoms shown in grey, whereas the atoms for the specific molecules indicated by the arrows.

The dissociation mechanism for all halogen molecules on Ti (110) surface was found to be similar. It was observed that all halogen molecules adsorption mechanism was found to prefer top site adsorption on Ti (110) surface, whereas, the HBr molecule prefers the bridging site. However, it can also be observed that the Br atom bonded to two Ti atoms after dissociation, this suggesting that Br prefers a short bridging position. The interaction of a halogen molecule with the Ti surface leads to halogen molecular bond breakdown and binding with the Ti atoms. It was observed that halogen molecules dissociate on the Ti (110) surface with the formation of a relatively stable bond of halogen and titanium atoms. The halide –Ti atom bonding is important in this section, in which it defines most of the processes that govern the halogen molecule dissociation and interaction with the Ti atom. The dissociation of all halogen molecules on Ti (110) surfaces accompanied by adsorption energy strength. Dissociation adsorption process is the most fundamental characteristic of the adsorption process that determines the adsorption strength of the molecule [260].

Adsorption energy refers to the energy released upon adsorption of halogen molecules on Ti (110) surface. The adsorption energy of halogen molecules on the Ti (110) surface was calculated using the expression (3-37) as discussed in section 3.8.2 (Chapter 3). In Figure 5-16, the adsorption energy dependence of halogen molecules on Ti (110) surface is presented. All the adsorption energies for halogen molecules were found to be negative indicating that the reaction is spontaneous. The large negative E_{ads} value shows the stable exothermically of the adsorption process mechanism whereby HF molecule found to be the most energetically favourable. HF molecule was found to be more thermodynamically favourable with adsorption energy (E_{ads}) of -3.523 eV while the HI molecule is the least favourable with an adsorption energy value of (-3.153 eV). According to our findings for halogen molecule adsorption on Ti (110) surface, it can be seen that the adsorption energy per molecule gradually increases following the order HF > HCl > HBr > HI (Figure 5-16).

A similar adsorption behaviour trend of this halogen was observed on the Iron surface by Guo *et al* [261] and the results are also consistent with the previous calculation of halogen adsorption on the metal oxide surface [262].

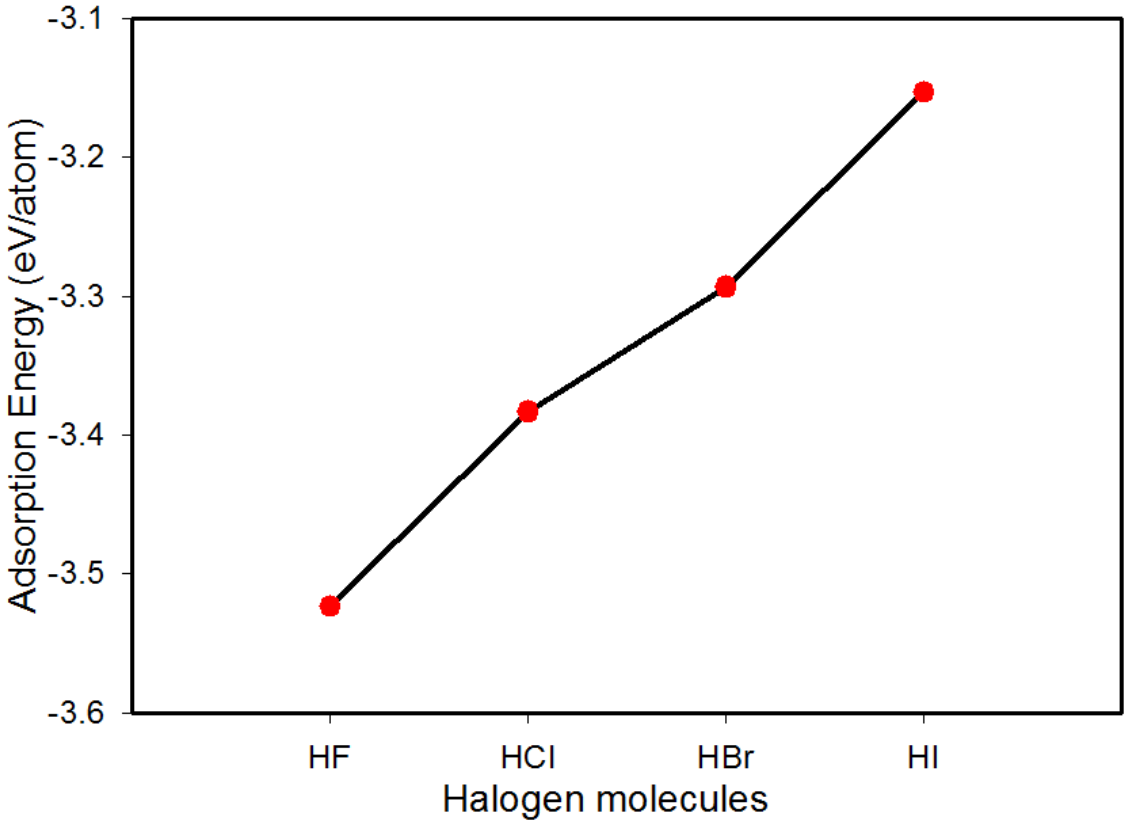

Figure 5-16: Adsorption energy dependence per halogen molecule adsorption on Ti (110) surface.

5.2.2. Adsorption energy of halogen ions on Ti (110) surface

In this section, the halogen ions adsorption on Ti (110) surface at different adsorption sites and their adsorption positions are investigated. Much focus is on ion adsorption on Ti (110) which is relevant to a surface chemical reaction, aqueous solution etching and corrosion [39]. In order to understand better the halogen ions interaction on Ti (110) surface, halogen ions are adsorbed on Ti (110) surface at different adsorption positions. The stability of the adsorption position is determined by the adsorption energy strength with respect to surface sites, their adsorption energies were calculated using the Eq. (3-37) and the results are listed in Table 5-2. Our results showed that all halogen ion

adsorbed spontaneously in all adsorption surface positions. Comparing the adsorption energies at different adsorption site, the top site position was found to more favourable followed by the hollow and bridging site for all halogen ion adsorption. This supports the observation found in section 6.1 on the halogen molecules adsorption mechanism. In order to investigate the order of halogen ion interacting with Ti (110) surface, their adsorption energies are analysed. There is a significant difference in the adsorption energies per halogen ion adsorption. The negative values of adsorption energies indicate that the adsorption of halogen ion on Ti (110) surface is energetically favourable.

Fluorine ion showed more preferential adsorption energy on both top (E_{ads}^{F}= -6.950 eV) and hallow sites (E_{ads}^{F}= -5.593 eV), whilst iodine is less stable for all adsorption sites. Chlorine is more preferential on the bringing site (E_{ads}^{Cl}= -4.730 eV). This indicates that F-ion exhibits the strongest adsorption strength on the Ti (110) surface followed by Cl and Br ion, and the least interaction is observed with I atom. This is comparable with the findings by Nguyen *et al* [247] on Si surface using spin-polarized DFT-PBE functional. In addition, similarities were observed by Pasti *et al* [171] on halogen (Cl, Br, and I) adsorption on crystallographic (111) planes of Pt, Pd, Cu and Au using PWscf code of the Quantum ESPRESSO distribution using PBE functional within GGA.

Table 5-2: Calculated adsorption energies (eV) for halogen ions at Ti (100), Cu (111) and Si surfaces at different adsorption site.

Adsorption site		**F^-**	**Cl^-**	**Br^-**	**I^-**
Present @ Ti (PBE)	Top	-6.950	-4.830	-4.349	-3.495
	Bridge	-4.403	-4.730	-4.185	-3.489
	Hollow	-5.593	-4.795	-4.288	-3.489
[247] @ Si (PBE)	-	-5.29	-3.22	-2.41	-1.29
[171, 166] @ Cu (PBE)	Top	-4.05	-3.13	-2.80	-2.41
	Bridge	-4.41	-3.46	-3.10	-2.71
	hcp	-4.49	-3.52	-3.16	-2.76

Figure 5-17 presents the adsorption energy dependence for each halogen ion species on Ti (110) surface. The adsorption energy values for each ion correspond to the top site adsorption configuration. The magnitude of adsorption energy decline with the increase of the atomic number of halogen atoms as seen in Figure 5-17. We found that the trend of adsorption energy strength varies in the order of F>Cl>Br>I for the top adsorption site. These findings are consistent with the previous observation on halogen-adsorbed silicene [247]. It was found the adsorption energy trend follows the periodic rule, $E_{ads}^{F} > E_{ads}^{Cl} > E_{ads}^{Br} > E_{ads}^{I}$ which is a similar progression of halogen electronegativity order.

The analysis of this fact shows that an anion with higher electronegativity (F^-) has a strong bond interaction strength than other halide ions like Cl^-, Br^- and I^- exhibit weakly bonding. The adsorption strength of fluorine on Ti (110) surface on top site is by 2.12 eV higher as compared to chlorine adsorption. Adsorption energy of bromine on the top site is 0.854 eV lower as compared to chlorine and is greater by 0.481 eV for iodine adsorption. Moreover, the difference in the adsorption energies

for iodine is significantly less for all adsorption site, this attributed to a different covalent radius. Present result revealed that the adsorption energies decreased with the increasing atomic size of the halogen. This confirms that fluorine adsorption on Ti surface is more preferential than Cl, Br, and I adsorption. Similar work by Pasti *et al* [171] also demonstrated that the halides adsorption energy on Pd, Pt, Cu and Au (111) surface decrease with an increase of ion radius.

In addition, the adsorption energies (E_{ads}) of halogen ion are significantly larger (less negative value) when compared to the adsorption energy strength of the halogen molecule in section 5.2.1. Therefore, the dissociative adsorption of halogen molecules is much less favourable than halogen ion adsorption. Adsorption energies for halogen molecule appear to be very close to each other, while the adsorption energy difference for halides differs by order of ~2 eV. Thus can be concluded that halide ions are mostly attractive towards Ti surfaces than halogen molecule. The adsorption energy of adsorbate is mostly dependent on the solvation energy (dissociation energy). For instance, HF/F has lower dissociation energy as shown in Table 4-1 (Chapter 4), hence it exhibits strongly chemical bonding, while HCl, HBr and HI show weakly chemical bonding with Ti atoms. Furthermore, the high electronegativity exhibits lead to appreciable levels of bonding and adsorption in which facilitates the influence of electrochemical reactivity. The chemical bonding of ionic species depends on electrostatic considerations.

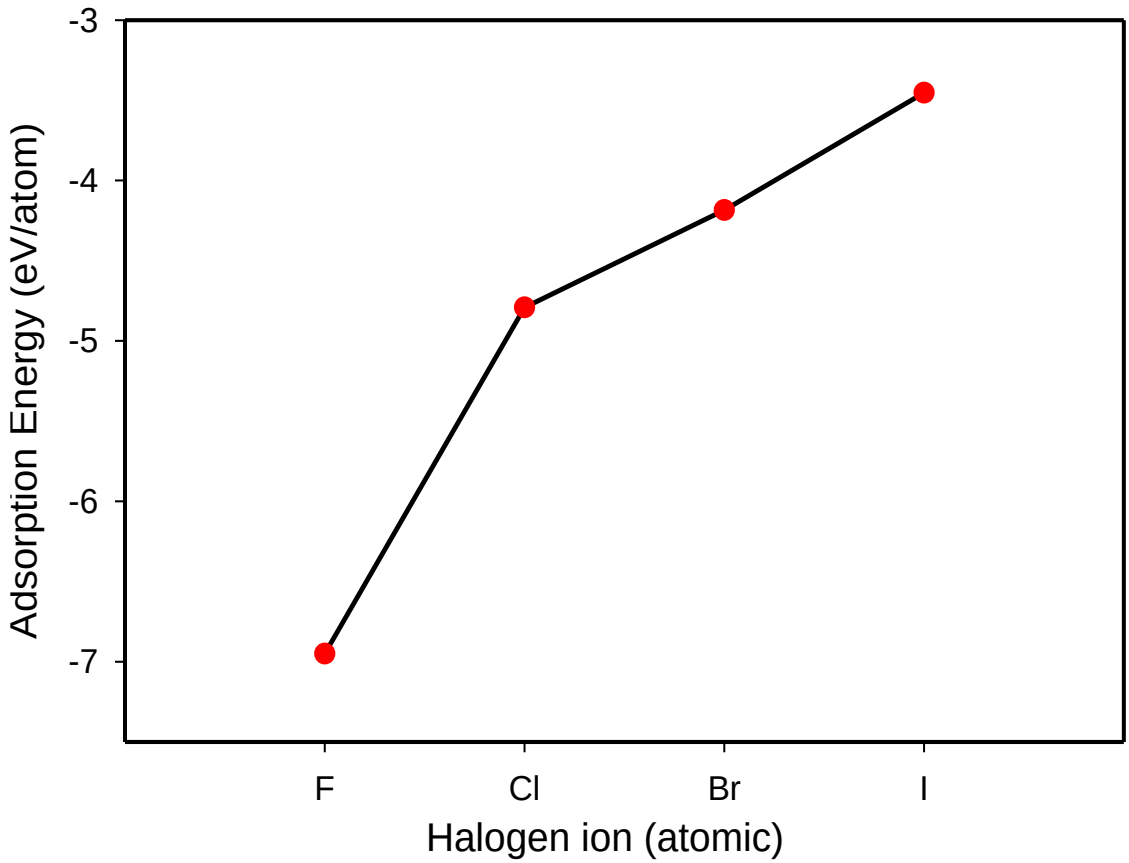

Figure 5-17: The adsorption energy of halogen ions (F, Cl, Br and I) on Ti (110) surface.

5.2.3. Adsorption geometry of halogen ions on Ti (110) surface

In this section adsorption of halogen ions (F^-, Cl^-, Br^-, I^-) on Ti (110) surface were analysed as it remains the same for an interaction between a Ti metal and electrolyte solutions. The metal-electrolyte interface is characterised by the presence of an electronic charge on the metal surface. Adsorption of a single halogen ion was considered and placed on top of the Ti (110) surface. Figure 5-18 (a-d) shows the atomistic model of halogen ions adsorption on Ti (110) surface. Initially, all halogen ions were placed at the same position height (2 Å) from the Ti atom surface. After optimisation, each halide ion forms a preferred bond with the Ti atom, for Ti-F (1.812 Å), Ti-Cl (2.268 Å), Ti-Br (2.434 Å) and Ti-I (2.859 Å).

Our results show that there is a very strong tendency for F^- to interact with Ti atom the interaction than Ti-I interaction. In general, surface interaction brought little change to the ion bond length. The bond length of Ti with halogen ions significantly increases from 1.81-2.85 Å (F^- to I^-) indicating a different nature of the interaction. Also, this is due to their different atomic radii, which is much bigger for I than that of F atom distance, the interaction bond length of Ti-I is larger than Ti-F bond distance [263].

Figure 5-19 depicts the adsorption energies of halogens on the Ti (110) surface as a function of adsorption bonding length at the top adsorption site whereby the analysis shows a linear relationship. The four data points show the smallest adsorption distances between surface titanium and F, Cl, Br and I increasing with decreasing adsorption energy strength. This trend suggests that there is a strong force of interaction between Ti and F atom than Ti and I atom. The displacement interaction of Ti surface with halogen atoms is in the sequence of F-Cl-Br-I, which is the decrease of adsorption energy whilst from more to less electronegativity. Present analysis of this fact shows that the adsorbate with the higher electronegativity (F^-) has a strongly bound solvation shell whilst other halides ions like Cl^-, Br^- and I^- exhibit weakly bound solvation shells [39].

Relative to the sum of atomic bond length of Ti atom with halide ions, the length increases with a decrease in electronegativity [241]. The electronegativity parameter is related to the chemical potential wherein a higher value indicates better chemical potential. In this calculation, I ion fail to have a stable configuration at the adsorption site as shown in Figure 5-18 (d), this because it tends to migrate to the other site during structural relaxation, with the corresponding adsorption energy of -3.493 eV was determined see Figure 5-18.

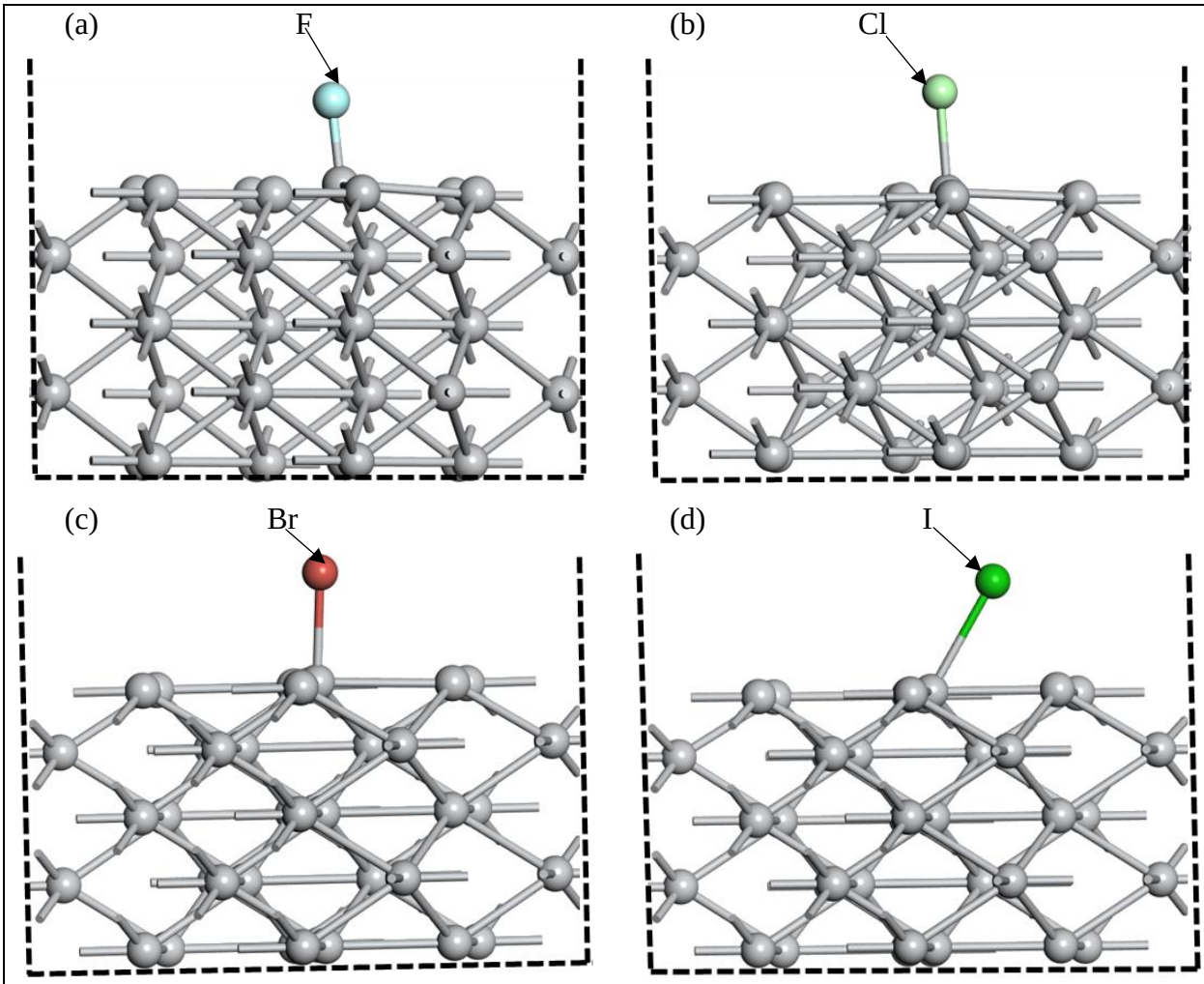

Figure 5-18: Optimised structure of halides ion adsorption on the Ti (110) surface: (a) F-adsorption, (b) Cl-adsorption, (c) Br-adsorption and (d) I-adsorption.

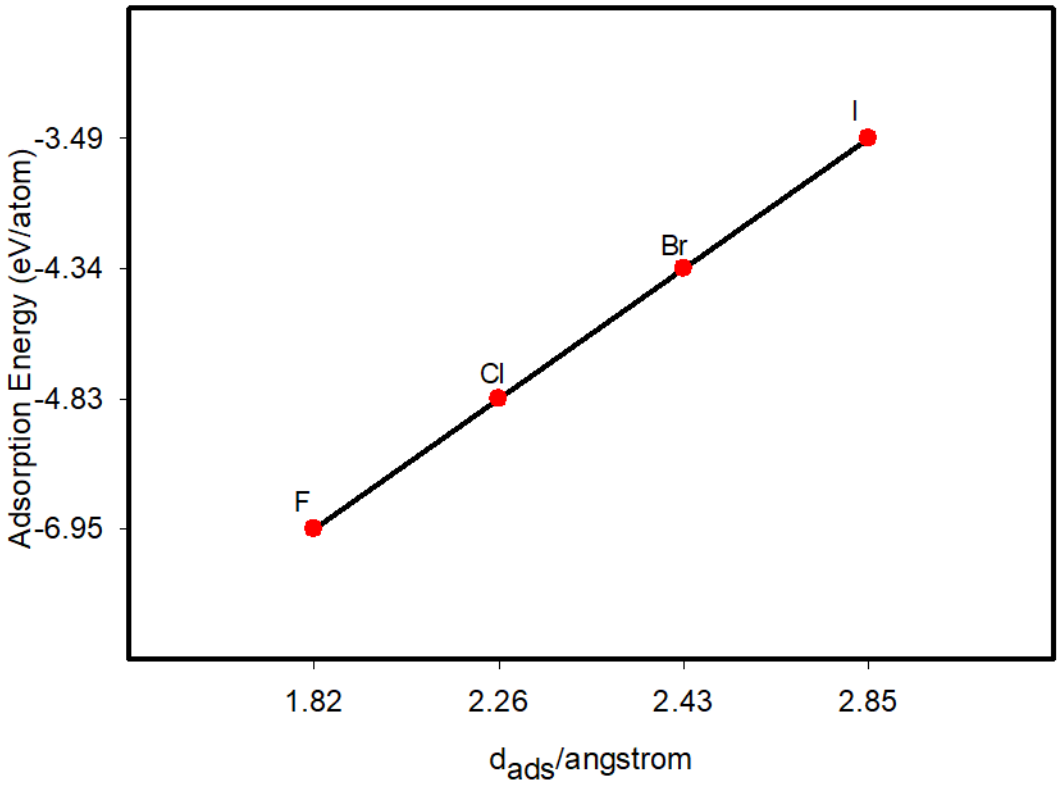

Figure 5-19: The adsorption energy of halogen ions with respect to adsorption distance.

5.2.4. Electronic properties of halogen adsorption on Ti (110) surface

5.2.4.1. Electron charge transfer

To further, gain some insight into the halogen interacting with Ti atom surfaces, Mulliken charge analysis was performed to calculate the electron transferred during adsorption. Since the halogen atoms have five-valence p- electrons, they try to attach to the Ti surface atom to get an extra electron to fill the outermost shell. The adsorption energy between halogen atoms and the metal surface typical reaches several electron-volts where it decreases with the rows of the periodic table for all halogen and metals [161]. Figure 5-20 shows the relationship between the adsorption energy with charge transferred (e^-) for each halogen atom. We see that the interaction between halogen atoms and Ti (110) surface result in a substantial amount (0.54 |e|) of charge transfer depending on the adsorption energy strength.

It was found that all the adsorbents are electron acceptors with 0.08-0.54 |e| obtained from Ti (110) surface. It has been reported that the dependence of electron transfer on halogen ion relies on the atomic electronegative strength and adsorption energy stability [169]. Since all the halogen molecules possess a higher electronegativity value than the Ti atom (1.5 eV), it suggests that the transfer of electrons from the surface to a molecule can occur. Furthermore, the halogen atom interacts strongly with Ti atoms lead to the acceptance of more charges from the surface. It can be said that electron transfer is induced by electronegativity. Fluorine accepts more charge (-0.54 |e|) than all other halogen atoms since it has a higher electronegativity. Thus, the trend in charge transferred strength is F (-0.54 |e|)> Cl (-0.35 |e|)> Br (-0.25|e|) > I (-0.08 |e|). The analysis indicates that the halogen ion behaves as a charge acceptor from the Ti (110) surface. Moreover, the large amount of charge transfer and the corresponding adsorption energies indicate the stronger interaction between the halogen ions (F, Cl, Br and I) and Ti atom.

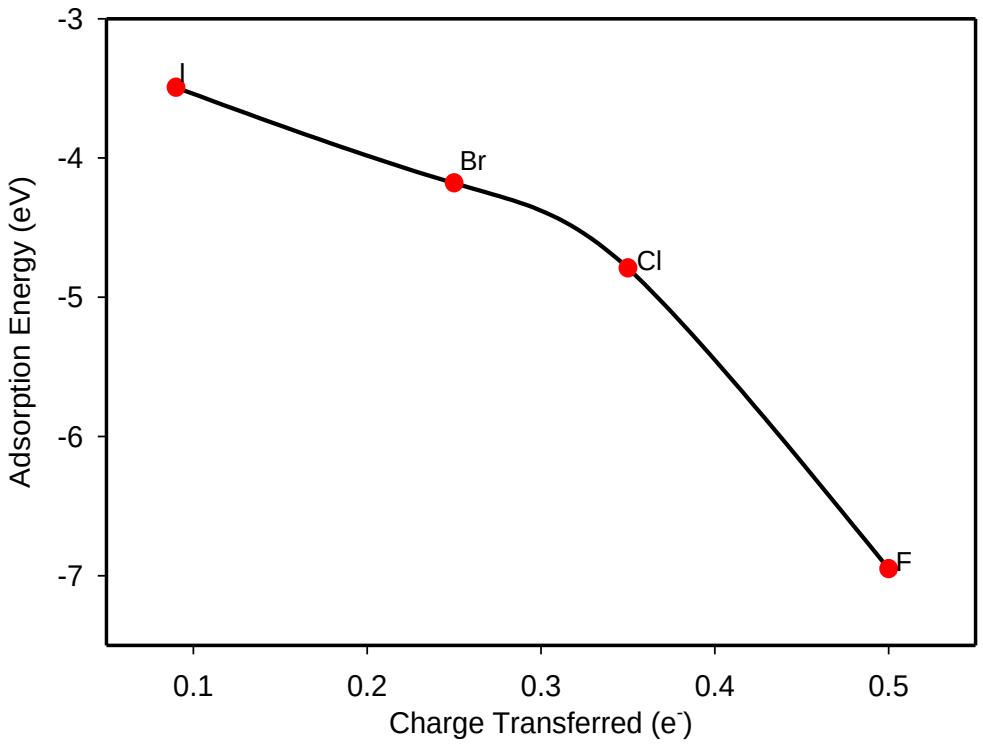

Figure 5-20: Charge transferred on Ti (110) surface after halogen ion adsorption.

5.2.4.2. Charge density difference

Adsorption of halogen ions on Ti (110) surfaces leads to charge redistribution due to electronic hybridisation between the orbitals of the halogen ions (adsorbate) and Ti atoms (adsorbent). The interaction between halogen ions with Ti atom surface implies a significant charge transfer at the interface. Charge density difference for halogen ion adsorption on Ti (110) surface was calculated using the same Eq. (3-38). The charge densities for substrate and ions were obtained from the same geometries as in the substrate and molecule interaction. Charge density difference shows how charges are shared among the atoms during bonding. Adsorption of halogen ion interaction with the Ti atom surface implies a significant charge transfer at the interaction. Therefore, since while charge transfer influences the redistribution of active species involved in the corrosion reaction it is important to analyse the charge transfer during adsorption.

Figure 5-21 (a-b) presents the charge density difference of the adsorbed halogen on Ti (110) surface for the top site. The magnitude of the charge is shown by different colours where blue and yellow represents charge accumulation and charge depletion, respectively. The plots show that titanium atom surface found to be polarised upon adsorption of halogen and electrostatic interaction play a crucial role in the attractive interaction. It was observed that the electron density is around the adsorptions atoms on the surface. We observe that charges are depleted from the Ti and accumulated on the halogen atom. Furthermore, a directional bonding of spherical shape is observed which suggest that the charge distribution between surface Ti and halogen exhibit ionic bonding behaviour. It is known that the change density difference for ionic bonding exhibit a charge density map that is localised on a single atom [264]. Generally, the chemical bond formed by halogen atoms with metals is intermediate between ionic and covalent [161] with the degree of bond ionicity depending on the particular halogen-metal pair.

We found that the degree of bond ionicity decreases down the row of periodic table F>Cl>Br>I. Interestingly, the charge density differences show that electrons transfer take place at the interface between halogens and Ti atoms. Both F and Cl atom accumulate large charge distribution closer to the atom while Br and I accumulate less charge distribution. The notable bond length change of Ti-F suggest a sizable charge redistribution. A localised electronic density depletion in the Ti atoms forms the bond with adsorbate and more delocalised depletion in the area of F-Ti bonding is observed. Furthermore, the charge density shape distribution remains similar for F and Cl, whereas for Br and I changes completely this is due to Ti-Br and Ti-I interaction weakened. The charge density plot shows a spherical charge distribution implying ionic bonding of Ti-halogen.

However, the polarisation in fluorine/chlorine is stronger than that in Br and I medium, which gave rise to large interaction energy. This explain why the interaction have a large adsorption energies of (-6.95 eV, -4.792 eV) for F^- and Cl^- than Br^- and I^- (-4.185 eV, -3.493 eV), respectively. The dependence of charge density and charge transfer is probably attributed to the dipole of the adsorbate halogen, demonstrating the weak Van der Waals interaction on Br and I than F and Cl on Ti atoms. This is reasonable for smaller charge and larger charge redistribution during the interaction.

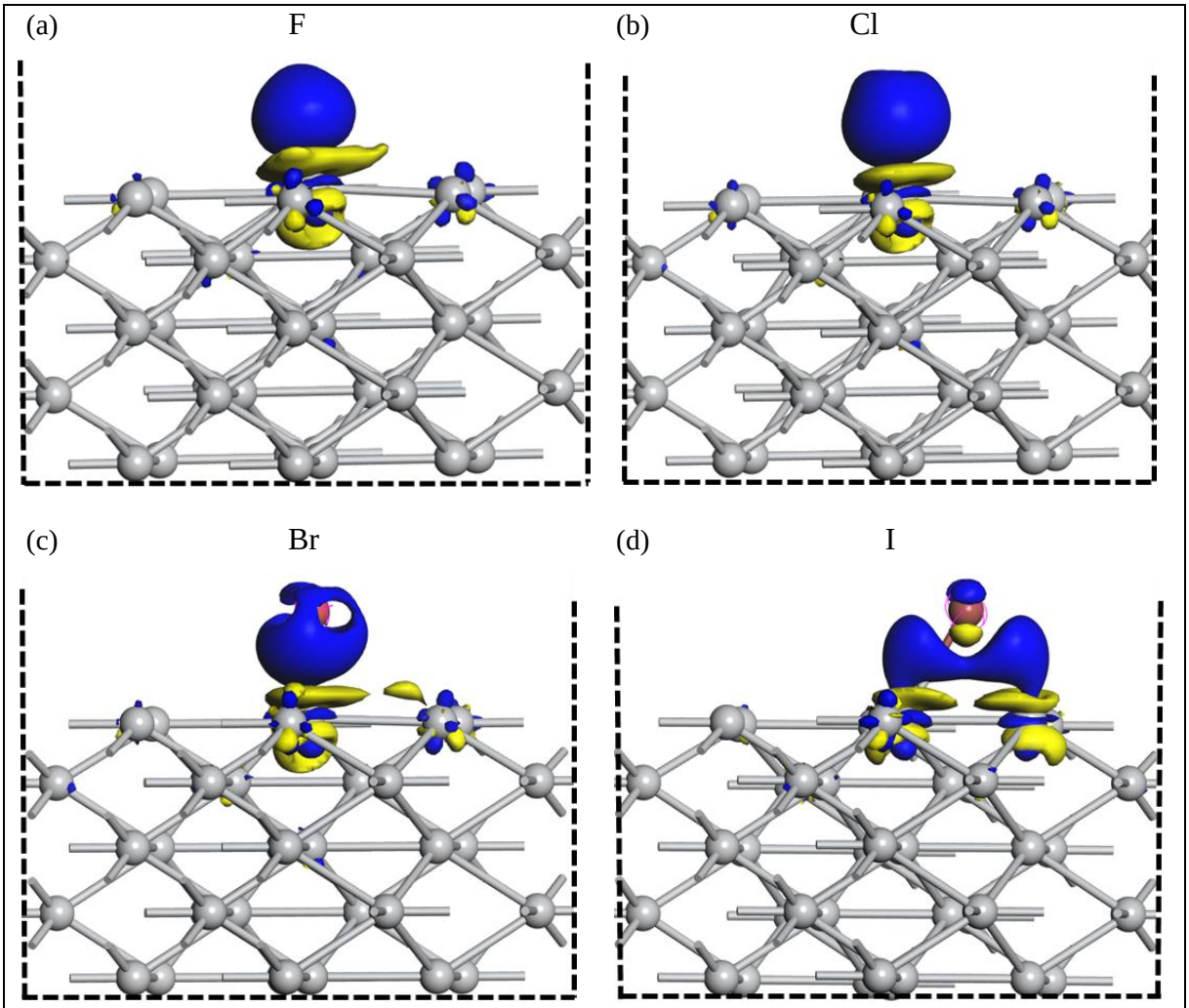

Figure 5-21: Charge density difference for (a) F-Ti, (b) Cl-Ti, (c) Br-Ti and (d) I-Ti. The blue region shows electrons accumulation while the yellow region shows electrons depletion.

5.2.4.3. Electron density map

Furthermore, the redistribution of charge for halogen ion adsorption was examined using electron density differences. Figure 5-22 (a-d) shows exhibits of electron density population of each halogen atom interaction with Ti atom. This facilitated the reaction between adsorbate and surface adsorbent. In this 2D plot, a loss of electrons is indicated by a blue region, while electron enrichment is indicated in the red region. It is clearly seen from Figure 5-22 that Ti atoms lost electrons and halogen ions gained electrons. This corresponds well with the aforementioned analysis of charge density difference analysis. The region of electron accumulation and loss differed with adsorbate which is due to the electron-accepting ability and the nature of bonding between the halogen adsorbate and adsorbent. For fluorine ion adsorption, the electron gain region is spherical and closely packed, while for chlorine, bromine and iodine we observed electron loss around the halogen atom. This is relative to the electronegativity and atomic radii of halogen ion.

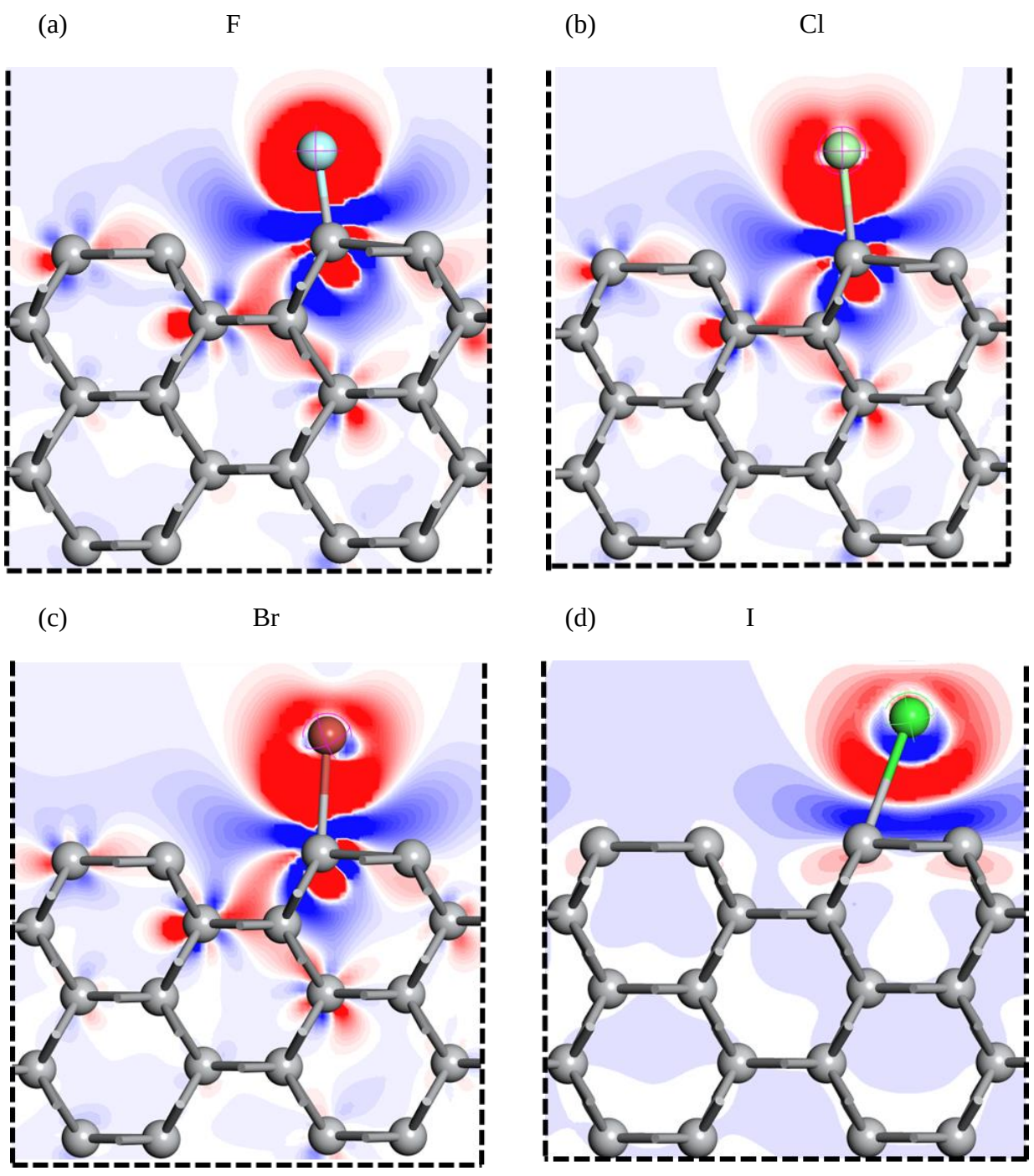

Figure 5-22: Electron density map of F, Cl, Br and I adsorption on Ti (110) surface, with spectrum from -0.02 to 0.02 and set value of 16 bands. Blue and red region indicate electron loss and gain, respectively.

5.2.4.4. Partial density of states

The projected density of states (PDOS) calculated to analyse the electronic structure free halogen molecules, Ti (110) surface and halogen-Ti bonding. Figure 5-23 shows the PDOS for pure HF molecule, clean Ti (110) surface and interaction of HF-Ti (110) surface. PDOS plots show the valence and conduction bands composed with the lowest energy band from -30 to +20 eV. The electronic peaks of Ti (110) surface consist mainly of $3s^2\ 3p^6\ 3d^2\ 4s^2$, with predominately 3d-orbital states and less contribution from s- and p-orbital at the Fermi level. Clearly, the states are well pronounced and overlap from the valence to conduction band (indicating metallic behaviour).

The PDOS for the clean and adsorbed Ti surface are characterised by a pseudogap at the Fermi energy (E_F) which emanate its contribution from d- and p-orbital. In all PDOS plots, the Fermi level is located in the deep pseudogap of the p-orbital peak. We observe a slight decrease in the magnitude of the halogen adsorbed PDOS peaks as compared to the clean Ti surface. The PDOS for molecular orbital of HF consists of $2s^2$ (-25.6 eV) and $2p^5$ with $\sigma_{H\text{-}F}$ (-5.5 eV) and lone pair of electrons of ρ_F orbital (-0.52 eV). The fluorine s- orbital lies very low around ~-25.6 eV and which contributes less minimum role in the bonding. PDOS for adsorbed HF/Ti (110) surface slightly decreased as compared to clean Ti surface, this suggests that the total energy decreases after molecule adsorption.

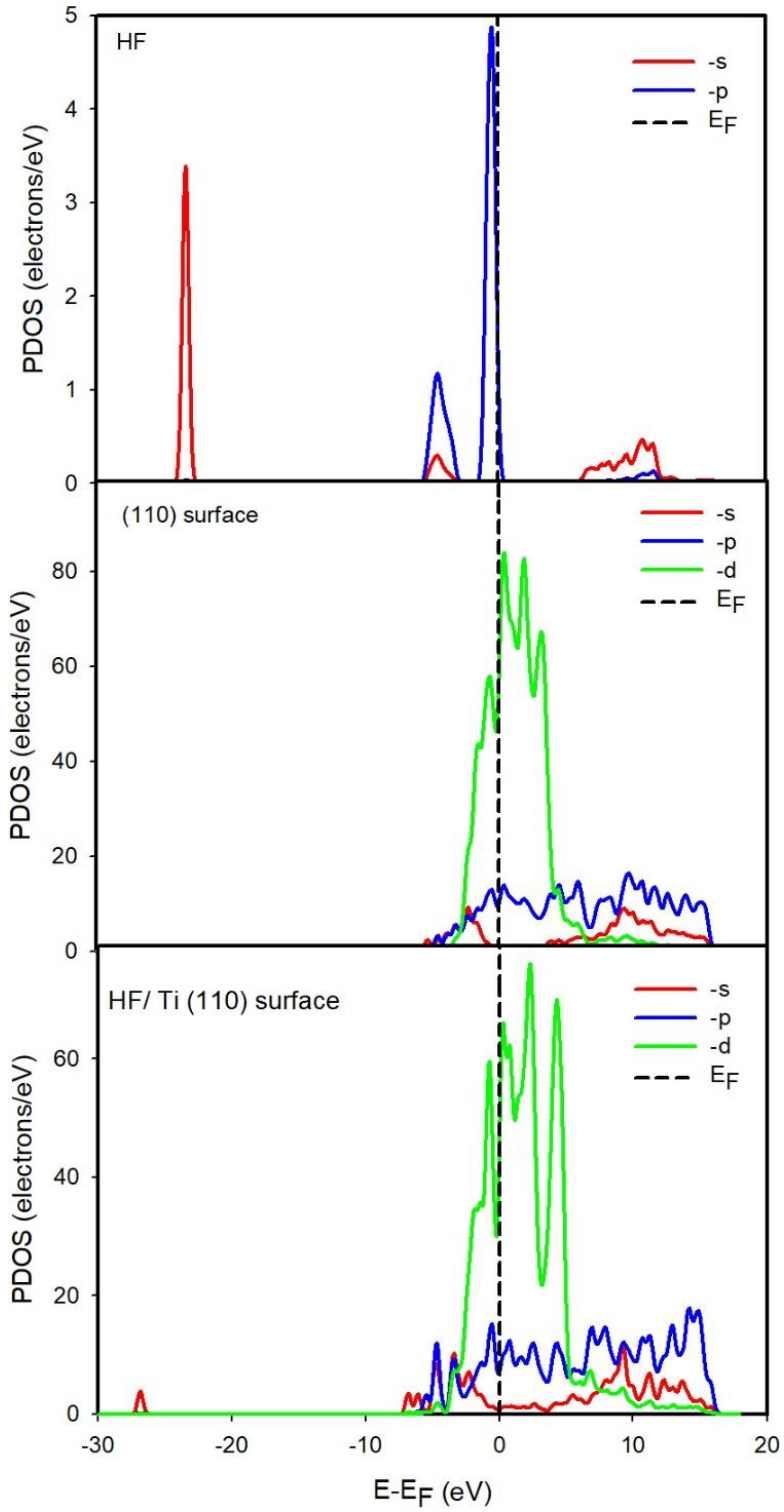

Figure 5-23: Partial density of states (PDOS) for HF free molecule, clean Ti (110) surface and HF/Ti (110) surface. The Fermi energy is taken as the energy zero.

In addition, after HF molecule adsorption new peaks appeared around -29 eV and -5.5 eV, the electronic peak of s- orbital (-29 eV) lies very deep and doesn't contribute to the role bonding. Moreover, the electronic peaks of s- and p- orbital appear around -5.5 eV denoting the sp-hybridisation. This revealed that the interaction of Ti-F bonding could be through F p- and Ti s-electrons. There is no significant difference for the HCl, HBr and HI PDOS as compared to the clean Ti surface, except that the states have shifted slightly to the conduction band after adsorption. This is consistent with the predicted adsorption energy of these halogen molecules.

Figure 5-24 presents the PDOS of free HCl molecule, clean Ti (110) surface and adsorbed HCl/Ti (110) surface. According to the PDOS curves, the molecular orbital of the free HCl molecule composed of the electronic peak of $3s^2$ (-13 eV) and $3p^5$ at -4.5 eV. After adsorption, the PDOS curve for Ti (110) and HCl/Ti (110) surface changes slightly. The electronic peak of $3s^2$ (-13 eV) shifted a little towards the left, while the electronic energy of the d- state decreases and become broader. In addition, for HCl/Ti (110) surface the electronic peak around -4 eV corresponding to p- and s- orbital, which reveal the formation of Ti-Cl interaction.

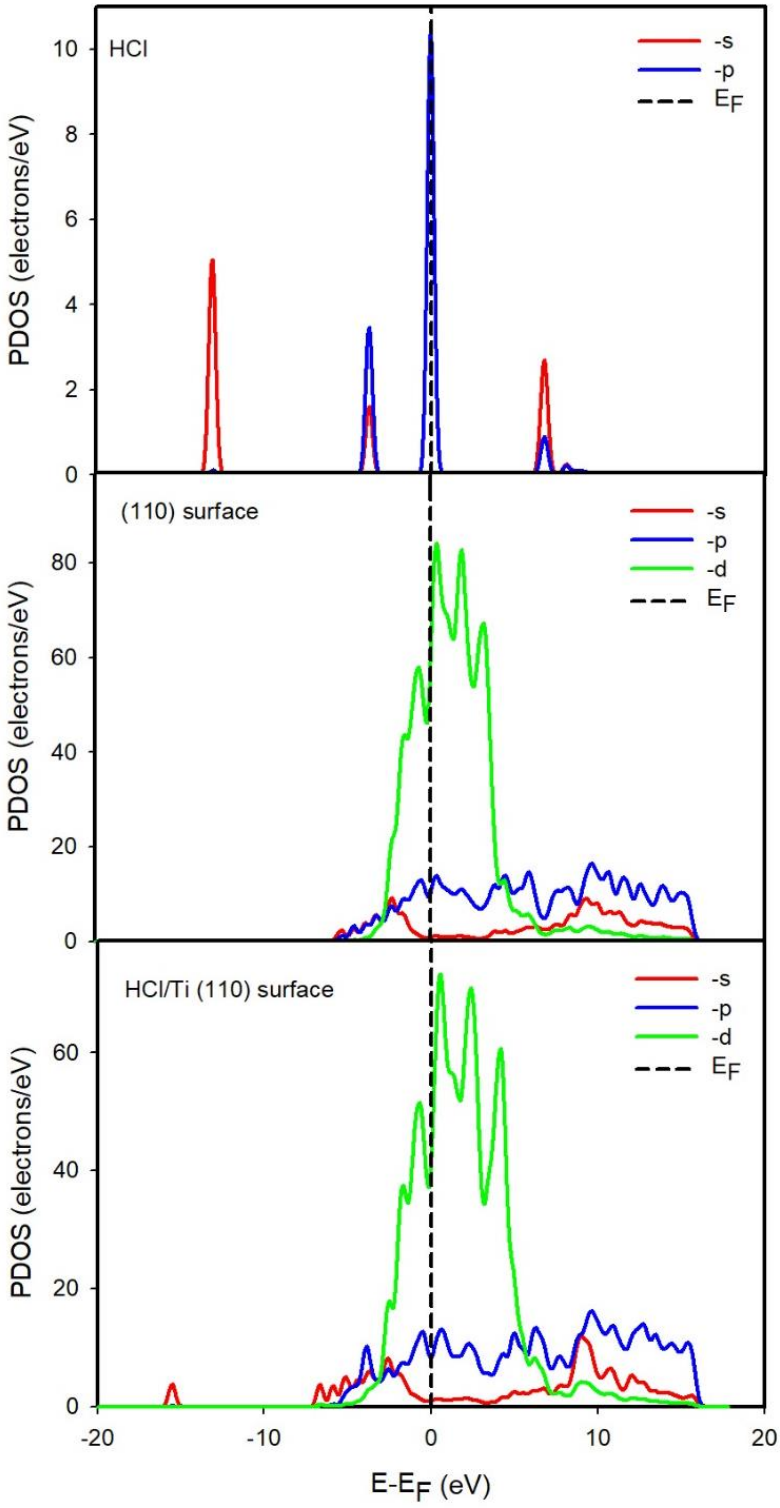

Figure 5-24: Partial density of states (PDOS) for HCl free molecule, clean Ti (110) surface and HCl/Ti (110) surface. The Fermi energy is taken as the energy zero.

The PDOS plots for a free HBr molecule clean Ti (110) surface as well as HBr/Ti (110) surface are presented in Figure 5-25. The PDOS of a free HBr molecular orbital consist of $4s^2$ (-12.5 eV) orbital and $\sigma_{H\text{-}Br}$ around (-3.6 eV) and ρ_{Br} orbital at (-0.4 eV). Electronic peak around -3.6 eV consists of Br $3p^5$ orbital with some contribution of s- state from the hydrogen atom. To evaluate the nature of the orbital for HBr/Ti (110) surface, after adsorption the new peaks appear around -15.6 eV and -3.8 eV, corresponding to the electrons from Br s- and p- states. Moreover, the adsorbed electronic peaks for s_{Br} –s orbital shifted to -15 eV as compared to the free molecules, this electronic peak lies very deep indicating no contribution in bonding. The electronic peak around -4 eV corresponds to the p- state of the Br atom and s- state of the Ti atom.

Figure 5-26 shows the PDOS curves for HI free molecule, pure Ti (110) surface and adsorbed HI/Ti (110) surface. The PDOS plot for free HI molecule presents the electronic peak around -12 eV and -3.2 eV, which correspond to s- and d- orbital states. After adsorption of HI molecule the electronic peak for p- orbital from the molecule hybridised with s- orbital from Ti atom, the electronic peaks hybridised around -3.2 eV. This suggests the bonding formation between Ti-I atoms. In addition, the electronic energy of d- orbital decreased after molecule interaction as compared to the d-electronic energy for pure Ti (110) surface. Moreover, it was found that the adsorption of halogen resulted in p- electronic peaks emerging at different energy level. The electronic peaks move from ~ -5.5 eV to -3.2 eV for F to I atom, respectively. This suggests the bonding formation between Ti-I atoms is less than the interaction of Ti-F.

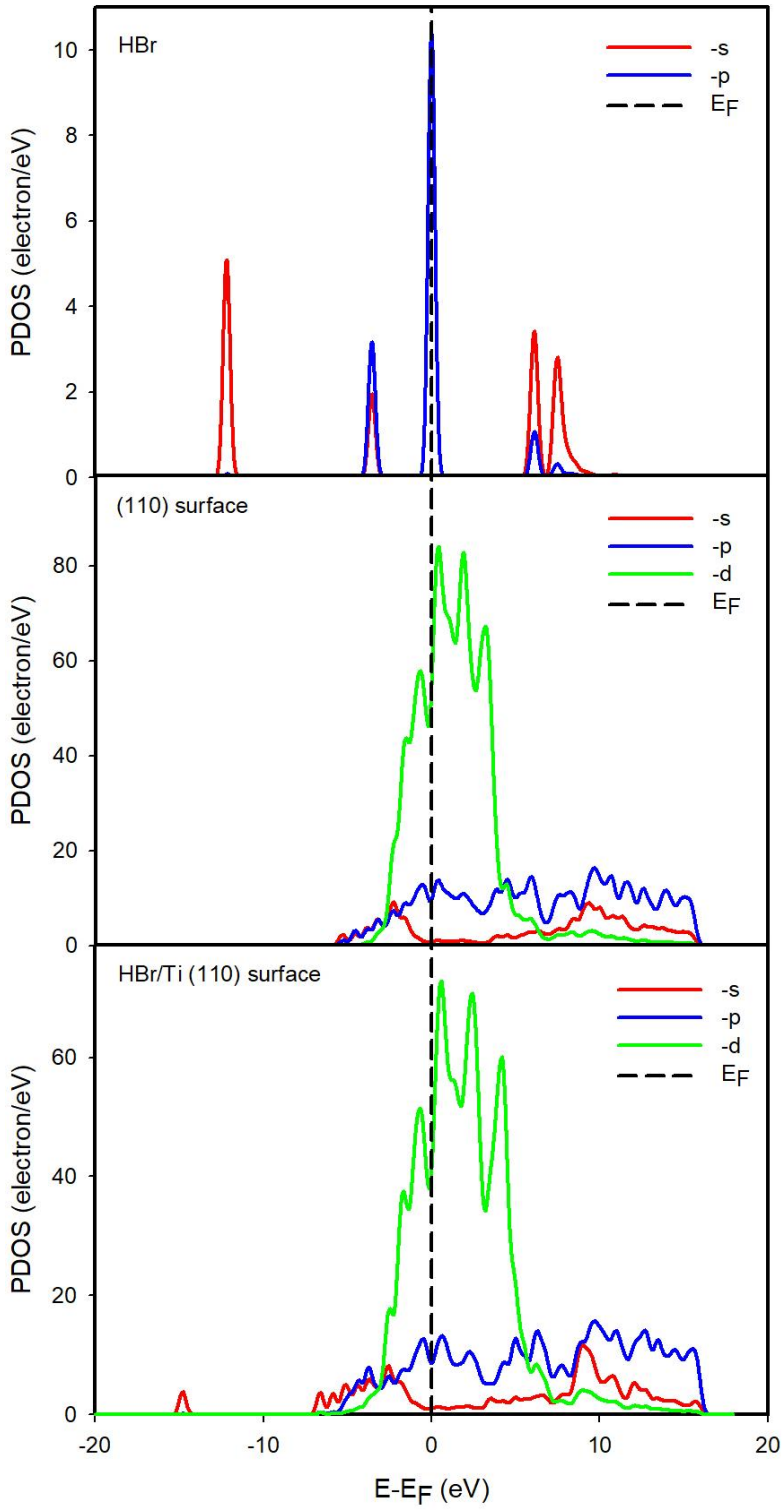

Figure 5-25: Partial density of states (PDOS) for HBr free molecule, clean Ti (110) surface and HBr/Ti (110) surface. The Fermi energy is taken as the energy zero.

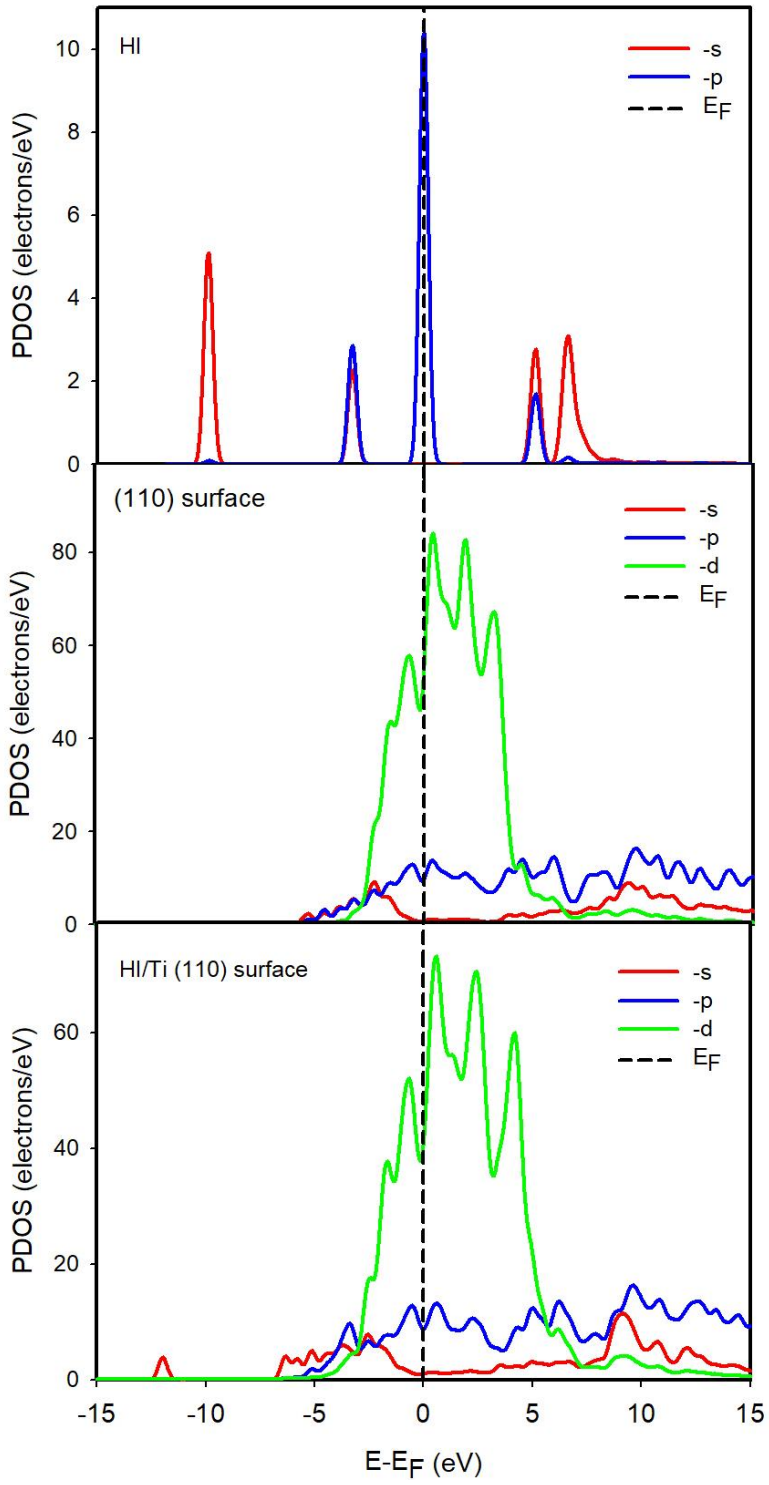

Figure 5-26: Partial density of states (PDOS) for HI free molecule, clean Ti (110) surface and HI/Ti (110) surface. The Fermi energy is taken as the energy zero.

5.2.5. Work function

Figure 5-27 shows the work function (Φ) of the adsorbed Ti (110) surface as a function of halogen ions for the top adsorption site. The presence of halogen ion on the Ti (110) surface increases the work function as compared to the clean Ti (110) surface (3.011 eV). Therefore, the calculated work function of F, Cl, Br and I adsorbed on Ti (110) surface is 3.559 eV, 3.707 eV, 3.707 eV and 3.434 eV, respectively. The induced work function is a result of a dipole involving a negative charge on the adsorbate [169]. We noted that the F atom increases the work function by 0.548 eV whilst both Cl and Br induce the Φ by 0.696 eV. It was noted that both Cl and Br lead to large values of the work function than F due to larger adsorption distance. On the other hand, the adsorption of I induces a lower (0.524 eV) work function than F and Cl adsorption. This trend can be interpreted as a result of the low electronegativity of the I atom. These present results are consistent with the observation reported by Roman *et al* [241].

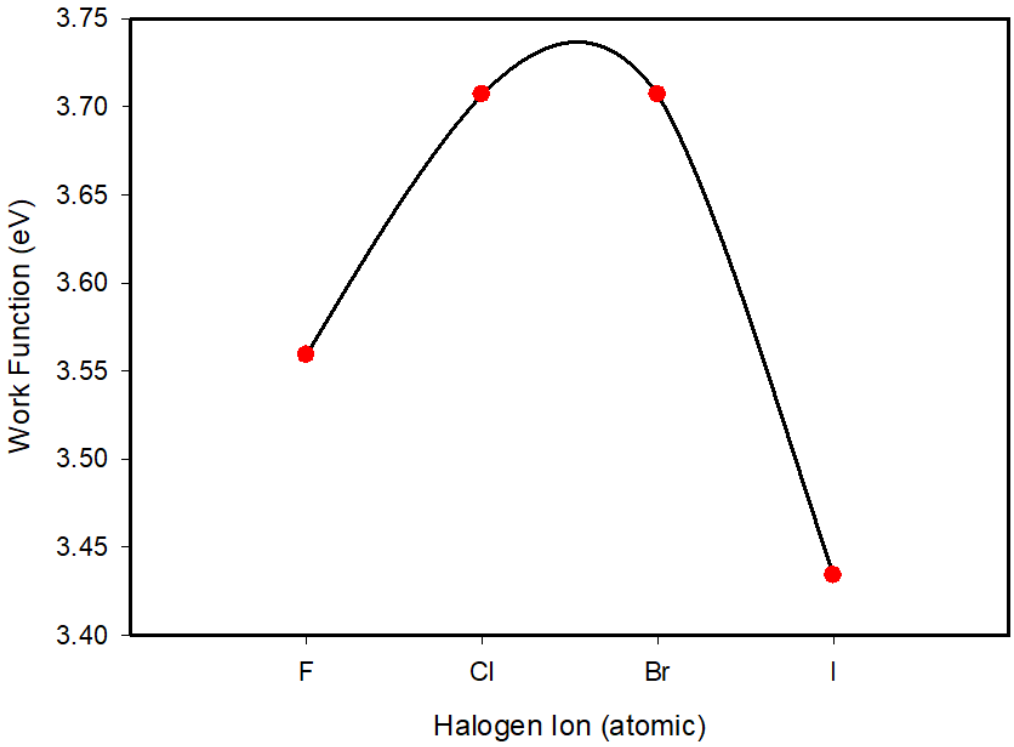

Figure 5-27: Calculated work function (Φ) against halogen ions adsorbed on Ti (110) surface.

5.3. Summary

In summary, the adsorption mechanism of halogen molecules and ions on Ti (100) and (110) surfaces have been analysed. Structural optimisation showed that all the halogen molecules dissociate completely by interaction and forming Ti-halide bonds (Ti-F, Ti-Cl, Ti-Br and Ti-I). It was observed that the binding between Ti-F atoms is stronger with a shorter bond length than other halogen atoms interaction (Ti-Cl, Ti-Br and Ti-I). Also, the study revealed that the adsorption energy of halogen molecules on Ti surfaces is negative denoting the spontaneous process. This mechanism suggests that the adsorption of halogen molecules is through surface redox reaction.

Present study revealed that the adsorption of halogen molecules on Ti surfaces is energetically favourable with the energy strength following the order of $E_{ads}^{HF} > E_{ads}^{HCl} > E_{ads}^{HBr} > E_{ads}^{HI}$. This suggests that the adsorption of the HF molecule on Ti surfaces is more thermodynamically stable than all halogen molecules. It was noted that the adsorption energy strength is consistent with the dissociation energy and electronegativity of free molecules. Our study found that the adsorption of halogen ions (F^-, Cl^-, Br^- and I^-) is more energetically preferential than the adsorption of halogen molecules (HF, HCl, HBr and HI) in both Ti surfaces.

In addition, adsorption sites were examined on Ti (100) and Ti (110) surfaces, and all the adsorption sites were found to possess negative adsorption energy indicating spontaneous reaction. This indicates that the Ti surfaces have reactive adsorption sites and adsorb all the halogen ions effectively. The bridge and top sites were observed to be the most preferential sites on Ti (100) and Ti (110) surface, respectively. Furthermore, it was noted that the adsorption energy follows the periodic role F>Cl>Br>I for all surface adsorption sites. This implies that adsorption energy changes slightly with the atomic difference of the adsorbates.

Our results revealed the average stable adsorption energy strength on Ti (100) than on Ti (110) surface for both F and Cl been the most stable adsorbate ions. Moreover, the interaction trend analysis followed by the electron-charge transfer, with all halogen ions been electron-charge accepting compounds. We also observed that the amount of charge transfer decrease from HF-HI molecule that is a similar correlation with the adsorption energy trend, implying that the stronger interaction there more electron-charge transferred. Present study also showed that there is a linear relationship between adsorption energy strength and electron-charge transferred. The charge transfer also determines the strength of binding showing that the halogen atoms are strongly bonded to Ti surfaces, which progressively decrease from fluorine to iodine adsorption.

Furthermore, the adsorption resulted in charge redistribution whereby the Ti atom surface showed an electron depletion region and halogen ion presented the accumulation region. The charge density difference was facilitated by the positive charge from the Ti atoms surface and the lone pair region of the adsorbates. We observed a spherical shape of charge density difference implying an ionic interaction between the halogen ions and Ti atoms. In addition, the PDOS plots revealed the electronic peak of the halogen ion interacting with the outermost Ti surface orbital. It was revealed that the adsorption of halogen resulted in p- electronic peaks emerging at different energy level. The electronic peaks move from ~ -5.5 eV to -3.2 eV for F to I atom, respectively. This suggests the bonding formation between Ti-I atoms is less than the interaction of Ti-F.

The adsorption of halogen atoms was found to affect the Ti surfaces work function and the adsorbed Ti surfaces have a higher work function as compare to the clean Ti surfaces. The magnitude of the induced work function varies from F>Cl>Br>I. It was noted that the adsorption of F atom increases the work function by approximately 0.548 eV, both Cl and Br ~0.669 eV while I increase by 0.523 eV. The induced work function is a result of a dipole involving a negative charge of the halogen ions.

Chapter 6

Coverage-depended of F_2 and Cl_2 molecules adsorption

As discussed in the previous Chapter, it is apparent that halogen ions have a propensity to adhere on Ti surfaces to a certain degree of adsorption energy. In this Chapter, adsorption of F_2 and Cl_2 diatomic molecules on Ti (100) surface at different coverage will be investigated. In particular, we will only examine the adsorption of both F^- and Cl^- ions on the Ti (100) surface. This follows from the observed stable average adsorption energy as presented in Chapter 5. Furthermore, we will not only investigate the ion-metal interaction but also the structural changes that link to possible volatile molecules formation and desorption, which are related to atomic etching products. It is worth noting that the important part of the etching mechanism is the formation of volatile species on the metal surface [265]. However, the research work focusing on the atomic etching of metal surface has been limited with regard to etching reactants and products.

6.1. Coverage adsorption of F_2 and Cl_2 molecules on Ti (100) surface

In this section, the adsorption of both F_2 and Cl_2 diatomic molecules at different coverage ranging from 1-3 molecule (ML) are studied. After geometry relaxation, it was found that both F_2 and Cl_2 molecules dissociate spontaneously into two atomic fragments and interact with the surface. To investigate the effect of F_2 and Cl_2 coverage adsorption on Ti (100) surface we computed the heats of formation, adsorption-desorption energy, and determine the structural parameters of the system. This will provide insight into the formation of specific compounds (etched molecules) and desorption energy mechanisms based on the formation of titanium halides compounds.

All the calculations were performed with similar computational details as described in Chapter 3.

6.1.1. Coverage adsorption of F_2 molecule on Ti (100) surface

Adsorption of F_2 diatomic molecules on Ti (100) surface at different coverage was studied to investigate the surface changes. Figure 6-1 (a and b) present the atomic structure of F_2 molecule adsorption on Ti (100) surface, (a) before and (b) after geometry optimisation. Based on the optimised atomistic models, it was seen that the F_2 molecule dissociates on the Ti (100) surface. The dissociation of diatomic F_2 molecule on Ti (100) surface involves a scenario of F-F bond breaking and Ti-F bond forming, the breaking and formation of atomic bonds is driven by F ions. Dissociation of F_2 molecule when interacting with the Ti (100) surface indicates a mutual repulsion between F ions, which accelerates them in the opposite direction as they make contact with the surface.

Moreover, it was found that dissociation of F_2 molecule form F-Ti-F and Ti-F-Ti interaction with a bond length of $d_{Ti\text{-}F}$ = 2.045 Å with the tilted angle of 98.4º and the bond distance between F atoms ($d_{F\text{-}F}$) was found to be 3.098 Å. The strength of Ti-F-Ti and F-Ti-F bridging bonds are capable of maintaining Ti_2F and TiF_2 dimers due to strong attractive force. This suggests that the diatomic bond breaking and displacement of surface atoms are driven by F ions, which result in forming titanium halide molecules (TiF_x). The dissociated molecule leads to the formation of ionic bonding with the positive charge of Ti atoms. The relative final state energy and adsorption energy of dissociated F_2 molecule on Ti (100) surface were found to be -0.049 eV/Å^2 and -10.90 eV, respectively. This suggests that the dissociation of the diatomic F_2 molecule on the Ti (100) surface is spontaneous.

(a) (b)

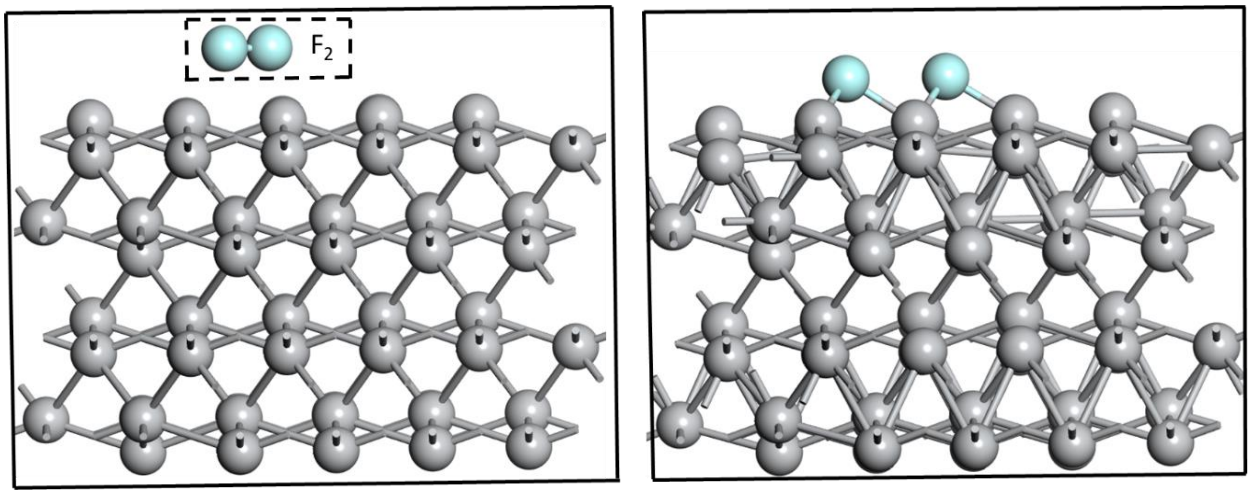

Figure 6-1: Atomistic structure for F_2 molecule adsorption on Ti (100) surface: (a) before and (b) after geometry optimisation.

Figure 6-2 and 6-3 presents the atomic structure of adsorbed two and three F_2 diatomic molecules on Ti (100) surface, respectively. After geometry optimisation, the adsorbate interacts with the titanium surface forming different Ti_xF_y clusters, where the molecules are displaced upwards from the Ti surface. The final atomic configuration results showed that the adsorbed F_2 molecules at different coverage reacted with the Ti surface and generated a minimum volatile species in the form of TiF_4 and Ti_2F_6 (see Figure 6-2 and 6-3).

In this scenario, the dissociation of two F_2 diatomic molecules generated volatile TiF_4 molecule, whilst the dissociation of three F_2 molecules form Ti_2F_6 species. This implies that the adsorption and dissociation of diatomic fluorine molecules at different coverage result in the formation of different Ti_xF_y species. It is important to note that the formation of Ti_xF_y clusters was observed to be pulled-up towards the vacuum, becoming isolated molecules that can be desorbed from the Ti (100) surface. This denotes that F ions are firstly adsorbed on the surface, forming volatile molecule and then desorption of Ti_xF_y cluster occur. Therefore, Ti_xF_y clusters are considered as etched species suggesting that the F_2 molecule has the potential to etch Ti surface.

In addition, the spontaneous formation of residual TiF_4 and Ti_2F_6 clusters on the Ti surface indicates that etching on titanium surfaces may take place in the early state of time if the TiF_4 molecule is generated. Therefore, the number of possible etched clusters (Ti_xF_y) increases with increasing adsorbate (F_2) coverage. This suggests that the etch rate is determined by how many metal fluoride (Ti_xF_y) are formed and can be removed or desorbed from the surface.

Moreover, our results showed that F_2 molecules are capable of removing up to one Ti atom from the surface by forming TiF_4 and two Ti atoms by creating Ti_2F_6 species. This implies that etching titanium surfaces by fluorination is isotropic etching mechanism. It is also noted that when diatomic F_2 molecules are used in the fluorination process the most etch products (TiF_4 and Ti_2F_6) are formed. These molecules are very volatile and can be easily detached from the Ti surface. Similar work was done on the exposure of F_2 molecule on metal Si (100) surface where the relative primary etching product such as SiF_2 and SiF_4 molecules were observed [266].

(a) Top view

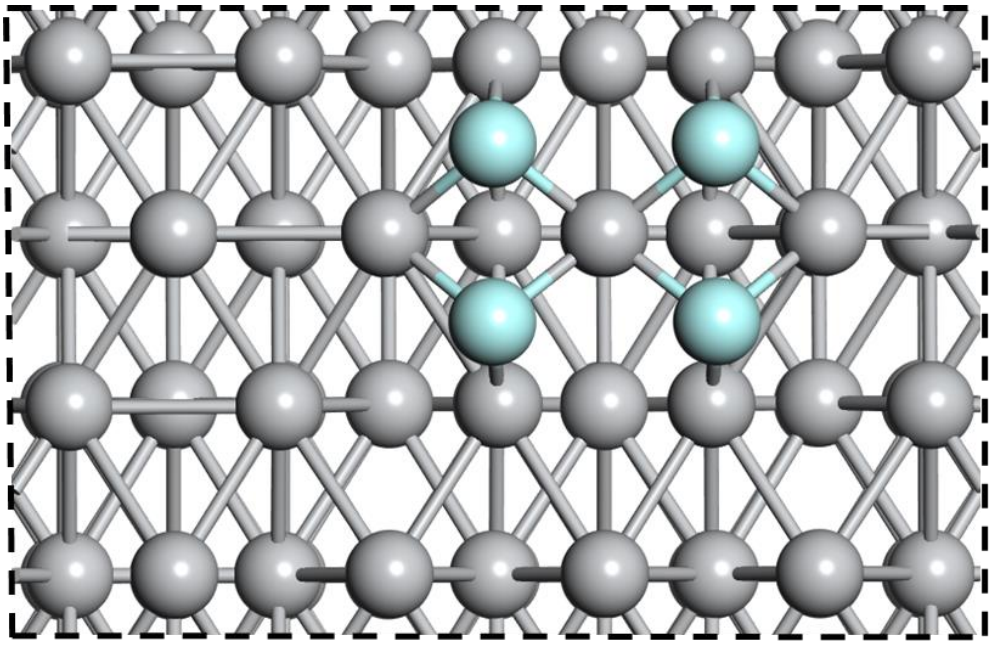

(b) Side view

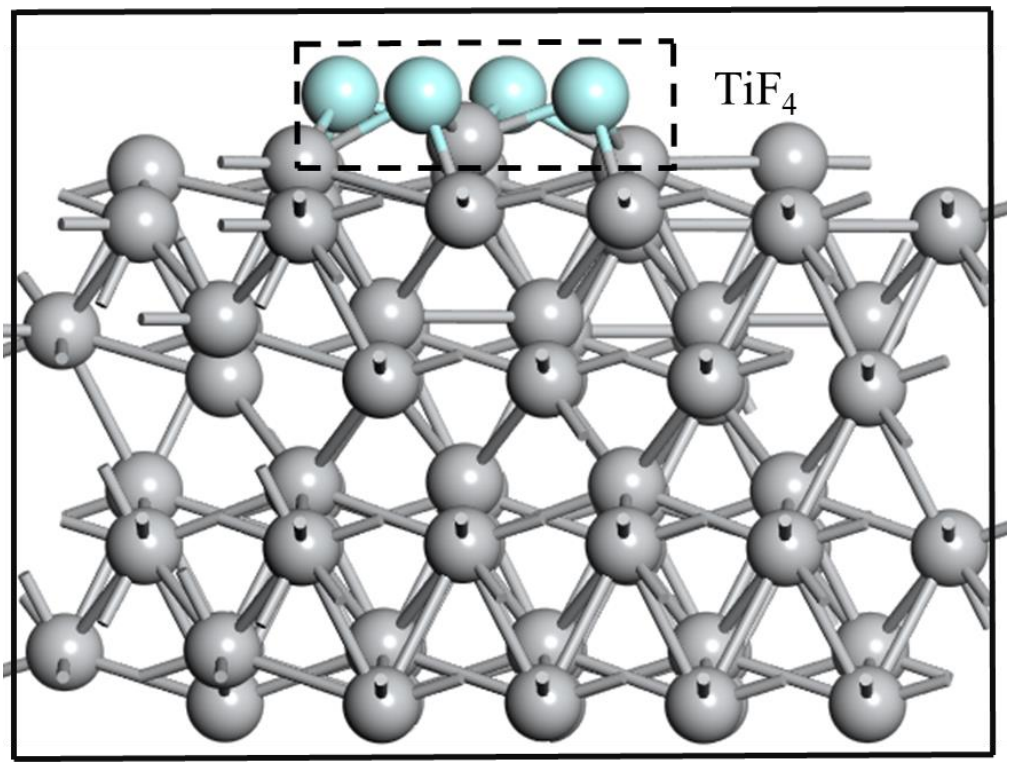

Figure 6-2: Optimised atomic structure for two F_2 diatomic molecules adsorption on Ti (100) surface: (a) Top view and (b) Side view.

(a) Top-View

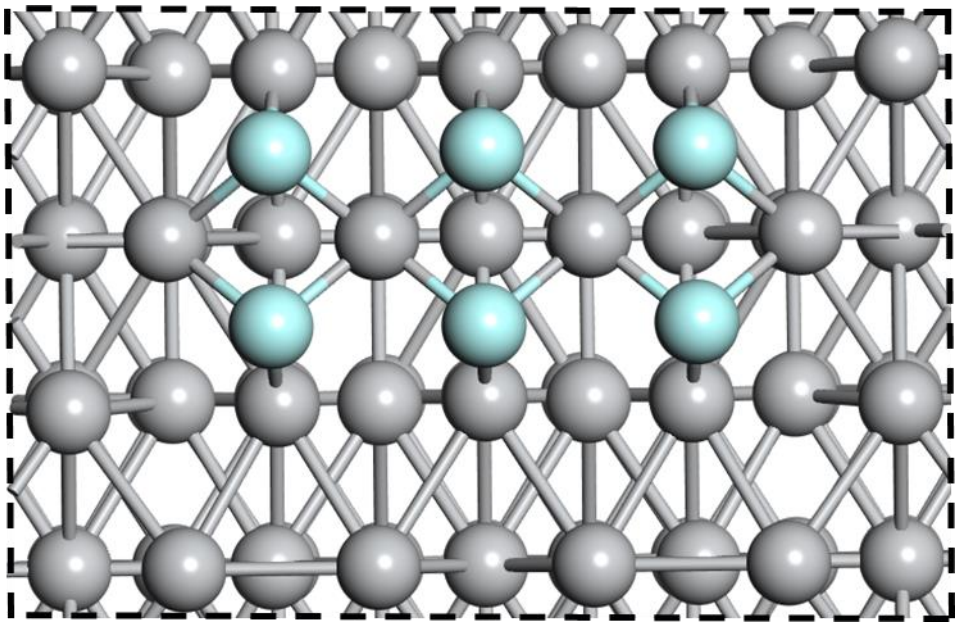

(b) Side-View

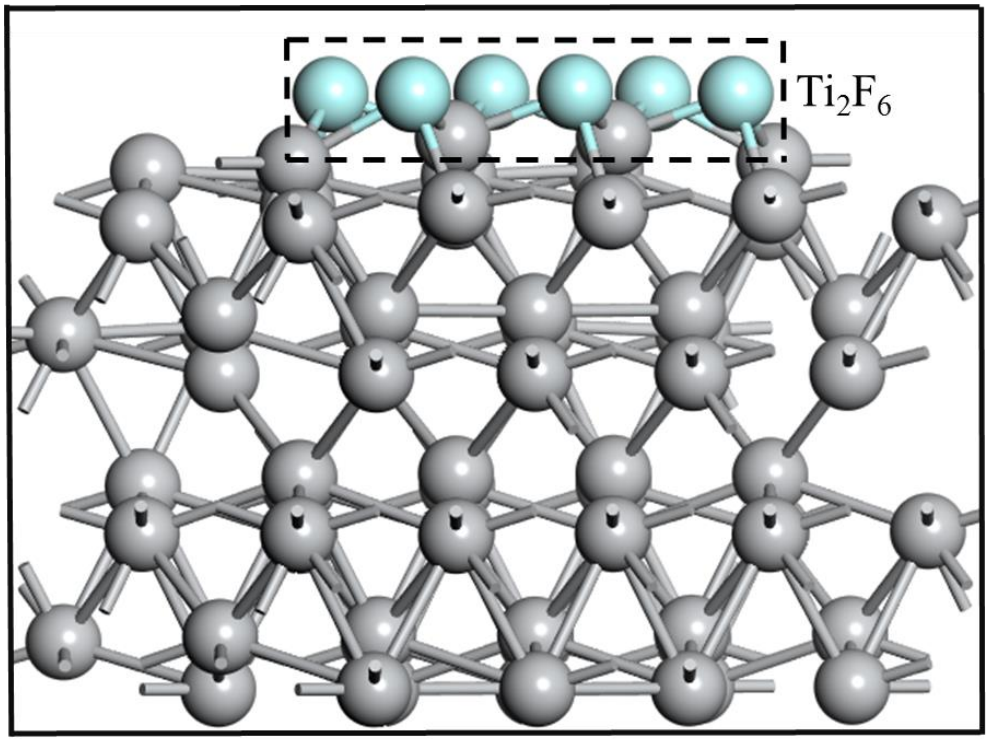

Figure 6-3: Optimised atomic structure for three F_2 diatomic molecules adsorption on Ti (100) surface: (a) Top view and (b) Side view.

6.1.2. Coverage adsorption of Cl_2 molecules on Ti (100) surface

Adsorption of Cl_2 diatomic molecule at different coverage was studied to investigate the structural changes on Ti (100) surface. Figure 6-4 illustrates dissociate and non-dissociative adsorptions of Cl_2 molecule on Ti (100) surface, we presented the initial and final configurations of the system. Figure 6-4 (a) present the atomistic schematic before optimisation and Figure 6-4 (b) after optimisation. Based on the final atomistic model, the adsorption of Cl_2 diatomic molecule on Ti (100) surface is by dissociation process that involves a scenario of Cl-Cl bond breaking and forming Ti-Cl bond. The Cl_2 molecule dissociates to form Cl-Ti-Cl and Ti-Cl-Ti interaction with a bond length of $d_{Ti\text{-}Cl}$ =2.494 Å, valence angle of 83.6º and the bond distance between Cl atoms ($d_{Cl\text{-}Cl}$) was found to be 3.326 Å.

Atomic bond breaking of Cl-Cl and formation of Ti-Cl is driven by Cl ions forming titanium halides bonding. Thus, one suggests that Cl_2 dissociate into two atomic fragments when the attraction between individual Cl ions and the Ti surface is greater than the Cl-Cl interaction. The relative final total energy and adsorption energy of dissociated Cl_2 molecule on Ti (100) surface were found to be -0.034 eV/Å^2 and -7.12 eV, respectively. This suggests that the dissociation of Cl_2 diatomic molecule on the Ti surface is exothermic. Both the final total energy and adsorption energy of Cl_2 are less stable as compare to F_2 diatomic adsorption in section 6.1.1.

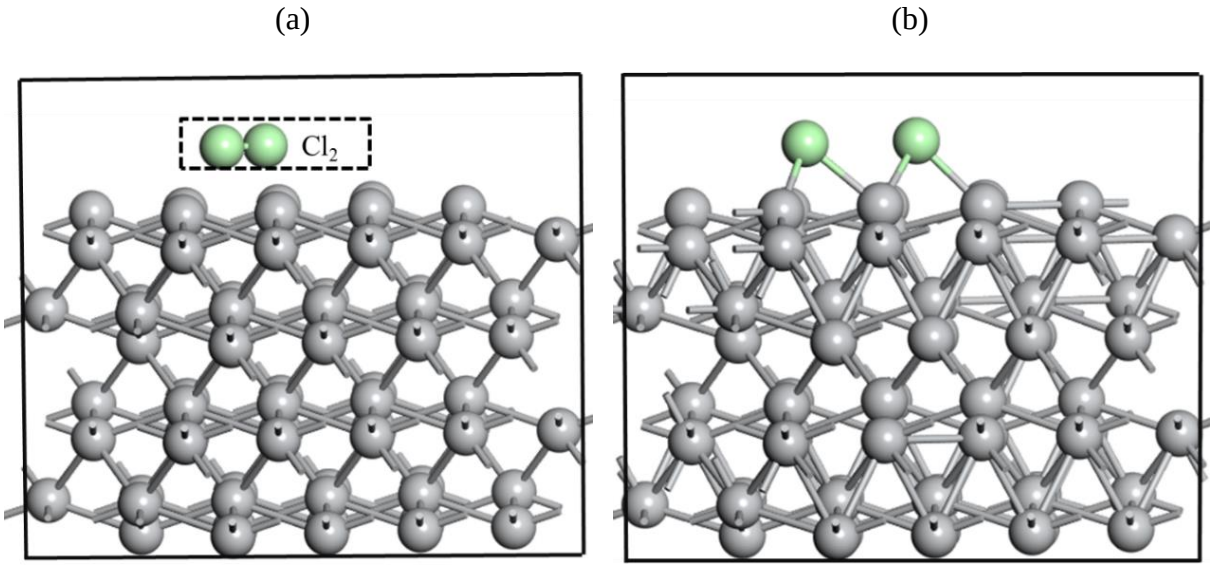

Figure 6-4: Atomistic structure for Cl_2 molecule adsorption on Ti (100) surface: (a) before and (b) after geometry optimisation.

Figures 6-5 and 6-6 presents the atomistic configuration of Cl_2 molecule adsorption at different coverage on Ti (100) surface. Final atomic structure shows that the incoming diatomic Cl_2 molecules react with the Ti surface to form equivalent Ti_xCl_y clusters. It was noted that the adsorption of two Cl_2 molecule form $TiCl_4$ whilst three Cl_2 generate Ti_2Cl_6 species. This indicates that the exposure of Cl_2 molecules on Ti (100) surface result in the continuous formation of $TiCl_x$ species. We observed that the formation of titanium chloride molecules ($TiCl_4$ and Ti_2Cl_6) were seen to be pulled-up to become isolated molecules that can be desorbed from the Ti (100) surface. This shows that when Cl_2 is considered as the surface etchant, it has the potential to remove the Ti atoms from the surface.

It was found that the adsorption of two Cl_2 diatomic molecules could remove one Ti atom and three Cl_2 etch two Ti atoms in the form of $TiCl_4$ and Ti_2Cl_6 clusters. This suggests that the etching Ti surface with Cl_2 diatomic etchant will be isotropic. Moreover, this indicates that when the Cl_2 molecule is adsorbed at high content there are more chances to form $TiCl_x$ volatile species. As such, titanium etching takes place in the early stage of time if a $TiCl_4$ cluster is formed. Furthermore, the number of etch molecules increases as the coverage adsorbate increases. The dissociation of Cl_2 diatomic molecules on Ti (100) surface and forming Ti_xCl_y species is similar to the above observation of F_2 molecule adsorbed as it forms Ti_xF_y as shown in section 6.1.1.

In this present study, the formation of Ti halides clusters (TiF_4, Ti_2F_6, $TiCl_4$ and Ti_2Cl_6) were observed from lower to higher coverage of the molecule adsorbate. This formed Ti_xF_y and Ti_xCl_y species is crucial for the initial stage of etching. Importantly these materials are very volatile and can be detached from the surface very easily. Therefore, it is necessary to emphasise that when F_2 and Cl_2 interact with the Ti surface ordered or disordered layers or molecules are being formed. Pavlova *et al* [119] reported similar observation when Cl ions were adsorbed on the Cu surface using DFT within VASP code with exchange-correction functional form of PBE employed. The volatile molecules formation and desorption took place in the form of CuCl, $CuCl_2$ and $CuCl_4$ molecules.

(a) Top-View

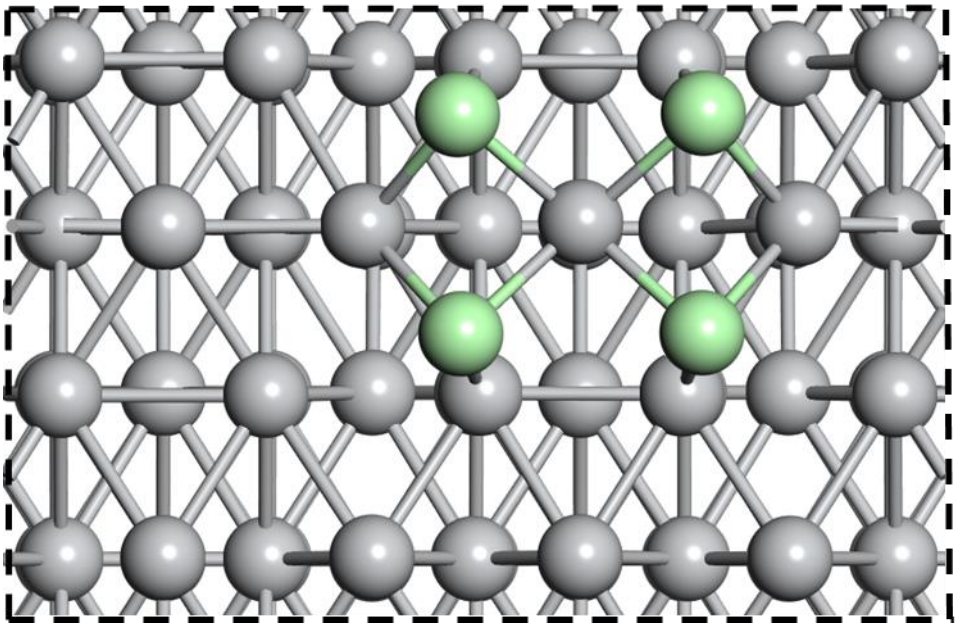

(b) Side-View

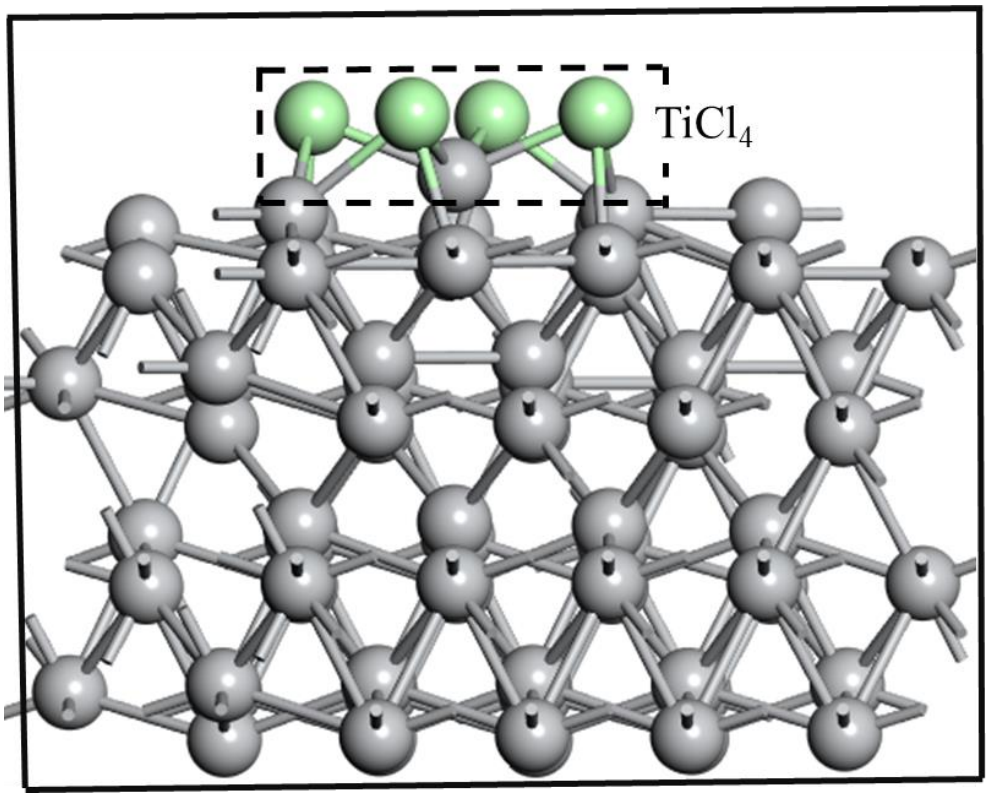

Figure 6-5: Optimised atomic structure for two Cl_2 diatomic molecules adsorption on Ti (100) surface: (a) Top-view and (b) Side-view.

(a) Top-View

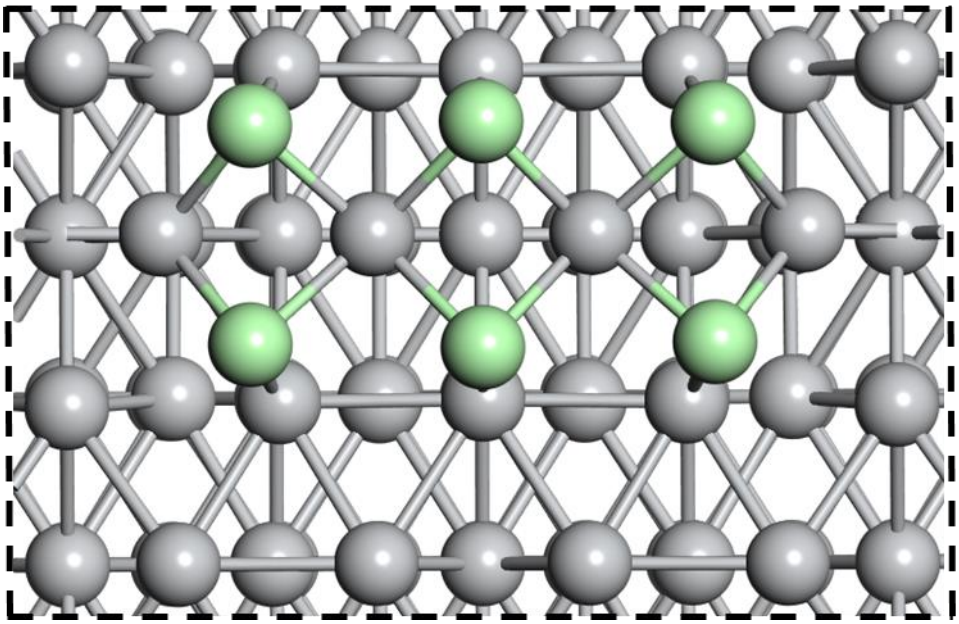

(b) Side-View

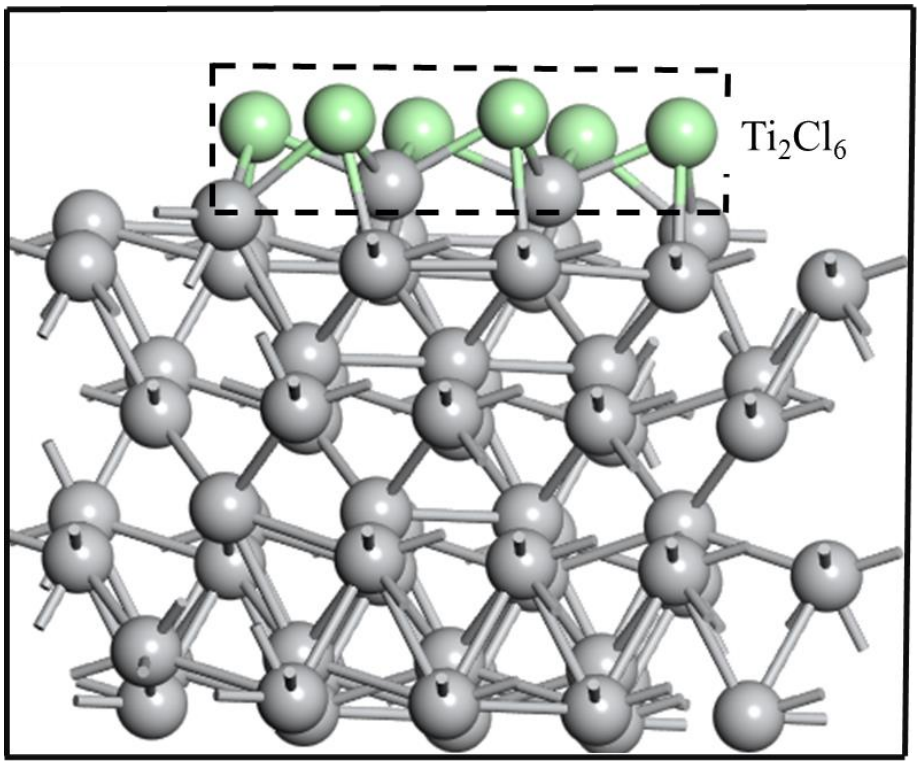

Figure 6-6: Optimised atomic structure for three Cl_2 diatomic molecules adsorption on Ti (100) surface: (a) Top-view and (b) Side-view.

6.1.3. Comparison of Ti_xF_y and Ti_xCl_y clusters

According to our findings, Ti_xF_y and Ti_xCl_y clusters formed on the surface indicates that when adsorbate ions at high content there is more chances to form etch products. It is important to emphasise that the etching titanium surface requires a substantial number of ions since TiX_4 (X= F or Cl) should be generated because is one of the dominant etched species. These current results finding are in good agreement with the observations by Kim *et al* [38]. In such, etching takes place on the surface in the early stage of time if TiX_4 (X=F or Cl) molecules are formed whereby the number of molecules increases as the adsorbate coverage increases.

Figures 6-7 and 6-8 presents the free optimised crystal structure for Ti_xF_y and Ti_xCl_y. The structures show both bond length and valance angle on the molecular structure, where the bond length between Ti-F varied from 1.76 to 1.978 Å while the bond length of Ti-Cl found to vary from 2.201 Å to 2.328 Å. Furthermore, the F-Ti-F valence angle for TiF_4 and Ti_2F_6 structures vary from 109.6º to 129.8º and the Cl-Ti-Cl valence angle for $TiCl_4$ and Ti_2Cl_6 range from 109.4º to 120.6º as shown in Figure 6-7 and 6-8, respectively. It was found that the structural parameters (bond lengths and valence angle) are slightly different from the ones formed on the Ti surface. The bond lengths between Ti and Cl are slightly larger than that of F and Ti where the shorter bond length indicates stronger tighter bonding between Ti-F interactions. It can be seen that there is a tendency for F^- to bond with Ti, which is in agreement with the results on the adsorption energy in Chapter 5. The bond length and valence angle for the free molecule are comparable with the bond angle parameter found on the volatile titanium halide molecules formed on the Ti (100) surface.

However, since the molecules are still attached to the Ti surface, the desorption energy of the molecules is required. In order to gain insight into the energy barrier of TiX_4 (X=F or Cl) molecules, their desorption and formation energies with respect to volatile species will be calculated in section 6.2. Since while these exposures are so closer to saturation, therefore, it is more likely that there is an intrinsic limit to the coverage due to other effects. A high increase in coverage adsorbate may result in repulsion between the neighbouring negative charge ions, which could lead to ions saturation coverage on a vacuum.

(a) (b)

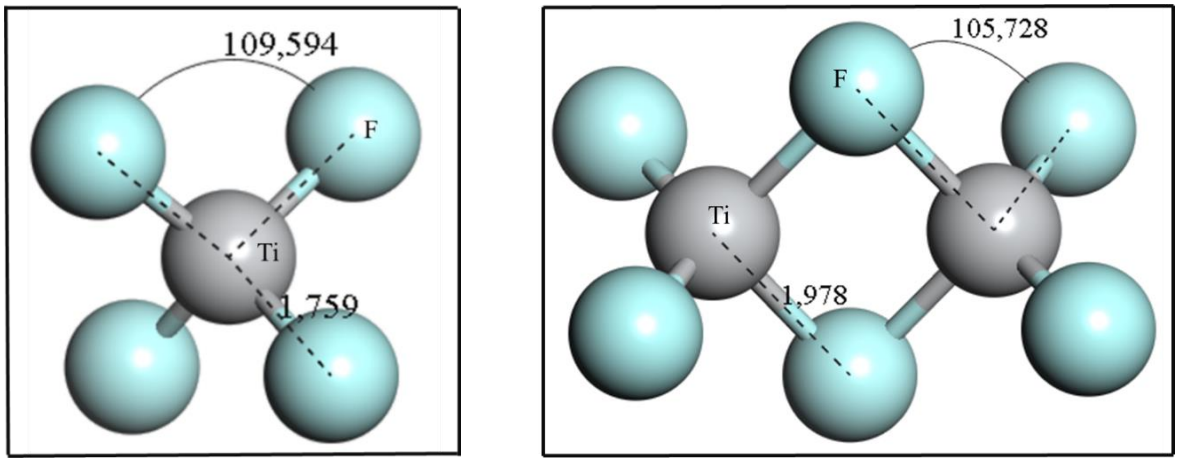

Figure 6-7: Optimised crystal structures of (a) TiF_4 and (b) Ti_2F_6.

(a) (b)

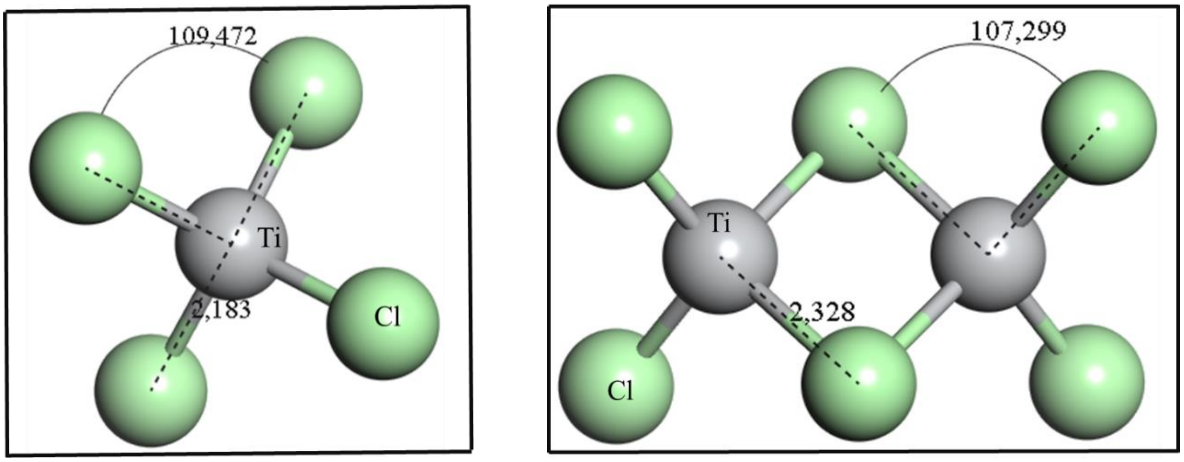

Figure 6-8: Optimised crystal structures of (a) $TiCl_4$ and (b) Ti_2Cl_6.

6.2. Heats of formation and desorption energy of Ti_xF_y and Ti_xCl_y clusters

In this section, the heats of formation and desorption energy of Ti_xF_y and Ti_xCl_y clusters formed on Ti (100) surface are investigated. Heats of formation for Ti_xF_y and Ti_xCl_y clusters are considered to understand the formation of etch products on titanium surface by F_2 and Cl_2 molecules. These Ti_xF_y and Ti_xCl_y materials are very volatile and can be detached from the surface very easily. However, since these molecules are still attached to the Ti surface, desorption energy is required. To characterise the stability and energy barrier of this molecule, the desorption energies (E_{des}) and heats of formation (E_{HF}) were calculated using Eq. 3-42 and 3-43, respectively.

Table 6-1 present the heats of formation, desorption energy and equilibrium bond length of Ti_xF_y and Ti_xCl_y clusters on the Ti (100) surface. All the E_{HF} values were found to be negative for both Ti_xF_y and Ti_xCl_y molecules implying an exothermic reaction process. In addition, this also implies that the formation of these volatile species (Ti_xF_y and Ti_xCl_y) is energetically favourable. We note that Ti_xF_y molecules possess the least value of E_{HF} than Ti_xCl_y, suggesting that the Ti_xF_y molecule is more stable and easier to be generated than Ti_xCl_y. In addition, the Ti_xF_y dimer is more stable due to a stronger Ti-F-Ti bridging bonding. Furthermore, the E_{HF} (-48.68 eV and -37.02 eV) for Ti_2F_6 and Ti_2Cl_6 are highly negative than TiF_4 and $TiCl_4$ clusters (-30.69 eV and -22.30 eV). This suggests that biomolecules (Ti_4F_6/Ti_4Cl_6) are more energetically favourable than single molecules (TiF_4/$TiCl_4$). In this regards the results show that the formation of volatile Ti_xF_y species is more exergonic than Ti_xCl_y clusters. This is because of a large number of F and Cl atoms contribution to efficient etching by a generation of many Ti-F and Ti-Cl bonds.

It is important to note that the heats of formation for the proposed volatile molecules are different, this is due to different bonding strength between Ti-F and T-Cl interaction. Moreover, this is in good agreement with the adsorption energy strength found in Chapter 5. The large negative heats of formation value of Ti_xF_y species suggest more stability and stronger interaction between the Ti-F atoms.

The great deviations between desorption energies of various Ti_xF_y and Ti_xCl_y species are listed in Table 6-1. Results showed that all the Ti_xF_y and Ti_xCl_y cluster possess a positive value of desorption energy implying a non-spontaneous process. The calculated desorption energy of TiF_4 was found to be lower than (58.61 eV) that of the $TiCl_4$ molecule (59.35 eV). This means that TiF_4 would be detached very easily from Ti (100) surface than $TiCl_4$ molecule. It is evident that TiF_4 species will be detached from the surface with an energy cost of 0.74 eV less than $TiCl_4$. In this case, the removal of TiF_4 is more favourable than the $TiCl_4$ species. This also denotes that Ti surface etching will be higher when using F_2 etchant as compare to Cl_2. In addition, the desorption energies of Ti_2F_6/Ti_2Cl_6 species is larger than that of TiF_4/$TiCl_4$ cluster denoting that detaching Ti_2F_6/Ti_2Cl_6 molecule requires more activation energy. The removal of Ti_2F_6 molecule is increasingly expensive with an energy barrier of 72.35 eV whilst desorption energy of TiF_4 is 58.61 eV.

Table 6-1: The heats of formation (E_{HF}), desorption energy (E_{des}) and equilibrium bond length of Ti_xF_y and Ti_xCl_y clusters.

Cluster	E_{HF} (eV)	E_{des} (eV)	Displacement (Å)	Bond length (Å)
TiF_4	-30.69	58.61	2.973	2.062
Ti_2F_6	-48.68	72.35	2.944	2.066
$TiCl_4$	-22.30	59.35	2.994	2.490
Ti_2Cl_6	-37.02	69.14	3.005	2.467

Similarly, the desorption of $TiCl_4$ cluster was found to be more favourable with a lower energy of 59.35 eV than Ti_2Cl_6 species (69.14 eV). This clearly indicates that single molecules (TiF_4/$TiCl_4$) are easily detached than double-clusters (Ti_2F_6/Ti_2Cl_6). Therefore, this implies that the etching velocity on the Ti (100) surface depends on the single TiF_x and $TiCl_x$ clusters formed. The desorption energy of single and biomolecules denotes that the etching of Ti surfaces occurs when the smallest volatile molecule is formed. Therefore, the amount of material removed is etched per TiF_x and $TiCl_x$ formed.

The desorption energy results prove that titanium halides (TiX_4: X= F, Cl) molecule can desorb from the surface. Our findings proved that the desorption of TiF_x molecule is less endothermic than $TiCl_x$ species indicating that Ti surface etching will be higher for F_2 reaction as compared to the Cl_2. These results confirm that the stability of the etch products with two F-Ti-F bridging bonds are the most stable than Cl-Ti-Cl implying that TiF_x dimers are the most desorbing molecules. The formation of TiF_4/$TiCl_4$ dimers and polymeric (Ti_2F_6/Ti_2Cl_6) products found in this study are in good agreement with the observation reported by Basher *et al* [267] on Ni/NiO surface etching by hexafluoro acetylacetone (hfach) using DFT with the B3LYP functional.

6.3. Partial density of states

To investigate the electronic interaction and formation of Ti_xF_y and Ti_xCl_y the partial density of states (PDOS) were analysed. The PDOS plots present the number of orbital states per unit energy, where the F_2 and Cl_2 diatomic molecule interacting with Ti (100) surface. Figure 6-9 present the PDOS curves of free TiF_4 structure, clean Ti (100) surface and TiF_4 molecule formed on Ti (100) surface. Electronic peaks for free crystal TiF_4 (Figure 6-9 top panel) consisting of s-, p- and d- with only p- orbital contributing more at the Fermi level (E_F). We observed pronounced electronic peaks at around -3 eV that correspond to p- and d- orbital for F and Ti atoms. This also indicates the p-d

hybridisation for Ti-F interaction. In addition, the PDOS plots for clean surface (Figure 6-9 middle panel) showed the Ti d- band contributing more to the Fermi level (E_F) and minimum contribution from both s- and p- orbitals. Slight changes were observed on PDOS plots for TiF_4 formed molecule (Figure 6-9 bottom panel) as compared to the clean Ti surface. New electronic peaks emerged at approximately -9 eV, which correspond to the p- electrons from F atoms. Furthermore, we noticed a slight decrease in the magnitude of the electronic peak for the formed TiF_4 formed molecule.

Figure 6-10 presents the PDOS of free Ti_2F_6 crystal structure, clean Ti (100) surface and Ti_2F_6 molecule formed on Ti (100) surface. PDOS curves for a free Ti_2F_6 crystal (Figure 6-10 top panel) consist mainly of s-, p- and d- orbital states with d- orbital state dominating more at the Fermi level (E_F). It was noted that the Ti_2F_6 PDOS plots display an electronic peak around -9 eV corresponding to the p- orbital from the F atom, which is a similar observation in Figure 6-10 (top panel) for the TiF_4 crystal structure. However, the PDOS peak for Ti_2F_6 free crystal molecule possesses a higher peak intensity than TiF_4 plots. Moreover, there is no significant difference between the form TiF_4 and Ti_2F_6 molecule, except for the higher magnitude of the electronic peaks.

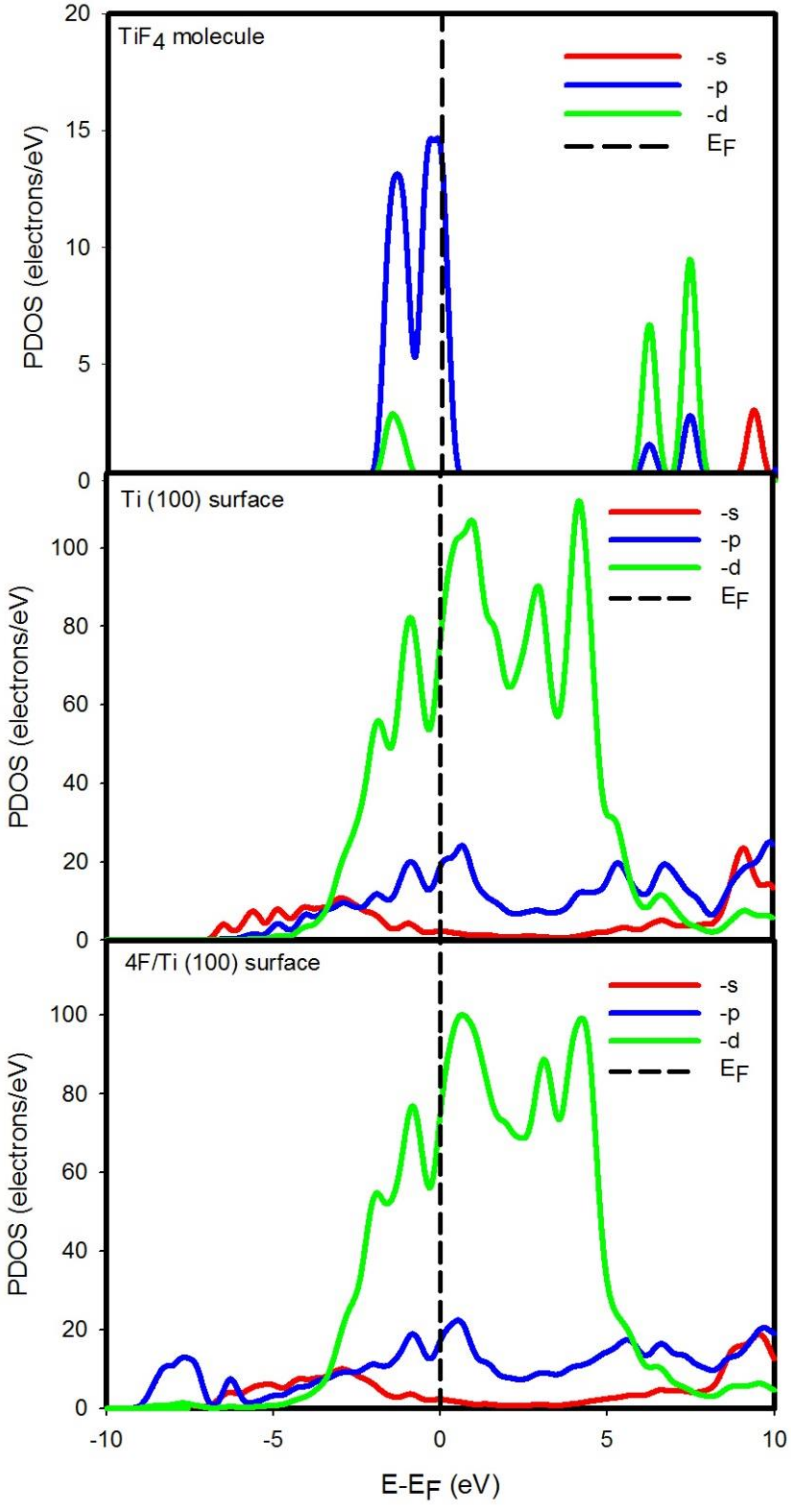

Figure 6-9: Partial density of states for TiF_4 crystal structure, clean Ti (100) surface and TiF_4 molecule formed on Ti (100) surface.

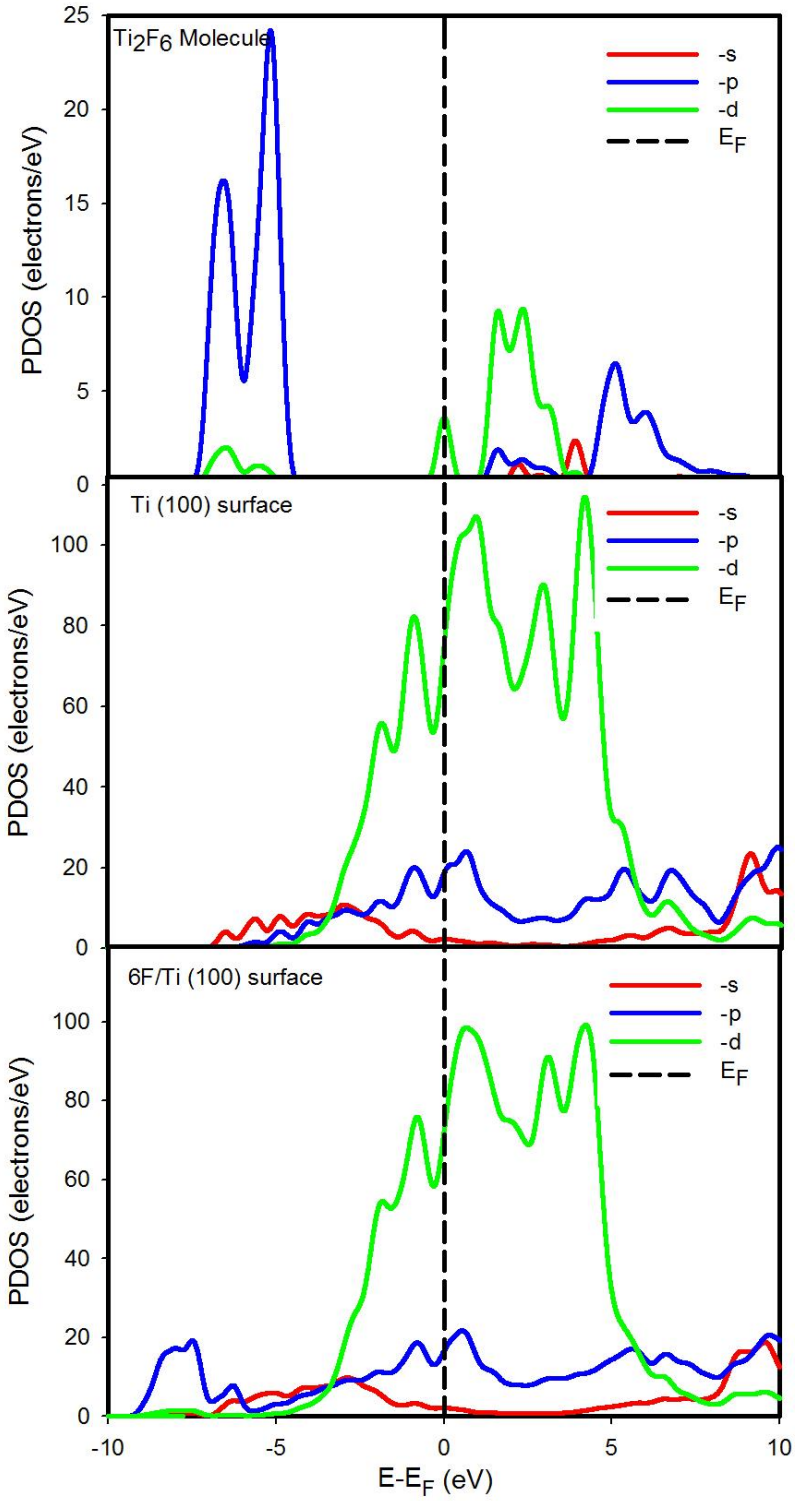

Figure 6-10: Partial density of states for Ti_2F_6 crystal structure, clean Ti (100) surface and Ti_2F_6 molecule formed on Ti (100) surface.

PDOS for $TiCl_4$ and Ti_2Cl_6 crystal structures, clean Ti (100) surface and $TiCl_4/Ti_2Cl_6$ molecules formed on Ti (100) surface were also investigated, to analyse the electronic interaction between the Ti and Cl orbitals. The PDOS plots present the number of orbital per unit energy for Cl^- ion interacting. Figure 6-11 shows the PDOS of $TiCl_4$ crystal structure, clean Ti (100) surface and $TiCl_4$ molecule formed on Ti (100) surface. The PDOS curves for $TiCl_4$ crystal structure (Figure 6-11 top panel) display the electronic peaks at approximately -13 eV corresponding to s- orbital from Cl^- atom. In addition, we observed electronic peaks around -2 eV corresponding to p-d hybridisation between the p- and d- orbitals from Cl and Ti atoms. Electronic peaks for clean Ti (100) surface (Figure 6-11 middle panel) consist of $3s^2$ $3p^2$ $3d^2$ $4s^2$ with d- electrons contributing highly of the Fermi level (E_F). Moreover, there is a significant change in PDOS peaks for $TiCl_4$ formed (Figure 6-11 bottom panel) as compared to the clean surface. We observed the emerged electronic peaks around -19 eV and -5 eV corresponding to s- and sp- orbital states for the Cl atom. Moreover, it was seen that the Ti d- band decreases after the $TiCl_4$ molecule formed on the surface as compared to the pure Ti (100) surface.

Figure 6-12 present the PDOS plot for Ti_2Cl_6 crystal structure, clean Ti (100) surface and Ti_2Cl_6 molecule formed on Ti (100) surface. The PDOS for free Ti_2Cl_6 crystal (Figure 6-11 top panel) present the electronic peaks at -19 eV and -5 eV corresponding to s- and p-d orbital states for Cl and Ti-Cl atoms, respectively. These electronic peak observations are similar to those appearing for the $TiCl_4$ structure (Figure 6-11 top panel). However, Ti_2Cl_6 electron peaks have a high magnitude than $TiCl_4$. The E_F lies on the p- orbital on $TiCl_4$ whereas on Ti_2Cl_6 structure lies on the –d orbital. In addition, the PDOS peaks of formed molecules (Figure 6-12 bottom panel) are slightly shifted downwards as compared with the electronic peak on a clean surface, which suggest that the total energy decrease after $TiCl_4$ and Ti_2Cl_6 molecules were formed.

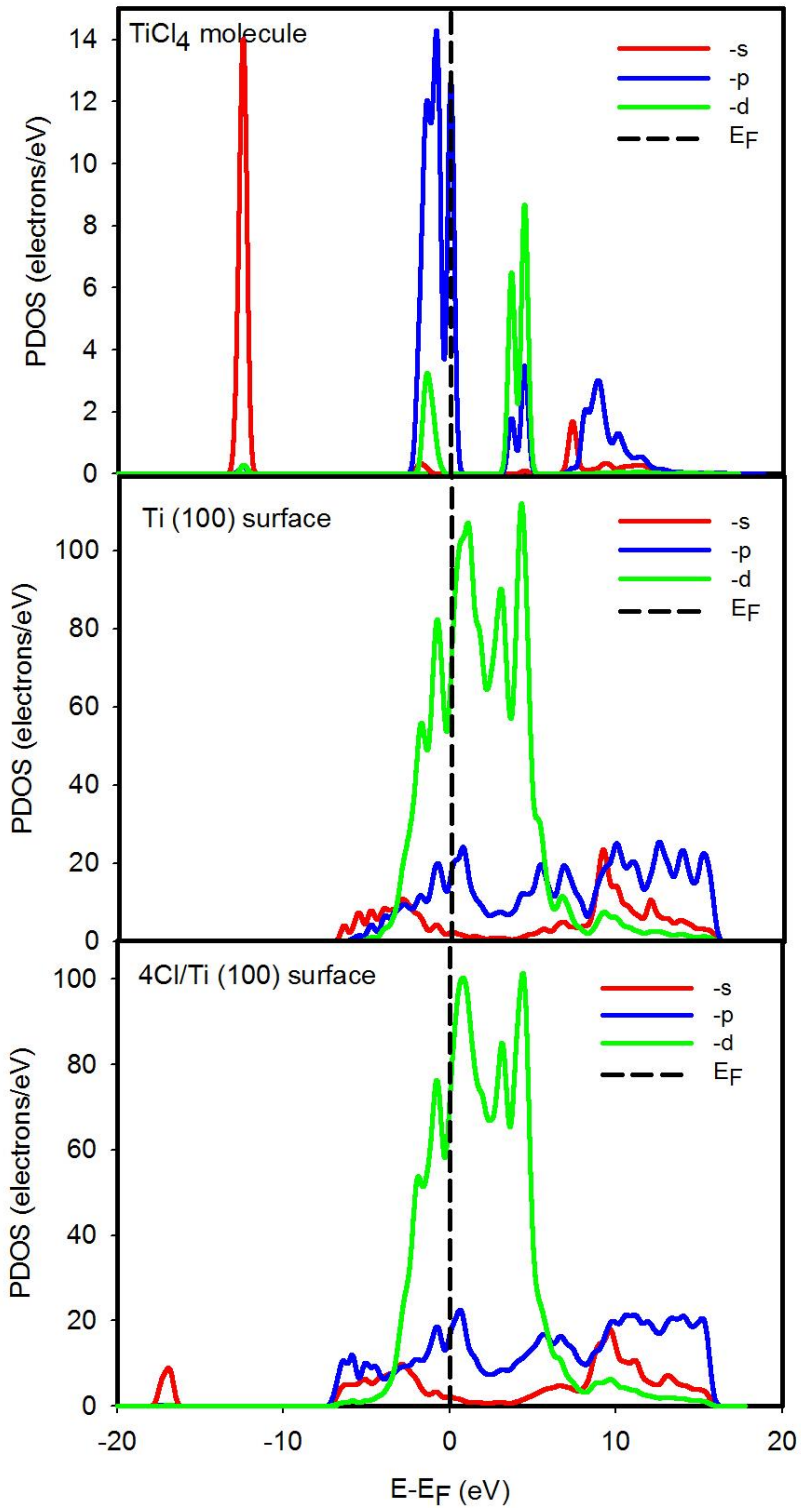

Figure 6-11: Partial density of states for $TiCl_4$ crystal structure, clean Ti (100) surface and $TiCl_4$ molecule formed on Ti (100) surface.

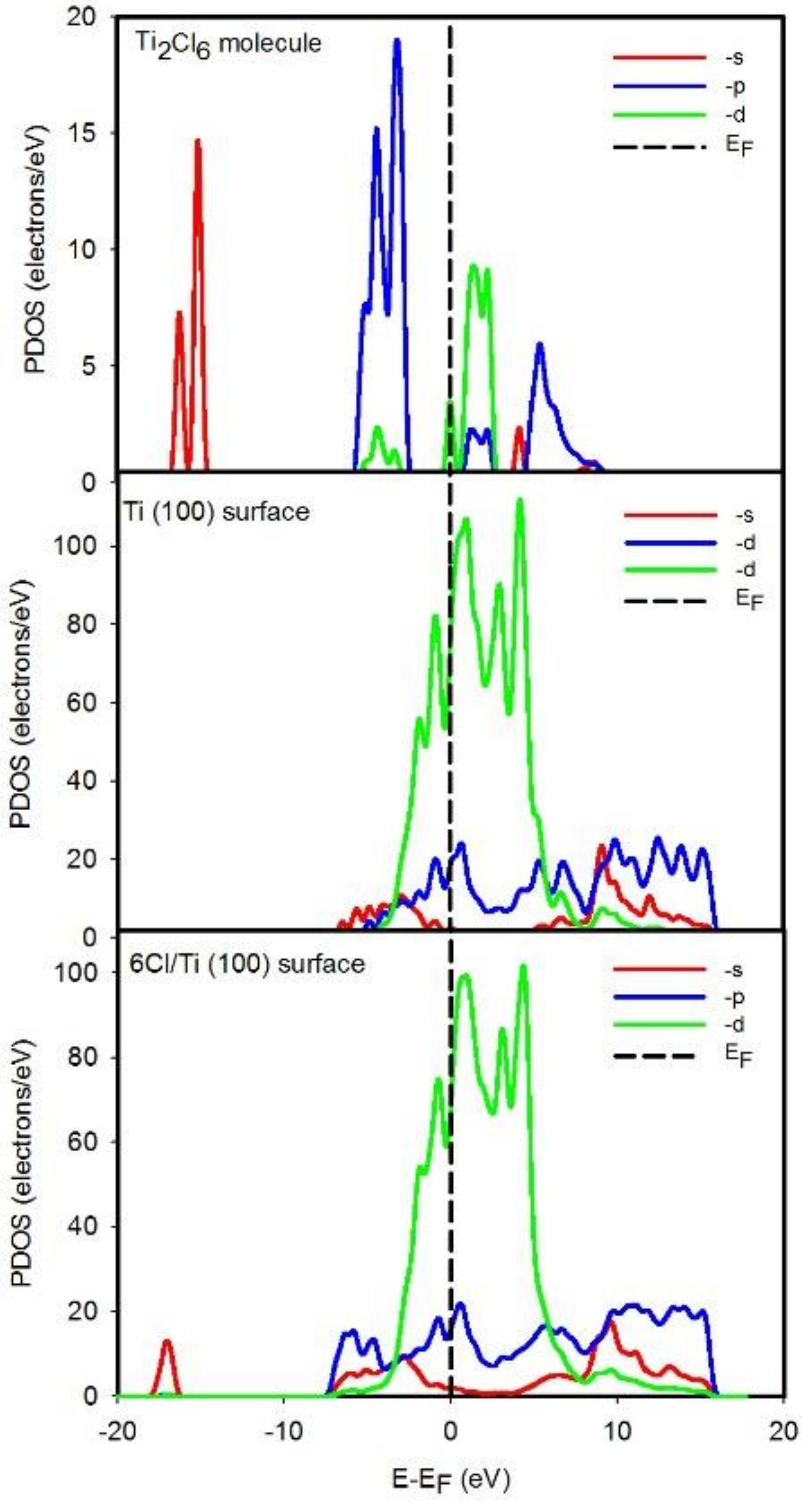

Figure 6-12: Partial density of states for Ti_2Cl_6 crystal structure, clean Ti (100) surface and Ti_2Cl_6 molecule formed on Ti (100) surface.

6.4. Charge density difference of desorption molecules

The estimation of total charge distribution of the titanium halides molecules was integrated to understand the changes of the profile with respect to different titanium halides formed and the nature of bonding. Figure 6-13 displays a 2D plot of the charge density difference ($\Delta\rho(r)$) for TiF_4 and Ti_2F_6 molecules. The plots show the electrons excess region (red colour) around the F atoms and the electron depletion region at the surface (blue region). The $\Delta\rho(r)$ shape changes with increasing fluorine atoms where the large charge depletion is observed located below the F atoms (see Figure 6-13 (a) as compared to Figure 6-13 (b)). The large negative charge $\Delta\rho(r) < 0$ between fluorine and titanium atoms occurs when the fluorine adsorption atoms are increased. This shows a mechanism of strong ionic interaction during halogen ion with titanium surface atom.

Formation of $TiCl_x$ molecules are analysed by means of a calculated charge density map. Figure 6-14 presents the 2D charge density difference for $TiCl_4$ and Ti_2Cl_6 molecules formed on Ti (100) surface. The top view plot reveals an accumulation charge in between the Cl atom with the neighbour's Ti atoms, indicating the formation of Ti-Cl bonds. Moreover, similar results were observed between Ti-F and Ti-Cl bonding, except that the electron density between Ti-F is larger. Comparing the isoline (iso-surfaces) between the TiF and TiCl, the high density of iso-surface (red-blue region) is seen from TiF_4 and Ti_2F_6 than on $TiCl_4$ and Ti_2Cl_6 molecules. This indicates their stronger bonding between Ti-F than Ti-Cl. The approximated strength of such bonding interaction can be estimated from isoline density. The Ti-Cl interaction is weakened due to the reduced density of iso-surface, as such the smaller magnitude of charge excess and deficit regions. Electron density plots of TiF_x showing the fluorine atom in TiF_x spherical charge distribution implying ionic bonding.

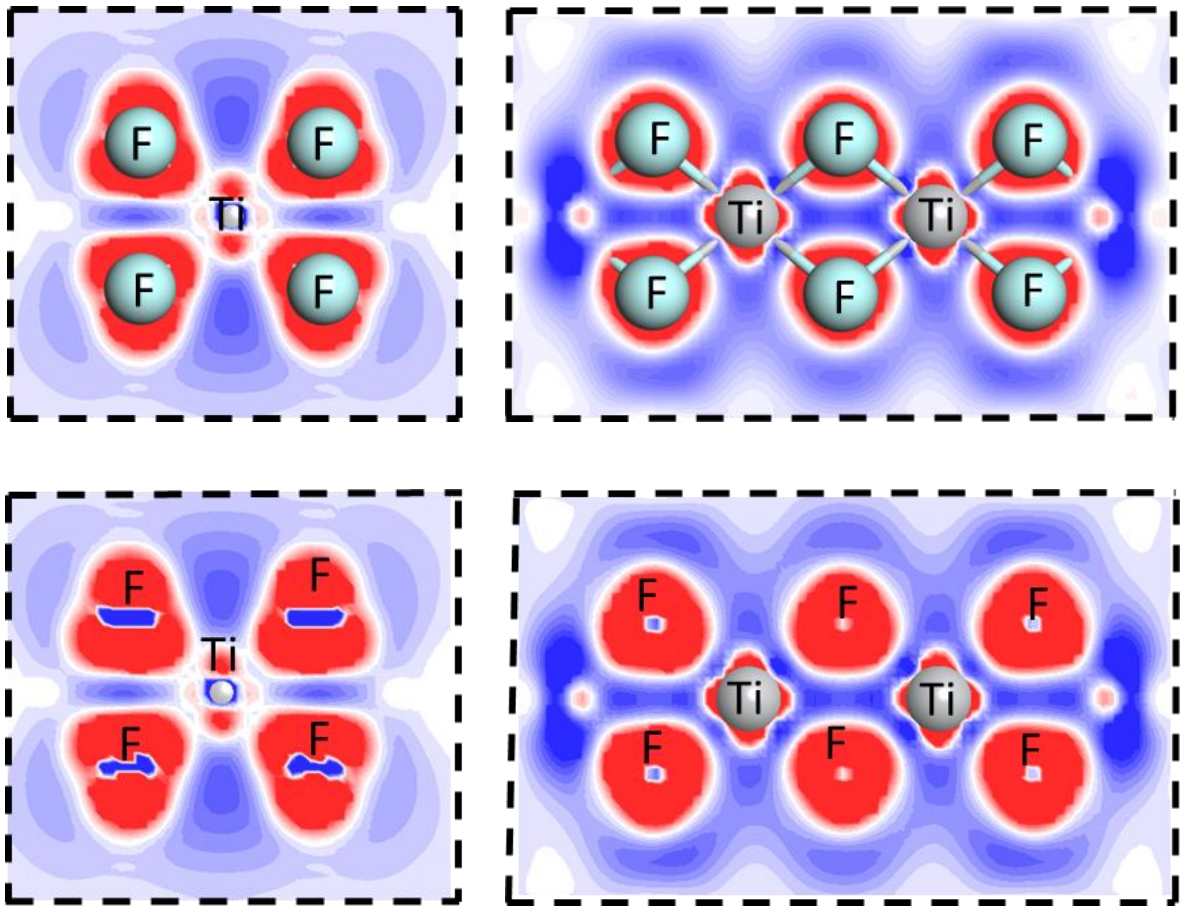

(a) (b)

Figure 6-13: Charge density difference for TiF_4 and Ti_2F_6 molecules formed on Ti (100) surface. Iso-surface of -0.05 eV to + 0.05 eV.

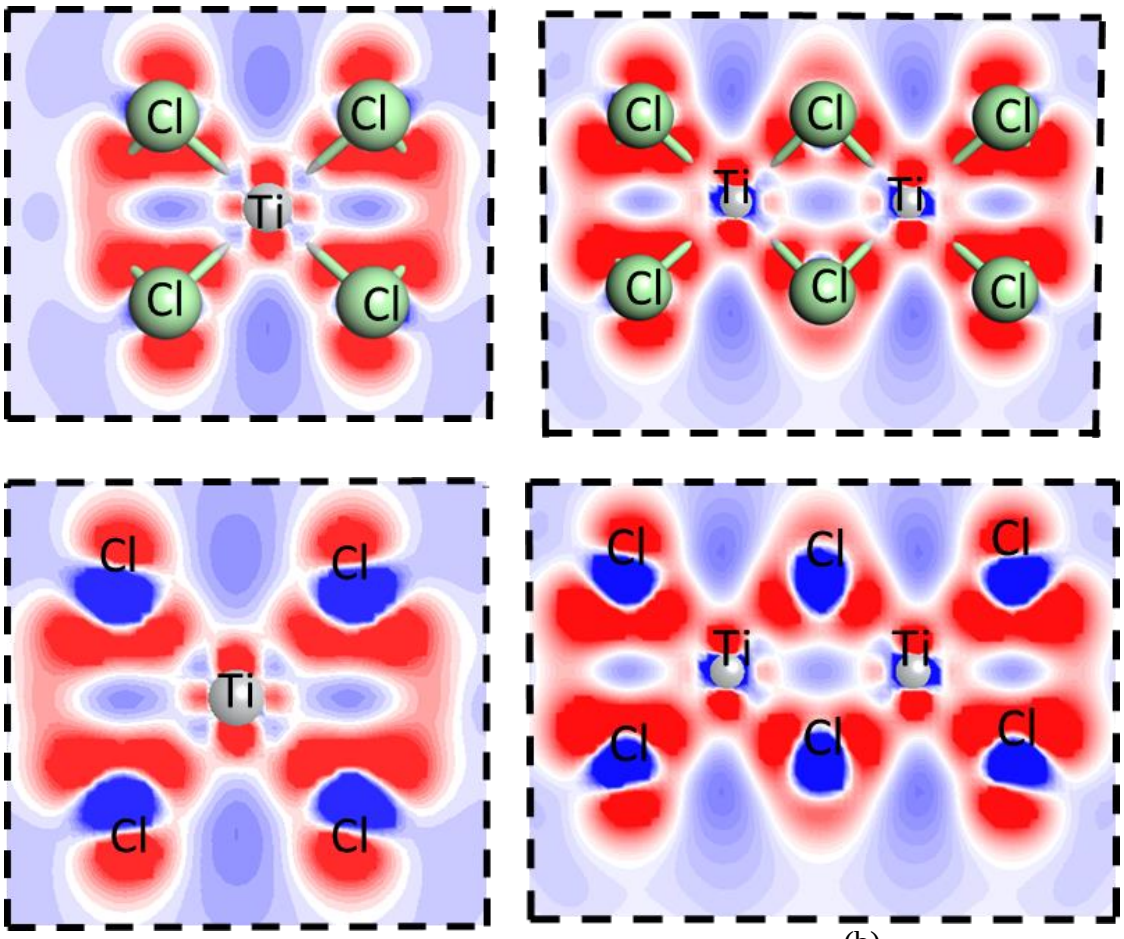

(a) (b)

Figure 6-14: Charge density difference for $TiCl_4$ and Ti_2Cl_6 molecules formed on Ti (100) surface. Isosurface of range from -0.05 eV to +0.05 eV.

Table 6-2 presents the atomic partial charges and population of formed volatile TiF_x and $TiCl_x$ molecules. Mulliken charge analysis shows that the Ti atoms are positively charged with a charge of 0.91-1.78 |e| while the F and Cl atoms have a charge of -1.76 |e| and -1.12 |e|, respectively. The charge of F atom adsorbed on the Ti surface is more negative than that of Cl atom. The more negative charge indicated that the Ti-F bond length is shorter than the Ti-Cl bond. It is also noted that the fluorine atom is highly negative charged which makes it highly polarization. Furthermore, the electronegativity of F (3.98) is greater than that of Cl (3.16) resulting in the fact that F atom obtains electrons from Ti easier than Cl atom when adsorbed on the Ti surface. In addition, the overlap population of Ti-F and Ti-Cl bonds are 0.26/0.29 and 0.45/0.50 on the TiF_4/Ti_2F_6 and

$TiCl_4/Ti_2Cl_6$ molecules. This indicates that the Ti-F bond is more ionic than that of Ti-Cl bond, which supports the charge density distribution analysis.

Table 6-2: Mulliken charge of several titanium halide molecules (TiF_x and $TiCl_x$)

Molecule	**Atoms**	**Charge (|e|)**	**population**
TiF_4	Ti; F	1.78; -1.76	0.26
Ti_2F_6	Ti;1F,2F	1.47;1.47;-1.02,-1.92	0.29, 0.15
$TiCl_4$	Ti; Cl	1.11;-1.12	0.45
Ti_2Cl_6	Ti; 1Cl, 2Cl	0.91, 0.19;-0.52, -1.28	0.50, 0.26

6.5. Summary

This Chapter presented the adsorption of F_2 and Cl_2 diatomic molecules on Ti (100) surface at different coverage mainly from 1-3ML. The nature of surface changes, volatile molecule formation and desorption energy received considerable attention in this Chapter. Our findings showed that when F_2 and Cl_2 diatomic molecule are adsorbed on Ti (100) surface result in the formation of volatile Ti_xF_y and Ti_xCl_y clusters on the Ti surface. Optimised structural results revealed that the obtained volatile molecules formed are TiF_4, Ti_2F_6, $TiCl_4$ and Ti_2Cl_6 with respect to coverage adsorption. We noted that the volatile molecules increase with increasing coverage adsorption of F_2 and Cl_2 molecule. This suggests that a large amount of F/Cl corresponding to an average interaction of F/Ti and Cl/Ti forming a volatile species. In addition, to understand clearly the formation of this molecule, the heats of formation were calculated.

It was found that all the TiF_x and $TiCl_x$ molecules possess negative heats of formation (E_{HF}) suggesting that the formation of these molecules is energetically favourable. Moreover, it asserts that there is no kinetic energy involved in the formation of TiF_x and $TiCl_x$ species. It was noted that the reaction of forming TiF_x cluster is more preferential with lower E_{HF} than the formation of $TiCl_x$

species. This means that fluorination is thermodynamically favourable on Ti surface because most metal fluorides are more stable than metal chloride. We also identified that the E_{HF} of Ti_2F_6 and Ti_2Cl_6 cluster are more stable than single TiF_4 and $TiCl_4$ species. Interestingly, it was seen that all these formed molecules were pulled-up from the Ti surface.

Furthermore, the Ti surface etching process can be described as the desorption mechanism taking place in the form of Ti_xF_y and Ti_xCl_y at any coverage. Therefore, the desorption process occurs energetically from the minimal barrier thus the desorption energy was calculated for each species. Comparing the energetic barrier for all possible desorption, the desorption energy for all molecules was found to be positive which implies a non-spontaneous process. However, the calculated desorption energy shows that the TiF_x molecule has a lower desorption barrier than $TiCl_x$. This implies that F can be the most stable reactant to form etch products as compare to Cl. This is consistent with the successful heat of formation for TiF_x clusters.

In addition, the dependence of the desorption energy present that a single molecule (TiF_4/$TiCl_4$) have minimal desorption energy than double (Ti_2F_6/Ti_2Cl_6) molecules. Pavlova *et al* reported similar observation analyses with Cl adsorption on cupper surface [119]. Etching mechanism via adatoms removal seems to be probable. This is reasonable that in the last step of fluorination and chlorination, the volatile TiF_4 and $TiCl_4$ molecules desorb. Therefore, both fluorination and chlorination reaction can be deployed for the titanium surface etching process. Moreover, the Mulliken charge analysis and electron density map show that the Ti-F is more ionic than the Ti-Cl interaction. This shows that charge transfer will be easy on Ti-F bonding which also causes stronger interaction than Ti-Cl.

Chapter 7

Conclusion and Recommendations

This chapter gives some prominent discoveries on the interaction of Ti surfaces with halogen molecules and ions. Some recommendations and future work are included, which may assist with further clarification and extending ideas on the etching mechanism. These encompass the titanium surfaces and fundamental studies of chemical interaction of halogen molecules/ions and Ti surfaces.

7.1. Conclusion

The present study has employed the first-principles approach to investigate the adsorption and etching of Ti surface with halogen molecules and ions. Two computational codes DMol^3 and CASTEP codes as embedded in Materials Studio were used. The DMol^3 code was utilised to simulate geometry optimisation of free halogen molecules while the CASTEP code was used for clean Ti surfaces and adsorbed surfaces calculations. The investigation of the etching process was described in three steps: (i) the interaction between the adsorbate-adsorbent, (ii) the formation of volatile molecules (etch products) on the surface and lastly, (iii) the desorption of the generated etch species on the surface. It was established that the selected etchant (HF, HC, HBr and HI) acids are potential to enhance the titanium surface.

Chapter 4 focused on the electronic properties of free halogen molecules and clean Ti (100), and (110) surfaces mainly to explore their reactivity and surface stability. It was found that the HF molecule is the most reactive etchant with lower dissociation energy of -5.12 eV than HCl, HBr and HI are -3.61 eV, -3.19eV and -2.87 eV, respectively. The dissociation energy decrease HF<HCl<HBr<HI. This is consistent with the observation reported by Lazarou *et al* [226].

Moreover, the electronegativity was highest for HF than other halogens indicating that HF is more reactive than HCl, HBr and HI molecules. The halogen molecules was found to follow the decrease stability order of HF> HCl> HBr> HI. Furthermore, we also found that Ti (110) surface is more stable with the lowest surface energy (0.141 eV/A^2) as compared to Ti (100) surface (0.126 eV/A^2). This is in agreement with the results reported by Hennig *et al* [237].

In Chapter 5, the adsorption of halogen molecules and ions on both Ti (100) and Ti (110) surfaces was studied to investigate the chemical interaction and their reactivity. This was determined by evaluating the adsorption energy, charge-electron transfer, charge density distribution and the work function. Three adsorption sites Top (T), Bridge (B) and Hollow (H) were examined and their reaction was spontaneous (E_{ads}<0). It was found that the bridge and top sites are the most favourable for Ti (100) and (110) surfaces, respectively. The order of reactivity for Ti (100) was B>T>H while for Ti (110) surface is T>H>Br. This trend is similar for all halogens adsorption on both surfaces. More importantly, the adsorption of halogen molecules on Ti surfaces are energetically favourable. Their adsorption strength show a periodic decreasing order of $E_{ads}^{HF} > E_{ads}^{HCl} > E_{ads}^{HBr} > E_{ads}^{HI}$. This interaction stability is similar to that of halogen dissociation energy and electronegativity. This implies that the adsorption of HF on these surfaces is thermodynamically stable than HCl, HBr and HI molecules. A similar observation was reported by Zhu *et al* [169] on the Al_2Pt surfaces. Similar observation was found when halogen ion is adsorbed on the surface. However, our results revealed that the adsorption of halogen ions is more preferential than that of halogen molecules. The F ion was found to be more reactive than Cl, Br and I ions resulting in the order F^->Cl^->Br^->I^-. It was evident that halogen ions cling to the Ti surface at different adsorption strength. Part of this work has been published [255].

Moreover, the interaction of halogen ions with Ti metal surfaces was deduced with regards to electron charge density. We found that all halogen ions are electron acceptors while the Ti surface atom is an electron donor. The amount of charge transferred depended on the adsorption energy strength. In particular, it was found that the F ion accepts more electrons than other halogen ions. The amount of charge transfer varies in the decreasing order F>Cl>Br>I, which is consistent with the adsorption energy strength. This is consistent with Bader net charge strength observed by Zhu *et al* [169] on the Al_2Pt surfaces. Furthermore, a directional bonding with a spherical shape was observed between halogen ion and surface atom. This suggests that the charge density distribution exhibit ionic bonding behaviour. Furthermore, it was also found that the adsorption of halogens induces the work function of Ti surfaces. The magnitude of the induced work function was observed to vary from halogen ionic in the order F>Cl>Br>I.

In order to describe the dependence of the surface coverage of adsorbed molecule, Chapter 6 presented the adsorption of F_2 and Cl_2 molecules at different coverage. We observed a substantial number of Ti_xF_y and Ti_xCl_y species formed on the metal Ti surface. This suggested the formation of the etch products that is TiF_4, Ti_2F_6, $TiCl_4$ and Ti_2Cl_6. The stability of the formed etch species was determined by calculating the heats of formation, desorption energy, the density of states and Mulliken population analysis. Our findings showed that the formation of Ti_xF_y and Ti_xCl_y clusters are energetically favourable (E_{HF}<0), suggesting an exergonic process. In addition, we also found that the Ti_xF_y species are more stable with the lowest heats of formation than Ti_xCl_y. It was also found that at high coverage, the formation of volatile Ti_xF_y is more favourable than the formation of Ti_xCl_y species. Mulliken population analysis of Ti-F is lower (0.29) than that of Ti-Cl (0.50) interaction. This indicates that the interaction of Ti-F is stronger and more ionic than that of Ti-Cl.

Moreover, the formed Ti_2F_6 and Ti_2Cl_6 are more stable than TiF_4 and $TiCl_4$, respectively. This suggests that the volatile biomolecules (Ti_2F_6, Ti_2Cl_6) were found to be more energetically stable than single molecules (TiF_4, $TiCl_4$). Thus, suggest the manifestation and second step of the etching process. Kim *et al* reported similar observation [38]. Furthermore, to understand the fundamental aspects of the etching process, the desorption energy of the formed Ti_xF_y and Ti_xCl_y species were calculated. It was found that all the etch products possess positive desorption energy which implied a non-spontaneous process. The desorption energy of the formed Ti_xF_y species was also found to be lower than Ti_xCl_y indicating that Ti_xF_y species desorb easily. This demonstrated that F_2 is suitable for Ti metal surface etching as compared to Cl_2. Thus, both fluorination and chlorination reaction can be deployed for the metal etching process.

In addition, the desorption energy of single TiF_4 and $TiCl_4$ is lower than the biomolecules Ti_2F_6 and Ti_2Cl_6 species. This suggests that the single etch product will desorb easier than the double etch species. The etching velocity depends on TiF_x and $TiCl_x$ clusters formed and desorbed. These findings are consistent with the work reported on the exposure of F_2 molecule on metal Si (100) surface where the relative primary etching product such as SiF_2 and SiF_4 molecules were observed [266]. Therefore, this implies that F_2 and Cl_2 etchants can be used for titanium metal surface etching. Moreover, the F_2 and Cl_2 etchants can be used as reactive gaseous and ions for dry or reacting ion etching method as described in Table 2-1 (Chapter 2). This is also consistent with literature for reactive ion etching for metal oxide surface [12], atomic layer etching of Si (100) and Si (111) surface by Cl_2 etchant [117] and Cu surface etching [119].

7.2. Recommendations

As results of the present work done, the following subjects are suggested for future work.

i. High adsorption coverage of halogen diatomic will be investigated using first-principle calculations.

ii. The development of Ti/F and Ti/Cl interatomic potential will be done using force field optimiser to describe the reaction of Ti-F and Ti-Cl.

iii. The temperature will be studied to investigate the etching mechanism at a different temperature, to measure the etch rate over the period.

iv. Adsorption of halogen molecules will be investigated at the different metal surfaces (aluminium, silicon or metal oxide surfaces) to study the etching mechanism.

v. An experimental study of halogen molecules adsorption at different coverage and etching will be studied in order to validate our predictions. Currently, HF molecule is used as a liquid etchant solution for metal surface etching, however, is more toxic and results in hydrogen embrittlement.

vi. Therefore it is recommended that both F_2 and Cl_2 molecules could be used as a gaseous etchant that mostly applicable for surface dry etching.

REFERENCES

[1] C. Leyens, M. Peters, Titanium and titanium alloys: Fundamentals and applications, Weinheim: Wiley-VCH, 2003.

[2] F. Campbell, Manufacturing technology for aerospace structural materials, Oxford: Elsevier, 2006.

[3] Z.M. Hu and T.A. Dean, "Aspects of forging of titanium alloys and the production of blade forms," Journal of Materials Processing Technology, vol. 111, pp. 10-19, 2001.

[4] R.C. Atwood, P.D. Lee and R.V. Curtis, "Modeling the surface contamination of dental titanium investment castings," Dental Materials, vol. 21, pp. 178-186, 2005.

[5] D. Mudaly, "Titanium and Magnesium Investment Casting Technology for Foundries," Accessed June 2017.

[6] S.Y. Sung, B.J. Choi, B.S. Han, H.J. Oh and Y.J. Kim, "Evaluation of alpha-case in titanium castings," Journal of Material Science and Technology, vol. 24, pp. 70-74, 2008.

[7] K.F. Lin and C.C. Lin, "Interfacial reactions between Ti-6Al-4V alloy and zirconia mold during casting," Journal of Materials Science, vol. 34, pp. 5899-5906, 1999.

[8] K.J. Kanarik, S. Tan, and R.A. Gottscho, "Atomic layer etching: rethinking the art of etch," Journal of Physical Chemistry Letters, vol. 9, pp. 4814-4821, 2018.

[9] P. Allongue, "Molecular imaging and local density of states characterization at the Si(111)/NaOH interface," Physical Review Letters, vol. 77, pp. 1986-1989, 1996.

[10] O.E. Tereshchenko, D. Paget, K.V. Toropetsky, V.L. Alperovich, S.V. Eremeev, A.V. Bakulin, S.E. Kulkova, B.P. Doyle and S. Nannarone, “Etching or stabilization of GaAs (001) under alkali and halogen adsorption,” Journal of Physical Chemistry C, vol. 116, pp. 8535-8540, 2012.

[11] K.J. Kanarik, S. Tan, W. Yang, T. Kim, T. Lill, A. Kabansky, E.A. Hudson, T. Ohba, K. Nojiri, J. Yu, R. Wise, I.L. Berry, Y. Pan, J. Marks and R.A. Gottscho, “Predicting synergy in atomic layer etching,” Journal of Vacuum Science and Technology A, vol. 35, pp. 05C302 (1)-05C302(7), 2017.

[12] M. David, R. Muhida, T. Roman, H. Nakanishi, W. Dino, H. Kasai, F. Takano, H. Shima and H. Akinaga, “First-principles calculations-based model for the reactive ion etching of metal oxide surfaces,” Vacuum, vol. 83, pp. 599-601, 2008.

[13] Y. Wang, H. Zhang, Y. Han, P. Liu, X. Yao and H. Zhao, “ A selective etching phenomenon on {001} faceted anatase titanium dioxide single crystal surfaces by hydrofluoric acid,” Chemical Communications, vol. 47, pp. 2829-2831, 2010.

[14] X. Liu, P. K. Chu and C. Ding, “Surface modification of titanium, titanium alloys and related materials for biomedical applications,” Materials Science and Engineering: Reports, vol. 47, pp. 49-121, 2004.

[15] M. Jamesh, S. Kumar and T.S.N.S. Narayanan, “Effect of thermal oxidation on corrosion resistance of commercially pure titanium in acid medium,” Journal of Materials Engineering and Performance, vol. 21, pp. 900-906, 2012.

[16] M.F. Lopez, J.A. Jimenez and A. Gutierrez, “Corrosion study of surface-modified vanadium-free titanium alloys,” Electrochimica Acta, vol. 48, pp. 1395-1401, 2003.

[17] J. Dini, “Chemical Milling,” International Metallurgical Reviews, vol. 20, pp. 29-56, 1975.

[18] J. Arrendondo, B. Colleary, S. Miskell and B. Sweet, “BS Project Report,” USA, 2010.

[19] M. Donachie, Titanium: a technical guide, USA: Material Park, 2000.

[20] Z.B. Wang, H.X. Hu and Y.G. Zheng, “Synergistic effects of fluorine and chlorine on general corrosion behavior of AISI 36 stainless steel and pure titanium in H2SO4 solution,” Corrosion Science, vol. 130, pp. 203-217, 2018.

[21] Z.B. Wang, H.X. Hu, C.B. Liu, H.N. Chen and Y.G. Zheng, “Corrosion behaviour of pure titanium and its weldment in simulalated desulfurized flue gas condensates in thermal power plant chimney,” Act Metallurgical Sinica (English letter), vol. 28, pp. 477-486, 2015.

[22] R.G.C.da Silva, M.R.S. Vieira, M.I.C. Malta, C.H. da Silva, S.H.de Oliveira and S.L.U. Filho, “Effect of initial surface treatment on obtaining a superhydrophobic surface on 5052 aluminum alloy with enhanced anticorrosion properties,” Surface and Coatings Technology, vol. 369, pp. 311-322, 2019.

[23] D. Knox and H.S. Grupp, “Chemical Milling, Increasing Efficiency at Wyman Gordon Company,” Worcester Polytechnic Institute, Worcester, MA, 2009.

[24] M. Niraula, K. Yasuda, N. Takai, M. Matsumoto,Y. Suzuki, Y. Tsukamoto, Y. Ito, S. Sugimoto,S. Kouno, D. Yamazaki and Y. Agata, “Surface processing of CdTe detectors using hydrogen bromide-based etching solution,” IEEE Electron Device Letters, vol. 36, pp. 856-858, 2015.

[25] H.H. Richter, M.A Aminpur, H.B. Erzgraber, A. Wolff, D. Kruger, A. Dehoff and M. Reetz, "Silicon dry etching in hydrogen iodide plasmas: surface diagnostics and technological apllications," Japane Journal of Applied Physics, vol. 36, pp. 4849-4853, 1997.

[26] N.O. Obi-Egbedi, I.B. Obot and M.I. El-Khaiary, "Quantum chemical investigation and statistical analysis of the relationship between corrosion inhibition efficiency and molecular structure of xanthene and its derivatives on mild steel in sulphuric acid," Journal of Molecular Structure, vol. 1002, pp. 86-96, 2011.

[27] V. Sharma, S. D. Elliott,T. Blomberg,S. Haukka, M. E. Givens, M. Tuominen and M. Ritala, "Thermal Atomic Layer Etching of Aluminum Oxide (Al2O3) Using Sequential Exposures of Niobium Pentafluoride (NbF5) and Carbon Tetrachloride (CCl4): A Combined Experimental and Density Functional Theory Study of the Etch Mechanism," Chemistry of Materials, vol. 33, pp. 2883-2893, 2021.

[28] S. K. Natarajan and S. D. Elliott, "Modeling the Chemical Mechanism of the Thermal Atomic Layer Etch of Aluminum Oxide: A Density Functional Theory Study of Reactions during HF Exposure," Chemistry of Matererials, vol. 30, pp. 5912-5922, 2018.

[29] H. Liu, M. Niinomi, M. Nakai and K. Cho, "A thermal and deformation-induced gamma phase transformations in biomedical beta-type alloy Ti-9Cr-0.2O," Acta Materialia, vol. 106, pp. 162-170, 2016.

[30] F. Trevisan, F. Calignano, A. Aversa, G. Marchese, M. Lombardi, S. Biamino, D. Ugues and D. Manfredi, "Additive manufacturing of titanium alloys in the biomedical field: processes, properties and applications," Applied Biomaterials and Functional Materials, vol. 16, pp. 57-67, 2017.

[31] P.T. Czekala, C. Panosetti, H. Lin and W.A. Hofer, “Van der Waals corrected DFT study of high coverage benzene adsorptions on Si(100) surface and STM simulations,” Surface Science , pp. 152-161, 2014.

[32] D.V. Tripkovic, D. Strmcnik, D. van der Vliet, V. Stamenkovic and N.M. Markovic, “The role of anoins in surface electrochemistry,” Faraday Discussions, vol. 140, pp. 25-40, 2009.

[33] O.M. Magnussen, “Ordered anion adlayers on metal electrode surfaces,” Chemical Reviews, vol. 102, pp. 679-726, 2002.

[34] G.N. Ankah, A. Pareek, S. Cherevko, A.A. Topalov, M. Rohwerder and F.U. Renne, “The influence of halides on the initial selective dissolution of Cu3Au (111),” Electrochimic Acta, vol. 85, pp. 384-392, 2012.

[35] Y.C. Lin, S. Lee, Y.C. Yang, P.W. Chiu, G.D. Lee and K. Suenaga, “Two-dimensional iodine-monofluoride epitaxy on WSe2,” Nature Partner Journals: 2D Materials and Applications, vol. 18, pp. 1-6, 2021.

[36] B.V. Andryushechkin, T.V. Pavlova and K.N. Eltsov , “Adsorption of halogens on metal surfaces,” Surface Science Reports, vol. 73, pp. 83-115, 2018.

[37] M.A. Gosalvez and R.M. Nieminen, “Surface morphology during anisotropic wet chemical etching of crystalline silicon,” New Journal of Physics, vol. 5, pp. 100(1)-100(28), 2003.

[38] S.Y. Kim and A.C.T. van Duin, “Simulation of titanium metal/titanium dioxide etching with chlorine and hydrogen chloride gases using the ReaxFF Reactive Force Field,” Journal of Physical Chemistry A, vol. 117, pp. 5655-5663, 2013.

[39] S. Ghosh and L. Manna, “The many facets of halide ions in the chemistry of colloidal,” Chemical Review, vol. 118, pp. 7804-7864, 2018.

[40] F. Vaz, P. Cerqueira, L. Rebouta, S.M.C. Nascimento, E. Alves, P. Goudeau, J.P. Riviere, K. Pischow and J de Rijk, “Structural, optical and mechanical properties of coloured TiNxOy thin films,” Thin Solid Films, vol. 448, pp. 449-454, 2004.

[41] D. Banerjee and J. Williams, “Perspectives on titanium science and technology,” Acta Materialia, vol. 61, pp. 844-879, 2013.

[42] Y. Liu, L. Chen, H. Tang, C.T. Liu, B. Liu and B. Huang, “Design of powder metallurgy titanium alloys and composites,” Materials Science and Engineering, vol. 418, pp. 25-35, 2006.

[43] B. Sefer, “Oxidation and Alpha–Case phenomena in titanium alloys used in aerospace industry: Ti–6Al–2Sn–4Zr–2Mo and Ti–6Al–4V,” PhD Thesis, pp. 1-112, 2014.

[44] G. Lütjering and J.C. Williams, Titanium, 2nd Edition, in: B. Derby (Ed.), Engineering Materials and Processes, Berlin: Springer, 2007.

[45] Y. Guilin, L. Nan, L. Yousheng and W. Yining, “The effects of different types of investments on the alpha-case layer of titanium castings,” Journal of Prosthetic Dentistry, vol. 97, pp. 157-164, 2007.

[46] T.A. Parthasarathy, W.J. Porter, S. Boone, R. John and P. Martin, “Life prediction under tension of titanium alloys that develop an oxygenated brittle case during use,” Scripta Materialia, vol. 65, pp. 420-423, 2011.

[47] S.Y. Sung, B.S. Han and Y.J. Kim, Formation of alpha case mechanism on titanium investment cast parts. In: Nurul Amin AKM ed. Titanium Alloys-Towards Achieving Enhanced Properties for Diversified Application, London: InTechOpen, 2012, pp. 29-42.

[48] E. Ezugwu and Z. Wang, "Titanium alloys and their machinability-a review," Journal of Materials Processing Technology, vol. 68, pp. 262-274, 1997.

[49] B.O. Odera, L.A. Cornish and M.J. Papo, "Electrolytic etching of platinum-aluminium based alloys," Platinum Metals Review, vol. 56, pp. 257-261, 2012.

[50] T.N. Pornsin-Sirirak, Y.C. Tai, H. Nassef and C.M. Ho,, "Titanium-alloy MEMS wing technology for a micro aerial vehicle application," Sensors and Actuators A: Physical, vol. 89, pp. 95-103, 2001.

[51] M.F. Aimi, M.P. Rao, N.C. Macdonald, A.S. Zuruzi and D.P. Bothman, "High-aspect-ratio bulk micromachining of titanium," Nature Materials, vol. 3, pp. 103-105, 2004.

[52] J.W. Coburn and H.F. Winters, "Plasma etching—A discussion of mechanisms," Journal of Vacuum Science and Technology, vol. 16, pp. 391-403, 1979.

[53] O. Cakir, "Chemical etching of aluminium," Journal of Material Processing Technology, vol. 199, pp. 337-340, 2008.

[54] V.M. Donnelly and A. Kornblit, "Plasma etching: Yesterday, today, and tomorrow," Journal of Vacuum Science and Technology A, vol. 31, pp. 050825(1)-050825(48), 2013.

[55] M.F.A. Muttalib, R.Y. Chen, S.J. Pearce and M.D.B. Charlton, "Optimization of reactive-ion etching (RIE) parameters for fabrication of tantalum pentoxide (Ta2O5) waveguide using Taguchi method," EPJ Web of Conferences, vol. 162, pp. 01003 (1)-01003 (5), 2017.

[56] H. Puliyalil and U. Cvelbar, “Selective plasma etching of polymeric substrates for advanced applications,” Nanomaterials, vol. 6, pp. 108(1)-108(24), 2016.

[57] A.l. Aria, B.J. Lyon and M. Gharib, “Morphology engineering of hollow carbon nanotube pillars by oxygen plasma treatment,” Carbon, vol. 81, pp. 376-387, 2015.

[58] F. Du, C. Lu, Mi, R. Huang, X. Han, Y. Shen and J. Shen, “Friction performance of aluminium-silicon alloy cylinder liner after chemical eching and laser finishing,” Metals, vol. 43, pp. 1-13, 2019.

[59] l.S. Manakasettharn, J.A. Taylor and T. Krupenkin, “Superhydrophobicity at micron and submicron scale,” Comprehensive Nanoscience and Technology, vol. 4, pp. 383-411, 2011.

[60] R. Zahran, J.I. Rosales Leal, M.A. Rodriguez Valverde and M.A. Cabrerizo Vilchez, “Effect of hydrofluoric acid etching time on titanium topography, chemistry, wettability, and cell adhesion,” PLoS One, vol. 11, pp. 1-12, 2016.

[61] H. Lee, H.D. Jung, M.H. Kang, J. Song, H.E. Kim and T.S. Jang, “Effect of HF/HNO3-treatment on the porous structure and cell penetrability of titanium (Ti) scaffold,” Materials and Design, vol. 145, pp. 65-73, 2018.

[62] V. Deshmukh, R. Kadam and S.S. Joshi, “Removal of alpha case on titanium alloy surfaces using chemical milling,” Machining Science and Technology, vol. 12, pp. 257-278, 2017.

[63] P. Rossouw, “Chemical milling infromation [Interview],” 2015.

[64] H.K. Jang, Y.D. Chung, S.W. Whangbo, I.W. Lyo, C.N. Whang, S.J. Lee and S. Lee, “Effects of chemical etching with hydrochloric acid on a glass surface,” Journal of Vacuum Science and Technology A, vol. 5, pp. 2563-2567, 2000.

[65] H.J. Oh, J.H. Lee, H.J. Ahn, Y. Jeong, N.J. Park, S.S. Kim and C.S. Chi, “Etching characteristics of high-purity aluminum in hydrochloric acid solutions,” Materials Science and Engineering A, vol. 449, pp. 348-351, 2007.

[66] A. Causier M. Bouttemy I. Gérard D. Aureau J. Vigneron and A. Etcheberry, “Aqueous bromine etching of InP: a specific surface chemistry,” Physica Status Solidi C, vol. 9, pp. 1408-1410, 2012.

[67] G.A. Grimes and G.K. Mor, TiO2, Nanotube Arrays: Synthesis, Properties and Applications, New York: Springer, 2009.

[68] C. Cardinaud, “Fluorine-based plasmas: Main features and application in micro-and nanotechnology and in surface treatment,” Comptes Rendus Chimie, vol. 21, pp. 723-739, 2018.

[69] J.H. Kim, A. Mirzaei, H.W. Kim and S.S. Kim, “Facile fabrication of superhydrophobic surfaces from austenitic stainless steel (AISI 304),” Applied Surface Science, vol. 439, pp. 598-604, 2018.

[70] M. Alhabeb, K. Maleski, T.S. Mathis, A. Sarycheva, C.B. Hatter, S. Uzun, A. Levitt and Y. Gogotsi, “Selective etching of silicon from Ti3SiC2 (MAX) to obtain 2D titanium carbide (MXene),” Angewandte Chemie Int.Ed, vol. 57, pp. 5444-5448, 2018.

[71] T. Rezayia and M.H. Entezari, “Toward a durable superhydrophobic aluminum surface by etching and ZnO nanoparticle deposition,” Journal of Colloid and Interface science, vol. 463, pp. 37-45, 2016.

[72] J.H. Kim, J.W. Bae, J.Y. Park, M.S. Im, B.O. Kim and J.H. Seo, “Effect of fluoride ions on wet etching of copper/ molybdenum in hydrogen peroxide solution,” Journal of Nanoscience and Nanotechnology, vol. 19, pp. 1714-1719, 2019.

[73] M. Ganjian, K. Modaresifar, H. Zhang, P.L. Hagedoorn, L.E.F Apachitei and A.A. Zadpoor, “Reactive ion etching for fabrication of biofunctional titanium nanostructures,” Scientific Report, vol. 9, pp. 18815(1)-18815(20), 2019.

[74] G. Cunge, M. Kogelschatz and N. Sadeghi, “Influence of reactor walls on plasma chemistry and on silicon etch product densities during silicon etching processes in halogen-based plasmas,” Plasma Sources Science and Technology, vol. 13, pp. 522-530, 2004.

[75] A.M. Cano, A.E. Marquardt, J.W. DuMont and S.M. George, “Effect of HF pressure on thermal Al2O3 atomic layer etch rates and Al2O3 fluorination,” Journal of Physical Chemistry C, vol. 123, pp. 10346-10355, 2019.

[76] W. Wang, P.R. Cha, G. Kim, M.J. Kim and K. Cho, “First principles study of Si etching by CHF3 plasma source,” Applied Surface Science, vol. 257, pp. 8767-8771, 2011.

[77] P. Sukkaew, Ö. Danielsson and L. Ojamäe, “Growth mechanism of SiC CVD: Surface etching by H2, H atoms and HCl,” Journal of Physical Chemistry A, vol. 122, pp. 2503-2512, 2018.

[78] J.L. Quan, B.T. Teng, X.D. Wen, Y. Zhao, R. Liu and M.F. Lu, “Hydrogen fluoride adsorption and reaction on the α-Al2O3 (0001) surface: A density functional theory study,” Journal of Chemical Physics, vol. 136, pp. 114701-114707, 2012.

[79] M.R. Arcos and C. Wangz, “Fluorine etching in porous silicon: An Ab-Initio Molecular Dynamics Study,” ECS Journal of Solid State Science and Technology, vol. 6, pp. P172-P177, 2017.

[80] T. Faraz, F. Roozeboom, H.C.M. Knoops and W.M.M. Kessels, “Atomic layer etching: What can we learn from atomic layer deposition,” ESC Journal of Solid State Science and Technology, vol. 4, pp. N5023-N5032, 2015.

[81] C.T. Carver, J.J. Plombon, P.E. Romero, S. Suri, T.A. Tronic and R.B. Turkot, “Atomic layer etching: An industry perspective,” ECS Journal Solid State Science and Technology, vol. 4, pp. N5005-N5009, 2015.

[82] K.J. Kanarik, T. Lill, E.A. Hudson, S. Sriraman, S. Tan, J. Marks, V. Vahedi and R.A. Gottscho, “Overview of atomic layer etching in the semiconductor industry,” Journal of Vacuum Science and Technology A, vol. 33, pp. 020802(1)-020802(14), 2015.

[83] Y. Lee and S.M. George, “Atomic layer etching of Al2O3 using sequential, self-limiting thermal reactions with Sn(acac)2 and hydrogen fluoride,” American Chemical Society Nano, vol. 9, pp. 2061-2070, 2015.

[84] S.M. George and Y. Lee, “Prospects for thermal atomic layer etching using sequential, self-limiting fluorination and ligand exchange reactions,” American Chemical Society, vol. 10, pp. 4889-4894, 2016.

[85] Y. Lee and S.M. George, “Thermal atomic layer etching of Al2O3, HfO2, and ZrO2 using sequential hydrogen fluoride and dimethylaluminum chloride exposures,” Journal of Physical Chemistry C, vol. 123, pp. 18455-18466, 2019.

[86] S.P. Walch, “Computed energetics for etching of the Si(100) surface byF and Cl atoms,” Surface Science, vol. 496, pp. 271-286, 2002.

[87] A. Migani, C. Sousa and F. IIIas, “Chemisorption of atomic chlorine on metal surfaces and the interpretation of the induced work function changes,” Surface Science , vol. 574, pp. 297-302, 2005.

[88] S.P. Chan, Z.F. Liu, W.M. Lau and J.S. Tse, “SiCl4 desorption in chlorine etching of Si (100)- a first principle study,” Surface Science, vol. 432, pp. 125-138, 1999.

[89] H.F. Winters and J.W. Coburn, “Surface science aspect of etching reactions,” Surface Science Reports, vol. 14, pp. 162-269, 1992.

[90] M. Peters, J. Kumpfert, C.H. Ward and C. Leyens, “Titanium alloys for aerospace applications,” Advanced Engineering Materials, pp. 419-427, 2003.

[91] Y. Li, C. Yang, H. Zhao, S. Qu, X. Li, and Y. Li, “New developments of Ti-based alloys for biomedical applications,” Materials, vol. 7, pp. 1709-1800, 2014.

[92] R.G. Hennig, D.R. Trinkle, J. Bouchet, S.G. Srinivasan, R.C. Albers and J.W. Wilkins, “Impurities block the α to ω martensitic transformation in titanium,” Nature of Materials, vol. 4, pp. 129-133, 2005.

[93] Y. Oshida, Bioscience and Bioengineering of Titanium Materials, Oxford: Elsevier, 2010.

[94] S.K. Nayak, C.J. Hung, V. Sharma, S.P. Alpay, A.M. Dongare, W.J. Brindley and R.J. Hebert , “Insight into point defects and impurities in titanium from first principles,” Computational Materials, vol. 11, pp. 1-10, 2018.

[95] F.U. Renner, G.N. Ankah and A. Pareek, “In-situ surface-sensitive X-ray diffraction study on the influence of iodide over the selective electrochemical etching of Cu3Au (111),” Surface Science, vol. 606, pp. L37-L40, 2012.

[96] O. Çakır, “Study of etch rate and surface roughness in chemical etching of stainless steel,” Key Engineering Materials, vol. 366, pp. 837-842, 2008.

[97] N. Buczek, Z. Huang, B. Fuhrmann and J. de Boor, “Model for the mass transport during metal-assisted chemical etching with contiguous metal films as catalysts,” Journal of Physical Chemistry C, vol. 24, pp. 13446-13451, 2012.

[98] H.H. Strehblow and P. Marcus, Mechanisms of pitting corrosion in corrosion mechanisms in theory and practise, P. Marcus editor: CRC Press, 2012, pp. 349-417.

[99] L.H. Liu, D.J. Michalak, T.P. Chopra, S.P. Pujari, W. Cabrera, D. Dick, J.F. Veyan, R. Hourani, M.D. Halls, H. Zuilhof and Y.J. Chabal, “Surface etching, chemical modification and characterization of silicon nitride and silicon oxide-selective functionalization of Si3N4 and SiO2,” Journal of Physics: Condensed Matter, vol. 28, pp. 094014-094020, 2016.

[100] H. Ohmi, J. Sato, Y. Shirasu, T. Hirano and H. Kakiuchi, “Significant improvement of copper dry etching property of a high-pressure hydrogen-based plasma by Nitrogen Gas Addition,” ACS Omega, vol. 4, pp. 4360-4366, 2019.

[101] E. Gileadi, “Charge and mass transfer across the metal/solution interface,” Isreal Journal of Chemistry, vol. 48, pp. 421-131, 2008.

[102] P. Acevedo-Pena and I. Gonzalez, “EIS characterization of the barrier layer formed over Ti during its potentiostatic anodization in 0.1 M HClO4/x mM HF (1 mM ≤ x ≤ 500 mM),” Journal of Electrochemical Society, vol. 159, pp. C101-C108, 2012.

[103] K. Fushimi, Y.Takabatake, T. Nakanishi and Y. Hasegawa, “Microelectrode techniques for corrosion research of iron,” Electrochimica Acta, vol. 113, pp. 741-747, 2013.

[104] P. Acevedo-Pena, L. Lartundo-Rojas and I. Gonzalez, “Effect of pH on the barrier layer of TiO2 nanoporous films potentiostatically grown in aqueous media containing fluoride ions,” Journal of Electrochemical Society, vol. 160, pp. C291-C297, 2013.

[105] C. Taylor, “The transition from metal-metal bonding to metal–solvent interactions during a dissolution event as assessed from electronic structure,” Chemical Physics Letters, vol. 469, pp. 99-103, 2009.

[106] Y.Y. Sun, S. Gulizia, C.H. Oh, D. Fraser, M. Leary, Y.F. Yang and M. Qian, “The influence of as-built surface conditions on mechanical properties of Ti-6Al-4V additively manufactured by selective electron beam melting,” Journal of The Minerals, Metals and Material Society, vol. 68, pp. 791-798, 2016.

[107] P. Jakob, Y.J. Chabal, K. Raghvachari, R.S. Becker and A.J. Becker, “Kinetic model of the chemical etching of Si (111) surface by buffered HF solution,” Surface Science, vol. 275, pp. 407-413, 1992.

[108] R. Ramakrishnaiah, A.A. Alkheraif, D.D. Divakar, J.P. Matinlinna and P.K. Vallittu, “The effect of hydrofluoric acid etching duration on the surface micromorphology, roughness, and wettability of dental ceramics,” International Journal of Molecular Science, vol. 17, pp. 822(1)-822(17), 2016.

[109] G. Juodzbalys, M. Sapragoniene and A. Wennerberg, “New acid etched titanium dental implant surface,” Journal of Stomatologija, Baltic Dental and Maxillofacial, vol. 5, pp. 101-105, 2003.

[110] L.L.E. Guehennec, A. Soueidan, P. Layrolle and Y. Amouriq, “Surface treatments of titanium dental implants for rapid osseointegration,” Dental Materials, vol. 23, pp. 844-854, 2007.

[111] K.Y. Hung, Y.C. Lin and H.P. Feng, “The effect of acid etching on the nanomorphological surface charateristics and activation energy of titanium medical materials,” Materials, vol. 10, pp. 1164(2)-1164(14), 2017.

[112] M.A. Gosalvez, A.S Foster and R.M. Nieminen, “Atomistic simulations of surface coverage effects in anisotropic wet chemical etching of crystalline silicon,” Applied Surface Science, vol. 202, pp. 160-182, 2002.

[113] S.A. Vitale, H. Chae and H.H. Sawin, “Silicon etching yields in F2, Cl2, Br2, and HBr high density plasmas,” Journal of Vacuum Science and Technology, vol. 19, pp. 2197-2206, 2001.

[114] M.A. Lieberman and A.J. Lichtenberg, Principles of Plasma Discharges and Materials Procesing, New York: Wiley, 2005.

[115] A.M. Efremov, D.B. Murin, V.B. Betelin and K.H. Kwon, “Special aspects of the kinetics of reactive ion etching of SiO2 in fluorine, chlorine and bromine containing plasma,” Russian Microelectronics, vol. 49, pp. 94-102, 2020.

[116] N. Lim, A. Efremov, H.G. Hwang and S. Nahm, “Etching kinetics and surface conditions for KNbxOy films with fluorine- and chlorine-based plasma chemistries,” Plasma Chemistry and Plasma Processing, vol. 40, pp. 625-640, 2020.

[117] S.D. Park, D.H. Lee and G.Y. Yeom, “Atomic layer etching of Si(100) and Si(111) Using Cl2 and Ar Neutral Beam,” Electrochemical and Solid-State Letters, vol. 8, pp. C106-C109, 2005.

[118] A. Agarwal and M.J. Kushner, “ Plasma atomic layer etching using conventional plasma equipment,” Journal Vacuum Science and Technology A, vol. 27, pp. 37-50, 2009.

[119] T.V. Pavlova, B.V. Andryushechkin and G.M. Zhidomirov, “First-principle study of adsorption and desorption of chlorine on Cu (111) surface: Does chlorine or copper chloride desorb,” Journal of Physical Chemistry C, vol. 120, pp. 2829-2836, 2016.

[120] E. Bright and D.W. Readey, “Dissolution Kinetics of TiO2 in HF-HCl solutions,” Journal of the American Ceramic Society, vol. 70, pp. 900-906, 1987.

[121] F. Fracassi and R. Dagostino, “Chemistry of titanium dry etching in fluorinated and chlorinated gases,” Pure and Applied Chemistry, vol. 5, pp. 703-707, 1992.

[122] H.G. Yang, C.H. Sun, S.Z. Qiao, J. Zou, G. Liu, S.C. Smith, H.M. Cheng and G.Q. Lu, “Anatase TiO2 single crystals with a large percentage of reactive facets,” Nature, vol. 453, pp. 638-641, 2008.

[123] X. Ma, Y. Dai, W. Wei, B. Huang and M.H. Whangbo, “Insights into how fluorine-adsorption and n-type doping affect the relative stability of the (001) and (101) surfaces of

TiO2: Enhancing the exposure of more active but thermodynamically less stable (001),” Journal of Physical Chemistry Letters, vol. 6, pp. 1876-1882, 2015.

[124] F. Gossenberger, T. Roman and A. Groß, “Equilibrium coverage of halides on metal electrodes,” Surface Science, vol. 631, pp. 17-22, 2015.

[125] N. de Leeuw, C. Nelson, C. Catlow, P. Sautet and W. Dong, “Density-functional theory calculations of the adsorption of Cl at perfect and defective Ag (111) surfaces,” Physical Review B, vol. 69, pp. 045419(1)-045419(12), 2004.

[126] A. Bouzoubaa, B. Diawara, V. Maurice, C. Minot and P. Marcus, “Ab initio modelling of localized corrosion: study of the role of surface steps in the interaction of chlorides with passivated nickel surfaces,” Corrosion Science, vol. 51, pp. 2174-2182, 2009.

[127] T.J. Grassman, G.C. Poon and A.C. Kummel, “Low coverage spontaneous etching and hyperthermal desorption of aluminum chlorides from Cl2/Al(1 1 1),” Journal of Chemical Physics, vol. 121, pp. 9018-9030, 2004.

[128] D.H. Kim, S.J. Kwak, J.H. Jeong, S. Yoo, S.K. Nam, Y.J. Kim and W.B. Lee, “Molecular Dynamics Simulation of Silicon Dioxide Etching by Hydrogen Fluoride Using the Reactive Force Field,” ACS Omega , vol. 6, pp. 16009-16015, 2021.

[129] S. Tinck, E.C. Neyts and A. Bogaerts , “Fluorine−silicon surface reactions during cryogenic and near room temperature etching,” Journal Physical Chemistry C , vol. 118, pp. 30315-30324, 2014.

[130] H. Ohta and S. Hamaguchi , “Molecular dynamics simulation of silicon and silicon dioxide etching by energetic halogen beams,” Journal Vacuum Science and Technology A , vol. 19, pp. 2373-2381, 2001.

[131] K.R. Williams, K. Gupta, M. Wasilik , “Etch Rates for Micromachining Processing -Part II,” Journal of Microelectromechanical Systems , vol. 12, pp. 761-778, 2003.

[132] C. Ellinger, A. Stierle, I.K. Robinson, A. Nefedov H. Dosch, “ Atmospheric Pressure Oxidation of Pt (111),” J. Phys.: Condens. Matter, vol. 20, pp. 184013(1)-184013(5), 2008.

[133] D. Kong, “The influence of fluoride on the physicochemical properties of anodic oxide films formed on titanium surfaces,” Langmuir, vol. 24, pp. 5324-5331, 2008.

[134] F. H. Froes H. Friedrich, J. Kiese and D. Bergoint, “Titanium in the family automobile: The cost challenge,” Journal of The Minerals, Metals and Material Society, vol. 56, pp. 40-44, 2004.

[135] S.B. Basame and H.S. White, “Pitting corrosion of titanium the relationship between pitting potential and competitive anion adsorption at the oxide film/electrolyte interface,” Journal of the Electrochemical Society, vol. 147, pp. 1376-1381, 2000.

[136] M. Mizuhata, S. Yamamoto and H. Maki, “Removal of surface scale from titanium metal by etching with HF–HNO3 Mixed Acid,” Materials Transactions, vol. 58, pp. 1280-1289, 2017.

[137] A.R. Shankar, N.S. Karthiselva and U.K. Mudali, “Thermal oxidation of titanium to improve corrosion resistance in boiling nitric acid medium,” Surface and Coatings Technology, vol. 235, pp. 45-53, 2013.

[138] Z.B. Wang, H.X. Hu, C.B. Liu and Y.G. Zheng, “The effect of fluoride ions on the corrosion behavior of pure titanium in 0.05 M sulfuric acid,” Electrochimica Acta, vol. 135, pp. 526-535, 2014.

[139] S. Ban, Y. Iwaya, H. Kono and H. Sato, “Surface modifaction of titanium by etching in concentrated sulfuric acid,” Dental Materials, vol. 22, pp. 1115-1120, 2006.

[140] M.S. Amrutha, F. Fasmin and S. Ramanathan, “Effect of HF concentration on anodic dissolution of titanium,” Journal of The Electrochemical Society, vol. 164, pp. H188-H197, 2017.

[141] Z. Liu, I.L. Tsai, G.E. Thompson, H. Liu and U. Donatus, “Chemical etching behaviour of titanium in bromine-methanol electrolyte,” Materials Chemistry and Physics, vol. 160, pp. 329-336, 2015.

[142] S.A. Cho and K.T. Park, “The removal torque of titanium screw inserted in rabbit tibia treated by dual acid etching,” Biomaterials, vol. 24, pp. 3611-3617, 2003.

[143] Z. Jiang, T. Norby and H. Middleton, “Evaluation of metastable pitting on titanium by charge integration of current transient,” Corrosion Science, vol. 52, pp. 3158-3161, 2010.

[144] J.T. Kim and S.A. Cho, “The effects of laser etching on shear bond strength at the titanium ceramic interface,” The Journal of Prosthetic Dentistry, vol. 101, pp. 101-106, 2009.

[145] L. Zhang, V.M. Menendez-Floresa, N. Murakami and T. Ohno, “Improvement of photocatalytic activity of brookite titanium dioxide nanorods by surface modification using chemical etching,” Applied Surface Science, vol. 258, pp. 5803-5809, 2012.

[146] C.M. Aldao and J.H. Weaver, “Halogen etching of Si via atomic-scale processes,” Progress in Surface Science, vol. 68, pp. 189-230, 2001.

[147] D. Sazou, K. Saltidou and M. Pagitsas, “Understanding the effect of bromides on the stability of titanium oxide films based on a point defect model,” Electrochimica Acta, vol. 76, pp. 48-61, 2012.

[148] H. Hocheng and P.S. Pa, “Electropolishing of cylindrical workpiece of tool materials using disc-form electrodes,” Journal Material Processing Technology, vol. 142, pp. 203-212, 2003.

[149] P.C. Lemaire and G.N. Parsons, “Thermal selective vapor etching of TiO2: Chemical vapor etching via WF4 and self-limiting atomic layer etching using WF6 and BCl3,” Chemistry of Materials , vol. 29, pp. 6653-6665, 2017.

[150] P.R. Mussini, S. Ardizzone, G. Cappelletti, M. Longhi, S. Rondinini and L.M. Doubova, “Surface screening effects by specifically adsorbed halide anions in the electrocatalytic reduction of a model organic halide at mono- and polycrystalline silver in acetonitrile,” Journal of Electroanalytical Chemistry, vol. 552, pp. 213-221, 2013.

[151] B.S. Hoener, C.P. Byers, T.S. Heiderscheit, A.S. De Silva Indrasekara, A. Hoggard, W. S. Chang, S. Link and C.F. Landes, “Spectroelectrochemistry of halide anion adsorption and dissolution of single gold nanorods,” Journal of Physical Chemistry C, vol. 120, pp. 20604-20612, 2016.

[152] R.W Revie and H.H Uhlig, Corrosion and corrosion control 4th ed, New Jersey: John Wiley & Sons, Hoboken, 2008.

[153] J.M. Bastidas, C. Fosca, B. Chico and E. Otero, “Corrosion behaviour of highly alloyed stainless steels in mixed chloride and fluoride aqueous solutions,” Material Corrosion, vol. 48, pp. 216-220, 1997.

[154] A.J. Samin and C.D. Taylor, “A computational thermodynamic and kinetic study of chlorine binding to the Zr (0001) surface,” Colloid and Surface A, vol. 539, pp. 92-100, 2018.

[155] E. Altman, Halogens on metals and semiconductors, Berlin: Springer, 2001, pp. 420-442.

[156] P. Mikolajczk and B. Stankiewicz, “Fluorine,chlorine and iodine adsorption on the Ge (001) surface: Comparative study for the coverage of 0.75 and 1 monolayer,” Applied Surface Science, vol. 256, pp. 4822-4828, 2010.

[157] M. Cordin, B.A. Lechner, P. Amann, A. Menzel, E. Bertel, C. Franchini, R. Zucca, J. Redinger, M. Baranov and S. Dieh, “Phase transitions driven by competing interactions in low-dimensional systems,” Europhysics Letters, vol. 92, pp. 26004P1-26004P5, 2010.

[158] B.V. Andryushechkin, G.M. Zhidomirov, K. N. Eltsov, Y.V. Hladchanka and A.A. Korlyukov, “Local structure of the Ag(100) surface reacting with molecular iodine: Experimental and theoretical study,” Physical Review B, vol. 80, pp. 125409-125419, 2009.

[159] J. Serafin, A. Liu and S. Seyedmonir, “Surface science and the silver-catalyzed epoxidation of ethylene: an industrial perspective,” Journal of Molecular Catalysis A: Chemical, vol. 131, pp. 157-168, 1998.

[160] A. Bouzoubaa, D. Costa, B. Diawara, N. Audiffren and P. Marcus, “Insight of DFT and atomistic thermodynamics on the adsorption and insertion of halides onto the hydroxylated NiO (111) surface,” Corrosion Science , vol. 52, pp. 2643-2652, 2010.

[161] A. Migani and F. Illas, “A systematic study of the structure and bonding of halogens on low-index transition metal surfaces,” Journal of Physical Chemistry B, vol. 110, pp. 11894-11906, 2006.

[162] J. Chiles, M. Malinowski, A. Rao, S. Novak, K. Richardson and S. Fathpour, “Low-loss, submicron chalcogenide integrated photonics with chlorine plasma etching,” Applied Physics Letter, vol. 106, pp. 111110(1)-111110(4), 2015.

[163] D.Y. Choi, S. Madden, A. Rode, R. Wang and B. Luther-Davies, “Dry etching characteristics of amorphous As2S3 film in CHF3 plasma,” Journal of Applied Physics, vol. 104, pp. 113305(1)-113305(6), 2008.

[164] E. Cheng and G.S. Hwang, “Dissociative chemisorption of methyl fluoride and its implications for atomic layer etching of silicon nitride,” Applied Surface Science , vol. 543, pp. 148557(1)-148557(6), 2021.

[165] J. Bjork, F. Hanke and S. Stafstrom, “Mechanisms of Halogen-Based Covalent Self-Assembly on Metal Surfaces,” Journal American Chemistry Society, vol. 135, pp. 5768-5775, 2013.

[166] I.A. Pasti, N.M. Gavrilov and S.V. Mentus, “Fluorine adsorption on transition metal surfaces – A DFT study,” Journal of the Serbian Chemical Society, vol. 78, pp. 1763-1773, 2013.

[167] A. Groß, “Ab initio molecular dynamics study of H2 adsorption on sulfur- and chlorine-covered Pd (100) surface,” Surface Science, vol. 608, pp. 249-254, 2013.

[168] Y. Duan, “Adsorption of fluorine and chlorine on Mg (0001) surface: A density functional theory investigation,” Transactions of Nonferrous Metals Society of China, vol. 24, pp. 1844-1852, 2014.

[169] Q. Zhu and S.Q. Wang, “First principles study of halogens adsorption on intermetallic surfaces,” Applied Surface Science, vol. 364, pp. 29-36, 2016.

[170] K. Tada, H. Koga, A. Hayashi, Y. Kondo, T. Kawakamia, S. Yamanaka and M. Okumura, “Effects of halogens on interactions between a reduced TiO2 (110) surface,” Applied Surface Science, vol. 411, pp. 149-162, 2017.

[171] I.A. Pasti and S.V. Mentus, “Halogen adsorption on crystallographic (111) planes of Pt, Pd, Cu and Au, and on Pd-monolayer catalyst surfaces: First-principles study,” Electrochimica Acta, vol. 55, pp. 1995-2003, 2010.

[172] B. Shen, Z. Fang, K. Fan and J. Deng, “Effect of halogen atoms (Cl, Br, I) on the structure and catalytic behavior of Ag(111) surface: a density functional,” Surface Science, vol. 459, pp. 206-212, 2000.

[173] Y. Wang, Q. Sun, K. Fan and J. Deng, “Interaction of halogen atom with Ag(110): ab initio pseudopotential density functional study,” Chemical Physics Letters, vol. 334, pp. 411-418, 2001.

[174] I.T. McCrum, S.A. Akhade and M.J. Janik, “Electrochemical specific adsorption of halides on Cu 111,100, and 211: A Density Functional Theory study,” Electrochimica Acta 173 (2015) 302–309, vol. 173, pp. 302-302, 2015.

[175] X.X. Wu, Q. Wang, F. Wang and Y. Zhou, “First-principles study on chemisorption of Cl on γ-TiAl (111) surface,” Acta Physica Sinica, vol. 59, pp. 7278-7284, 2010.

[176] H. Okada, K. Inagaki, H. Goto, K. Endo, K. Hirose and Y. Mori, “First-principles molecular-dynamics calculations and STM observations of dissociative adsorption of Cl2 and F2 on Si(0 0 1) surface,” Surface Science, vol. 515, pp. 287-295, 2002.

[177] H. Xionga, Y. Shi and Z. Wang, “Reactive ion etching of Ge-Sb-Se ternary chalcogenide glass films in fluorine plasma,” Microelectronic Engineering, vol. 225, pp. 111259 (1)-111259(8), 2020.

[178] A. Jenichen and C. Engler, “Etching of GaAs(100) surfaces by halogen molecules: density functional calculations on the different mechanisms,” Journal of Physical Chemistry B, vol. 105, pp. 1956-1960, 2001.

[179] H.M. Badran, Kh.M. Eid and H.Y. Ammar, “DFT and TD-DFT studies of halogens adsorption on cobalt-doped porphyrin: Effect of the external electric field,” Results in Physics, vol. 23, pp. 103964(1)-103964(14), 2021.

[180] R. Zhang, K. Kuang, P. Zhang and S. Chen, “Study on density functional theory of Cl surface,” Materials Science and Engineering of Powder Metallurgy, vol. 15, pp. 433-438, 2010.

[181] S.A. Saraireh, M. Altarawneh and M.A. Tarawneh, “Nanosystem’s density functional theory study of the chlorine adsorption on the Fe (100) surface,” Nanotechnology Reviews, vol. 10, pp. 719-721, 2021.

[182] M. Liu, Y. Jin, C. Zhang, C. Leygraf and L. Wen, “Density-functional theory investigation of Al pitting corrosionin electrolyte containing chloride ions,” Applied Surface Science , vol. 357, pp. 2028-2038, 2015.

[183] A. Wander, C.L. Bailey, B.G. Searle, S. Mukhopadhyay and N.M. Harrison, “Identification of possible lewis acid sites on the β-AlF3 (100) surface: An ab initio total energy study,” Physical Chemistry Chemical Physics, vol. 7, pp. 3989-3993, 2005.

[184] J. Acker, S. Bucker and V. Hoffmann , “Impact of the chemical form of different fluorine sources on the formation of AlF molecules in a C2H2/N2O flame,” Journal of Analytical Atomic Spectrometry, vol. 31, pp. 902-909, 2016.

[185] “Material Studio, DS BIOVIA. Dassault System BIOVIA,” 2000.

[186] S.J. Clark, M.D. Segall, C.J. Pickard, P.J. Hasnip, M.J. Probert, K. Refson and M.C. Payne,, “First principle Methods Using CASTEP,” Zeitschrift für Kristallographie, vol. 220, pp. 567-570, 2005.

[187] B. Delley, “From molecules to solids with the DMol3,” Journal of Chemical Physics, vol. 113, pp. 7756-7764, 2000.

[188] P. Hohenberg and W. Kohn, “Inhomogeneous electron gas,” Physical Review B, vol. 136, pp. 867-871, 1964.

[189] W. Kohn and L.J. Sham, “Self-consistent equations including exchange and correlation effects,” Physical Review A, vol. 140, pp. A1133-A1138, 1965.

[190] L.H. Thomas, “The Calculation of Atomic Fields,” Proceedings Cambridge Philosophical Society, vol. 23, pp. 542-548, 1926.

[191] E. Fermi, “Theory for Atomic Systems,” Zeitschrift Physics, vol. 48, pp. 73-79, 1928.

[192] D.R. Hartree, “The Wave Mechanics an Atom with a Non-Coulomb Central Field. Part1 Theory and Methods,” Proceeding Cambridge Philosophical Society, vol. 24, pp. 89-110, 1928.

[193] V. Fock, “Approximate Method for the Solution of the Quantum Mechanical Problems,” Z. Phys., vol. 61, pp. 126-148, 1930.

[194] J.C. Slater, “A simplification of the Hartree-Fock Method,” Physical Review, vol. 81, pp. 385-390, 1951.

[195] J.C. Slater, Quantum Theory of Molecules and Solids 4, New York: McGraw-Hill, 1974.

[196] M. U. Guide, Materials Design Manual, Materials Design Inc, 2018.

[197] M.C. Payne, M.P. Teter and T.A. Allan, “Iterative minimization techniques for ab initio total-energy calculations: Molecular dynamics and conjugate gradients,” Reviews of Modern Physics, vol. 64, pp. 1050-1051, 1992.

[198] J.P. Perdew, K. Burke and M. Ernzerhof, “Generalised gradient approximation made simple,” Physical Review Letter, vol. 77, pp. 3865-3868, 1996.

[199] J.P. Perdew and Y. Wang, “Accurate and simple density functional for the electronic exchange energy: General Gradient Approximation,” Journal of Physical Review B, vol. 33, pp. 8800-8802, 1986.

[200] J.P. Perdew, J.A. Chevary, S.H. Vosko, K.A. Jackson, M.R. Pederson, D.J. Singh and C. Fiolhais, “Atoms, molecules, solids and surface: Application of the generalized gradient

approximation for exchange and correction.," Journal of Physical Review B, vol. 46, pp. 6671-6687, 1992.

[201] A.E. Mattsson, P.A. Schultz, M.P. Desjarlais, T.R. Mattsson and K. Leung, "Desinging meaningful density functional theory calculations in materials science– a Primer," Modelling and Simulation of Material and Engineering, vol. 11, pp. R1-R31, 2005.

[202] W. Koch and M.C. Holthausen, A chemist's guide to density functional theory, Weinheim: Wiley-VCH, 2001, pp. 75-77.

[203] K. Burke, P. Perdew and M. Ernzerhof,, "Why the generalized gradient approximation works and how to go beyond it," International Journal Quantum of Chemistry, vol. 293, pp. 61-64, 1997.

[204] J. Tao, J.P. Perdew, V.N. Staroverov and G.E. Scuseria, "Climbing the density functional ladder: nonempirical meta-generalized gradient approximation designed for molecules and solids," Physical Review Letters, vol. 91, pp. 146401(1)-146401(4), 2003.

[205] P. Blochl, "Theory and practice of density-functional theory," Institute for Theoretical Physics: Clausthal University of Technology, pp. 1-43, 2011.

[206] J. Harvey, "DFT computation of relative spin-state energetics of transition metal compounds," Structure and Bonding, vol. 112, pp. 151-183, 2004.

[207] J. Hafner, "Ab initio simulation of material using VASP: Density Function Theory and Beyond," Journal of Computational Chemistry, vol. 29, pp. 2045-2078, 2008.

[208] J.R. Chelikowsky and M.L. Cohen, Pseudopotentials for semiconductors, in Handbook of Semiconductors, Amsterdam: Elsevier, 1992.

[209] D.J. Chadi and M.L. Cohen, “Special Points in the Brillouin Zone,” Physical Review B, vol. 8, pp. 5747-5753, 1973.

[210] N. Troullier and J.L. Martins, “Efficient pseudopotential for plane-wave calculations,” Journal of Physical Review B, vol. 43, pp. 1993-2006, 1991.

[211] D. Vanderbilt, “Soft self-consistent pseudopotentials in a generalized eigenvalue formalism,” Physical Review B, vol. 41, pp. 7892-7895, 1992.

[212] S.G. Louie, S. Froyen and M.L. Cohen, “Nonlinear ionic pseudopotentials in spin-density-functional calculations,” Physical Review B, vol. 26, pp. 1738-1742, 1982.

[213] P. Blöchl, “Projector augmented-wave method,” Physical Review B, vol. 50, pp. 17953-17979, 1994.

[214] D. Singh, Plane Waves, Pseudopotentials and the LAPW Method, Norwell, MA: Kluwer Academic, 1994..

[215] G. Kresse and D. Joubert, “From ultrasoft pseudopotentials to the projector augmented-wave method,” Physical Review B, vol. 59, pp. 1758-1775, 1999.

[216] Y.H. Dai, “Covergence Properties of the BFGS algorimthm,” SIAM Journal on Optimization, vol. 13, pp. 693-701, 2002.

[217] M.D. Segall, P.J.D. Lindan, M.J. Probert, C.J. Hasnip, S.J. Clark and M.C. Payne, “First Principle simulation: Ideas, illustrations and CASTEP code,” Journal of Physics: Condensed Matter, vol. 14, pp. 2717-2744, 2002.

[218] B. Delley, “An all-electron numerical method for solving the local density functional for polyatomic molecules,” Journal of Chemical Physics, vol. 92, pp. 508-517, 1990.

[219] R.R. Nazmutdinova, T.T. Zinkicheva, M. Probst, K. Lust and E. Lust, “Adsorption of halide ions from aqueous solutions ata Cd(0001) electrode surface: quantum chemicalmodelling and experimental study,” Surface Science , vol. 577, pp. 112-126, 2005.

[220] K.F. Khaled, N.S. Abdelshafi, A.A. El-Maghraby, A. Aouniti, N. Al-Mobarak and B. Hammouti, “Alanine as corrosion inhibitor for iron in acid medium: a molecular level study,” International Journal of Electrochemical Science, vol. 7, pp. 12706-12719, 2012.

[221] C. Fall, “Ab initio study of the work functions of the elemental metal crystals,” PhD Thesis, pp. 1-144, 1999.

[222] L. Markus, “Adsorption of Simple molecules on structured surfaces,” PhD Thesis, pp. 1-117, 2003.

[223] R. Tran, X.G. Li, J.H. Montoya, D. Winston, K.A. Persson and S.P. Ong, “Anisotropic work function of elemental crystals,” Surface Science, vol. 687, pp. 48-55, 2019.

[224] H.J. Monkhorst and J.D. Pack, “Special points for Brillouin-zone integrations,” Physical Review B, vol. 13, pp. 5188-5192, 1976.

[225] C.L. Reis, J.M. Pacheco and J.L. Martins, “First-principles norm-conserving pseudopotential with explicit incorporation of semicore states,” Physical Review B, vol. 68, pp. 155111(1)-155111(6), 2003.

[226] Y.G. Lazarou, A.V. Prosmitis, V.C. Papadimitriou and P. Papagiannakopoulos, “Theoretical calculation of bond dissociation energies and enthalpies of formation for halogenated molecules,” Journal of Physical Chemistry A, vol. 105, pp. 6729-6742, 2001.

[227] R. Petrucci, “Genereal Chemistry 9th Ed,” in Principles and Modern Applications, New Jersey, Pearson Education Inc, 2007, pp. 920-928.

[228] C. Housecroft and A.G. Sharpe , Inorganic Chemistry (3rd, Third Edition), New Jersey: Prentice Hall, 2007.

[229] G. Cavallo, P. Metrangolo, R. Milani, T. Pilati and A. Priimagi, “The Halogen Bond,” Chemical Reviews, vol. 116, pp. 2478-2601, 2016.

[230] A.Y. Musa, A.A.H. Kadhum, A.B. Mohamad, A.A.B. Rahoma and H Mesmari, “Electrochemical and quantum chemical calculations on 4, 4-dimethyloxazolidine-2-thione as inhibitor for mild steel corrosion in hydrochloric acid,” Journal of Molecular Structure, vol. 969, pp. 233-237, 2010.

[231] D. Al-Amiedy, “Spin-orbital coupling, spin-spin, and electric properties of hydrogen floride (HF), hydrogen chloride molecules(HCl) and hydrogen bromide molecule,” STM Journals: Emerging Trends in Chemical Engineering, vol. 2, pp. 1-3, 2015.

[232] M. Amati, S. Stoia and E.J. Baerends, “The electron affinity as the highest occupied anion orbital energy with a sufficiently accurate approximation of the Exact Kohn-Sham Potential,” Journal of Chemical Theory and Computation, vol. 16, pp. 443-452, 2020.

[233] T. Mineva, N. Neshev, E. Sicilia and M. Toscano, “Density functional orbital reactivity indices: Fundamentals and applications,” Advances in quantum chemistry, vol. 33, pp. 273-292, 1998.

[234] E. Wers, H. Oudadesse, B. Lefeuvre, A. Lucas-Girot, J. Rocherulle´and R. Lebullenger, “Excess entropy and thermal behavior of Cu- and Ti-dopedbioactive glasse,” Journal of Thermal Analysis and Calorimetry, vol. 117, pp. 579-588, 2014.

[235] A. Dwivedi, V. Baboo and A. Bajpai, “Fukui function analysis and optical, electronic, and vibrational properties of tetrahydrofuran and Its derivatives: A complete quantum chemical study,” Journal of Theoretical Chemistry, pp. 1-11, 2015.

[236] R.R. Contreras, P. Fuentealba, M. Galván and P. Pérez, “A direct evaluation of regional Fukui functions in molecules,” Chemical Physics Letters, vol. 304, pp. 405-413, 1999.

[237] R.G. Hennig, T.J. Lenosky, D.R. Trinkle, S.P. Rudin and J.W. Wilkins, “Classical potential describes martensitic phase transformations between the alpha, beta and gamma titanium phases,” Physical Review B, vol. 78, pp. 0541211-05412110, 2008.

[238] R. Tran, Z. Xu, B. Radhakrishnan, D. Winston, W. Sun, K.A. Persson and S.P. Ong, “Surface energies of elemental crystals,” Scientific Data , vol. 3, pp. 160080(1)-160080(13), 2016.

[239] H.Y. Wang, N. Wang, S. Zhang, X.Y. Deng, D.J. Li and H.Q. Gu, “First-principles study on stability and electronic properties of W(001), W(110) and W(111) surfaces,” Surface and Coatings Technology, vol. 229, pp. 55-59, 2013.

[240] N.E. Singh-Miller and N. Marzari, “Surface energies, work functions, and surface relaxations of low-index metallic surfaces from first principles,” Physical Review B, vol. 80, pp. 1-9, 2009.

[241] T. Roman, F. Gossenberger, K. Forster-Tonigold and A. Groß, “Halide adsorption on close-packed metal electrodes,” Physical Chemistry Chemical Phyics, vol. 16, pp. 13630-13634, 2014.

[242] W. Wei, K. Wu, X. Zhang, J. Liu, P. Qiu and L. Cheng, “In-situ characterization of initial marine corrosioninduced by rare-earth elements modifiedinclusions in Zr-Ti deoxidized low-alloy steels,” Journal of Materials Research and Technology, vol. 9, pp. 1412-1424, 2020.

[243] K. Christmann, “Some basic processes at surfaces exemplified by means of hydrogen interaction with transition metals,” Surface Science and Electrochemistry, pp. 213-220, 2018.

[244] D.M. Tshwane, R. Modiba, H.R. Chauke, G. Govender and P.E. Ngoepe, “First-principle study of HF molecule adsorption on TiO2 (110) surface,” Material Science and Engineering, vol. 655, pp. 012043(1)-012043(9), 2019.

[245] B.J. Lee, A. Efremov, J. Lee and K.H. Kwon, “Etching kinetics and mechanisms of SiC Thin Films in F, Cl and Br based plasma chemistries,” Plasma Chemistry and Plasma Processing, vol. 39, pp. 325-33, 2019.

[246] F. Paesani, P. Bajaj and M. Riera, “Chemical accuracy in modeling halide ion hydration from many-body representations,” Advances in Physics: X, vol. 4, pp. 1-30, 2019.

[247] D.K. Nguyen, N.T.T. Tran, Y.H. Chiu and M.F. Lin, “Concentration diversified magnetic and electronic properties of halogen adsorbed silicene,” Scientific Reports Nature Research, vol. 9, pp. 13746(1)-13746(16), 2019.

[248] S. Zong, Y. Zhang, N. Lu, P. Ma, J. Wang and X.R. Shi, “A DFT screening of M-HKUST-1 MOFs for nitrogen-containing compounds adsorption,” Nanomaterials MDPI, vol. 8, pp. 958(1)-958(16), 2018.

[249] K. Pradhan, G.L. Gutsev and P. Jena, “Negative ions of transition metal-halogen clusters,” The Journal of Chemical Physics, vol. 18, pp. 1443011-1443018, 2010.

[250] Z. Huang, N. Geyer, P. Werner, J. de Boor and U. Gosele, “Metal assisted chemical etching of silicone: A Review,” Advanced Materials, vol. 23, pp. 285-308, 2011.

[251] B.W. Tian, T.H. Huang, J.Y. Guo, H.B. Shu, Y. Wang and J. Dai , “Gas adsorption on the pristine monolayer GeP3: a first-principles calculation,” Vacuum, vol. 164, pp. 181-185, 2019.

[252] Z. Ma, R. Sa, Q. Li and K. Wu, “Interfacial electronic structure and charge transfer of hybrid graphene quantum dot and graphitic carbon nitride nanocomposites: insights into high effeciency for photocatalytic solar water splitting,” Physical Chemistry Chemical Physics, vol. 18, pp. 1050-1058, 2016.

[253] G. Kastlunger, P. Lindgre and A.A. Peterson, “Controlled-potential simulation of elementary electrochemical reaction: Proton discharge on metal surface,” Journal of Physical Chemistry C, vol. 122, pp. 12771-12781, 2018.

[254] G. Guo, H. Wu, J. Liu, Y. Zhang and Z. Xie, “Tuning the electronic and magnetic properties of monolayer germanium triphosphide adsorbed by halogen atoms: Insights from first principles study,” Physica E, vol. 127, pp. 114537(1)-114537(7), 2021.

[255] D.M. Tshwane, R. Modiba, G. Govender, P. E. Ngoepe and H.R. Chauke, “The adsorption of halogen molecules on Ti (110) surface,” Journal of Materials Research, pp. 592-601, 2021.

[256] L.P. Wolters and F. M. Bickelhaupt, “Halogen Bonding versus Hydrogen Bonding: A Molecular Orbital Perspective,” ChemistryOpen , vol. 1, pp. 96-105, 2012.

[257] D.M Tshwane, R Modiba, H.R Chauke, G Govender and P.E Ngoepe, “Computer simulation studies of HF adsorption on TiO2 (001) and (110) surfaces,” The Proceedings of SAIP2019, the 64th Annual Conference of the South African Institute of Physics, Vols. ISBN: 798-0-620-88875-2, pp. 23-28, 2020.

[258] B.V. Andryushechkin, V.V. Zheltov, V.V. Cherkez, G.M. Zhidomirov, A.N. Klimov, B. Kierren, Y. Fagot-Revurat, D. Malterre and K.N. Eltsov, “Chlorine adsorption on Cu(111) revisited: LT-STM and DFT study.,” Surface Science, vol. 639, pp. 7-12, 2015.

[259] H. Xu and I. Harrison,, “Dissociative adsorption of Br2 on Pt (111): hot atom dynamics,” Journal of Physical Chemistry B, vol. 103, pp. 11233-11236, 1999.

[260] K. Christmann, “Some Basic Processes at Surfaces Exemplified by Means of Hydrogen Interaction With Transition Metals,” Encyclopedia of Interfacial Chemistry: Surface Science and Electrochemistry, pp. 213-220, 2018.

[261] L. Guo, Y. Ou, X. Shen, S. Kaya, W. Shi, R. Zhang, X. Zheng and J. Wang, “Specific adsorption of halide ions on Iron surface: A combined electrochemical and Monte Carlo simulation investigation,” International Journal of Electrochemical Science, vol. 12, pp. 7064-7074, 2017.

[262] A.S. Shalabi, “F+ tunable laser activity and interaction of atomic halogens (F, Cl and Br) at the low coordinated surface sites of SrO:Ab initio and DFT calculations,” Journal of Molecular Modeelling , vol. 8, pp. 314-326, 2002.

[263] S. Batsanov, “Van der Waals Radii of Elements,” Inorganic Materials, vol. 37, pp. 871-885, 2001.

[264] R.F.W. Bader and W.H. Henneker, “Molecular Charge Distributions and Chemical Binding,” Journal of Chemical Physics, vol. 46, p. 3341, 1967.

[265] A.V. Bakulin, S.E. Kulkova, S.V. Eremeev and O.E. Tereshchenko, “Early stages of halogen adsorption on cation-rich InAs (001): surface etching mechanism,” Journal of Physical Chemistry C, vol. 118, pp. 10097-10105, 2014.

[266] A. Chatterjee, T. Iwasaki and T. Ebina, “Adsorption and structural energetics of chemisorbed F atom on Si(100)-a density functional theory (DFT) study,” The Japan Society of Applied Physics, vol. 39, pp. 4279-4284, 2000.

[267] A.H. Basher, M. Krstić, T. Takeuchi, M. Isobe and T. Ito, “Stability of hexafluoroacetylacetone molecules on metallic and oxidized nickel surfaces in atomic-layer-etching processes,” Journal of Vacuum Science and Technology A, vol. 38, pp. 022610(1)-022610(8), 2020.

[268] A. Agarwal and M.J. Kushner, “Plasma atomic layer etching using conventional plasma equipment,” Journal of Vacuum Science and Technology A, vol. 27, pp. 37-50, 2009.

[269] I.L. Geada, H.R. Dakhel, T. Jamil, M. Sulpizi and H. Heinz, “Insight into induced charges at metal surfaces and biointerfaces using a polarizable Lennard–Jones potential,” Nature Communication, vol. 9, pp. 716 (1)-716(14), 2018.

[270] A.D. Buckingham , “Molecular and Chemical Physics,” Journal of the Chemical Society, Faraday Transactions 2, vol. 83, pp. 1743-1750, 1987.

[271] P. Gkeka, “Molecular dynamics studies of peptide-membrane interactions: insights from coarse-grained models,” PhD Thesis, 2010.

[272] G.W. Watson, E.T. Kelsey, N.H. de Leeuw, D.J. Harris and S.C. Parker, “Atomistic simulation of dislocations, surfaces and interfaces in MgO,” Chemical Society Faraday Transactions , vol. 92, pp. 433-438, 1996.

[273] S. Li and D.A. Dixon, “Chapter 2-Structural and Electronic Properties of Group 6 Transition Metal Oxide Clusters,” New and Future Developments in Catalysis, pp. 21-61, 2013.

[274] K.T. Tang and J.P. Toennies, “A simple theoretical model for the van der Waals potential at intermediate distances. I. Spherically symmetric potentials,” The Journal of Chemical Physics, vol. 66, pp. 1496-1506, 1977.

[275] V.V. Ogorodnikov and Y.I. Rogovoi, “Buckingham-potential parameters and relations between them for solids,” Powder Metallurgy and Metal Ceramics, vol. 33, pp. 327-333, 1995.

[276] H. Nienhaus, “Electronic excitations by chemical reactions on metal surfaces,” Surface Science Reports, vol. 45, pp. 1-78, 2002.

[277] P. Metrangolo and G. Resnati, “Halogen bonding: A Paradigm in supramolecular chemistry,” Chemistry- A European Journal, vol. 7, pp. 2511-2519, 2001.

[278] H. Grubmüller, H. Heller, A. Windemuth and K. Schulten, “Generalized Verlet Algorithm for Efficient Molecular Dynamics Simulations with Long-range Interactions,” Molecular Simulation, vol. 6, pp. 121-142, 1991.

[279] W.J. Kim, S. Xing, G. Kremer, M. Sicot, B. Kierren, D. Malterre, G. Contini, J. Rault, P. Le Fèvre, F. Bertran, D. Rocca, Y. Fagot-Revurat and S. Lebègue, “Electronic structure of heavy halogen atoms adsorbed on the Cu(111) surface: A combined ARPES and first principles calculations study,” Journal of Physical Chemistry C, vol. 123, pp. 26309-26314, 2019.

APPENDIX A

PUBLICATIONS AND CONFERENCE PRESENTATIONS

Publications

1. D.M Tshwane, R. Modiba, H.R Chauke, G. Govender, P.E Ngoepe, The adsorption of Halogen molecules on Ti (110) surface. Journal Material Research 36 (3) 592-601, 2021

2. D.M Tshwane, R. Modiba, H.R Chauke, G. Govender, P.E Ngoepe, First principle study of HF molecule adsorption on TiO_2 (110) surface, IOP Conference Series: Materials Science and Engineering 655 (1), 012043, 2019

3. D.M Tshwane, R. Modiba, H.R Chauke, G. Govender, P.E Ngoepe, Computer simulation studies of HF adsorption on TiO_2 (001) and (110) surfaces: The Proceedings of SAIP2019, the 64th Annual Conference of the South African Institute of Physics, 23-28. ISBN: 798-0-620-88875-2

4. D.M Tshwane, R. Modiba and A.S Bolokang, Surface analysis of the stress-induced, impurity driven face centered cubic titanium phase and the ranging lattice parameter sizes, Materials Today Communications 24 101168, 2020

5. D.M Tshwane, R. Modiba, H.R Chauke, G. Govender, P.E Ngoepe, Computational study of chlorine-ion adsorption on Ti (100) surface. To be published.

6. D.M Tshwane, R. Modiba, H.R Chauke, G. Govender, P.E Ngoepe, Computer simulation studies of F_2 molecule adsorption on Ti (100) surface at different coverage. To be published

7. D.M Tshwane, R. Modiba, H.R Chauke, G. Govender P.E Ngoepe, First-principle studies of HF molecule adsorption on Titanium (100) and (110) surfaces. To be published

Presentation at the conference

1. D M Tshwane, R Modiba, H R Chauke, G Govender, P E Ngoepe, First principle study of HF and HCl molecule adsorption on Ti (100) surface, 12th Centre for High Performance Computing (CHPC) National Conference 2018

2. D M Tshwane, R Modiba, H R Chauke, G Govender, P E Ngoepe, Computer simulation studies of HF adsorption on TiO_2 (110) surfaces, Annual Conference of the South African Institute of Physics 2019.

3. D M Tshwane, R Modiba, H R Chauke, G Govender, P E Ngoepe, Computer simulation studies of HF adsorption on TiO_2 (001) and (110) surfaces, Faculty of Science and Agriculture Research, October, Polokwane 2019.

4. D M Tshwane, R Modiba, H R Chauke, G Govender, P E Ngoepe, Computer simulation studies of HF adsorption on TiO_2 (110) surfaces, Conference of South African Advanced Material Initiative 2019

5. D M Tshwane, R Modiba, H R Chauke, G Govender, P E Ngoepe, Adsorption of Cl_2 molecule on Ti (100) surface at different coverage, 6th African School on Electronic Structure Methods and Applications (ASESMA-21) 2021

6. D M Tshwane, R Modiba, H R Chauke, G Govender, P E Ngoepe, Adsorption-desorption of F_2 molecule on Ti (100) surface at different coverage, Conference of South African Advanced Material Initiative 2021

Achievements Awards

1. First Price for PhD DPCMM student presentation award 64th Annual Conference of the South African Institute of Physics, July 2019

2. First Price for PhD student presentation award 10th Postgraduate Research Day, Faculty of Science and Agriculture, University of Limpopo, September 2019